

***Development of Inorganic Dyes for the  
Application of Photocatalytic CO<sub>2</sub>  
Reduction.***

**By**

**Nadia Coburn, B.Sc. (Hon.)**



A Thesis presented to Dublin City University

for the

Degree of Master of Science.

Under the supervision of Prof. J. G. Vos &

Dr. Mary. T. Pryce,

School of Chemical Sciences, Dublin City University.

**2011.**

***Authors Declaration.***

I hereby certify that this material, which I now submit for assessment on the programme of study leading to the award of M.Sc. is entirely my own work, that I have exercised reasonable care to ensure that the work is original, and does not to the best of my knowledge breach any law of copyright, and has not been taken from the work of others save and to the extent that such work has been cited and acknowledged within the text of my work.

**Signed:** \_\_\_\_\_ **ID No.:** \_\_\_\_\_

**Date:** \_\_\_\_\_

## *Acknowledgements*

There are so many people to thank that I am not sure I could do them all justice! But here it goes:

Firstly, I would like to thank Prof. Han Vos for all his time, patience and guidance throughout my time here and Dr. Mary Pryce for the opportunity of working with her and all of her support and guidance.

To my parents Patrick and Olive without whose love and support this research would not have been possible. Also I would like to thank my aunt May, for I would not be the person I am today without her love and guidance (and well for those who know her, her good natured stubbornness!) My brothers (Joe and Eugene) and sisters (Brenda and Fiona) who have spoiled me rotten for the last 28 years, thank you.

To everyone past and present from the HVRG: the girls, Lynda, Laura, Yvonne and Jane and the boys, Rob, Dan, Bill, Declan, Hamid, Gourmet, Avi and Suraj and of course all the of the exchange students. I would especially like to thank Dan and Rob for their immense patience and or all of the times spent out of the lab you made my time here very special, There are too many times when both of you have helped me, to mention.

Laura you get paragraph of your own, for without the everyday chats, guidance and honesty I never would have finished. Thank you, you are truly an amazing person and I wish you all the best.

I would not have been able to get through the ups and downs of life at DCU without thanking two very special people, Nora and Sharon, for without the girly nights, dance classes, tea, cocktails and advice, life would have been truly gloomy. You two are ladies and don't worry the Wisp and Dice are a coming!

A thank you to all of the people across science for the help, laughs, parties, tea, ranting etc., Jamie, Will, Andy, Fadi, Siabh, Dennis, Dave, Kev, Debbie, Sonia, Ross, Ann-marie, David and to anyone I have forgotten please forgive me.

An infinite number of thank yous to my non DCU friends: Mark, Liz, Dermot, John H., Cheryl, Eilish, Eilis, Clare, Aoife, Dave, Mick, Ger, Erin, Orla, John S. and

Eimear. A special thank you to Erin for all the breakfast and coffee mornings, they won't be forgotten and neither will your dancing skills!

A million and one thank you's to John for your love and support. I appreciate everything you have done for me over the last while no one has made me happier or laugh as much as you (or made me so many cups of tea!).

To the DKC without you I would never have worked out my creativity. There are too many of ye to thank individually so collectively have a big THANK YOU for the knit nights, meetings and general excuses to meet for tea and cakes and laughter all of you brought to my life.

Finally I would like to thank the chemistry technicians of DCU (past and present); John, Brendan, Damien, Vinnie, Veronica, Mary, Ambrose, Colette, Claire, Susanna for without you none of my experiments would ever have come to completion and I would have lost my sanity. Your' patience has no limits and I appreciate everything you have done over the years.

*Be inspired to be brilliant, for we stand on the shoulders of giants, even if we hear nothing but the rain. –Anon.*

## ***Abstract.***

The work presented in this thesis focuses on the synthesis and characterisation of inorganic dyes which may be used as potential catalysts for CO<sub>2</sub> reduction. Chapter 1 is an introductory chapter concerned with introducing the area of CO<sub>2</sub> reduction and the complexes developed to date. It begins with a brief overview of the area of CO<sub>2</sub> reduction before introducing the significant photocatalysts developed to date for this purpose. The chapter concludes with an introduction to the photocatalysts developed within this research.

Chapters 3 and 4 of this thesis describe the synthesis and characterisation of mononuclear and dinuclear ruthenium (II) and rhenium (I) complexes using various synthetic routes and ligands. The experimental methodology (i.e. the materials, methods and instrumentation) used while conducting this research, is described in Chapter 2.

The investigation into the preparation of photocatalysts begins in chapter 3 with the development of homonuclear and heteronuclear supramolecular complexes containing ruthenium and rhenium metal centers using the “*complexes as metals / complexes as ligands*” approach. A range of ‘azole’ type bridging ligands 3,5-bis(pyridin-2-yl)-1,2,4-triazole (Hbpt), 3,5-bis(pyridin-2-yl)-1,2,4-triazole (Hbpzt), 2,5-Bis(2-pyridyl)-1,3,4-thiadiazole (dptd) were prepared to connect these two centres with an aim to study the effect of bridging ligands on catalytic activity. Characterisation was carried out by <sup>1</sup>H NMR, and CHN with a discussion of their electronic properties included.

Chapter 4 continues with a description of a synthetic study to prepare [Ru(bpy)<sub>2</sub>(tpphz)Re(CO)<sub>3</sub>Cl](PF<sub>6</sub>)<sub>2</sub>. Synthesis of the bridging ligand, tetrapyrido[3,2-a:2',3':3'',2''-h:2'''',3'''-j]phenazine (tpphz) is described with subsequent novel synthetic routes leading to the development of ruthenium and rhenium precursor complexes. Further investigation in the preparation of [Ru(bpy)<sub>2</sub>(tpphz)Re(CO)<sub>3</sub>Cl](PF<sub>6</sub>)<sub>2</sub> is detailed and characterisation is carried out by <sup>1</sup>H NMR and IR.

Chapter 5 details the analysis of  $[\text{Ru}(\text{bpy})_2(\text{bpt})\text{Re}(\text{CO})_3\text{Cl}]\text{PF}_6$  conducted by ion chromatography using a Dionex ICS-1500 system for oxalate and formate. System installation, calibration and validation are described with respect to the detection of oxalate and formate. Irradiation studies of the heteronuclear complex using blue light over a twenty four hour period are described.

Chapter 6 concludes this thesis with a summary of the work completed during this research. Possible future work is also described before concluding remarks.

### Abbreviations

**Bpy** = 2,2'-bipyridine

**BNAH** = 1-benzyl-1,4-dihydronicotinamide

**CO<sub>2</sub>** = carbon dioxide

**CP** = Cobalt porphyrins

**cyclam** = 1,4,8,11-tetraazacyclotetradecane

**CoTTP** = cobalttetra-m-tolylporphyrin.

**DMF** = dimethylformamide

**DMSO** = dimethylsulfoxide

**Et<sub>3</sub>N** = triethylamine

**FeP** = Iron porphyrins

**GHG** = Greenhouse gases

**HA**= ascorbic Acid

**Me<sub>2</sub>phen** = 2,9-Dimethyl-1,10-phenanthroline

**Mfibpy** = 4-methyl-4'-[1,10]phenanthroline-[5,6-d]imidazol-2-yl)bipyridine

**MebpyC<sub>2</sub>H<sub>4</sub>Mebpy** = 1,2-bis(4'-methyl-[2,2']bipyridinyl-4-yl)-ethane

**MebpyC<sub>4</sub>H<sub>8</sub>Mebpy** = 1,4-bis(4'-methyl-[2,2']bipyridinyl-4-yl)-butane

**MebpyC<sub>6</sub>H<sub>12</sub>Mebpy** = 1,6-bis(4'-methyl-[2,2']bipyridinyl-4-yl)-hexane

**MP** = metalloporphyrin

**MN** = metallocorrin

**MPc** = metallophthalocyanine

**MC** = metallocorrole.

**MLCT** = metal to ligand charge transfer

**NHE** = Normal Hydrogen Electrode

**OER** = one electron reduced

**Pr-cyclam** = 6-((p-methoxybenzyl)pyridin-4-yl)methyl-1,4,8,11 -  
tetraazacyclotetradecan

**Pcat** = photocatalyst

**Phen** = 1,10-phenanthroline

**Phendione** = 1,10-phenanthroline-5,6-dione

**Rubisco** = Ribulose-1,5 -biphosphatecarboxylase: oxygenase

**TEA** = triethanolamine

**TEOA** = triethanolamine

**TPP** = tetraphenylporphyrin,

**TFPP** = TPP containing a 3-F group

**T<sub>3</sub>CF<sub>3</sub>PP** = TPP containing a 3-CF<sub>3</sub> group

**TF<sub>5</sub>PP** = TPP with a perflourinated group



**THF** = tetrahydrofuran

**TN<sub>co</sub>** = turnover number for CO

**TMS** = trimethylsilane

## ***Table of Contents***

### ***Chapter One – Introduction.***

1.0	Introduction.	2
1.1	Artificial Photosynthesis.	3
1.1.1	Dark Reactions – The Calvin Cycle	4
1.2	Photocatalytic CO <sub>2</sub> Reduction.	6
1.2.1	Thermodynamic / Kinetic Considerations	6
1.2.2	Excited State Electron Transfer Considerations	8
1.2.3	Mechanistic Considerations	9
1.3	Type I Catalysts.	11
1.3.1	Tetraaza-macrocycles ( Cyclams)	13
1.3.2	Supramolecular Complexes	18
1.4	Type II Catalysts.	23
1.4.1	Metallomacrocycles	24
1.4.1.1	Metalloporphryins	25
1.4.1.2	Metallocorrolles	28
1.4.1.3	Metallocorrins	29
1.4.1.4	Metallophthalocyanines	31
1.4.2	Rhenium Mononuclear Complexes	36
1.5	Bibliography	42

### ***Chapter Two – Instrumental Methods.***

2.0	Introduction	50
2.1	General	51
2.2	Instrumental Methods	51
2.2.1	NMR Spectroscopy	51
2.2.2	Infrared Spectroscopy (IR).	51
2.2.3	Ultra Violet/Visible Spectroscopy. (UV/Vis)	52
2.2.4	Emission Spectroscopy.	52

2.2.5 Mass Spectrometry.	52
2.2.6 Elemental Analysis.	53
2.2.7 High Performance Liquid Chromatography. (HPLC)	53
2.2.8 Ion Chromatography.	53
3.0 Synthetic Considerations.	54
3.1 Apparatus Setup.	54
3.2 Glassware Preparation.	54
3.3 Sample Collection.	55

***Chapter Three - Synthetic approaches to the preparation of mononuclear and dinuclear photocatalysts using azole ligands.***

3.0 Introduction.	56
3.1 Aim.	61
3.2 Synthetic Procedures.	
3.2.1 Preparation of Ligands.	64
3.2.2 Preparation of Mononuclear Complexes.	66
3.2.3 Preparation of Dinuclear Complexes.	68
3.3 Characterisation and Discussion.	
3.3.1 Synthetic Procedures.	71
3.3.2 <sup>1</sup> HNMR Spectroscopy.	75
3.3.3 Infra-red Spectroscopy.	86
3.3.4 Absorption Spectroscopy.	89
3.3.5 Emission Spectroscopy.	94
3.4 Conclusions.	98
3.5 Bibliography.	99

***Chapter Four – Synthetic applications to the design of  
[Ru(bpy)<sub>2</sub>(tpphz)Re(CO)<sub>3</sub>Cl](PF<sub>6</sub>)<sub>2</sub>.***

4.0	Introduction .	103
4.1	Aim.	106
4.2	Synthetic Procedures.	
4.2.1	Preparation of Ligands.	109
4.2.2	Preparation of Mononuclear Complexes.	110
4.2.3	Preparation of Dinuclear Complexes.	113
4.2.4	Attempted Synthesis.	115
4.3	Results and Discussion.	
4.3.1	Synthesis.	116
4.3.2	<sup>1</sup> HNMR Spectroscopy.	123
4.3.3	Infra-red Spectroscopy.	134
4.4	Conclusion.	137
4.5	Bibliography.	138

***Chapter Five – Detection of Formate and Oxalate using Ion  
Chromatography.***

5.0	Introduction	141
5.1	Aim	150
5.2	System Installation and Calibration.	
5.2.1.	System Installation.	151
5.2.2	Chemicals and Reagents.	152
5.2.3.	Separation and Resolution.	152
5.2.4.	Reproducibility and Efficiency	154
5.2.5.	Conclusion.	155
5.3	Method Development for the Analysis of Oxalate and Formate.	
5.3.1	Determination of Retention Times and Reproducibility.	156
5.3.2.	Calibration and Quantification.	158
5.3.3	Detection Limits .	159
5.4.	Photochemical CO <sub>2</sub> Reduction Experiment.	160

5.5 Conclusions and Future Work	162
5.6 Bibliography	162
 <i>Chapter Six – Final Conclusions and Future Work.</i>	 163
<i>Appendix A: List of Figures.</i>	
<i>Appendix B: List of Tables.</i>	

## ***Chapter 1 – Introduction.***

### ***Chapter 1: Introduction.***

*Chapter one acts as an introduction to CO<sub>2</sub> reduction and the research that has been carried out to date. A brief discussion of artificial photosynthesis is presented, however the main focus of the chapter are those systems that are prepared to photocatalytically reduce CO<sub>2</sub>.*

## **1.0 Introduction**

One of the greatest challenges facing our generation, is the reduction of greenhouse gases (GHG) in our atmosphere, thereby reducing the effect of climate change. As the world population grows, the demand for energy production increases, releasing yet more GHG and directly contributing to global warming. To combat this, scientists around the world are working together to locate alternative fuel sources and to reduce carbon dioxide emissions. CO<sub>2</sub> accounts for the largest share in the worlds GHG emissions<sup>1 2</sup>, inspiring scientists to inexpensively reduce CO<sub>2</sub> to useful organic compounds. From this view point, the research reported here, was undertaken to prepare a series of transition metal complexes that would photocatalytically reduce CO<sub>2</sub>.

Within the last twenty years a great deal of time and effort has been employed into the development of artificial systems that have the ability to reduce CO<sub>2</sub>. Research has mainly been divided into type I and type II catalysts:

**Type I catalysts:** Use a biomolecular or supramolecul approach to CO<sub>2</sub> reduction.

**Type II catalysts:** Are comprised of one single compound, which acts as both the photosensitiser and the catalytic centre for reduction.

As the body of work reported here deals with artificial photocatalytic systems, these systems will be described in detail in the following subsections. The following section describes the initial research into the development of photocatalysts for CO<sub>2</sub> reduction.

## **1.1 Artificial Photosynthesis**

The sun delivers  $\sim 120,000$  TW of energy to the earth's surface on average per second, the amount of energy that could potentially be harnessed is 4 times that of the current global energy requirement.<sup>3</sup> As current solar energy conversion technologies cannot compete with the energy generated from fossil fuels, scientists have turned to systems like artificial photosynthesis as a method of alternative energy production. Artificial photosynthesis is a direct pathway to produce fuel from carbon dioxide and water using solar energy, in an integrated system without the use of charge carriers.<sup>4,5,6</sup> The main role of research into this area is to learn from the processes occurring in green plants and algae and to reproduce or 'mimic' this transistion to produce energy in a form that can be utilised in our everyday life. This system also has the added advantage of reducing the amount of  $\text{CO}_2$  in our atmosphere.

Figure 1.1 below shows the overview of photosynthesis, as shown this can be broken down into light and dark reactions (Calvin cycle). The light reactions are governed by photosystem I and photosystem II mediated by an electron transport chain, producing  $\text{O}_2$  from  $\text{H}_2\text{O}$ .<sup>4,5,6</sup> The energy produced from the light reactions is subsequently consumed by the dark cycle where  $\text{CO}_2$  is fixated. As  $\text{CO}_2$  is the main focus of this thesis only the dark reaction will be discussed further.

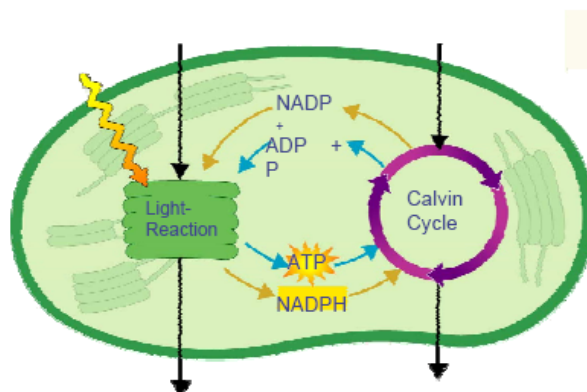


**Figure 1.1** General scheme of photosynthesis occurring within a chloroplast.



## Chapter 1 – Introduction.

### 1.1.1 Dark Reactions – The Calvin Cycle.

Dark reactions deal predominately with carbon dioxide fixation and reactions that occur within the Calvin cycle where rubisco (*Ribulose-1,5 -biphosphatecarboxylase: oxygenase*) is the most abundant enzyme of the biosphere<sup>7</sup>. In 1989 a breakthrough in the structural elucidation of rubisco<sup>8</sup> led to two decades of further research into improving the catalytic efficiency of the enzyme by genetic engineering.<sup>9,10,11,12,13,14,15,16,17,18</sup> In 1996, T. J. Andrews published an article in *Nature* entitled “*The Bait in the Rubisco Mousetrap*”<sup>19</sup> which describes the unusual activation mechanism of rubisco in the presence of CO<sub>2</sub> as described in Figure 1.2 below. Figure 1.3 that follows shows the structure of the metal containing active site of the rubisco structure.

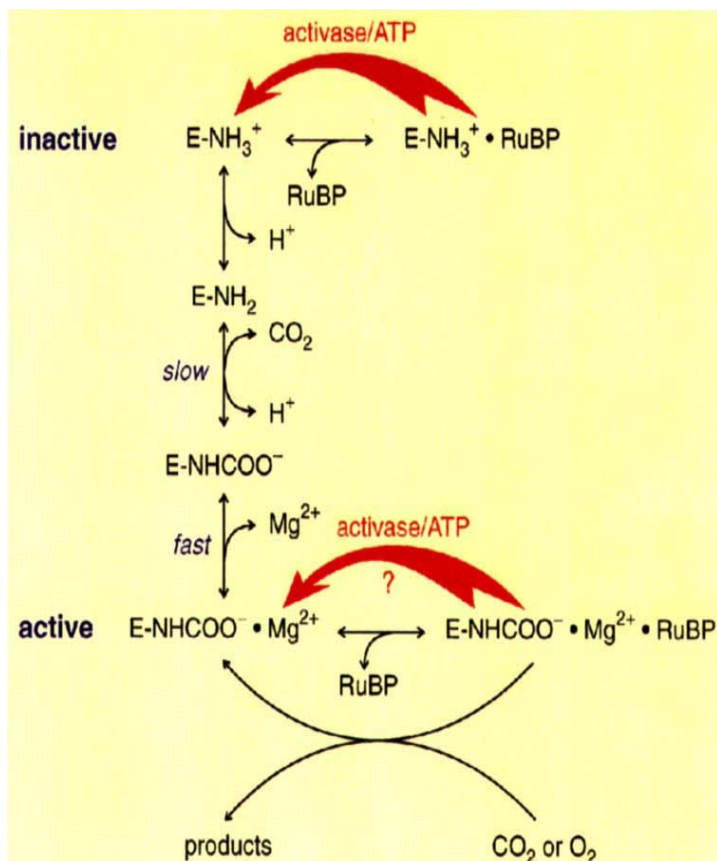


**Figure 1.2:** Activation mechanism of rubisco in the presence of CO<sub>2</sub>.

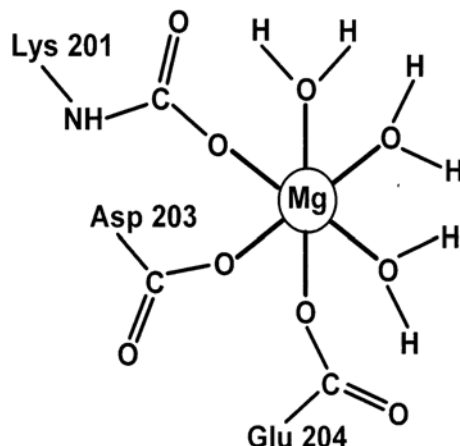


**Figure 1.3:** Structure of the metal containing segment of rubisco.

Rubisco is an enzyme consisting of eight large subunits (52,000 M<sub>r</sub>) containing the active sites as depicted in Figure 1.2 along with eight smaller subunits of 13,000 M<sub>r</sub>. As shown in Figure 1.3, carbon dioxide is bound in the form of a carbamate to the ε-amino group of lysine located within a cofactor attached to the protein. The cofactor then allows for further reaction with the active sites containing the divalent Mg<sup>2+</sup>. In 1996 T.C. Taylor *et al.* reported that this carbamate ligand was found to have monodentate coordination, while the magnesium ion prefers to be penta-coordinated in substrate containing structures and octahedral coordination when substrate free.<sup>20</sup> CO<sub>2</sub> fixation is then completed by a carbamylation reaction of lysine 201 converting a cationic side chain to an anionic one. More current research within this area has shown that crystal structure site-mutagenesis have met with limited success on catalytic activity and research has currently moved to bioselection as an alternative random mutagenic approach<sup>21</sup> along with subunit loop alterations<sup>22</sup> with the aim of increasing catalytic activity.

## **1.2 Photocatalytic CO<sub>2</sub> Reduction**

Artificial photocatalytic systems that use light energy to reduce CO<sub>2</sub> are the main focus of this thesis and will be discussed in detail. These systems in principle consist of:

- A Photocatalyst: This contains the light harvesting species and the catalyst that will reduce CO<sub>2</sub>.
- An electron relay : This acts as a mediator and is typically an iodide/triiodide species
- A sacrificial donor: typically triethylamine.

Typically transition metal complexes are reported for use<sup>23</sup> within these artificial systems as they have long lived excited states, which are capable of electron transfer, and have the ability to absorb light in the visible range.<sup>25</sup> Development of these systems is complex as the reduction of carbon dioxide to form formate, carbon monoxide or methanol has a number of difficult scientific challenges due to the stability of CO<sub>2</sub> as the most oxidized carbon compound.<sup>24</sup> A number of considerations must be taken into account in order to develop an effective system, which has the ability to reduce CO<sub>2</sub> photocatalytically.

### **1.2.1 Thermodynamic / Kinetic Considerations**

Kinetically there is an excess of energy produced or an ‘overvoltage’ during a one electron reduction from CO<sub>2</sub> to CO<sub>2</sub><sup>•-</sup> due to the structural differences between linear CO<sub>2</sub> and bent CO<sub>2</sub><sup>•-</sup>.<sup>25</sup> Thermodynamically, the high reduction potential required for the one electron activation of CO<sub>2</sub> (-1.9 vs. NHE), is not only unfavorable but also produces the unstable CO<sub>2</sub><sup>•-</sup>. This poses a challenge that may be overcome by introducing a multi electron transfer into the reduction of CO<sub>2</sub>. By introducing a step by step reduction the amount of energy required is reduced making the reduction of CO<sub>2</sub> more practical.

## Chapter 1 – Introduction.

Figure 1.4 below details the redox reactions and the reduction potentials for these reactions at pH 7 at 25°C.<sup>26</sup> These two electron reductions are shown to be more favorable at a low pH becoming less favorable than H<sub>2</sub>O reduction above pH 6.5. This is described in an experiment carried out by Fujita *et al.* shown in Figure 1.5 below where the reduction potentials are shown against varying pH. Inflections were observed at the pK<sub>a</sub> of the carbon dioxide oxidant (6.3 and 10.5) and of the formate product (3.5).

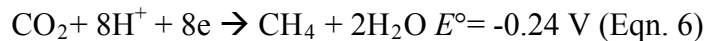
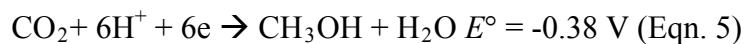
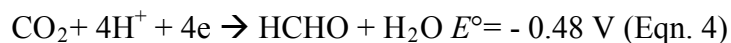
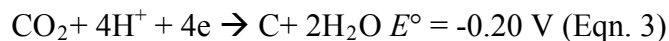
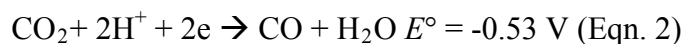


**Figure 1.4:** Redox potentials vs. NHE for the multi electron reduction of CO<sub>2</sub> at pH 7 / 25°C.<sup>27</sup>

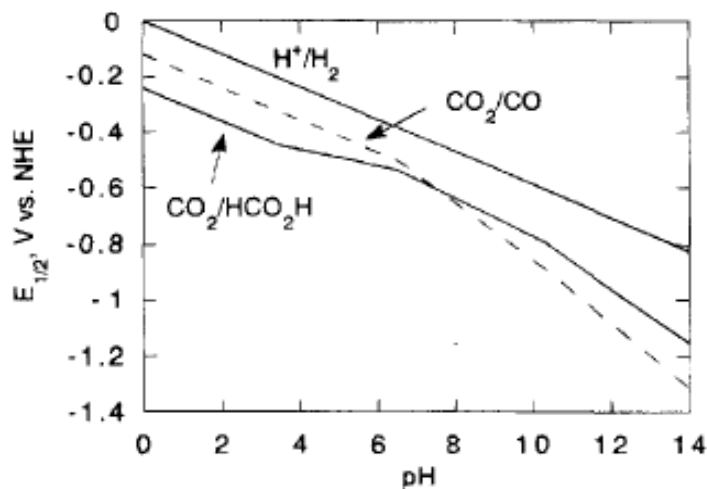


**Figure 1.5:** Shows the two electron reduction potentials as a function of pH for carbon dioxide to carbon monoxide, carbon dioxide to formic acid and hydrogen ion /water to dihydrogen.

## ***Chapter 1 – Introduction.***

When taking into consideration the equations in Figure 1.4 above, the stable reduction products of CO<sub>2</sub>, CO (-0.53 V eqn 2) and formate (-0.61 V, eqn 1) occur at much lower potentials than the one electron reduction of CO<sub>2</sub> (-1.9 V) This reduces the amount of energy required at each step indicating that a multi electron reduction route is more viable for CO<sub>2</sub> reduction, and must be considered during the development of catalysts for this purpose.

The same considerations apply to photochemical CO<sub>2</sub> reduction, the strong reducing agents that are required to reduce carbon dioxide to CO<sub>2</sub><sup>•-</sup> are difficult to obtain via photochemical methods. Generally photochemical electron transfer is a one electron process; a catalyst must be employed here to facilitate a multi-electron reduction of CO<sub>2</sub>, in addition to the photosensitiser.

### ***1.2.2 Excited State Electron Transfer Considerations***

Electron transfer is of vital importance in these systems as the photosensitiser has to be regenerated to its ground state after excitation, as well as electron transfer to the catalytic center. This occurs via a bimolecular approach from an independent sensitiser or covalently within a supramolecular complex and the understanding of electron movement is crucial.

The two main types of electron transfer are oxidative and reductive quenching depending on whether an electron is donated (oxidative) from the excited state or accepted (reductive) from the substrate (quencher). Figure 1.6 below details examples of electron transfer pathways under discussion.

## Chapter 1 – Introduction.

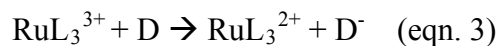


**Figure 1.6:** Shows the oxidative and reductive quenching equations as described by E. Fujita. Where A = strong reducing agent and D = sacrificial donor.

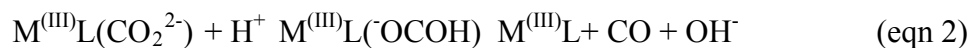
As mentioned previously strong reducing agents are required to reduce  $\text{CO}_2$  to  $\text{CO}^-$ , here oxidative quenching forms  $\text{RuL}_3^{3+}$  (a strong oxidant, eqn. 1) while reductive quenching forms  $\text{RuL}_3^{+}$  (a strong reductant, eqn. 2). The sacrificial agent D (eqn. 3) is needed to reduce the strong oxidant  $\text{RuL}_3^{3+}$ . Regeneration to the ground state is carried out by the sacrificial donor D, most commonly being triethylamine (TEA), nitilotriethanol (TEOA), ascorbic acid ( $\text{H}_2\text{A}$ ) and ethylenediaminetetraacetate (EDTA). This reduction and regeneration process introduced here is employed in the photocatalytic systems under discussion within this thesis and will be discussed in subsequent sections within specific systems.

### 1.2.3 Mechanistic Considerations

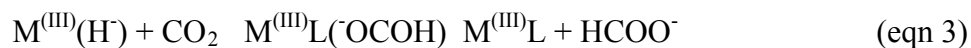
The mechanism of  $\text{CO}_2$  reduction is still under investigation in most systems that have previously been prepared. Most of these difficulties arise as the reduction of  $\text{CO}_2$  can occur via two pathways as shown below, and are governed by the route that  $\text{CO}_2$  takes when introduced to the catalyst.

1. *Oxidative addition:* This involves the addition of the neutral  $\text{CO}_2$  ligand to  $\text{M}^{(\text{I})}\text{L}$ , oxidising the metal by  $2e^-$  to form a metallacarboxylate  $\text{M}^{(\text{III})}\text{L}(\text{CO})^-$ . The formation of the carboxylate species allows for stabilization of the reduced moiety, which further reacts with  $\text{H}^+$  to form  $\text{M}^{(\text{III})}\text{L}$ , CO and  $\text{OH}^-$ , as shown in equations 1 and 2.<sup>28</sup>

**Chapter 1 – Introduction.**



2. *CO<sub>2</sub> Insertion:* Here CO<sub>2</sub> “inserts” itself between a metal hydride bond causing the formation of a formato complex. This insertion is kinetically favoured over the formation of the carboxylate species.<sup>29,30</sup>



These reaction pathways as mentioned above, were described by Fujita *et al.* as shown in Figure 1.7 below.

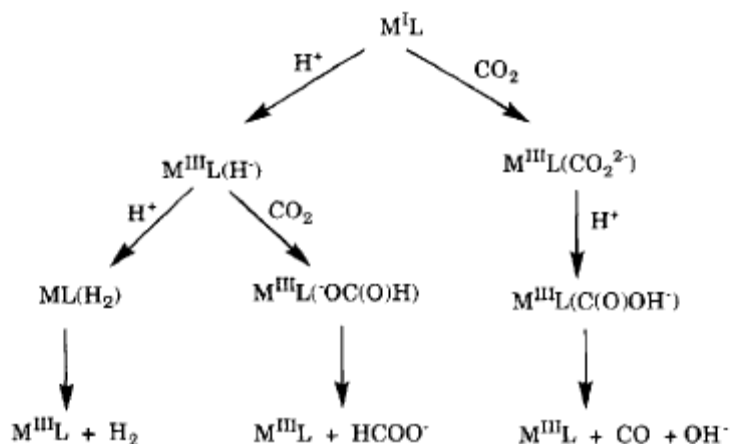


**Figure 1.7:** Possible CO<sub>2</sub> reduction pathways as described by Fujita *et al.*

Taking these considerations into account many photocatalytic systems have been developed with one of the above methods in mind. The mechanistic advancements will be shown per individual catalyst as follows, which will be divided into type I and type II as most recently described by Morris *et al.*<sup>31</sup>

### **1.3 Type I Catalysts**

Morris *et al.* describe type I catalysts as a photosensitized approach to CO<sub>2</sub> reduction using either a bimolecular process or a supramolecular complex. The bimolecular approach is described in Figure 1.8 below.

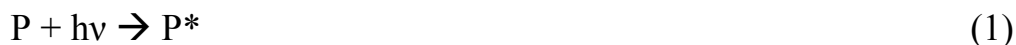


**Figure 1.8:** Equations for the bimolecular process for CO<sub>2</sub> reduction.

In this process a molecular light absorber (P) is promoted to its excited state (P\*) (eq 1). This then undergoes reductive quenching (as described previously in section 1.2) by a sacrificial donor (D) to obtain the reduced sensitizer (P<sup>-</sup>) and oxidized donor (D<sup>·+</sup>) (eq 2) electron transfer then occurs from the reduced sensitizer (P<sup>-</sup>) to the catalyst (eq 3) where a reduced active site is generated (one electron reduced species OER) so CO<sub>2</sub> reduction may occur (eq 3 + 4).

Equations 5 and 6 above show the ability of the amine sacrificial donor to undergo hydrogen abstraction and radical rearrangements that can produce a carbon centered radical species. This species is known to have the ability to reduce a second photosensitizer.<sup>32</sup> Tables 1.1 and 1.2 below describe a series of photocatalytic experiments carried out using type I catalysts. However catalytic systems based on this approach are known to have problems with the selectivity of products formed and



## Chapter 1 – Introduction.

the efficiency of CO<sub>2</sub> reduction due to competing reaction of hydrogen evolution from the intermediate complexes.<sup>33</sup> Tables 1.1 and 1.2 that follow describe the photocatalysts under discussion in detail in the following subsections.

	Photosensitiser	Catalyst	Reductant	Product	$\Phi_{\text{mol}}$ Einstein <sup>-1</sup>	Ref
1	[Ru(bpy) <sub>3</sub> ] <sup>2+</sup>	Co <sup>2+/</sup> bpy	TEA	CO, H <sub>2</sub> ,		27
2	[Ru(bpy) <sub>3</sub> ] <sup>2+</sup>	Co <sup>2+/</sup> Me <sub>2</sub> phen	TEA	CO, H <sub>2</sub>	0.012 (CO) 0.065 (H <sub>2</sub> )	34
3	[Ru(bpy) <sub>3</sub> ] <sup>2+</sup>	[Ru(bpy) <sub>2</sub> (CO)(H)] <sup>+</sup>	TEOA	HCOO <sup>-</sup>	0.15	35
4	[Ru(bpy) <sub>3</sub> ] <sup>2+</sup>	[Nicyclam] <sup>2+</sup>	HA	CO, H <sub>2</sub>	0.001 (CO)	36, 37
5	[Ru(bpy) <sub>3</sub> ] <sup>2+</sup>	[NiPr-cyclam] <sup>2+</sup>	HA	CO, H <sub>2</sub>	0.005 (CO)	38
6	[Ru(bpy) <sub>3</sub> ] <sup>2+</sup>	[Ru(bpy) <sub>2</sub> (CO) <sub>2</sub> ] <sup>2+</sup>	BNAH	HCOO <sup>-</sup> , CO	0.03(HCOO <sup>-</sup> ) 0.15 (CO)	39, 40,41
7	[Ru(bpy) <sub>3</sub> ] <sup>2+</sup>	[Ru(bpy) <sub>2</sub> (CO) <sub>2</sub> ] <sup>2+</sup>	TEOA	HCOO <sup>-</sup>	0.14	39,40, 41
8	<i>p</i> -Terphenyl	[Cocyclam] <sup>3+</sup>	TEOA	CO,HCOO <sup>-</sup> , H <sub>2</sub>	0.25 (CO + HCOO <sup>-</sup> )	42, 43
9	<i>p</i> -Terphenyl	[CoHMD] <sup>2+</sup>	TEOA	CO,HCOO <sup>-</sup> , H <sub>2</sub>	-	42, 44
10	<i>Phenazine</i>	Cocyclam <sup>3+</sup>	TEOA	HCOO <sup>-</sup>	0.07	45

**Table 1.1:** Summary of Type I catalyst experiments for CO<sub>2</sub> reduction via bimolecular process, where

TEOA= triethanolamine,, TEA = triethylamine, bpy =2,2'-bipyridine, Me<sub>2</sub>phen = 2,9-Dimethyl-1,10-phenanthroline, BNAH = 1-benzyl-1,4-dihydronicotinamide, HA = ascorbic acid, cyclam = 1,4,8,11-tetraazacyclotetradecane and Pr-cyclam,6-((NR)pyridin-4-yl)methyl-1,4,8,11-tetraazacyclotetradecane where R = *p*-methoxybenzyl and benzyl.

	Compound	Reductant	Product	$\Phi$ mol Einstein-1	TNco	Ref
1	Ru(mfibpy)Re	BNAH		-		46
2	Re(mfibpy)Ru	BNAH		-		46
3	b <sub>2</sub> Ru-Re	BNAH		-		46
4	d <sub>2</sub> Ru-Re	BNAH	CO	0.120		46
5	tfbRu-Re	BNAH		-		46
6	RuRe <sub>3</sub>	BNAH	CO	0.093		46
7	Ru(phen) <sub>2</sub> (phen-cyclam-Ni)	ascorbate	CO	0.09 <sup>a</sup> (microliters)		47
8	Ru <sub>2</sub> Re	BNAH	CO	-	110 <sup>b</sup>	61
9	RuRe <sub>2</sub>	BNAH	CO	-	190 <sup>b</sup>	61
10	RuC <sub>3</sub> (OH)Re	BNAH	CO	-	-	62
11	RuC <sub>2</sub> (OH)Re	BNAH	CO	0.13 <sup>b</sup>	180	62
12	RuC <sub>4</sub> (OH)Re	BNAH	CO	0.11 <sup>b</sup>	120	62
13	RuC <sub>6</sub> (OH)Re	BNAH	CO	0.11 <sup>b</sup>	120	62

**Table 1.2:** Summary of Type I catalyst experiments for CO<sub>2</sub> reduction via bimolecular process, where

*BNAH* = 1-benzyl-1,4-dihydronicotinamide

*mfibpy* = 4-methyl-4'-[1,10]phenanthroline-[5,6-d]imidazol-2-yl)bipyridine

*a* = microliters of CO not  $\Phi$ mol Einstein<sup>-1</sup>

*b* = calculated on complex concentration.

### 1.3.1 Tetraaza-macrocycles ( Cyclams)

Research into the use of cyclams, in the development of photocatalysts for CO<sub>2</sub> reduction, initially used the bimolecular approach discussed previously, using [Ru(bpy)<sub>3</sub>]<sup>2+</sup>,<sup>36,37,38</sup> p- Terphenyl<sup>42,43</sup> and phenazine as sensitizers. In 1990 Craig *et al.* reported the use of [Ni(14-aneN<sub>4</sub>)]<sup>2+</sup> and [Ni(12-aneN<sub>4</sub>)]<sup>2+</sup> (Figure 1.9 below) to investigate catalytic ability, as previous investigations by Sauvage<sup>48,49</sup> indicated a high selectivity for the electrochemical reduction of CO<sub>2</sub> over that of water.

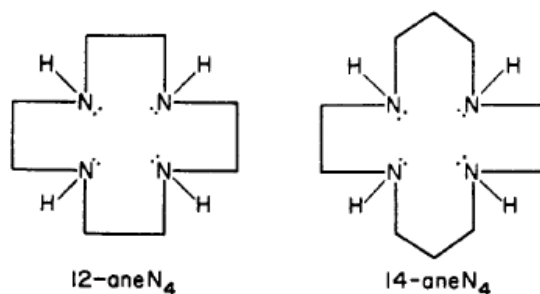


**Figure 1.9:** Structures of [Ni(14-aneN<sub>4</sub>)]<sup>2+</sup> and [Ni(12-aneN<sub>4</sub>)]<sup>2+</sup> investigated by Craig *et al.*<sup>33</sup>

Photochemical studies by Craig of the 1,4,7,10-tetraazacyclotetradecanes confirmed that these complexes have the catalytic ability to reduce carbon dioxide, in the presence of a [Ru(bpy)<sub>3</sub>]<sup>2+</sup> sensitizer with H<sub>2</sub> as a minor product. These complexes displayed interesting differences during photochemical experiments; the [Ni(12-aneN<sub>4</sub>)]<sup>2+</sup> produced CO and formate as expected, while the [Ni(14-aneN<sub>4</sub>)]<sup>2+</sup> produced only CO. This was explained by the structural differences of the two complexes with a view to further flash photolysis studies to determine the reason for these differences.

That same year Kimura *et al.*<sup>50</sup> reported the preparation of a 1,4,8,11-tetraazacyclotetradecane covalently bound to a ruthenium bipyridine moiety as shown below in Figure 1.10. However this was found to have limited catalytic activity due to

## Chapter 1 – Introduction.

the configuration of the Ni(cyclam) unit and the rapid dissociation of the Ru(bpy)<sub>2</sub> moiety upon irradiation.<sup>51</sup> This led to the development of the supramolecular complex, ([Ru(phen)<sub>2</sub>(phen-cyclam-Ni)(ClO<sub>4</sub>)<sub>4</sub>].2H<sub>2</sub>O) illustrated in Figure 1.11 below, to inhibit the photolability of the ruthenium sensitizer and increase catalytic activity.

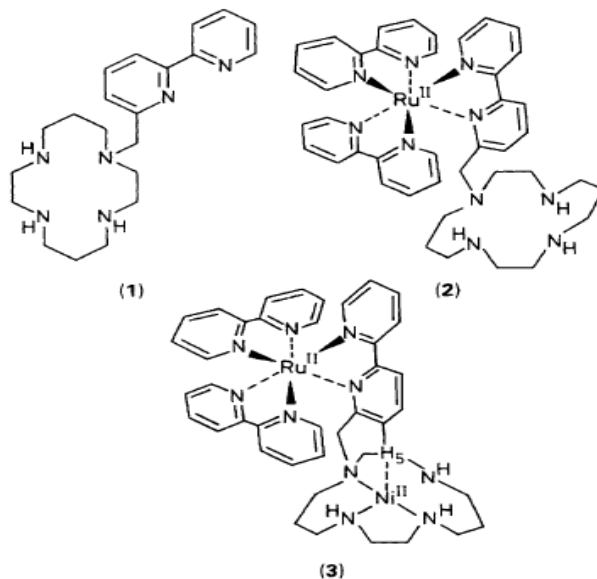


**Figure 1.10:** Preparation of the supramolecular complex [Ru<sup>(II)</sup>(bpy)<sub>2</sub>(bpy-cyclam)Ni<sup>(II)</sup>] (ClO<sub>4</sub>)<sub>4</sub>·2H<sub>2</sub>O(3) via [Ni<sup>(II)</sup>cyclam] (1) and [Ru(bpy)<sub>2</sub>(bpy-H<sub>2</sub>cyclam<sup>2+</sup>)](ClO<sub>4</sub>)<sub>4</sub>·3H<sub>2</sub>O.<sup>50</sup>

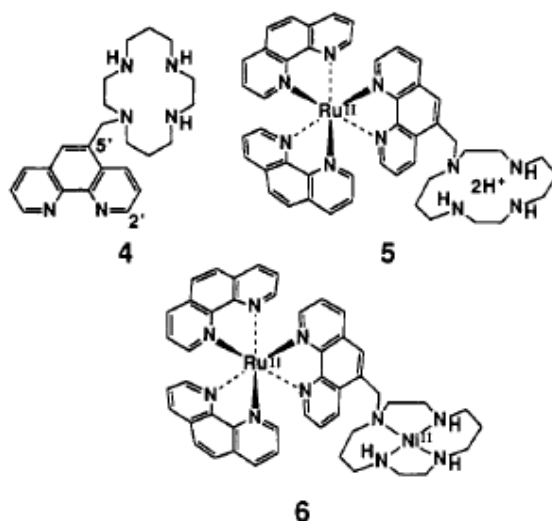


**Figure 1.11:** Preparation of the supramolecular complex  $[Ru(phen)_2(phen-cyclam-Ni)(ClO_4)_4] \cdot 2H_2O$  from the Ni(II) cyclam ligand (1) and  $Ru(phen)_2(phen-cyclam-H_2)(ClO_4)_4 \cdot 3H_2O$  (2).

Subsequent photochemical studies of  $[Ru(phen)_2(phen-cyclam-Ni)(ClO_4)_4] \cdot 2H_2O$  using  $[Ru(phen)_3]^{2+}$  and  $[Ni(cyclam)]^{2+}$  as a reference system, displayed increased stability of  $[Ru(phen)_2(phen-cyclam-Ni)(ClO_4)_4] \cdot 2H_2O$  over the reference system and the previous bipyridine analogue ( $[Ru(bpy)_2(bpy-cyclam-Ni)(ClO_4)_4] \cdot 2H_2O$ ) while prolonged irradiation in the presence of  $CO_2$  showed increased CO formation over the previous reported systems in conjunction with increased selectivity.<sup>51</sup> The small amount of CO produced was reportedly due to the hindered access of  $CO_2$  to the cyclam catalytic site.  $[Ru(bpy)_2(bpy-cyclam-Ni)(ClO_4)_4] \cdot 2H_2O$  because of steric hindrance, formed from the trans I configuration<sup>38</sup> while  $[Ru(phen)_2(phen-cyclam-Ni)(ClO_4)_4] \cdot 2H_2O$  retained the more usual trans II configuration. However the emission lifetime of the  $Ru(phen)_2$  moiety was found to be too short to allow the reductive quenching of the excited state which led to the preparation of the supramolecular type I catalyst  $[Ru(bpy)_2(4-((4-methylpyridinium-1-yl)methyl)-4'-methyl-2,2'-bipyridine)](ClO_4)_3$  shown in Figure 1.12 below.

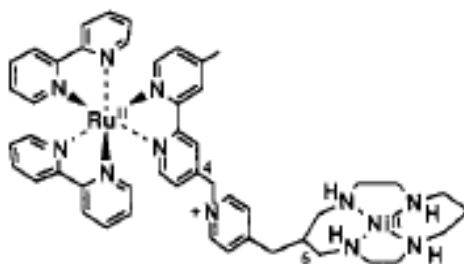


**Figure 1.12:** Structure of  $[Ru(bpy)_2(4-((4\text{-methylpyridinium-1-yl)methyl})-4'\text{-methyl-2,2'-bipyridine})](ClO_4)_3$ .

During the photochemical measurements of  $[Ru(bpy)_2(4-((4\text{-methylpyridinium-1-yl)methyl})-4'\text{-methyl-2,2'-bipyridine})](ClO_4)_3$ , the photodissociation of the  $Ru(bpy)_2$  moiety was again observed along with increasing CO formation upon the exchange of the methyl group on the bipyridine ring with the more electron withdrawing p-methoxybenzyl group and benzyl groups respectively, though further research in to these systems by Kimura has yet to be reported.

The research of cyclams as potential catalysts for  $CO_2$  reduction was also reported by Fujita *et al.* with both Ni<sup>52</sup> and Co<sup>53,54,55,56</sup> centers. These systems were similar to that of Kimura *et al.* but Fujita investigated the effect on bimolecular quenching<sup>52</sup> on the Ni cyclam unit by ligand exchange, before moving on to the development of Co cyclams and further Co macrocycles.

Fujita *et al.* investigated the use of cobalt macrocycles as stabilizers when using p-terphenyl as a sensitizer for  $CO_2$  reduction. Previously Matsuoka *et al.*<sup>43,54,57</sup> had reported the use of p-terphenyl (TP) to p-sexiphenyl as sensitizers during the photoreduction of  $CO_2$  to formate, though a competing photo-Birch reduction of the TP caused loss of photocatalytic activity of the TP rendering it useless. Fujita hoped to increase the amount of formate formed (and the amount of  $CO_2$  reduced) due to the stabilization of the TP by rapid electron transfer from the TP radical anion to the macrocycle. Investigation showed the increased yield of formate from 7.2 % to 25 % by using the macrocycle and a tertiary amine as a sacrificial donor.

## Chapter 1 – Introduction.

Fujita *et al.* also studied a series of 14-membered macrocycles for the factors governing the binding of CO and CO<sub>2</sub>. Here Fujita reports the importance of back bonding upon the attachment of CO to the square planar low spin d<sup>8</sup> cobalt (I) center, which was identified by a decrease of CO stretching frequencies as binding constants increase. Charge transfer from cobalt to CO is also mentioned as an important factor in the stabilization of the CO adducts formed during CO<sub>2</sub> reduction. This paper led to further research into the mechanisms of CO<sub>2</sub> reduction for macrocycles, which are still not fully understood. Figure 1.13 describes the mechanisms researched so far for CO<sub>2</sub> reduction by metaltetraaza-macrocycles described by Morris *et al.*

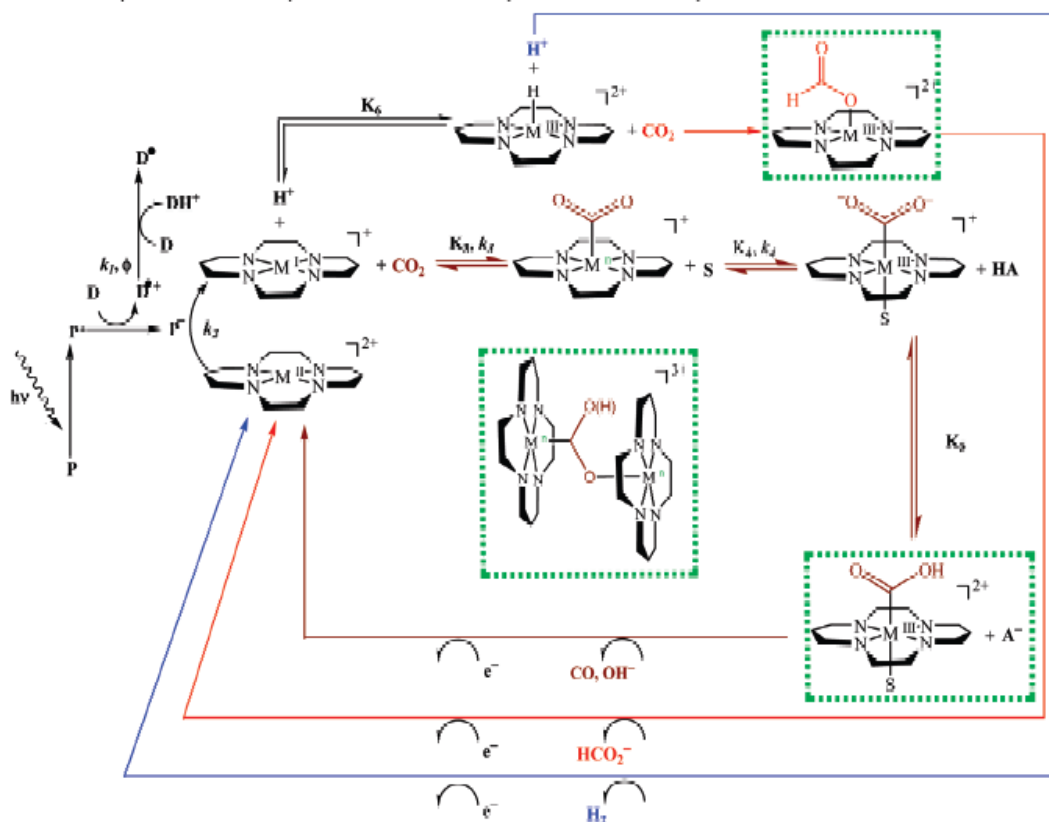


**Figure 1.13:** Proposed mechanisms for CO<sub>2</sub> reduction for metal metaltetraaza-macrocycles.

### **1.3.2 Supramolecular Complexes**

Research into the development of supramolecular complexes for CO<sub>2</sub> reduction i.e., attachment of a sensitizer to a catalytic center capable of CO<sub>2</sub> reduction, was conducted with the premise of increasing the efficiency of excited- state electron transfer between the donor (sensitizer) and acceptor (catalyst) thereby increasing the amount of CO<sub>2</sub> reduced. Table 1.2 on page 13 has a brief summary of supramolecular photocatalysts. It was suggested that a supramolecular complex based on this design would have the following benefits:<sup>59</sup>

1. Efficient formation of the one electron reduced species (OER) due to rapid quenching of the donor excited state by a sacrificial donor.
2. Efficient reduction of CO<sub>2</sub> adducts.
3. Rapid loss of the monodentate ligand from the OER and its rapid reaction with CO<sub>2</sub>.
4. Efficient reproduction of the parent ligand –complex by re-coordination of the ligand to the rhenium center after CO formation.

As previously discussed, the supramolecular complexes containing cyclams by Kimura and Fujita, showed increased stability and turnover numbers. Complexes containing rhenium as a catalytic center have been investigated by Ishitani *et al.* over recent years.<sup>58, 59, 60</sup> Examples of the Ru(II)- Re(I) systems investigated are shown in Figure 1.14 below.



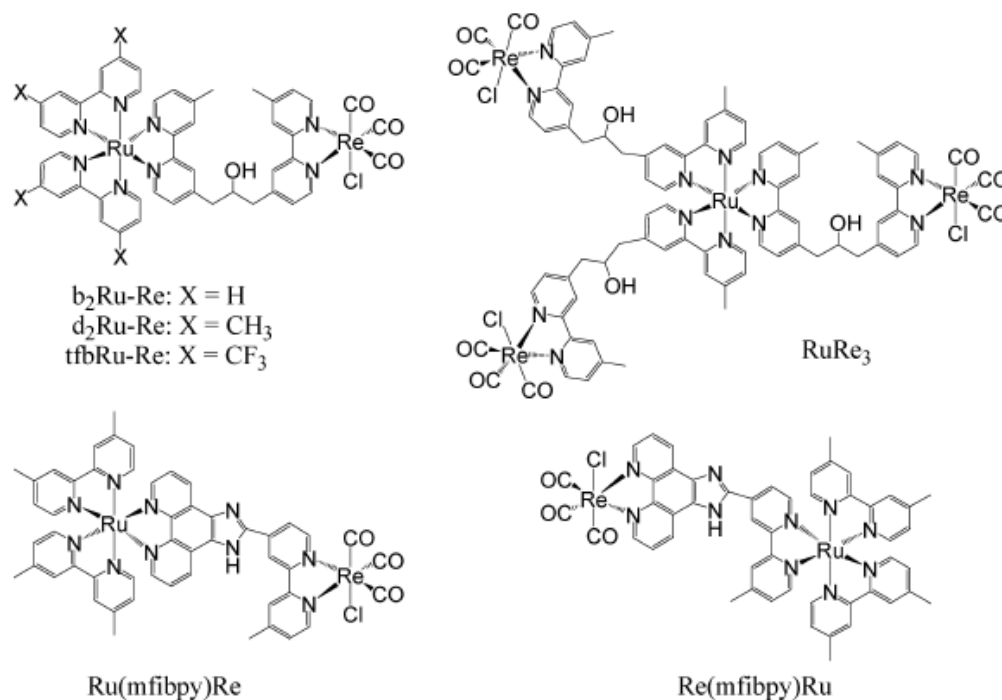


**Figure 1.14:** Supramolecular complexes studied by Ishitani *et al.*

Photocatalytic experiments of the heterogeneous systems described above in Figure 1.14 and Table 1.2, ( $tfbRu-Re$ ,  $b_2Ru-Re$  and  $d_2Ru-Re$ ), were shown to have efficient quenching of the Ru moiety in the presence of BNAH (1-benzyl-1,4-dihydronicotinamide) though no quenching was observed in the presence of TEA.<sup>46</sup> In the case of  $tfbRu-Re$  and  $b_2Ru-Re$  the OER formation was found to be endothermic ( $(\Delta G) +0.55$  and  $+0.05$  eV respectively,) inhibiting the formation of the OER species, however the  $tfbRu-Re$  complex produced a small amount of CO.

These photocatalytic experiments also indicated the importance of the bridging ligand chosen to covalently bind the sensitizer to the catalytic center. For the complexes  $Ru(mfibpy)Re$  and  $Re(mfibpy)Ru$  (Figure 1.14) photocatalytic ability was low. However strong electronic communication between the sensitizer and catalytic center was indicated to decrease photocatalytic activity but maintain rapid electron transfer,

## Chapter 1 – Introduction.

concluding that communication between the two moieties is essential but a slow transfer rather than a rapid transfer is required, as reaction of the catalytic site with CO<sub>2</sub> is slow.<sup>45</sup>

Using this information Ishitani *et al.* in 2008<sup>61</sup> further investigated the effect of a bridging ligand and rates of electron transfer between the Ru(II) and Re(I) centers, using tris[(4'-methyl-2,2'-bipyridyl-4-yl)methyl]-carbinol as described in Figure 1.15 that follows. This allowed for the study of trinuclear supramolecular complexes, using either two Ru centres and one Re centre or one Ru centre and two Re and the effects of this structure on catalytic ability under visible irradiation. Turnover numbers (TNco) for Ru<sub>2</sub>LRe and RuLRe<sub>2</sub> were calculated as 110 and 190 respectively based on complex concentration. These experiments were repeated using corresponding mononuclear complexes to determine catalytic efficiency for example for Ru<sub>2</sub>LRe (0.05mM, TNco:110), [Ru(dmb)<sub>3</sub>]<sup>2+</sup> (0.05 mM) and [(dmb)-Re(CO)<sub>3</sub>Cl] (0.025 mM) (TNco:55) were used. These experiments showed increased CO formation for the trinuclear complexes with RuLRe<sub>2</sub> showing the most catalytic activity. As this complex has one sensitizer to two catalytic sites, this appears to confirm that a slow electron transfer to the catalytic site is preferred for CO<sub>2</sub> reduction to be efficient.

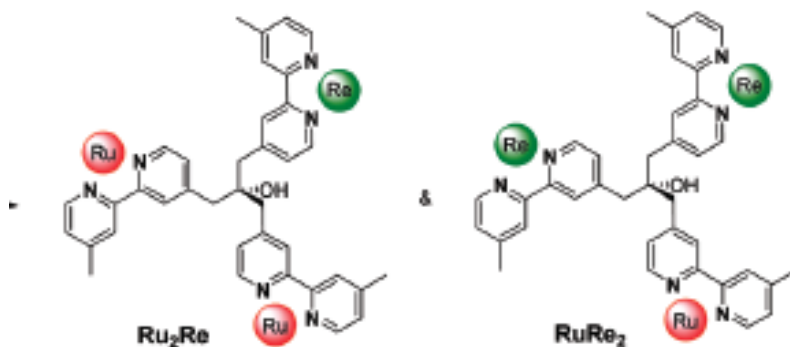


**Figure 1.15:** Diagram of the trinuclear supramolecular structures investigated by Ishitani *et al.*

## Chapter 1 – Introduction.

Most recently in 2009 Ishitani *et al.* investigated this theory further using 1,2-bis(4'-methyl-[2,2']bipyridinyl-4-yl)-ethane (**MebpyC<sub>2</sub>H<sub>4</sub>Mebpy**), 1,4-bis(4'-methyl-[2,2']bipyridinyl-4-yl)-butane (**MebpyC<sub>4</sub>H<sub>8</sub>Mebpy**), and 1,6-bis(4'-methyl-[2,2']bipyridinyl-4-yl)-hexane (**MebpyC<sub>6</sub>H<sub>12</sub>Mebpy**) as shown in Figure 1.16 below.<sup>62</sup>

Using these bridging ligands, structural rigidity is reduced allowing free rotation around the alkyl chains, in theory providing a less inhibited catalytic site for the attachment of CO<sub>2</sub>. However RuC<sub>2</sub>Re was found to have the best catalytic efficiency producing a turnover number of 180 while RuC<sub>4</sub>Re and RuC<sub>6</sub>Re yielded turnover numbers of 110 CO, similar to that of the reference complex RuC<sub>3</sub>(OH)Re. This increase in catalytic activity was due to the weak interaction between the Ru (II) and Re (I) centers observed only in the RuC<sub>2</sub>Re complex, resulting in increased reductive quenching by BNAH and subsequently increased CO<sub>2</sub> reduction. Research within this area is ongoing as the mechanism for CO<sub>2</sub> reduction using supramolecular complexes is still under investigation.

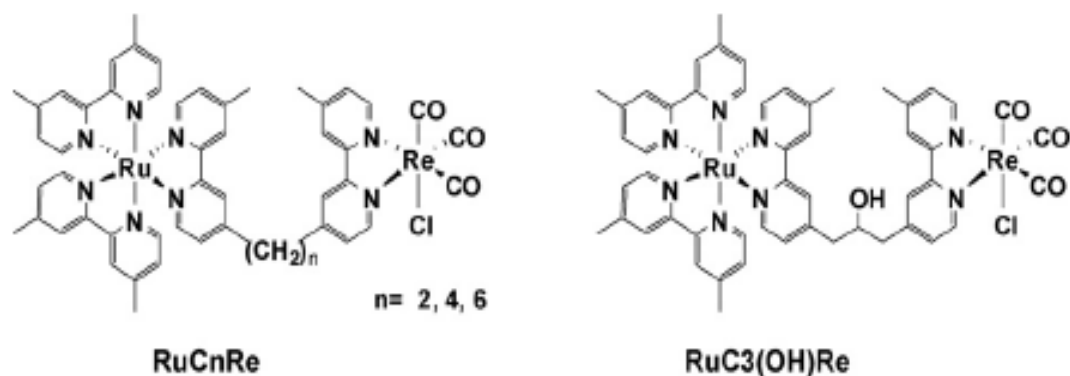


**Figure 1.16:** Structures of Re(II)-Re(I) complexes using MebpyC<sub>2</sub>H<sub>4</sub>Mebpy, MebpyC<sub>4</sub>H<sub>8</sub>Mebpy, MebpyC<sub>6</sub>H<sub>12</sub>Mebpy and corresponding alcohol (1,3-bis(4-methyl-[2,2']bipyridinyl-4-yl)-propan-2-ol) as bridging ligands.<sup>62</sup>

### **1.4 Type II Catalysts**

Type II catalysts, as described by Morris *et al.*, are those where one single compound acts as both the photosensitiser and the catalyst. Here the necessity for an electron mediator is negated as the excited photocatalyst (Pcat\*) is reduced by an amine donor (Et<sub>3</sub>N). This reductive quenching occurs in the same manner as described for type I catalysis in section 1.3 above. The Pcat<sup>•-</sup> now in its active state can react with CO<sub>2</sub> as shown in equations 10,11 and 12 below. During type II catalysis the oxidized amine donor (Et<sub>3</sub>N<sup>•+</sup>) is capable of further reactions to form another reduced catalyst allowing for further reaction with CO<sub>2</sub> (eqn 13 and 14).

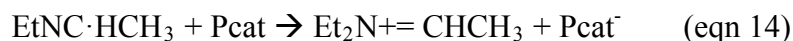
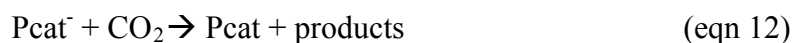


**Figure 1.17:** Equations describing type II catalysis.

Compounds that have been reported for type II catalysis for CO<sub>2</sub> reductions are metallomacrocycles and mononuclear complexes containing Co, Ru and Re metal centers. These compounds will be discussed in the following sections. Mechanistic details for CO<sub>2</sub> reduction of these compounds are still under investigation and will not be discussed in detail. Table 1.3 that follows gives a brief overview of the compounds investigated.<sup>63, 64, 65</sup>

	<i>Compound</i>	<i>Reductant</i>	<i>Product</i>	<i>TN<sub>co</sub></i>	<i>Ref</i>
1	[Co <sup>II</sup> Tpp]	Et <sub>3</sub> N	CO, HCO <sub>2</sub> <sup>-</sup>	>300	63
2	[Co <sup>II</sup> TFPP]	Et <sub>3</sub> N	CO, HCO <sub>2</sub> <sup>-</sup>	>150	63
3	[Co <sup>II</sup> T <sub>3</sub> CF <sub>3</sub> PP]	Et <sub>3</sub> N	CO, HCO <sub>2</sub> <sup>-</sup>	>150	63
4	[Co <sup>II</sup> TF <sub>5</sub> PP]	Et <sub>3</sub> N	CO, HCO <sub>2</sub> <sup>-</sup>	>150	63
5	[Fe <sup>III</sup> TM <sub>2</sub> PyP]	Et <sub>3</sub> N	CO	~ 70	64
6	[Co <sup>II</sup> TTP]	Et <sub>3</sub> N	CO, HCO <sub>2</sub> <sup>-</sup>	3.1 <sup>a</sup>	65
7	[Fe <sup>II</sup> TTP]	Et <sub>3</sub> N	CO, HCO <sub>2</sub> <sup>-</sup>	2.1 <sup>a</sup>	65

**Table 1.3:** Summary of Type II catalyst experiments for CO<sub>2</sub> reduction where:  
*A* = mmolL<sup>-1</sup> CO, Et<sub>3</sub>N = triethylamine, TPP = tetraphenylporphyrin, TFPP = TPP containing a 3-F group, T<sub>3</sub>CF<sub>3</sub>PP = TPP containing a 3-CF<sub>3</sub> group, TF<sub>5</sub>PP = TPP with a perfluorinated group. CoTTP = (cobalttetra-*m*-tolylporphyrin).

### **1.4.1 Metallomacrocycles.**

A number of metallomacrocycles were investigated for CO<sub>2</sub> reduction including corroles, corrins, porphyrins<sup>63,64</sup> and pthathocyanies containing iron and cobalt centers as depicted in Figure 1.18. The reason for such interest in this area is due to the wide visible spectral absorption displayed by these macrocycles and the ability to tune these bands by the addition of differing metals within their structure. These macrocycles proceed via a stepwise reduction to their active redox states, allowing for the stepwise reduction of CO<sub>2</sub> accounting for the thermodynamic considerations mentioned earlier in section 1.2.

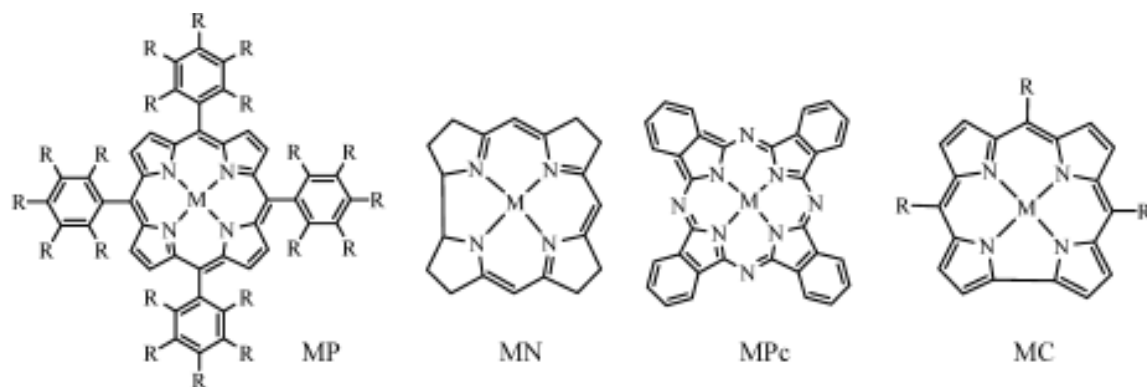


**Figure 1.18:** Metallomacrocycles investigated for CO<sub>2</sub> reduction where MP = metalloporphyrin, MN = metallocorrin, MPc = metallophthalocyanine, MC = metallocorrole.

#### 1.4.1.1 Metalloporphyrins.

Cobalt porphyrins (CP) and Iron porphyrins (FeP) have been reported to reduce CO<sub>2</sub> in homogenous solutions.<sup>63,64,65</sup> Closely related structurally to cyclams and tetrazamacrocycles, the rate of formation of CO is also strongly related to ligand structure and hence the steric effects of CO<sub>2</sub> attachment that were problematic for the previous macrocycles are also a problem for metalloporphyrins. Generally porphyrins reduce CO<sub>2</sub> in the active redox state of zero, which is obtained by either photochemical or chemical radiation techniques.<sup>31,63,64,65</sup> Prolonged photolysis often shows increasing CO production over time with the eventual degradation of the photocatalyst.<sup>63,64,65</sup>

Grodzowski *et al.* investigated the use of an iron porphyrin Fe<sup>(III)</sup>TPP (tetraphenylporphyrin) for photochemical CO<sub>2</sub> reduction, reporting the stepwise reduction of Fe<sup>(III)</sup> to Fe<sup>(0)</sup> in three distinct steps.<sup>64</sup> This stepwise photoreduction is typical of porphyrin compounds where the initial reduction from Fe<sup>III</sup> to the stable Fe<sup>II</sup> is known to occur for iron porphyrins at the MLCT (Metal to Ligand Charge Transfer) band i.e. wavelengths below the Soret band, allowing the axial ligand to become oxidized. Subsequent reduction to Fe<sup>(I)</sup> was reportedly much more difficult and occurred in small concentrations under prolonged photolysis in the presence of CO<sub>2</sub>, leading to the eventual destruction of the porphyrin complex. However,

## Chapter 1 – Introduction.

turnover numbers of CO reached a maximum of 40 before the destruction of the catalyst via the chlorin intermediate. The yield of CO increased with photolysis time, though destruction of the porphyrins occurred before a turnover number of 100 was achieved, which is much lower than the reported values of electrochemical CO<sub>2</sub> reduction.<sup>66</sup>

Behar *et al.* continued the investigation of metalloporphyrins, for photochemical CO reduction using a cobalt center instead of iron as previous electrochemical studies showed formation of formate and CO upon CO<sub>2</sub> reduction.<sup>63</sup> Co<sup>(II)</sup>P (cobalt tetraphenylporphyrin) and derivatives were investigated photochemically with acetonitrile as a solvent in the presence of TEA. As for the iron porphyrins, this lead first to the formation of Co<sup>(II)</sup>P and subsequently Co<sup>(I)</sup>P before producing formate and CO. Turnover numbers here were greater than the previously investigated iron macrocycles as CoP showed TN > 300. Behar *et al.* also indicated that the low turnover numbers in the other cobalt derivatives was due to the ineffective binding of TEA to the cobalt center in the Co<sup>II</sup> and Co<sup>I</sup> complexes, and indicated that a sensitizer such as p-terphenyl may increase the quantum yield.

These experiments lead to the development of a type I catalyst with cobalt porphyrins and p-terphenyl sensitizer, which was carried out by Fujita *et al.* displaying that indeed the quantum yield is increased in the presence of p-terphenyl as a reductive quencher. Here the p-terphenyl was photoreduced by TEA to form TP<sup>•-</sup> which has a higher reductive ability to reduce cobalt and iron porphyrins to their M<sup>0</sup>P (M = metal) state rapidly. The production rates of the M<sup>0</sup>P state was also found to be diffusion controlled by a series of pulse radiolysis experiments. The photochemical reduction results of which are shown below in Figure 1.19.

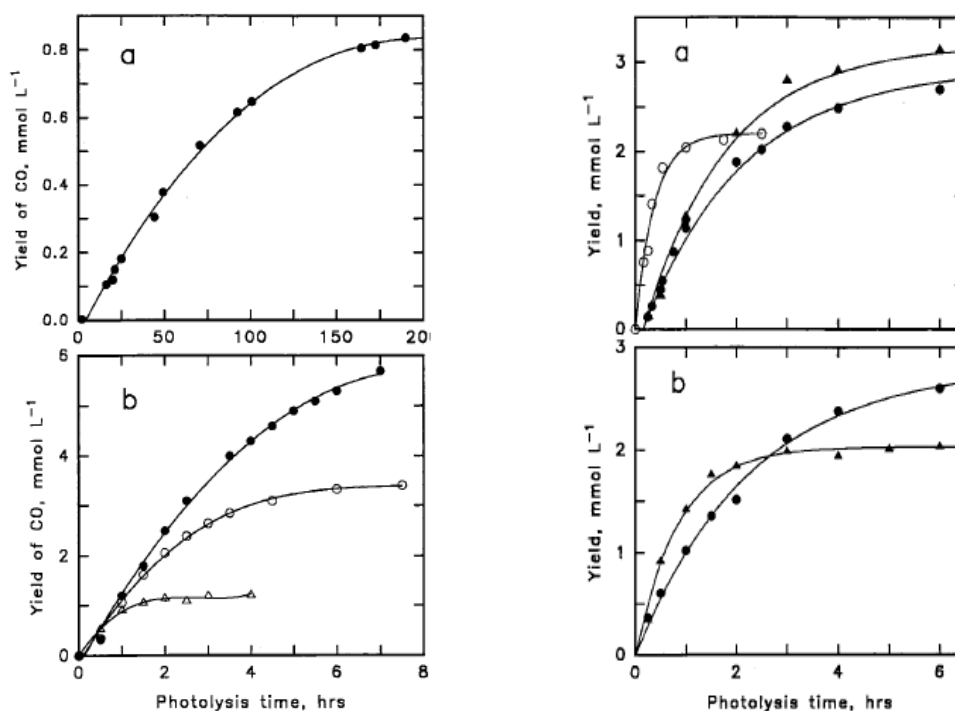


**Figure 1.19:** Results of Photochemical production of CO in CO<sub>2</sub>-saturated acetonitrile solutions containing 5% TEA and Co porphyrin conducted by Fujita *et al.*<sup>65</sup>

Graph A(LHS):  $1 \times 10^{-5} \text{ mol L}^{-1} \text{ Co}^{\text{II}} \text{ TPP}$  with no TP; Graph B:  $3 \times 10^{-3} \text{ mol L}^{-1} \text{ TP}$  and various concentrations of  $\text{Co}^{\text{II}} \text{ T3FPP}$ , (●)  $9 \times 10^{-5} \text{ mol L}^{-1}$ , (O)  $2.4 \times 10^{-5} \text{ mol L}^{-1}$ , (Δ)  $7 \times 10^{-6} \text{ mol L}^{-1}$ . Graph A (RHS): Yield of formate (O) without porphyrin; yield of formate (●) and CO (▲) with  $1 \times 10^{-4} \text{ mol L}^{-1} \text{ CoTTP}$ .

Graph B(RHS) depicts the photochemical production of HCOO<sup>-</sup> and CO in CO<sub>2</sub><sup>-</sup> saturated acetonitrile solutions containing 5% TEA and  $3 \times 10^{-3} \text{ mol L}^{-1} \text{ TP}$ . Graph B(RHS): Yield of formate (●) and CO (▲) with  $1 \times 10^{-4} \text{ mol L}^{-1} \text{ FeTTP}$ .

On a separate line of research porphyrin diads have been reported by Tokumaru *et al.*<sup>67</sup> Hammerstrom *et al.*<sup>68</sup> Perutz *et al.*<sup>69</sup> and finally Ishitani *et al.* in 2009 who reported the synthesis of a zinc porphyrin – rhenium diad type I catalyst, as shown in Figure 1.20 that has the ability to reduce CO<sub>2</sub>.<sup>70</sup> These series of diads fall outside the



## Chapter 1 – Introduction.

working principle behind the type II photocatalyst and for that reason will not be discussed in more detail here.

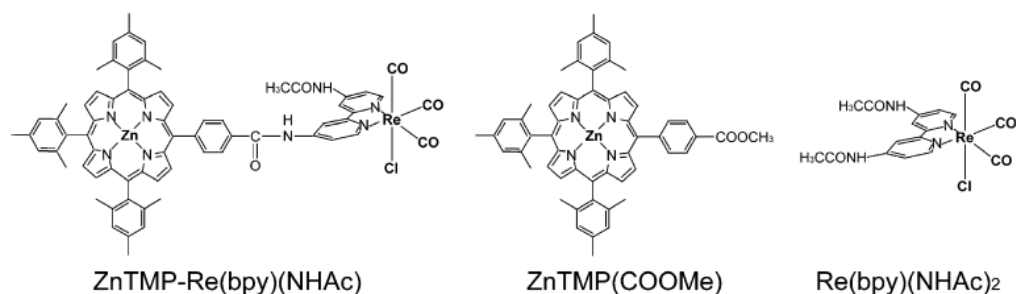


**Figure 1.20:** Structures of the zinc porphyrin diad prepared by Ishitani *et al.*<sup>70</sup>

### 1.4.1.2 Metalloporroles.

Progressing from the metalloporphyrins, Fujita *et al.* studied the effect of iron and cobalt corroles on CO<sub>2</sub> reduction.<sup>71</sup> Predominately one major drawback of all metallomacrocycles are the often long and tedious synthetic and purification methods required to produce the complexes. Recently synthetic aspects have improved allowing research within this area to expand.<sup>72, 73, 74, 75</sup>

As shown previously in Figure 1.18 metalloporroles contain one less meso bridge than metalloporphyrins and therefore have a smaller metal cavity. The corrole structure contains nitrogens with three protons where the porphyrins have nitrogens containing only two protons, this allows stabilization of the metal centre at a higher oxidation state which in turn has an effect on their reduction reactions for CO<sub>2</sub> activity. This allows the metalloporroles to have a more negative reduction potential which increases the probability of reducing CO<sub>2</sub> and in turn makes the metalloporrole a viable catalyst.

Continuing the photoreduction experiments, Fujita *et al.* carried out CO<sub>2</sub> reduction experiments of iron and cobalt corroles (type I) catalysts in deoxygenated acetonitrile in the presence of TEA with p-terphenyl as a sensitizer foreseeing the problems that

## ***Chapter 1 – Introduction.***

would arise from the lack of TEA binding. Formation of the p-terphenyl radical anion is highly efficient and is formed from the singlet state of the TEA. This allows for a fast reduction of the metallocorrole reducing the chance of unwanted side reactions occurring.  $\text{ClFe}^{\text{(IV)}}(\text{tpfc})$  (where tpfc is the trianion of 5,10,15-tris-(pentafluorophenyl)corrole) was shown to exhibit  $[\text{Fe}^{\text{(II)}}(\text{tpfc})]^-$  as the first reduction product and was shown to strongly bind with CO to form  $[(\text{CO})\text{Fe}^{\text{(II)}}(\text{tpfc})]^-$ . This is in contrast to the cobalt corrole ( $[\text{Co}^{\text{II}}(\text{tpfc})]^-$ ) as no CO binding activity was observed during these experiments. Prolonged photolysis of the metallocorroles leads to the destruction of the metallocorroles complex. Apart from the metallocorroles' reaction with  $\text{CO}_2$  in their  $\text{M}^{\text{I}}$  oxidation state, comparison of these corroles with their corresponding metalloporphyrin showed no increased catalytic activity.

### ***1.4.1.3 Metallocorrins.***

As research into metallomacrocycles provided some interesting results as potential catalysts for  $\text{CO}_2$  reduction, Grodkowski and Neta<sup>76</sup> investigated the activity of metallocorrins with cobalt as a metal center and to compare these to corresponding porphyrin macrocycle. Structurally metallocorrins are smaller in size having a similar tetrapyrrole structure but containing only six double bonds in comparison to the porphyrin's eleven, which may add stability to the structure as the probability of proton attack during the photochemical experiments is reduced. This was best described in Figure 1.18 previously.

In contrast to the previous metallomacrocycles, the metallocorin,  $\text{B}_{12}$  used by Grodkowski and Neta was found to be insoluble in deoxygenated acetonitrile so a mixture of acetonitrile / methanol (9:1 v/v) was used along with TEA and p-terphenyl as a sensitizer. To allow accurate comparison of the corrin with the corresponding porphyrin parallel experiments with CoTTP (cobalt(*m*-tolyporphyrin)) were carried out, the results of which are described in Figure 1.21 that follows. Confirmation that the CO was produced from  $\text{CO}_2$  was controlled by parallel experiments carried out in the presence of He. These experiments indicated that the metallocorrins were stable

## Chapter 1 – Introduction.

for longer reaction times that the porphyrin and also as a consequence had higher yield of formate.

The results of these experiments indicated that the mechanism of reduction of  $\text{CO}_2$  is similar in both the metallocorrin and metalloporphyrin systems. Production of hydrogenated complexes as side reaction also occurred along with the photodecomposition of the metallocorrin and accumulation of CO in solution. Grodkowski and Neta indicate that protection of the complex from hydrogenation may increase the catalyst activity and inhibit deactivation of the corrin.

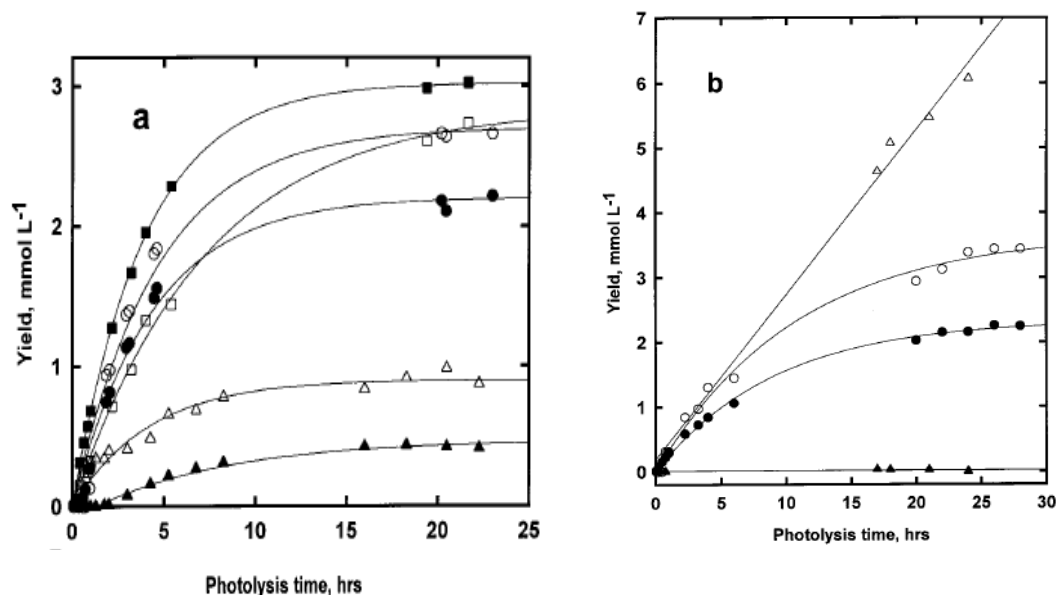


**Figure 1.21:** Photochemical production of CO preformed by Grodkowski and Neta (solid symbols) and  $\text{H}_2$  (open symbols). (a)  $\text{CO}_2$ -saturated acetonitrile/methanol (9/1 v/v) solutions containing 5% TEA, 3 mmol L<sup>-1</sup> TP, and 0.05 mmol L<sup>-1</sup> cobalt complex: cyanocobalamin (circles), cobinamide (squares), and CoTTP (triangles). (b) Similar solutions containing hydroxocobalamin under  $\text{CO}_2$  (circles) and under He (triangles).

#### 1.4.1.4 Metallophthalocyanines.

Metallophthalocyanines like their metallocorrin relatives above, have shown the ability to reduce  $\text{CO}_2$  at a redox state of +1 with a reduced phthalocyanine ring  $[\text{M}^{\text{I}}\text{Pc}^{\cdot-}]^{2-}$ .<sup>31</sup> Research into the use of phthalocyanines as a catalyst for  $\text{CO}_2$  reduction was carried out due to their wide spectral range of absorbance in the visible region, though research into this area is much more recent than its predecessors' discussed above due to the long and difficult preparations of the complexes. In 2007 Zhao *et al.* reported the development of a zinc-phthalocyanine that was loaded on to a titania support using a sol gel technique as shown in Figure 1.22 that follows.<sup>77</sup> The immobilization of the catalyst on a solid support offered a new approach to the reduction of  $\text{CO}_2$  while making the most out of small synthetic yields of catalyst, as smaller amounts of dye is required for catalytic reactions. As a comparison  $\text{TiO}_2$  was also prepared with the catalyst by direct impregnation using both titanium dioxide and titanium butoxide powders.

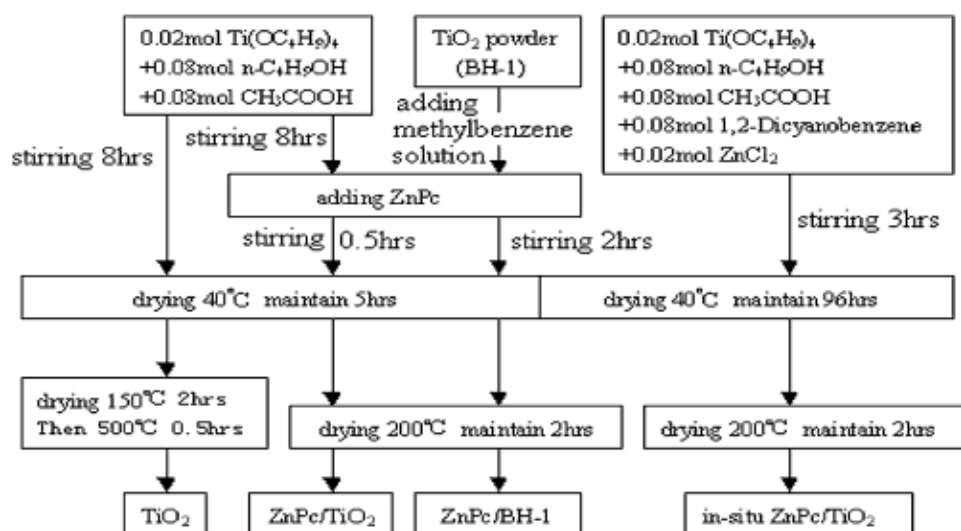


**Figure 1.22:** Preparation of the Zn-Phthalocyanine catalyst reported by Zhao *et al.*<sup>77</sup>

The subsequent photocatalytic experiments carried out by Zhao *et al.*, were conducted using a pyrex glass cell with a 100 ml volume. The catalyst was placed in 0.1 M NaOH and illuminated using a 500 W tungsten – halogen lamp. The presence of formic acid was determined using a UV – Vis spectrophotometer and subsequent gaseous products using a GC – TCD system. The results of the photocatalytic reactions indicated the preferential formation of formic acid, CO and methane via the Zn – phthalocyanine / TiO<sub>2</sub> rather than the butoxide derivative. The optimal loading of catalyst was found to be 1.0 wt % with an optimal CO<sub>2</sub> conversion rate of 0.37%. Figure 1.23 below shows the dependence of catalyst loading weight along with time of illumination.

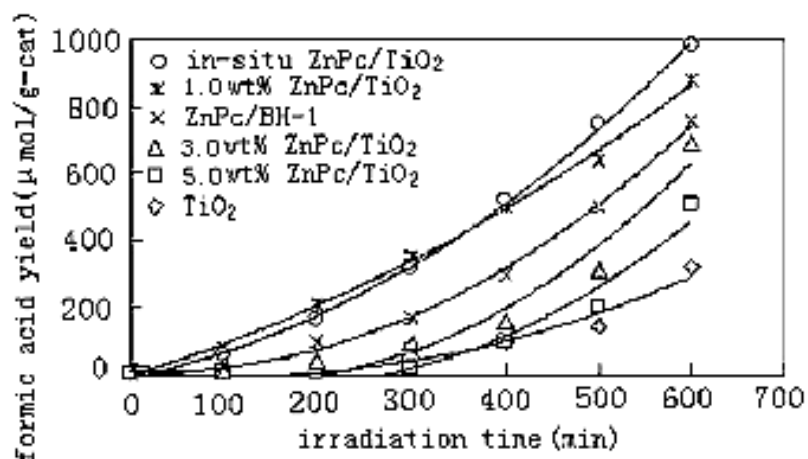


**Figure 1.23:** Time dependence of formic acid yields of the various catalysts prepared by Zhao *et al.*<sup>77</sup>

In 2009 Zhao *et al.*<sup>78</sup> continued this line of approach to CO<sub>2</sub> reduction using a cobalt phthalocyanine loaded on to TiO<sub>2</sub> using an improved sol-gel technique as shown in Figure 1.24 below. The photocatalytic reactions were carried out as described above

using a 1.0% catalyst loading. Here phthalocyanine containing Ni, Co and Zn metal centers were tested for photocatalytic ability with the CoPc/TiO<sub>2</sub> producing the most reduction products. Interestingly Zhao reported that the location of the catalyst on the TiO<sub>2</sub> is very important as the isolated CoPc was found to be the primary active site for photoreduction, therefore the distribution of the catalyst on the TiO<sub>2</sub> particles will have an effect on the amount of CO<sub>2</sub> reduced.

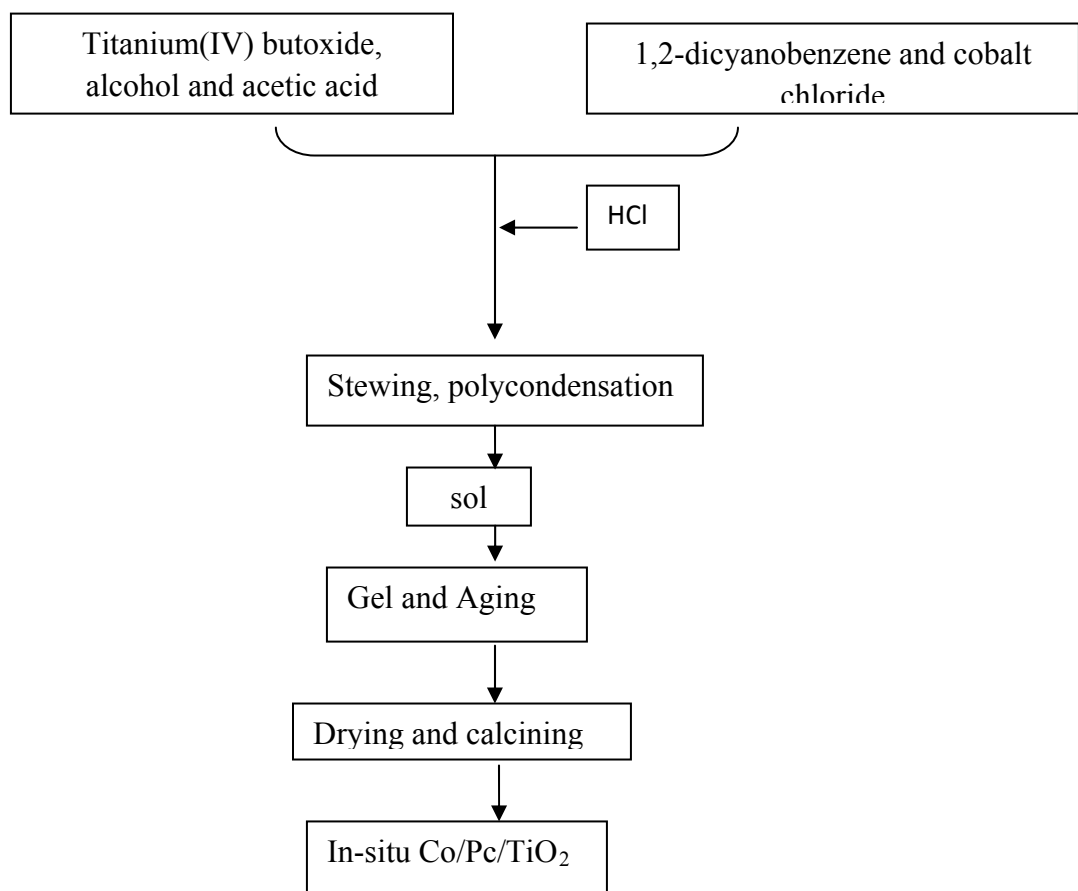


**Figure 1.24:** Improved sol-gel technique by Zhao et al.<sup>78</sup>

Unlike the previously discussed metallomacrocycles the mechanism of reduction of CO<sub>2</sub> proceeds initially with the catalysts acceptance of an electron from the TiO<sub>2</sub> surface. Visible light allows the excitation of the metallophthalocyanine and the formation of electron hole pairs occurs as shown in Figure 1.25 below. The TiO<sub>2</sub> then

## Chapter 1 – Introduction.

traps the electron which inhibits recombination. As the  $\text{TiO}_2$  is acting as an electron trap the metallophthalocyanine continues to transfer excited electrons to the  $\text{TiO}_2$  conduction band, increasing the separation of the electron hole pairs and in turn increases photoefficiency. However Zhao has indicated that excess catalyst loading inhibits the reduction of  $\text{CO}_2$  as the catalyst can then mask the  $\text{TiO}_2$  surface which stops the  $\text{CO}_2$  from accessing an electron.

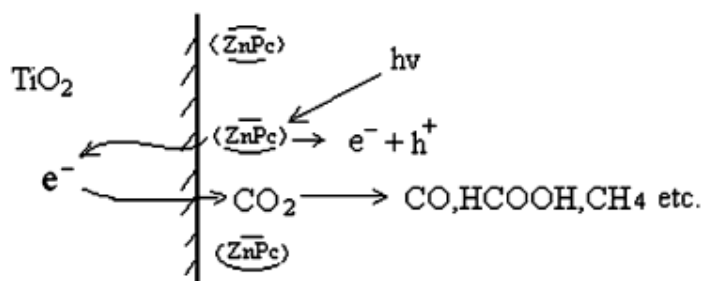


**Figure 1.25:** Illustration of photo-catalytic reduction of  $\text{CO}_2$  at  $\text{ZnPc}$  absorbed  $\text{TiO}_2$ .<sup>77</sup>

In addition to the research conducted by Zhao, Premkumar and Ramaraj reported the photocatalytic reduction of metalloporphyrin and metallophthalocyanine irreversibly absorbed on a Nafion membrane.<sup>79</sup> However the photocatalytic experiments here were carried out in the presence of a sacrificial donor (TEA) where the catalyst coated membranes were dipped in a saturated  $\text{CO}_2$  solution and subsequently illuminated. Both the porphyrin and phthalocyanine catalysts produced reduction products and both membranes were shown to be highly stable and produced reproducible results though turnover numbers were between 2 and 4 for both catalysts.

The metallomacrocycles discussed above are a small indication of a wider area of research of these catalysts for  $\text{CO}_2$  reduction. In summary the active catalytic states found by cyclic voltammetry are a formal oxidation state of zero for metalloporphyrins  $[\text{M}^0\text{P}]^{2-}$  and corrins  $[\text{M}^0\text{N}]^{2-}$ , +1 for corroles  $[\text{M}^1\text{C}]^{2-}$ , and +1 with a reduced phthalocyanine ring  $[\text{M}^1\text{Pc}^\bullet]^{2-}$  with the turnover numbers ranging in the region of 40 – 300. Research into the individual methods of  $\text{CO}_2$  reduction are still under

investigation, though the best representative mechanisms were reported by *Morris et al.* and are shown in Figure 1.26 below.

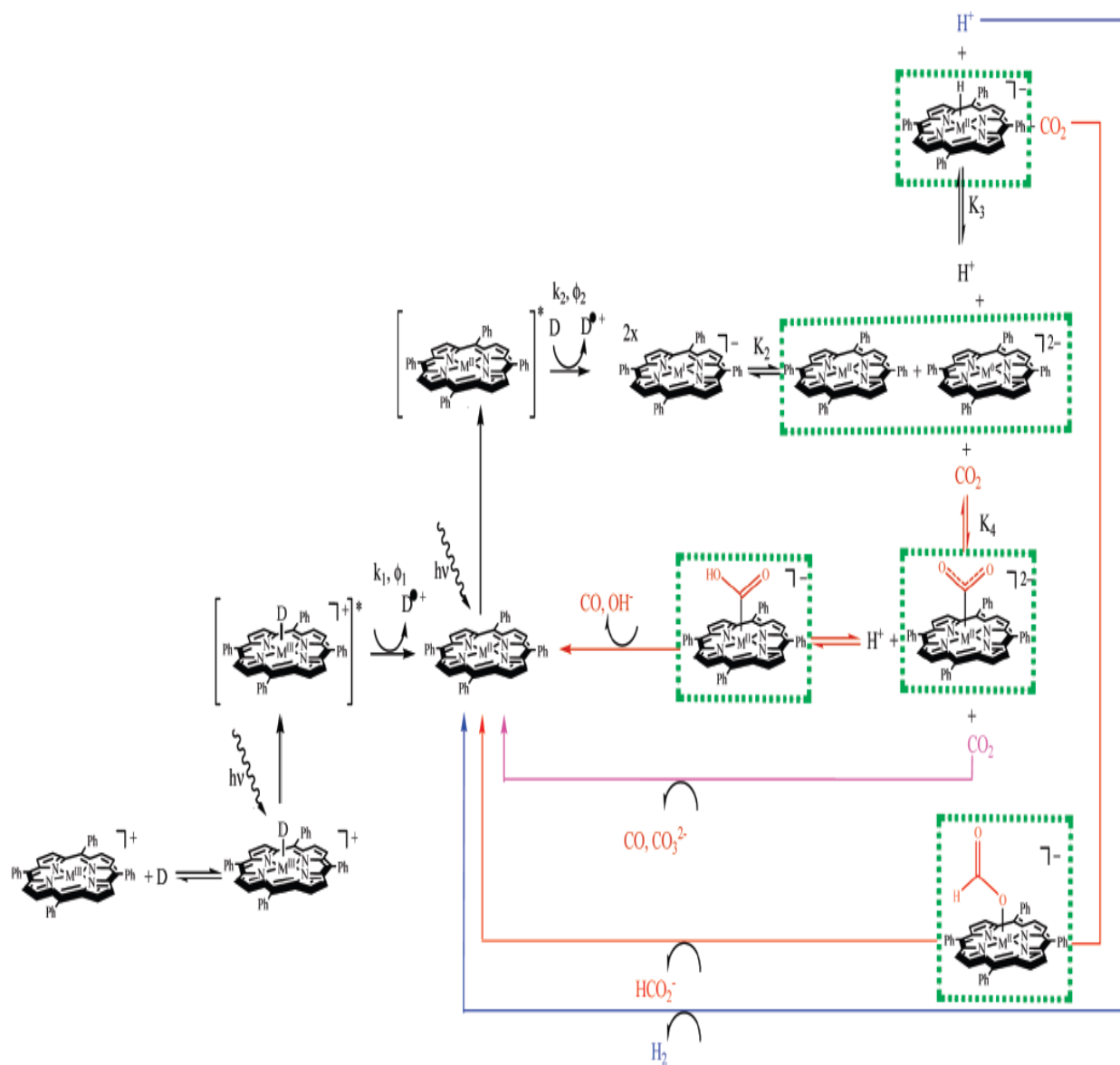


**Figure 1.26:** Proposed Mechanistic Steps in the Reduction of CO<sub>2</sub> by Metal Porphyrin Derivatives (M = Fe or Co) via a Type II catalysts by Morris et al. Where: Hydrogen production (blue), formate production (red), CO formation (brown and pink), and putative intermediates (green); as a representative compound, metalloporphyrin is illustrated.



### 1.4.2 Rhenium Mononuclear Complexes.

Rhenium (I) carbonyl complexes are one of the most intensely studied complexes for CO<sub>2</sub> reduction. Initially investigated by Hawecker *et al.* in 1983 using *fac*-[Re(L)(CO)<sub>3</sub>X]<sup>80</sup> where L = 4,4'-R<sub>2</sub>-2,2'-bipyridine (R = H, CH<sub>3</sub>) or 1,10-phenanthroline and X = Cl<sup>-</sup> or Br<sup>-</sup>, results showed the selective formation of CO with a quantum yield of 0.14 when chlorine is in the axial position.<sup>81</sup> Due to the success of these investigations Sullivan *et al.* carried out a dark reaction in the presence of CO<sub>2</sub> using *fac*-[Re(bpy)(CO)<sub>3</sub>H]<sup>82</sup> in which he investigated the first kinetic study of CO<sub>2</sub> insertion into the metal hydride bond. Here Sullivan discussed the solvent effects upon insertion reporting that *fac*-[Re(bpy)(CO)<sub>3</sub>H] undergoes a thermally activated reaction with CO<sub>2</sub> in THF, acetone and acetonitrile to produce the formate complex *fac*-[Re(bpy)(CO)<sub>3</sub>OC(O)H]. Sullivan also discussed the remarkable solvent effects that occurred with increasing dielectric constant. These results are displayed in Figure 1.27 below.

Solvent	[CO <sub>2</sub> ],M	k <sub>obsd</sub> S <sup>-1</sup>	K <sub>i</sub> , M <sup>-1</sup> s <sup>-1</sup>	D <sub>s</sub>	(D <sub>s</sub> -1)/(2D <sub>s</sub> +1)
Tetrahydrofuran (THF)	0.33	(6.50 ± 0.23) x 10 <sup>-5</sup>	(1.97 ± 0.07) x 10 <sup>-4</sup>	7.32	0.404
1/7 Ac/THF	0.32	(9.73 ± 0.04) x 10 <sup>-5</sup>	(3.04 ± 0.11) x 10 <sup>-4</sup>	9.1	0.422
1/2 Ac/THF	0.30	(1.84 ± 0.07) x 10 <sup>-4</sup>	(6.13 ± 0.23) x 10 <sup>-4</sup>	12.1	0.440
Acetone (Ac)	0.28	(7.05 ± 0.27) x 10 <sup>-4</sup>	(2.52 ± 0.05) x 10 <sup>-3</sup>	20.7	0.465
Dimethylformamide	0.23	(2.21 ± 0.09) x 10 <sup>-3</sup>	(9.67 ± 0.39) x 10 <sup>-3</sup>	36.7	0.480
Acetonitrile	0.14	(7.62 ± 0.14) x 10 <sup>-3</sup>	(5.44 ± 0.10) x 10 <sup>-2</sup>	36.1	0.480

**Figure 1.27:** Kinetic results reported for CO<sub>2</sub> insertion for *fac*-[Re(bpy)(CO)<sub>3</sub>H] by Sullivan *et al.*<sup>82</sup>

These results were the beginning of an ever expanding research area for rhenium tricarbonyl complexes within CO<sub>2</sub> reduction. Progressing from these results Ishitani *et al.* have conducted over a decade of research into this area with a strong focus on

deciphering the mechanism of reduction, though today this is still under much discussion. Ishitani continued research using complexes of the type  $[\text{XRe}(\text{CO})_3(\text{LL}')] ]$  reporting that these complexes contain low lying MLCT states that when excited at these wavelengths are better oxidants and reductants than in the corresponding ground states.<sup>83</sup> Ishitani also reported that in the excited state these complexes can undergo substitution reactions more readily than in the ground state.<sup>83</sup> This led to the first photochemical synthesis and isolation of *mer*- $[\text{Re}(\text{bpy})(\text{CO})_3\text{Cl}]$  as shown below in Figure 1.28 along with further investigations into photochemical ligand substitutions of *fac*- $[\text{Re}(\text{bpy})(\text{CO})_3\text{Cl}]$ .<sup>84</sup>

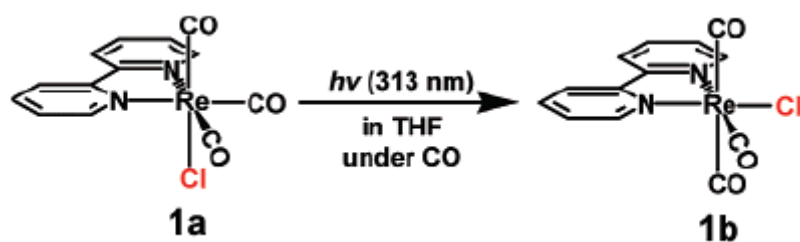


**Figure 1.28:** First reported photochemical synthesis of *mer*- $[\text{Re}(\text{CO})_3(\text{bpy})\text{Cl}]$ .

In 2008 in order to develop a better catalyst for photochemical  $\text{CO}_2$  reduction, Ishitani *et al.* studied three rhenium (I) complexes: *fac*- $[\text{Re}(\text{bpy})(\text{CO})_3\text{L}]$  ( $\text{L} = \text{SCN}^-$  (1-NCS),  $\text{Cl}^-$  (1-Cl), and  $\text{CN}^-$  (1-CN)) focusing on how they reduced  $\text{CO}_2$  with the premise that if one knows the mechanism of  $\text{CO}_2$  reduction then development of a catalyst becomes more manageable.<sup>85</sup> The initial steps of reduction are known; the *fac*- $[\text{Re}(\text{bpy})(\text{CO})_3\text{L}]$  is excited at its MLCT which in turn is quenched by a tertiary amine which produces a one electron reduced species (OER). The production of the OER species has been proven by laser flash photolysis studies<sup>85,86</sup> but a number of questions still remain unanswered. It is unknown as to how the OER species interacts and reduces  $\text{CO}_2$ , the source of the second electron for the reduction is not known along with how the photocatalyst is regenerated after the reduction. These questions are what prompted Ishitani to use the anionic ligands mentioned above to determine

## ***Chapter 1 – Introduction.***

which (if any) ligand is removed from the OER complex during reduction experiments.

The initial results of the experiments showed that 1-CN could not act as a photocatalyst while the complexes 1-Cl and 1-NCS produced turnover numbers of 15 and 30 respectively. To prove that the first steps in the reduction process were the excitation of the MLCT and quenching by the amine, the compounds were studied by flow cell electrolysis, which showed the formation of the OER species in both cases but the 1-Cl complex formed in a much smaller yield. The decay profiles of these complexes were then followed immediately after excitation in the dark in the presence and absence of CO<sub>2</sub>. Both decay profiles showed faster decays in the presence of CO<sub>2</sub> indicating an interaction between the OER and CO<sub>2</sub>. Using the 1-CN species as a control, the experiments were repeated, the decay profile of which showed no acceleration in the presence of CO<sub>2</sub> proving the requirement of formation of the OER for the reduction of CO<sub>2</sub>.

To determine which of the ligands were lost during the reaction the solutions were studied by HPLC and capillary electrophoresis pre and post photocatalytic experiments. These results showed the formation of SCN<sup>-</sup> and Cl<sup>-</sup> at the time when CO production occurred. From here Ishitani followed the work reported by Fujita *et al.*,<sup>87</sup> where the reduced species [Re(bpy<sup>-</sup>)(CO)<sub>3</sub>] rapidly takes up a solvent molecules such as THF or acetonitrile to produce [Re(bpy<sup>-</sup>)(CO)<sub>3</sub>S] which in turn slowly reacts with CO<sub>2</sub>. Ishitani also reported that recombination of the dissociated ligand depended strongly on the ligands chosen as the formation of the solvent complexes compete with recombination of the ligand. From these experiments Ishitani was able to propose the mechanism shown in Figure 1.29 that follows.

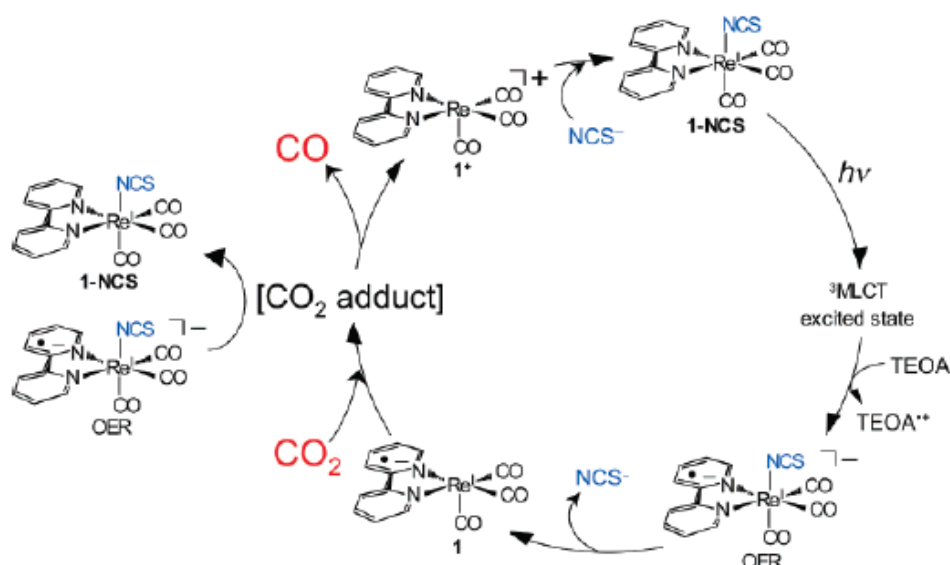


**Figure 1.29:** Proposed mechanism for  $\text{CO}_2$  reduction using a rhenium mononuclear complex by Ishitani *et al.*

From these experiments Ishitani proposed that a photocatalyst for  $\text{CO}_2$  reduction should consist of the following properties:

1. Efficient formation of the OER species by quenching of the  $^3\text{MLCT}$  excited state by the reducing reagent.
2. Effective production of  $[\text{Re}(\text{LL})(\text{CO})_3]$  by dissociation of the ligand from the OER species. Where  $\text{LL} = 2,2\text{-bipyridine}$
3. Efficient reduction of the  $\text{CO}_2$  adduct(s) by a further OER species.
4. High-yield recovery of the starting complex by recoordination of a ligand after CO formation.

To determine if the above properties did indeed have an effect, the complexes *fac*- $[\text{Re}(\text{bpy})(\text{CO})_3(\text{MeCN})]^+$  and *fac*- $[\text{Re}\{4,4'-(\text{MeO})_2\text{bpy}\}(\text{CO})_3\{\text{P}(\text{OEt})_3\}]^+$  were prepared as photosensitizers at a ratio of 1:25 respectively and analysed in the same manner as above. The results of this experiment showed the quantum yield of CO formation to be 0.59 which is the highest reported for a homogeneous system.<sup>85</sup> More recently Ishitani *et al.* reported that the  $\text{CO}_2$  adduct formed (Figure 1.29) is reduced

## ***Chapter 1 – Introduction.***

by another OER species of a rhenium complex, reporting that the most effective photocatalyst would be a mixture of two rhenium complexes.<sup>88</sup>

### ***1.5 Scope of Thesis.***

The work presented in this thesis details investigations into the development of a supramolecular photocatalyst that can potentially reduce CO<sub>2</sub> containing a ruthenium moiety and a rhenium tri carbonyl species. Research discussed above has indicated that the architecture of which is by no means trivial. The photocatalyst itself must be engineered on a molecular level in such a way as to allow electron exchange between the light absorbing species and the catalytic center in a manner that is efficient and nondestructive.

Rhenium was chosen as the catalytic center as the most promising photocatalyst to date is one that contains a rhenium tricarbonyl complex due to its relatively high quantum yields and high selectivity of products.<sup>80,81,83</sup> However, there are many unanswered questions with rhenium as a catalyst. As discussed above the controlling parameters surrounding structural requirements and electrochemical properties have not been investigated fully and the mechanism for CO<sub>2</sub> reduction is not fully understood. Rhenium also has a weak absorptivity in the visible region which has been overcome by the attachment of a ruthenium bipyridyl moiety via a mediating bridging ligand. The pairing of these three individual components (i.e. photosensitiser bridge and catalytic centre) are crucial as electron transport from the Ru center must be able to cross the bridging ligand and reach the rhenium metal center to allow regeneration of the catalyst after the formation of the one electron reduced species. For this reason the bridging ligands Hbpt, Hbpzt and tpphz have been chosen as electron transport has been shown to progress from the ruthenium center to the bridging ligand. Figure 1.30 below describes the complexes that have been investigated.

## Chapter 1 – Introduction.

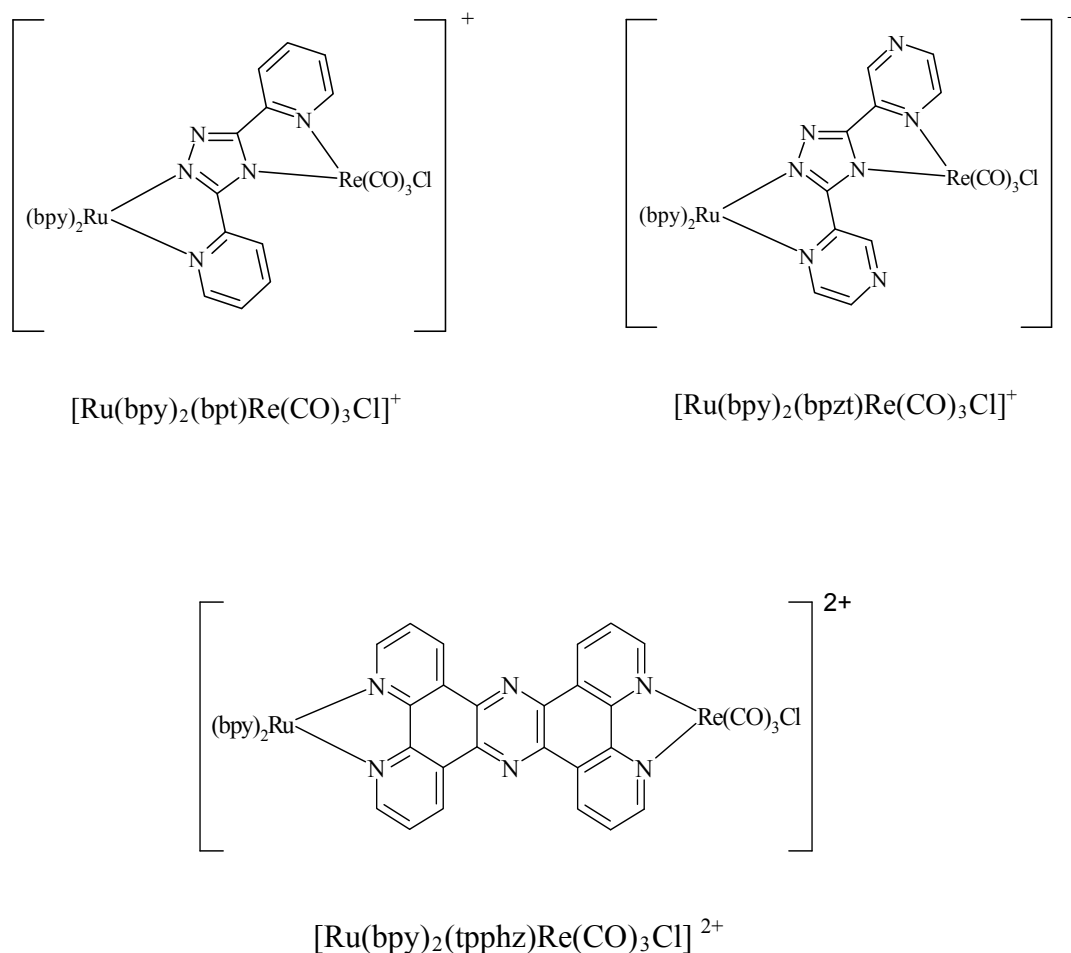


**Figure 1.30:** Dinuclear complexes prepared as potential photocatalysts for  $\text{CO}_2$  reduction. (bpy = 2,2-bipyridine).

This thesis is comprised of six chapters. Chapter one describes the research carried out to date, chapter two details the instrumental methods and chemical reagents used throughout this body of work. Chapter three relays the synthesis and characterisation of a series of ruthenium (II)/ rhenium (I) complexes containing azole type bridging ligands while chapter four deals with the number of routes taken to synthesise  $[\text{Ru}(\text{bpy})_2(\text{tpphz})\text{Re}(\text{CO})_3\text{Cl}]2(\text{PF})_6$ . Chapter five contains the analysis of  $[\text{Ru}(\text{bpy})_2(\text{bpt})\text{Re}(\text{CO})_3\text{Cl}](\text{PF})_6$  and its ability to reduce  $\text{CO}_2$  by ion exchange chromatography to determine the presence of formate. Chapter six concludes this body of work with reference to future work to be carried out.

## **1.5 Bibliography.**

- 
- <sup>1</sup> Garg, A., Bhattacharya, S., Shukla, P.R., Dadhwal, P.K., *Atmos. Environ.* 35, **2001**, 2679.
- <sup>2</sup> Apadula, F., Gotti, A., Pignini, A., Longhetto, A., Rocchetti, F., Cassardo, C., Ferrarese, S., Forza, R., *Atmos. Environ.* 37, **2003**, 3757.
- <sup>3</sup> Gust, D., Moore, T.A., Moore, A.L., *Acc. Chem. Res.*, 42, **2009**, 1890.
- <sup>4</sup> Alstrum – Acevedo, J.H., Brennaman, M.K., Meyer, T.J., *Inorg. Chem.*, 44, **2005**, 20.
- <sup>5</sup> Meyer, T.J., *Acc. Chem. Res.* 22, **1989**, 5.
- <sup>6</sup> Wasielewski, M.R., *Chem Rev.*, 92, **1992**, 435.
- <sup>7</sup> Walther, D., Ruben, M., Rau, S., *Coord. Chem. Rev.*, 182, **1999**, 67.
- <sup>8</sup> Anderson, I., Knight, S., Schneider, G., Lindqvist, Y., Lundqvist, T. Branden, C.I., Lorimer, G.H., *Nature*, 337, **1989**, 229.
- <sup>9</sup> Lundquist, E.G., Folting, K., Huffman, J.C., Caulton, K.G., *Inorg. Chem.*, 26, **1987**, 205.
- <sup>10</sup> Erijman, L., Lorimer, G.H., Weber G., *Biochemistry*, 32, **1993**, 5187.
- <sup>11</sup> Lorimer, G.H., Chen, Y.R., Hartman, F.C., *Biochemistry*, 32, **1993**, 9018.

## ***Chapter 1 – Introduction.***

---

<sup>12</sup> Thow,G., Zhu,G., Spreitzer R.J., *Biochemistry*, 33, **1994**, 5109.

<sup>13</sup> Salvucci, M.E., Chavan, A.J., Klein, R.R., Rajagopalan, K., Haley B.E., *Biochemistry*, 33, **1994**, 14879.

<sup>14</sup> Larson, E.A., Larimer, F.W., Hartman, F.C., *Biochemistry*, 34, **1995**, 4531.

<sup>15</sup> Hong, S.B., Kuo, J.M., Mullins, L.S., Raushel F.M., *J. Am. Chem. Soc.*, 117, **1995**, 7580.

<sup>16</sup>Gibson,K., Lorimer, G.H., Rendina,A.R. Taylor, W.S., Cohen, G., Gatenby A.A., Payne, W.G., Roe, D.C., Lockett, B.A., *Biochemistry*, 34, **1995**, 10976.

<sup>17</sup>Hutchison, R.S., Groom, Q., Ort D.R., *Biochemistry*, 39, **2000**, 6679.

<sup>18</sup>Karkehabadi,S., Peddi, S.R., Anwaruzzaman, M., Taylor, T.C., Cederlund, A., Genkov, T., Andersson, I., Spreitzer R.J., *Biochemistry*, 44, **2005**, 9851.

<sup>19</sup>Andrews T.J., *Nat. Struct. Bio.*, 3, **1996**, 3.

<sup>20</sup>Taylor, T.C., Andersson, I., *Nat. Struct. Biol.* 3, **1996**, 95.

<sup>21</sup> Mueller-Cajar, O., Morell, M., Whitney S.M., *Biochemistry*, 46, **2007**, 14067.

<sup>22</sup>Karkehabadi, S., Satagopan, S., Taylor, T.C., Spreitzer, R.J., Andersson, I., *Biochemistry*, 46, **2007**, 11080.



- <sup>23</sup>Sutin, N., Creutz, C., *Pure Appl. Chem.*, 52, **1980**, 2717.
- <sup>24</sup>Takeda, H., Ishitani O., *Coord. Chem. Rev.*, 254, **2010**, 346.
- <sup>25</sup>Fujita E., *Coord. Chem. Rev.*, 185, **1999**, 373.
- <sup>26</sup>Sutin, N., Creutz, C., Fujita, E., *Inorg. Chem.*, 19, **1997**, 67.
- <sup>27</sup>Lehn, J.M., Zeisel, R., *Proc. Natl. Acad. Sci. USA.*, 79, **1982**, 701.
- <sup>28</sup>Creutz, C., Sullivan, P., *Electrochemical and Electrocatalytic Reactions of Carbon Dioxide*, B., Ed., Elsevier Science Publishers, Amsterdam, The Netherlands, Chpt. 2., **1993**, 1947.
- <sup>29</sup>Sullivan, B.P., Meyer, T.J., *J. Chem. Soc., Chem. Commun.*, **1984**, 1244.
- <sup>30</sup>Palmer, D.A., Eldik, R.V., *Chem. Rev.*, 83, **1983**, 731.
- <sup>31</sup>Morris, A.J., Meyer, T.J., Fujita, E., *Acc. Chem. Res.*, 42, **2009**, 1983.
- <sup>32</sup>Whitten, D.G., *Acc. Chem. Res.*, 13, **1980**, 83.
- <sup>33</sup>Krishnan, C.V., Sutin, N., *J. Am. Chem. Soc.*, 103, **1981**, 2141.
- <sup>34</sup>Ziesel, R., Hawecker, J., Lehn, J.M., *Helv. Chim. Acta.*, 69, **1986**, 1065.
- <sup>35</sup>Lehn J.M., Ziessel, R., *J. Organomet. Chem.* 382, **1990**, 157.

**Chapter 1 – Introduction.**

---

<sup>36</sup>Craig, C.A., Spreer, L.O., Otvos, J.W., Calvin, M., *J. Phys. Chem.*, 98, **1990**, 7957.

<sup>37</sup>Grant, J.L., Goswami, K., Spreer, L.O., Otvos, J.W., Calvin, M., *J. Chem. Soc. Dalton Trans*, **1987**, 2105.

<sup>38</sup>Kimura, E., Wada, S., Shionoya, M., Okazaki, Y., *Inorg. Chem.*, 33, **1994**, 770.

<sup>39</sup>Ishida, H., Tanaka, K., Tanaka, T., *Chem. Lett.*, **1988**, 339.

<sup>40</sup>Ishida, H., Tanaka, K., Tanaka, T., *Organometallics*, 6, **1987**, 181.

<sup>41</sup>Ishida, H., Tanaka, K., Tanaka, T., *Inorg. Chem.*, 29, **1990**, 905.

<sup>42</sup>Matsuoka, S., Yamamoto, K., Ogata, T., Kusaba, M., Nakashima, N., Fujita, E., Yanagida, S., *J. Am. Chem. Soc.* 115, **1993**, 601.

<sup>43</sup>Matsuoka, S., Yamamoto, K., Pac, C., Yanagida, S., *Chem. Lett.*, **1990**, 2099.

<sup>44</sup>Ogata, T., Yanagida, S., Brunschwig, B.S., Fujita, E., *J. Am. Chem. Soc.* 117, **1995**, 6708.

<sup>45</sup>Grodzowski, J., Behar, D., Neta, P., Hambright, P., *J. Phys. Chem. A*, 101, **1997**, 248.

<sup>46</sup>Gholamkhash, B., Mametsuka, H., Koike, K., Tanabe, T., Furue, M., Ishitani, O., *Inorg. Chem.*, 44, **2005**, 2326.

---

<sup>47</sup>Kimura, E., Bu, X., Shionoya, M., Wada, S., Maruyama, S., *Inorg. Chem.*, 31, **1992**, 4542.

<sup>48</sup> Beley M.; Collin, J. P.; Ruppert, R.; Sauvage, J. P., *J. Chem. Soc., Chem. Commun.* **1984**, 1315.

<sup>49</sup> Beley, M.; Collin, J.-P.; Ruppert, R.; Sauvage, J. P. *J. Am. Chem. Soc.*, 108, **1986**, 7461.

<sup>50</sup> Kimuara E., Wada S., Shionoya M., Takahashi, T., Litakac, Y., *J. Chem. Soc. Chem. Commun.*, **1990**, 397.

<sup>51</sup>Kimura, E., Bu, X., Shionoya, M., Wada, S., Maruyama, S., *Inorg. Chem.*, 31, **1992**, 4542.

<sup>52</sup>Fujita, E., Milder, S.J., Brunschwig, B.S., *Inorg. Chem.*, 31, **1992**, 2079.

<sup>53</sup>Fujita, E., Szalda, D.J., Creutz, C., Sutin, N., *J. Am Chem.. Soc.*, 110, **1988**, 4870.

<sup>54</sup>Matsuoka, S., Yamamoto, T., Ogata, T., Kusaba, M., Nakashima, N., Fujita, E., Yanagida, S., *J. Am. Chem. Soc.*, 115, **1993**, 601.

<sup>55</sup>Fujita, E., Creutz, C., Sutin, N., Szalda, D.J., *J. Am. Chem. Soc.*, 113, **1991**, 343.

<sup>56</sup>Fujita, E., Creutz, C., Sutin, N., Brunschwig, B.S., *Inorg. Chem.*, 32, **1993**, 2657.

<sup>57</sup> Matsuoka, S., Kohzuki, T., Pac, C., Ishida, A., Takamuku,S., Kusaba, M., Nakashima, N., Yanagida, S., *J. Phys. Chem.*, 96, **1992**, 4437.

---

<sup>58</sup> Bian, Z.Y., Sumi, K., Furue, M., Sato, S., Koiko, K., Ishitani, O., *Inorg. Chem.*, 47, **2008**, 10801.

<sup>59</sup> Takeda, H., Ishitani, O., *Coord. Chem., Rev.*, 254, **2010**, 346.

<sup>60</sup> Takeda, H., Koike, K., Inoue, H., Ishitani, O., *J. Am. Chem. Soc.*, 130, **2008**, 2023.

<sup>61</sup> Bian, Z. Y., Sumi, K., Furue, M., Sato, S., Koike, K., *Inorg. Chem.*, 47, **2008**, 10801.

<sup>62</sup> Koike, K., Naitob, S., Satob, S., Tamakib, Y., Ishitani, O., *J. Photochem. Photobio. A. Chem.*, 207, **2009**, 109.

<sup>63</sup> Behar D., Dhanasekaran T., Neta P., Hosten C. M., Ejeh D., Hambright P., Fujita., *J. Phys. Chem. A.*, 102, **1998**, 2870 .

<sup>64</sup> Hambright P., Grodkowski J., Behar D., Neta P., *J. Phys. Chem. A.*, 101, **1997**, 248.

<sup>65</sup> Dhanasekaran T., Grodkowski J., Neta P., Hambright P., Fujita E., *J. Phys. Chem. A*, 103, **1999**, 7742.

<sup>66</sup> Hammouche M., Lexa D., Saveant J.-M., Momenteau M., *J. Electroanal. Chem. Interfacial Electrochem.* 249, **1988**, 347.

<sup>67</sup> Tokumaru, K., *J. Porphyrins Phthalocyanines*, 5, **2001**, 77.

<sup>68</sup> Le Gourrierrec, D., Andersson, M., Davidsson, J., Mukhtar, E., Sun, L., Hammarstrom, L., *J. Phys. Chem. A.*, 103, **1999**, 557.

<sup>69</sup> Gabrielsson, A., Hartl, F., Zhang, H., Lindsay, S. J. R., Towrie,

M., Vlcek, A., Jr; Perutz, R. N., *J. Am. Chem. Soc.*, 128, **2006**, 4253.

<sup>70</sup> Kiyosawa, K., Shiraishi, N., Shimada, T., Masui, D., Tachibana, H., Takagi, S., Ishitani, O., Tryk, D.A., Inoue H., *J. Phys. Chem. C*, 113, **2009**, 11667.

<sup>71</sup> Grodkowski J., Neta P., Fujita E., Mahammed A., Simkhovich L., Gross Z., *J. Phys. Chem. A*, 106, **2002**, 4772.

<sup>72</sup> Gross Z., Galili N., Saltsman I., *Angew. Chem., Int. Ed.*, 38, **1999**, 1427.

<sup>73</sup> Koszarna B., Gryko D. T., *J. Org. Chem.*, 71, **2006**, 3707.

<sup>74</sup> Gryko D. T., *J. Porphyrins Phthalocyanines*, 12, **2008**, 906.

<sup>75</sup> Goldberg D. P., *Acc. Chem. Res.*, 40, **2007**, 626.

<sup>76</sup> Grodkowski J., Neta P., *J. Phys. Chem. A*, 104, **2000**, 1848.

<sup>77</sup> Zhao Z., Fan, J., Wang Z., *Journal of Cleaner Production*, 15, **2007**, 1894.

<sup>78</sup> Zhao Z., Fan, J., Xie, M., Wang, Z., *Journal of Cleaner Production*, 17, **2009**, 1025.

<sup>79</sup> Premkumar J., Ramaraj P., *J. Photochem. Photobio. A. Chem.*, 110, **1997**, 53.

<sup>80</sup> Hawecker J., Lehn J.M., Ziessel R., *J. Chem. Soc., Chem. Commun.* **1983**, 536.

<sup>81</sup> J. Hawecker, J.-M. Lehn, R. Ziessel, *Helv. Chim. Acta*, 69, **1986**, 1990.

<sup>82</sup> Sullivan, B. P., Meyer, T. J., *Organometallics*, 5, **1986**, 1500.

---

<sup>83</sup> Ishitani, O., George, M. W., Ibusuki, T., Johnson, F. P. A., Koike K., Nozaki K., Pac, C., Turner, J. J., Westwell J. R., *Inorg. Chem.*, 33, **1994**, 4712.

<sup>84</sup> Sato, S., Sekine, A., Ohashi, Y., Ishitani, O., Blanco-Rodríguez, A. M., Vlcek, A., Unno, T., Koike, K., *Inorg. Chem.*, 46, 9, **2007**, 3531.

<sup>85</sup> Takeda, H., Koike, K., Inoue, H., Ishitani, O., *J. Am. Chem. Soc.*, 130, **2008**, 2023

<sup>86</sup> Kutal, C., Corbin, A. J., Ferraudi, G., *Organometallics*, 6, **1987**, 553.

<sup>87</sup> Shinozaki, K., Hayashi, Y., Brunschwig, B. S., Fujita, E., *Res. Chem. Intermed.*, 33 **2007**, 27.

<sup>88</sup> Takeda, H., Ishitani, O., *Coord. Chem. Rev.* 254, **2010**, 346.

***Chapter Two:  
Instrumentation.***

*Chapter two describes the instrumentation and techniques used within this thesis. The instrument models and accessories are described along with chemicals, reagents and any special techniques required. Software packages are also described where ever possible.*

## **2.1. General.**

The synthetic materials and reagents used throughout this thesis were of reagent grade or better. The compounds 2,2'-bipyridine (bpy), 1,10-phenanthroline (phen), 1,10-phenanthroline-5,6-dione (phendione) were purchased from Aldrich and used without further purification. All solvents were used as purchased. Column chromatography was performed using neutral activated aluminum oxide (150 mesh) with an acetonitrile/methanol mobile phase. Alumina TLC plates used during the purification processes were purchased from Aldrich and used as received.

## **2.2. Instrumental Methods**

### **2.2.1 NMR Spectroscopy.**

$^1\text{H}$  NMR and  $^1\text{H}$  NMR COSY spectra were obtained on a Bruker Advance 400 NMR Spectrometer at 400 MHz. Analysis was carried out in deuterated solvents (DMSO,  $d_3$ -ACN,  $d_3$ -Acetone and  $\text{CDCl}_3$ ) depending on substance solubility. Spectra were calibrated using either the relevant solvent peaks or TMS was added to the NMR tube as an internal reference. Some solutions required sonication for approximately five to ten minutes to ensure a fully dissolved solution due to low compound solubility. Samples containing a rhenium carbonyl species or the ligand tpphz were analysed immediately in the dark to ensure no photodecomposition.

### **2.2.2 Infrared Spectroscopy (IR).**

Infrared spectra of compounds in solution were measured using  $\text{CH}_2\text{Cl}_2$  or THF as solvents. A Perkin Elmer 2000 FTIR spectrometer was used and scans were carried out initially in the  $4000\text{ cm}^{-1}$  to  $600\text{ cm}^{-1}$  range before reducing to the carbonyl stretching frequency  $2200\text{ cm}^{-1}$   $1800\text{ cm}^{-1}$ . An average of 25 scans was carried out per sample using an Omni cell with NaCl windows. To obtain a clear spectrum, resolution was set to 4 cm and an interval of 1 cm were used.



### **2.2.3 Ultra Violet/Visible Spectroscopy. (UV/Vis)**

UV–Vis absorption spectra were recorded on a Shimadzu 3100 UV-Vis instrument. Sample measurements were carried out using 1 cm quartz cells and a relevant solvent blank. Solvents used for UV-Vis analysis were spectroscopy grade ethanol, DCM or acetonitrile. Cleaning of the quartz cells were carried out using a Kuvettol cleaning solution used as directed or an acid solution of 1:1 (v/v) conc.  $\text{H}_2\text{SO}_4/\text{HNO}_3$  to remove any remaining metal residue followed by washing with water. As the latter leads to glass etching and eventually the destruction of the cell it was only used in severe cases.

### **2.2.4 Emission Spectroscopy.**

Emission spectra were collected on a Perkin-Elmer LS50B luminescence spectrometer equipped with a red sensitive Hamamatsu R928 detector. A 1 cm, 4 sided quartz cell was used. Emission and excitation slit widths were typically 3, 5 or 10 nm depending on individual circumstances. Cuvettes were cleaned and cared for as described above.

### **2.2.5 Mass Spectrometry.**

Mass spectra were recorded with a Bruker-Esquire LC-00050 electrospray ionisation mass spectrometer at positive polarity with cap-exit voltage of 167 V. Each spectrum was recorded by summation of 20 scans. The experiments were performed on a Bruker Esquire LC\_00050 electro spray interface (ESI). Spectra were collected by constant infusion of the analyte dissolved in acetonitrile, with a positive ion polarity.

## ***Chapter 2 – Instrumentation.***

### **2.2.6 Elemental Analysis.**

Carbon, hydrogen and nitrogen (CHN) elemental analyses were carried out on an Exador Analytical CE440 by the Microanalytical Department, University College Dublin. The CHN analyzer used an Exador analytical CE440.

### **2.2.7 High Performance Liquid Chromatography. (HPLC)**

HPLC measurements were performed on a JVA analytical HPLC system consisting of a Varian Prostar HPLC pump using a Partisil P10 SCX-3095 cation exchange column (HiChrom) and a Varian Prostar photodiode array detector. A 20  $\mu\text{L}$  injection loop delivered the sample to the column using typically 0.08 M  $\text{LiClO}_4$  in  $\text{MeCN}/\text{H}_2\text{O}$  (80/20) mobile phase at a flow rate of  $1.8 \text{ cm}^3 \text{ min}^{-1}$ . The chromatogram was monitored at 280 nm and analysed using Varian proStar software.

### **2.2.8 Ion Chromatography.**

Ion Chromatography was carried out using a Dionex ICS 1500 system with the *Chromeleon* software package. Separation was achieved using an IonPac AS22 column with an attached IonPac AG22 guard column. The ICS 1500 system employs the use of an ASRS 300 4 mm self - regenerating 4mm suppressor with a DS6 heated conductivity cell for detection. A Mobile phase of 4.5 mM  $\text{Na}_2\text{CO}_3$  / 1.4 mM  $\text{NaHCO}_3$  (pH = 11.8) was used in all cases with a flow rate of  $1.2 \text{ cm}^3/\text{min}$ .

### 3.0 Synthetic Considerations.

This section describes the techniques employed to carry out synthetic reactions including apparatus set up and any special requirements carried out.

#### 3.1 Apparatus Setup.

Glassware set up and reflux reactions were carried out as shown in Figure 2.1. In some cases reactions were carried out in the presence of nitrogen where the drying tube is replaced with a nitrogen bubbler connected to a constant, steady nitrogen flow. Sand baths were used in general, apart from the synthesis of the ruthenium bipyridine dichloride starting material where a blue heating mantle with glass wool was employed along with the addition of a cracking tube.

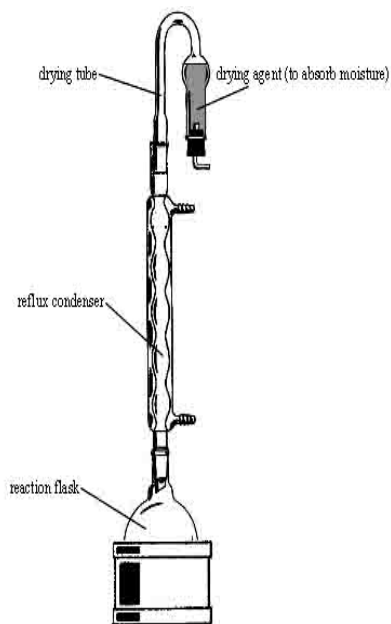


**Figure 2.1:** Diagram of Reflux Setup.<sup>1</sup>

#### 3.2 Glassware Preparation.

Synthetic reactions containing the rhenium pentacarbonyl starting material required very clean dry glassware. All glassware was taken directly from the oven and allowed to cool to room temperature. Reflux setup was shown above with the addition of a nitrogen bubbler. In some cases metal residue was removed from glassware using a small acid wash consisting of 1:1 (v/v)  $\text{HNO}_3:\text{H}_2\text{SO}_4$ , which was then neutralised and placed into relevant waste containers.

---

<sup>1</sup> <http://www.uvkchem.com/checm3ab/checm3ab.htm>

***Chapter 3: Synthetic Approaches  
to the preparation of  
mononuclear and dinuclear  
photocatalysts using azole  
ligands.***

*The subject of the work presented in this chapter is the development of an alternative synthetic pathway to prepare the heteronuclear complex  $[Ru(bpy)_2(tpphz)Re(CO)_3Cl](PF_6)_2$ . Synthesis and characterisation of the ruthenium(II) and rhenium(I) mononuclear complex intermediates are described. Preparation of the symmetric tetrapyrrodo[3,2-a:2',3':3'',2''-h:2''',3'''-j]phenazine (tpphz) ligand is discussed along with the mononuclear and dinuclear complexes containing this ligand.*

### 3.0 Introduction.

Previously in chapter 1 the development of photocatalysts has been discussed. This chapter and the work described herein, details the synthetic strategies using the “complexes as metals / complexes as ligands approach”<sup>1,2,3</sup> to prepare these photocatalysts. The main work in this chapter is the discussion of the procedures involved in the preparation of these metal complexes which are described in Tables 3.1, 3.2, and 3.3 that follow. The synthesis involved is a multi step procedure, involving the preparation and purification of precursor complexes before the final synthesis of the more complex photocatalysts.

To design these supramolecular complexes, the [Ru(bpy)<sub>2</sub>] moiety was chosen as a light absorbing centre. This offers a decent starting point due to the well documented electrochemical and photochemical properties, reported as early as the late 1960’s by Crosby and co-workers<sup>4,5</sup> and subsequently by Gafney and Adamson<sup>6</sup> in the seventies and by Hage and co-workers in the eighties and early nineties.<sup>7,8,9</sup> This Ru (II) centre was then combined with a [Re(CO)<sub>3</sub>Cl] moiety to act as a catalytic centre for CO<sub>2</sub> reduction. Rhenium was chosen as the metal of choice to act as the centre for CO<sub>2</sub> reduction due to its relatively high quantum yields and high selectivity of products during the reduction process as described in detail previously in chapter 1.<sup>10,11,12,13</sup> As demonstrated from the supramolecular photocatalysts discussed in chapter 1, the potential for CO<sub>2</sub> reduction to occur while using these two metal centres relies heavily on the bridging ligand chosen and its ability to allow a communication pathway between them.

The triazole ligands and their derivatives Hbpt (3,5-bis(pyridin-2-yl)-1,2,4-triazole) and Hbpzt (3,5-bis(pyrazin-2-yl)-1,2,4-triazole) were chosen due to their well documented properties<sup>7,8,9,10,14</sup> The first reported bis(bpy) ruthenium complexes containing 1,2,4-triazoles was as in the eighties by Vos and co – workers who studied these ligands due to their  $\sigma$ -donor properties and the differing coordination isomers that formed. These investigations and subsequent reports are important to the synthesis and characterisation of the complexes discussed in this chapter, as these studies found that the metal ion can coordinate via the N4 or the N2 sites on the triazole ligand as shown in Figure 3.1 below.

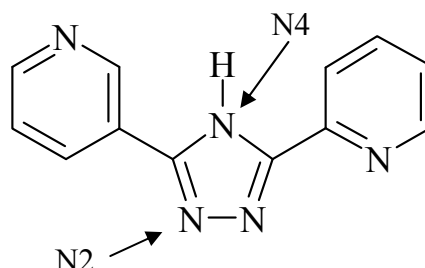


**Figure 3.1:** An example of the triazole ligand Hbpt with the coordination sites N2 and N4 available.

Another important finding from these investigations was the stronger donating ability of the N2 site over that of the N4 which has been shown to affect the electronic and electrochemical properties of the complex. The favorability of coordination occurring of the N2 site over the N4 site is highly dependent on the substituents present (if any) on the five membered ring of the triazole.<sup>15,16</sup>

Apart from the coordination modes available and the  $\sigma$  – donating abilities of the triazole ligands, another important feature of these metal complexes of the type  $[(\text{Ru}(\text{bpy})_2)_2(\text{bpt})](\text{PF}_6)_3$  are the well documented electronic spectra which are dominated by intense adsorption bands between 450 – 470 nm. This is the result of CM3CT (metal to ligand charge transfer) band and a  $d\pi-\pi^*$  interaction occurring at lower energy; the ligand  $\pi-\pi^*$  transitions are also observed in the 250 – 300 nm region. These findings were of particular use during the synthesis and characterisation of the complexes under discussion in this chapter.

The complexation reaction described by Vos and co-workers was of great interest as the “metals as ligands / metals as complexes” approach was used which gave a solid starting point from the preparation of such complexes within this chapter. Figures 3.2, 3.3 and 3.4 that follow demonstrate the general synthetic approach taken to prepare the supramolecular photocatalysts under discussion in this chapter:

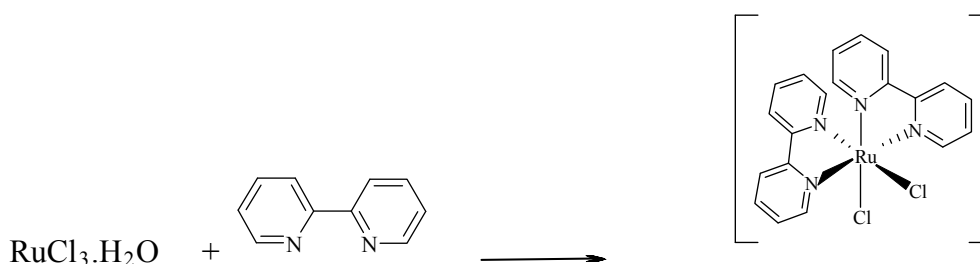


**Figure 3.2:** General synthesis of a mononuclear complex.

Figure 3.2 above details the preparation of a mononuclear complex by the reaction of a metal with free ligand. As shown above this mononuclear complex has two chlorine groups attached which allow for further reaction with coordinating ligands such as the triazole ligands mentioned earlier. Synthesising mononuclear precursors like that in Figure 3.2 allows for the preparation of homonuclear and heteronuclear complexes as shown in Figure 3.3 and 3.4 below. The synthesis of the homonuclear complex is a relatively straightforward synthesis that requires the addition of the metal precursor in a 2:1 ratio to bridging ligand.

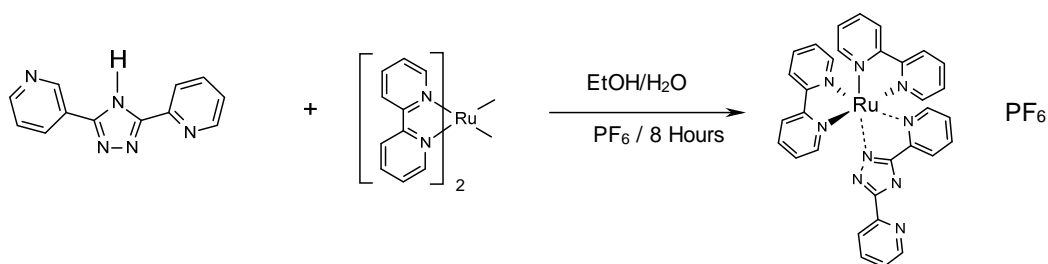


**Figure 3.3:** Example of a homonuclear complex synthesis.

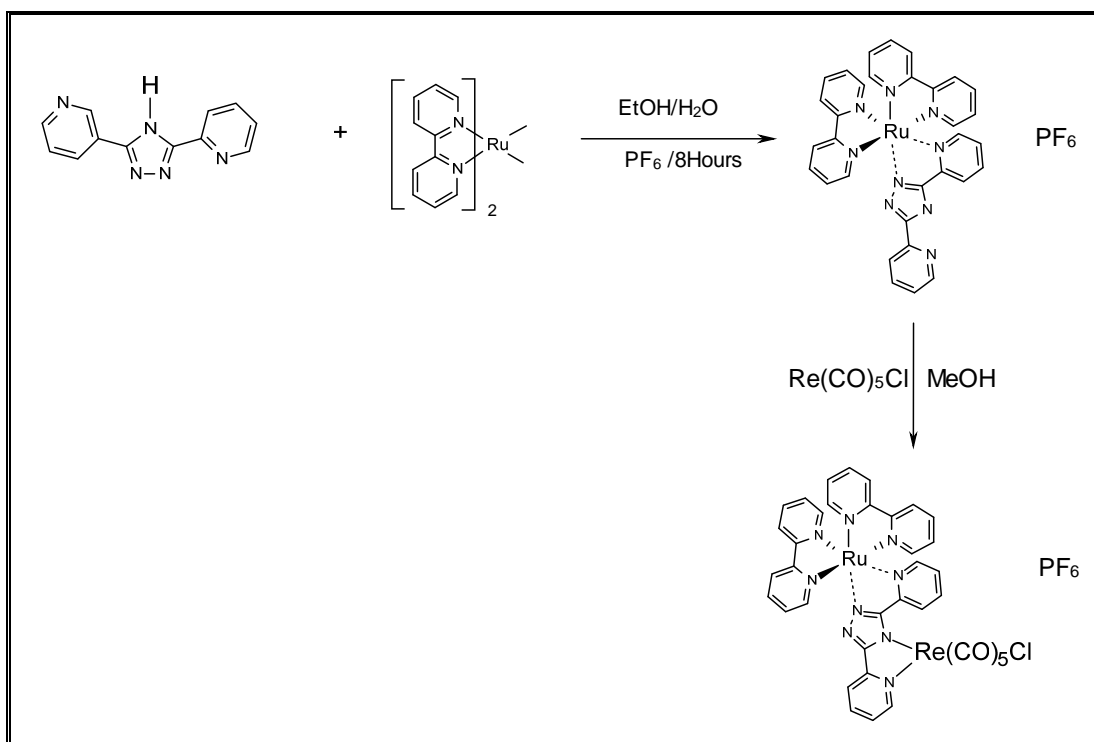


**Figure 3.4:** Example of a heteronuclear complex synthesis.

The work outlined in this chapter generally requires the synthesis of heteronuclear complexes. This is achieved by the addition of a second metal centre to a mononuclear complex. This is a challenging synthesis which requires the preparation of a pure mononuclear complex before the addition of the second metal centre. This is the traditional method used for the synthesis of metal complexes of this type and the subsequent sections will detail the synthesis of the mixed ligand systems as shown above.



### 3.1 Aim.

The synthesis and characterisation of ruthenium (II) and rhenium (I) mono- and dinuclear complexes containing the asymmetric ligands 3,5-bis(pyridin-2-yl)-1,2,4-triazole (Hbpt), 3,5-bis(pyridin-2-yl)-1,2,4-triazole (Hbpzt) and 2,5-Bis(2-pyridyl)-1,3,4-thiadiazole (dptd) are described. The structures of the ligand employed and metal complexes are described in Figures 3.5, 3.6 and 3.7.

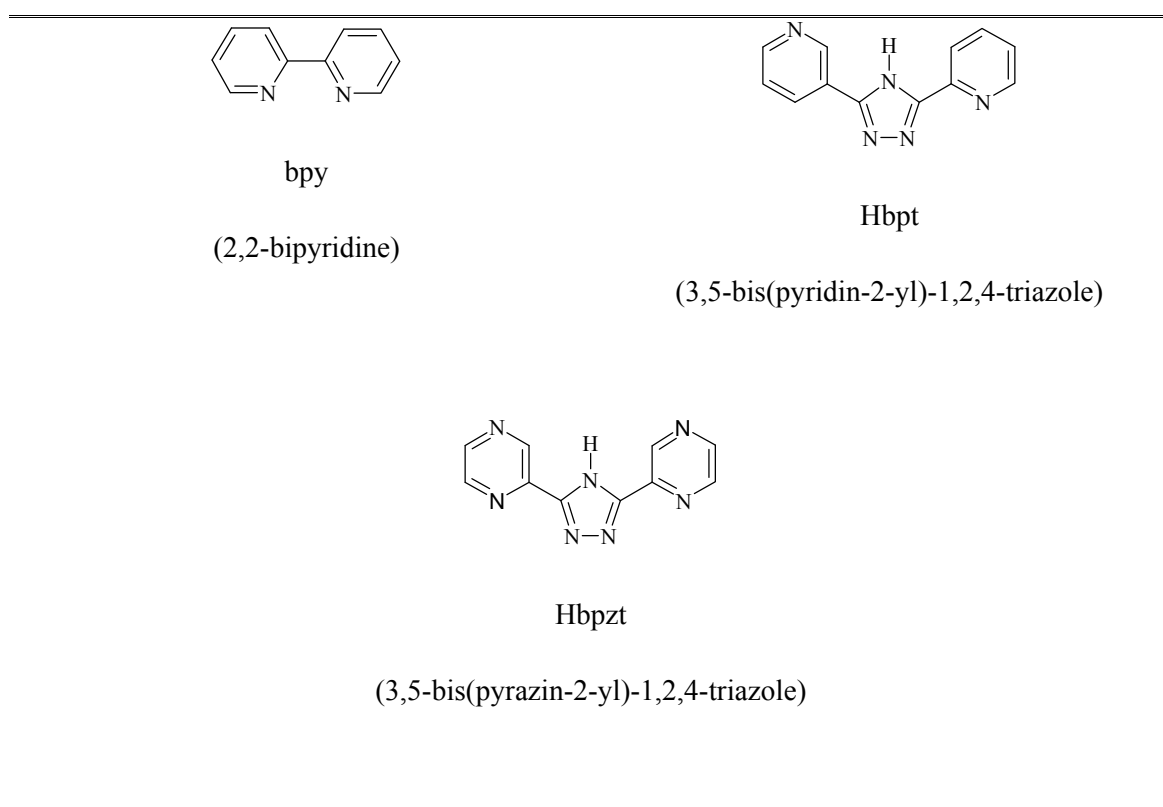


**Figure 3.5:** Depicts the structures of the ligands discussed in this section.

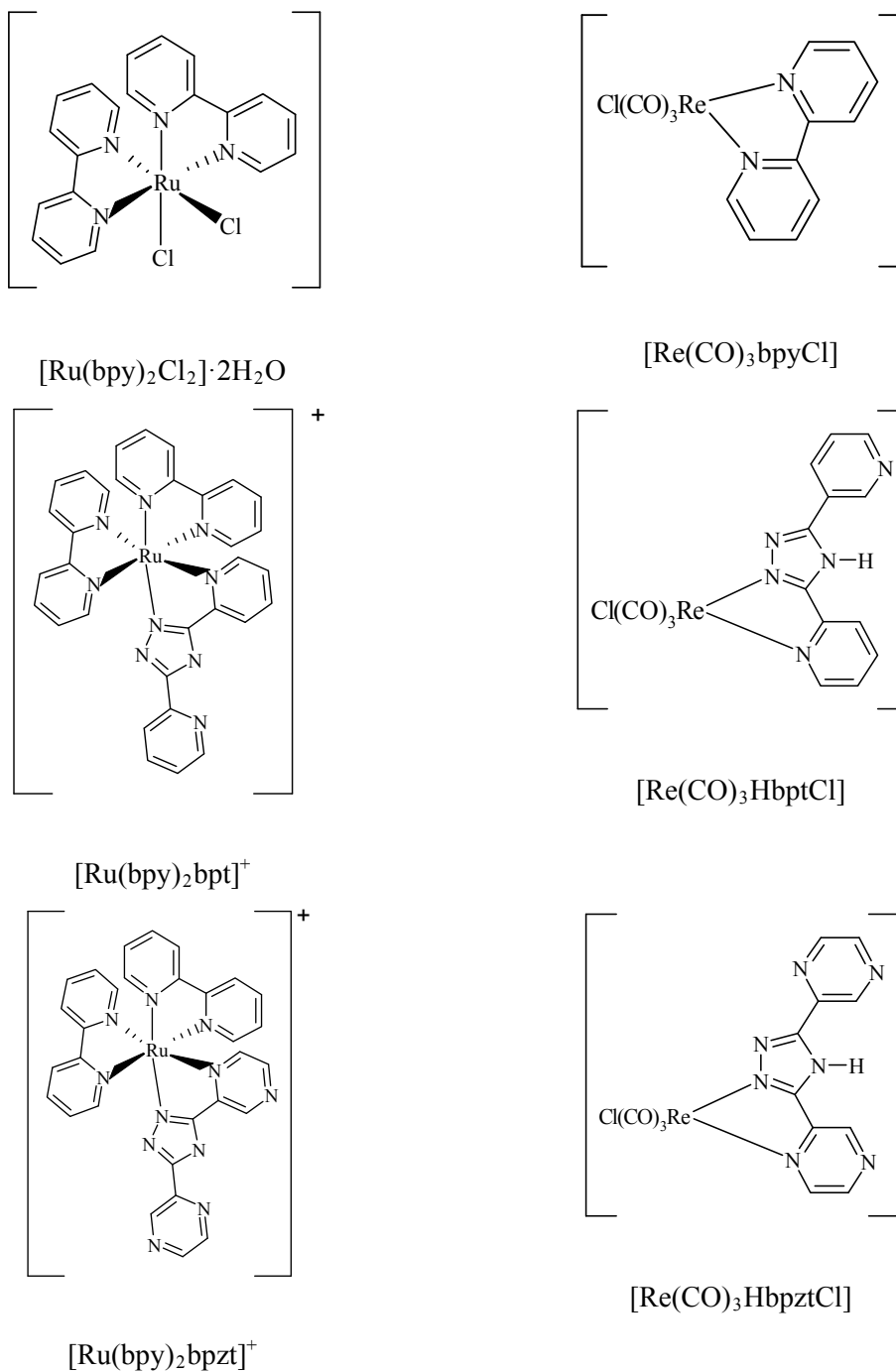


**Figure 3.6:** Depicts the structures of the mononuclear complexes discussed in this section.

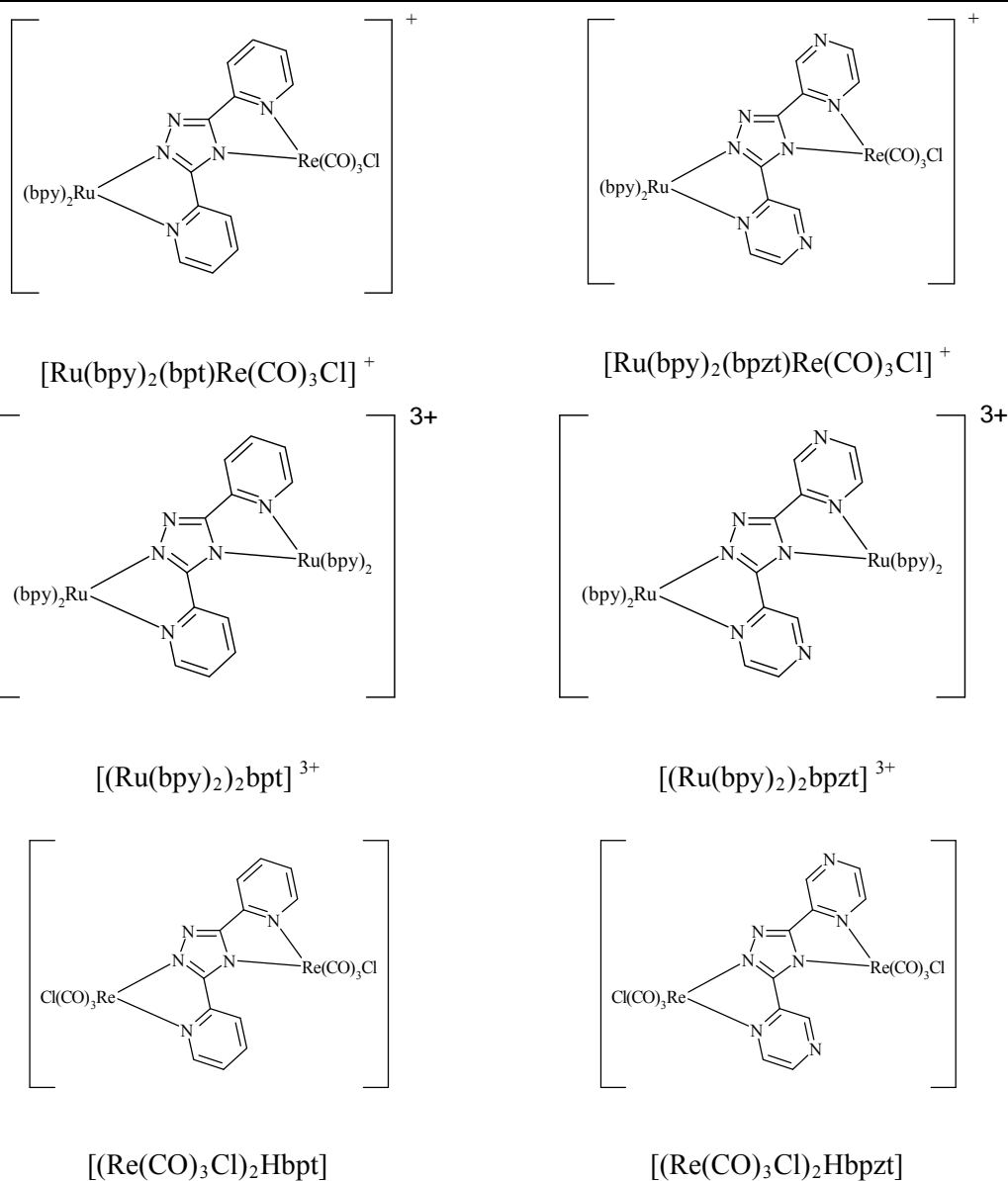


**Figure 3.7:** Depicts the structures of the dinuclear complexes discussed in this section. (bpy = 2,2-bipyridine).

## 3.2 Synthetic Procedures.

### 3.2.1 Ligand Preparation

#### *3,5-bis(pyridin-2-yl)-1,2,4-triazole (Hbpt)*

##### *3,5-bis(pyridin-2-yl)-4-amino-1,2,4-triazole*

2-cyanopyridine (10 g, 96.2 mmol) and hydrazine monohydrate (4.95 cm<sup>3</sup>, 96.2 mmol) were heated for three hours under reflux at 100°C. The orange product that was formed was collected by vacuum filtration, washed with cold ethanol and diethyl ether. The orange solid was then dissolved in 2M HCl (20 cm<sup>3</sup>) and stirred for thirty minutes. This was then cooled to room temperature and made alkaline by the addition of ammonia. This was then cooled to +4 °C. After 2 hours the tan product was washed with alkaline H<sub>2</sub>O to yield the intermediate 3,5-bis(pyridin-2-yl)-4-amino-1,2,4-triazole. Yield: 6.87 g, 28.8 mmol, 30 %. <sup>1</sup>HNMR (DMSO, 400 MHz) δ in ppm: 8.79 (d, 2H), 8.20 (d, 2H), 8.02 (dd, 2H), 7.88 (s, 1H), 7.43 (dd, 2H).

##### *3,5-Bis(pyridin-2-yl)-1,2,4-triazole*

The intermediate was then dissolved in boiling 5M nitric acid (11 cm<sup>3</sup>). This was then immediately cooled to 0°C and sodium nitrite solution was added slowly until no brown fumes were noticed, the solution was allowed to stir for 2 hours and a white precipitate was formed. This was collected by filtration and dissolved in aqueous ammonia and boiled for 5 minutes. The white product was then formed by evaporation of the liquid phase and was recrystallised from ethanol. Yield: 5.95 g, Calc for C<sub>12</sub>H<sub>11</sub>N<sub>5</sub>, Mw: 224.23 g/mol. <sup>1</sup>HNMR (DMSO, 400MHz) δ in ppm: 7.50 (dd, 2H), 7.98 (dd, 2H), 8.12 (d, 2H), 8.75 (d, 2H).

**3,5-bis(pyrazin-2-yl)-1,2,4-triazole (Hbpzt)** <sup>17</sup>

2-Pyrazinecarboxylic acid (8.0 g, 65 mmol) and conc. H<sub>2</sub>SO<sub>4</sub> (2 cm<sup>3</sup>) were heated at reflux in EtOH for 3 h. Sodium carbonate was added to neutralize the H<sub>2</sub>SO<sub>4</sub> after which excess hydrazine hydrate (5.05 g, 101 mmol) was added. The solution was stirred at 0°C for 3 h. The precipitate was filtered and washed with cold EtOH. 2-Cyanopyrazine (4.2 g, 40 mmol) was converted to 2-pyrazylmethyylimidate by heating it at reflux with Na metal in MeOH for 3 h. The hydrazide from above was added and the solution heated for an additional 1 h. The yellow precipitate was filtered and washed with cold EtOH. 3,5-(pyrazin-2-yl)-1,2,4-triazole was obtained by heating the pyrazine-2-carboxylic acid N'-(imino-pyrazin-2-yl-methyl)-hydrazide at reflux in ethylene glycol for 1 h. The product was then recrystallised from ethanol. Yield 6.0 g, 27 mmol, 42%. Calc for C<sub>10</sub>H<sub>7</sub>N<sub>7</sub>, Mw: 226.23 g/mol <sup>1</sup>HNMR (DMSO, 400MHz) δ in ppm: 9.35 (s, 2H), 8.81 (d, 2H), 8.78 (d, 2H).

### 3.2.2 Preparation of Mononuclear Complexes

#### ***[Ru(bpy)<sub>2</sub>Cl<sub>2</sub>].2H<sub>2</sub>O*<sup>18</sup>**

2,2'-bipyridine (6.02 g, 38.5 mmol), RuCl<sub>3</sub>·H<sub>2</sub>O (4.00 g, 7.7 mmol) and LiCl (1.15 g, 26.7 mmol) were placed in 30 cm<sup>3</sup> of DMF and refluxed for 4 hours. The solution was then cooled to room temperature and transferred to 80 cm<sup>3</sup> of acetone along with washings from the condenser and left overnight at -4 °C. The dark purple crystals were recovered by vacuum filtration and washed with water and acetone respectively until the filtrate became clear. Yield: 5.60 g, 10.8 mmol, 78 %. Calc for C<sub>20</sub>H<sub>18</sub>N<sub>4</sub>O<sub>2</sub>Cl<sub>2</sub>Ru<sub>1</sub>, Mw: 520.21 g/mol. <sup>1</sup>HNMR (DMSO, 400 MHz) δ in ppm: 7.12 (dd, 2H), 7.56 (d, 2H), 7.63 (dd, 2H), 7.69 (dd, 2H) 8.49 (dd, 2H), 8.63 (d, 2H), 9.79 (d, 2H).

#### ***[Ru(bpy)<sub>2</sub>bpt](PF<sub>6</sub>).1/2H<sub>2</sub>O***

[Ru(bpy)<sub>2</sub>Cl<sub>2</sub>].2H<sub>2</sub>O (1.16 g, 2.23 mmol) was dissolved in 30 cm<sup>3</sup> of solvent (EtOH: H<sub>2</sub>O (2:1 v/v)) and brought to 90 °C. Hbpt (500 mg, 2.22 mmol) was dissolved in 20 cm<sup>3</sup> of the solvent and added slowly to the [Ru(bpy)<sub>2</sub>Cl<sub>2</sub>].2H<sub>2</sub>O in small portions. This was then brought to reflux temperature (120 °C) and left for 6 hours. The reaction was then cooled to room temperature and the ethanol removed by rotary evaporation. 10 cm<sup>3</sup> of H<sub>2</sub>O was then added and aqueous NH<sub>4</sub>PF<sub>6</sub> was added dropwise until no more precipitate was formed. The reaction was then left at +4 °C overnight. The orange solid was then recovered by vacuum filtration and allowed to dry. This was then purified using alumina with acetonitrile mobile phase then recrystallised from acetone: H<sub>2</sub>O (1:1v/v). Yield: 0.33g, 0.417 mmol, 19 %. Calc for C<sub>32</sub>H<sub>26</sub>N<sub>9</sub> Ru<sub>1</sub>PF<sub>6</sub>(1/2H<sub>2</sub>O), Mw: 790.45 g/mol. <sup>1</sup>HNMR (DMSO, 400 MHz) δ in ppm: 7.05 (dd, 1H), 7.15 (dd, 1H), 7.19 (dd, 1H), 7.30 (m, 3H) 7.44 (d, 1H), 7.65 (dd, 1H), 7.74 (dd, 2H), 7.78 (d, 4H), 7.78 (m, 5H), 8.05 (d, 1H), 8.35 (m, 4H), 8.45 (d, 1H).

***[Ru(bpy)<sub>2</sub>bpzt](PF<sub>6</sub>)<sup>19</sup>***

As for [Ru(bpy)<sub>2</sub>bpt](PF<sub>6</sub>).1/2H<sub>2</sub>O except [Ru(bpy)<sub>2</sub>Cl<sub>2</sub>] · 2H<sub>2</sub>O (500 mg, 0.96 mmol) and Hbpzt (500 mg, 2.21 mmol) was used. Yield: 0.29g, 0.37 mmol, 38 %. Calc on C<sub>30</sub>H<sub>22</sub>N<sub>11</sub> Ru<sub>1</sub>PF<sub>6</sub> Mw: 783.43 g/mol. <sup>1</sup>HNMR (DMSO, 400 MHz) δ in ppm: Ring A: (H<sub>3</sub>, 9.34), (H<sub>5</sub>, 7.58), (H<sub>6</sub>, 8.55), Ring B: (H<sub>3</sub>, 8.86), (H<sub>5</sub>, 7.21), (H<sub>6</sub>, 8.22), bpy: 8.48 (dd, 2H), 8.60 (dd, 2H), 7.43 (dd, 2H), 7.62 (dd, 2H), 8.13 (m, 4H), 8.78 (m, 4H).

***[Re(CO)<sub>3</sub>(bpy)Cl]***

20 cm<sup>3</sup> of anhydrous toluene was purged for 5 minutes. [Re(CO)<sub>5</sub>Cl] (100 mg, 0.277 mmol) was weighed out carefully under nitrogen and added to the toluene along with of 2,2'-bipyridine (0.0432g, 0.276 mmol). This was heated to reflux and left for 2.5 hours. The reaction had turned a dark yellow colour and was allowed to cool to room temperature and placed at +4 °C overnight. The yellow product was collected by vacuum filtration and to ensure the entire product was collected the toluene was evaporated. Yield: 0.124, 97%. Calc on C<sub>13</sub>H<sub>8</sub>N<sub>2</sub>O<sub>3</sub>ClRe<sub>1</sub> Mw: 461.78 g/mol. <sup>1</sup>HNMR (acetone, 400 MHz) δ in ppm: 7.82 (m, 2H), 8.35 (m, 2H), 8.69 (d, 2H), 9.11 (d, 2H).

***[Re(CO)<sub>3</sub>Cl(Hbpt)]***

As For [Re(CO)<sub>3</sub>(bpy)Cl] except [Re(CO)<sub>5</sub>Cl] (100 mg, 0.277 mmol) and Hbpt (70 mg, 0.312 mmol) was used. Yield: 88 mg, 0.166 mmol, 60 %. Calc on C<sub>15</sub>H<sub>11</sub>N<sub>5</sub>O<sub>3</sub>Cl Re<sub>1</sub> Mw: 529.89 g/mol. <sup>1</sup>HNMR (acetone, 400 MHz) δ in ppm: Ring A: (H<sub>3</sub>, 8.42), (H<sub>4</sub>, 8.26), (H<sub>5</sub>, 7.52), (H<sub>6</sub>, 9.05) Ring B: (H<sub>3</sub>, 8.40), (H<sub>4</sub>, 8.22), (H<sub>5</sub>, 7.52), (H<sub>6</sub>, 8.78). E.A for ReC<sub>15</sub>H<sub>9</sub>N<sub>5</sub>O<sub>3</sub>Cl: Calculated: C 34.1, H 1.8, N 13.3, Found: C 33.64, H 1.93, N 12.87.

### 3.2.3 Preparation of Dinuclear Complexes

#### ***[Ru(bpy)<sub>2</sub>(bpt)Re(CO)<sub>3</sub>Cl](PF<sub>6</sub>).3H<sub>2</sub>O***

(200 mg 0.256 mmol) of [Ru(bpy)<sub>2</sub>bpt](PF<sub>6</sub>)1/2.H<sub>2</sub>O was reacted with (100 mg, 0.277 mmol) of [Re(CO)<sub>5</sub>Cl] in 50cm<sup>3</sup> of methanol for 6 hours. The solvent was then removed. The complex was then recrystallised from acetone/ethanol (2/1 v/v). Yield: 0.3493 g, 0.306 mmol, 115%. Calc on C<sub>35</sub>H<sub>32</sub>N<sub>9</sub>O<sub>6</sub>ClRu RePF<sub>6</sub> Mw: 1141.02 g/mol. <sup>1</sup>HNMR (DMSO, 400 MHz) δ in ppm: 6.74 (dd, 1H), 6.91( dd,1H), 7.02 (dd, 1H), 7.13 (dd, 1H), 7.26 (m 2H), 7.32(dd,2H), 7.38(m, 2H), 7.43 (dd, 2H), 7.58 (m,3H), 7.81 (m, 4H), 8.09 (dd, 1H), 8.12( dd, 1H), 8.20 (dd 1H), 8.38 (m, 1H). E.A for Ru<sub>1</sub>Re<sub>1</sub>C<sub>35</sub>H<sub>27</sub>N<sub>9</sub>O<sub>6</sub>ClPF<sub>6</sub>: Calculated: C 38.6, H 2.4, N 11.6, Found: C 35.42, H 2.72, N 10.47.

#### ***[{Ru(bpy)<sub>2</sub>}<sub>2</sub>bpt](PF<sub>6</sub>)<sub>3</sub>***

[Ru(bpy)<sub>2</sub>Cl<sub>2</sub>].2H<sub>2</sub>O (1.00g, 1.922 mmol) and Hbpt (0.186g, 0.830 mmol) were placed in 50cm<sup>3</sup> of 2:1 ethanol:H<sub>2</sub>O and refluxed for 6 hours. The reaction was then brought to room temperature and the ethanol removed by rotary evaporation. The orange product was precipitated by the addition of NH<sub>4</sub>Pf<sub>6</sub> and the solution was left at +4°C overnight. The crude product was then collected by filtration. Purification was carried out using an alumina column with acetonitrile as a mobile phase and recrystallised from 1:1 acetone: H<sub>2</sub>O. Yield: 683 mg, 0.46 mmol, 55 %. Calc on C<sub>52</sub>H<sub>42</sub>N<sub>13</sub>Ru<sub>2</sub>P<sub>3</sub>F<sub>18</sub> Mw: 1484.58 g/mol

<sup>1</sup>HNMR (DMSO, 400 MHz) δ in ppm: 6.68 (dd, 1H), 6.84 (dd, 1H), 7.04 (dd, 1H), 7.13(dd, 1H), 7.23(m, 2H), 7.38( m, 2H), 7.48(m, 2H), 7.63(m, 2H), 7.73 (m, 2H), 7.85(m, 1H), 7.93(dd, 1H), 8.28 (m,2H), 8.36 (dd, 1H), 8.51(m, 2H), 8.58 (dd, 1H), 8.68 (m, 2H), 8.82( dd,2H).



***[{Ru(bpy)<sub>2</sub>}<sub>2</sub>bpzt](PF<sub>6</sub>)<sub>3</sub>*<sup>7</sup>**

As for [{Ru(bpy)<sub>2</sub>}<sub>2</sub>bpt](PF<sub>6</sub>)<sub>3</sub> except that [Ru(bpy)<sub>2</sub>Cl<sub>2</sub>].2H<sub>2</sub>O (1g, 1.922 mmol) and Hbpzt (0.186g, 0.822 mmol) were reacted. Yield: 576 mg, 0.387 mmol, 47 %. Calc on C<sub>50</sub>H<sub>39</sub>N<sub>15</sub>Ru<sub>2</sub>P<sub>3</sub>F<sub>18</sub> Mw: 1486.56 g/mol. <sup>1</sup>HNMR (DMSO, 400 MHz) δ in ppm: 6.62 (dd, 1H), 6.93 (dd, 1H), 7.23 (dd, 1H), 7.53(m, 2H), 7.42(m, 2H), 7.51 (, 2H), 7.36(m, 2H), 7.72 (m, 2H), 8.02(m, 2H), 8.28(m, 2H), 8.43(m, 2H), 8.63 (m, 2H), 9.19 (dd, 1H).

***[{Re(CO)<sub>3</sub>Cl}<sub>2</sub>bpt]***

20cm<sup>3</sup> of anhydrous toluene was purged for 5 minutes. [Re(CO)<sub>5</sub>Cl] (0.2g, 0.553 mmol) was weighed out carefully under nitrogen and added to the toluene along with of Hbpt (0.06g, 0.268 mmol). This was heated to reflux and left for 2.5 hours. The reaction had turned a dark yellow colour and was allowed to cool to room temperature and placed at +4°C overnight. The yellow product was collected by vacuum filtration and to ensure the entire product was collected the toluene was evaporated. The product was then recrystallised from acetone. Yield: 0.1385g, 0.166 mmol, 62%. Calc on C<sub>18</sub>H<sub>10</sub>N<sub>5</sub>O<sub>6</sub>Cl<sub>2</sub>Re<sub>2</sub>Mw: 834.37 g/mol. <sup>1</sup>HNMR (DMSO, 400 MHz) δ in ppm: 8.25 (dd, 2H), 7.68 (m, 2H), 9.02 (dd, 2H).

***[{Re(CO)<sub>3</sub>Cl}<sub>2</sub>bpzt]***

As for [{Re(CO)<sub>3</sub>Cl}<sub>2</sub>bpt] except Re(CO)<sub>5</sub>Cl (100 mg, 0.277 mmol) and Hbpzt (0.06g, 0.265 mmol) was used. Yield: 68 mg, 0.081 mmol, 31 %. Calc on C<sub>18</sub>H<sub>10</sub>N<sub>5</sub>O<sub>6</sub>Cl<sub>2</sub>Re<sub>2</sub>Mw: 834.37 g/mol. <sup>1</sup>HNMR (DMSO, 400 MHz) δ in ppm: 9.38 (s, 2H), 8.82 (dd, 2H), 8.79 (dd, 2H).

### 3.2.4 Attempted Synthesis.

#### ***[Ru(bpy)<sub>2</sub>(bpzt)Re(CO)<sub>3</sub>Cl](PF<sub>6</sub>)***

As for [Ru(bpy)<sub>2</sub>(bpt)Re(CO)<sub>3</sub>Cl]PF<sub>6</sub> except (100 mg 0.128 mmol) of [Ru(bpy)<sub>2</sub>bpzt]PF<sub>6</sub> was reacted with (100 mg, 0.277 mmol) of [Re(CO)<sub>5</sub>Cl]. The desired product was not obtained.

#### ***[Re(CO)<sub>3</sub>Cl(Hbpzt)]***

As For [Re(CO)<sub>3</sub>bpyCl] except [Re(CO)<sub>5</sub>Cl] (100 mg, 0.277 mmol) and Hbpzt (72 mg, 0.314 mmol) was used. The desired product was not obtained.

### 3.3 Results and Discussion.

#### 3.3.1 Synthetic Procedures - Ligand Preparation.

The Hbpt synthesis used was that previously reported by L. Cassidy, as this method did not employ the use of sodium metal and also offered an increased yield compared to previously reported synthesis by Hage and earlier by Geldard.<sup>20</sup> The ligand was prepared in two stages firstly preparing the 3,5-bis(pyridin-2-yl)-4-amino-1,2,4-triazole intermediate, then refluxing this in concentrated  $\text{HNO}_3$ . This can be seen in Figure 3.8 below. The synthesis of the ligand can be problematic and care must be taken during the addition of the sodium nitrite solution. The reaction at that point must be allowed to stir until the brown fumes are no longer seen and a clear solution is obtained. The white precipitate does not always form at this point but the addition of concentrated ammonia and reduction of the mother liquor generally yields the required ligand.

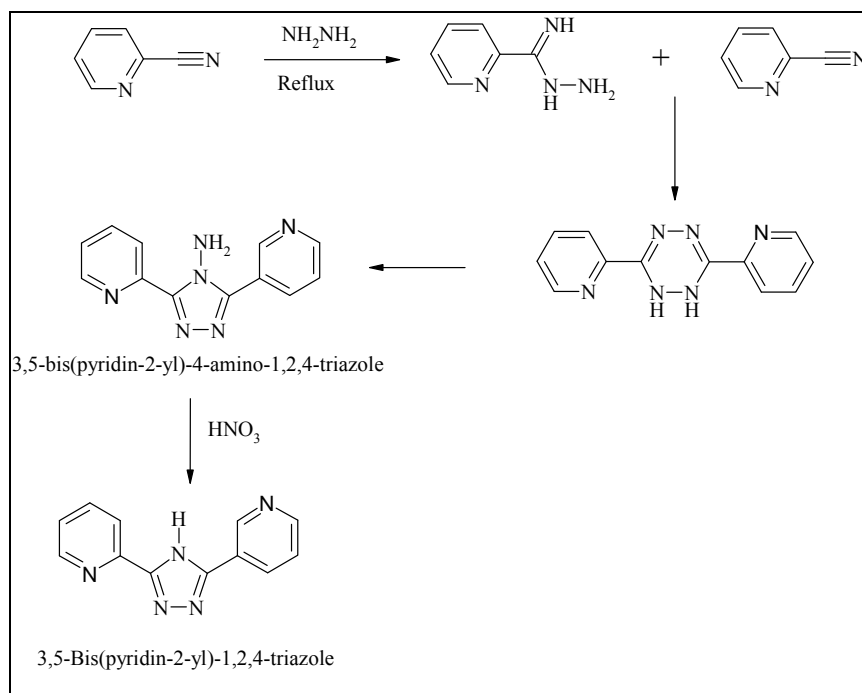


**Figure 3.8:** Synthetic route used to synthesise Hbpt.

The synthesis of the pyrazine analogue, Hbpzt was carried out as previously reported by Hage and co-workers.<sup>7,9</sup> The most problematic part of this synthesis was the intramolecular ring closure. It was found that the ligand was obtained pure and in high yield when the ligand was heated until molten and allowed to stir at this temperature for an hour. Upon cooling the ligand was obtained. Figure 3.9 below details the steps taken during this synthesis.

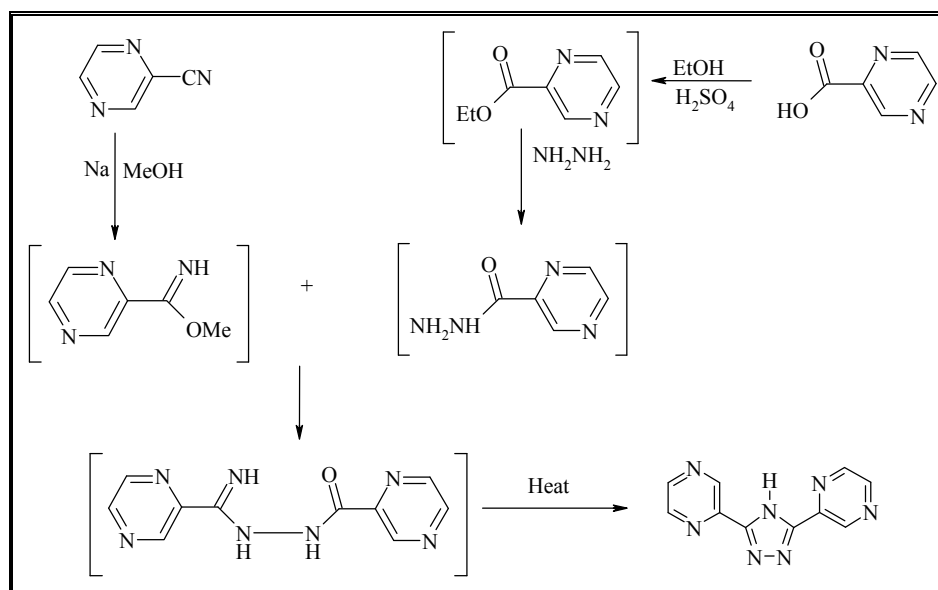


**Figure 3.9:** Route used to synthesise Hbpzt.

### 3.3.2 Synthetic Procedures - Preparation of Mononuclear Complexes.

The synthetic preparation of the ruthenium mononuclear complexes were relatively straightforward. The starting material  $\text{cis-}[\text{Ru}(\text{bpy})_2\text{Cl}_2]\cdot 2\text{H}_2\text{O}$  was prepared by refluxing  $\text{RuCl}_3\cdot \text{H}_2\text{O}$  for four hours in the presence of 2,2-bipyridine as previously reported by Meyer in 1978,<sup>18</sup> the only difference to those methods reported, was the increase of refluxing temperature and a decrease in the time the solution was refluxed which was reduced to four hours. The deuteriated form was also prepared in this manner but using the deuterated 2,2-*d*-bipyridyl. This was used in subsequent analysis as a starting and a reference compound. Yields for the deuteriated and non deuteriated reactions were typically around 70%.

The formation of the Ru(II) mononuclear complex  $[\text{Ru}(\text{bpy})_2(\text{bpt})]^+$  was carried out as previously reported by Hage *et al.*,<sup>7</sup> the only difference was in the purification procedure where the mononuclear complex was separated on neutral alumina using acetonitrile as a mobile phase. The synthesis of the  $[\text{Ru}(\text{bpy})_2(\text{bpzt})]^+$  complex was more complicated, it was found that the best purification was using neutral alumina with acetonitrile with a methanol gradient.

The preparation of the Rhenium(I) mononuclear complexes  $[\text{Re}(\text{CO})_3\text{HbptCl}]$  and  $[\text{Re}(\text{CO})_3\text{bpyCl}]$  were carried out as previously reported with no variations. These reactions were followed using infra-red analysis by monitoring the disappearance of the rhenium pentacarbonyl peaks and the formation of the tricarbonyl species. The one important difference between the preparations of both of these mononuclear complexes was the time required to reach completion. The rhenium(I) complexes required 3-3.5 hours of refluxing time to reach completion, were the Ru(II) complexes required 6 hours.

For the formation for both the ruthenium and rhenium mononuclear species, it was important to fully dissolve the ligand before the addition of either the  $[\text{Ru}(\text{bpy})_2\text{Cl}_2]\cdot 2\text{H}_2\text{O}$  or the rhenium pentacarbonyl. This limited the amount of dinuclear species formed along with using a 1:1.2 metal to ligand ratio. This often meant, that during the purification procedure only the unreacted ligand needed to be removed.

### 3.3.3 Synthetic Procedures - Preparation of Dinuclear Complexes.

The preparation of the homonuclear dinuclear complexes,  $[\{\text{Ru}(\text{bpy})_2\}_2\text{bpt}]^{3+}$  and  $[\{\text{Re}(\text{CO})_3\text{Cl}\}_2\text{Hbpt}]$  were carried out as previously reported using the *complexes as metals* and *complexes as ligands* strategies.<sup>21, 22</sup> The purification procedure employed here for  $[\{\text{Ru}(\text{bpy})_2\}_2\text{bpt}]^{2+}$  was a neutral alumina column instead of the reported sephadex SP C-25 resin.<sup>75</sup> The heteronuclear complex  $[\text{Ru}(\text{bpy})_2(\text{bpt})\text{Re}(\text{CO})_3\text{Cl}]$  was prepared as reported previously with no variations. The same method was employed for the synthesis of the  $[\text{Ru}(\text{bpy})_2(\text{bpzt})\text{Re}(\text{CO})_3\text{Cl}]^+$  and  $[\text{Ru}(\text{bpy})_2(\text{bptd})\text{Re}(\text{CO})_3\text{Cl}]^{2+}$  complexes. Below is a schematic representation of the formation of the dinuclear complexes.

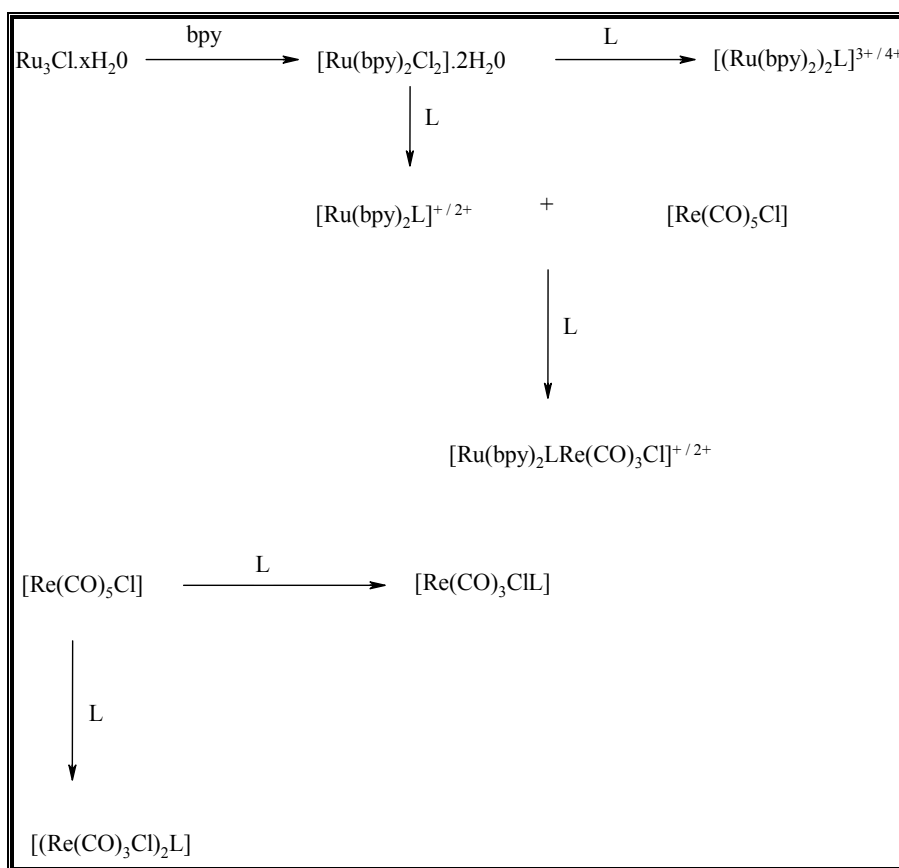


**Figure 3.10:** Schematic representation of the pathways employed in the synthesis of the dinuclear metal complexes. ( $\text{L} = \text{Hbpt}, \text{Hbpzt}, \text{dptd}$ ).

To determine the formation and purity of the mononuclear and dinuclear complexes discussed the  $^1\text{H}$ NMR spectra of the mononuclear complex was compared to that of the intermediate  $[\text{Ru}(\text{bpy})_2\text{Cl}_2] \cdot 2\text{H}_2\text{O}$  and that of the free ligand, an example of which is detailed in Figure 3.11 below.

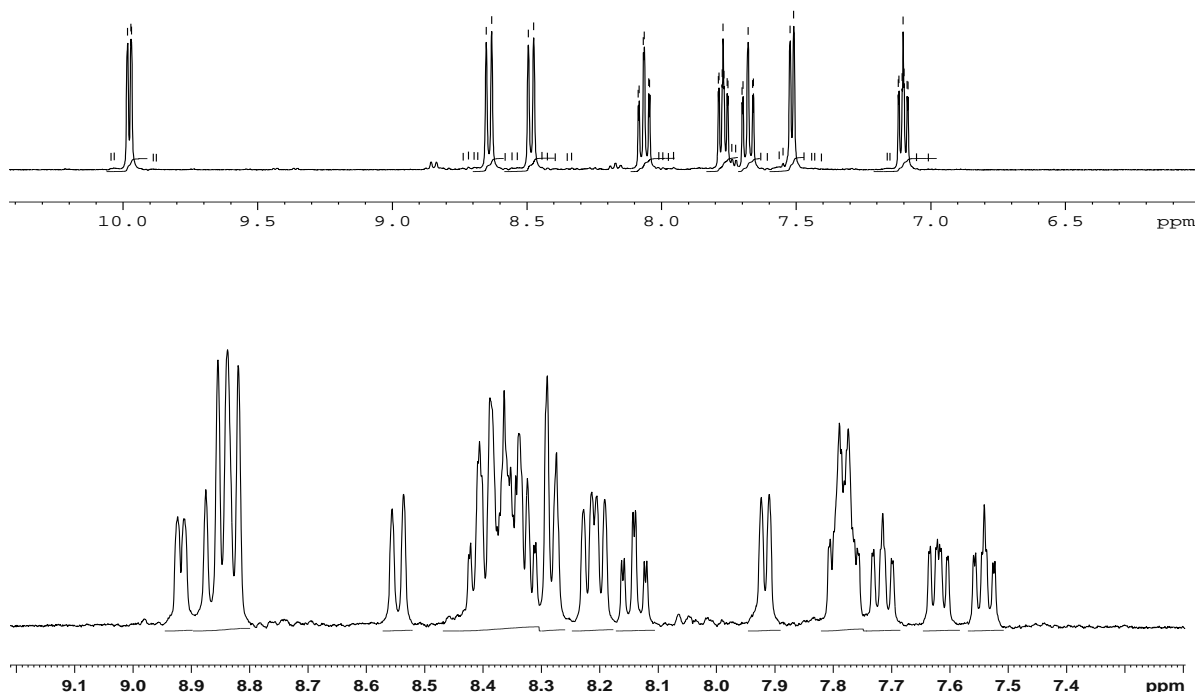


**Figure 3.11:**  $^1\text{H}$ NMR spectra for  $[\text{Ru}(\text{bpy})_2\text{Cl}_2]$  and  $[\text{Ru}(\text{bpy})_2\text{bpt}]^+$  carried out in DMSO at 298K.

#### 3.3.4. $^1\text{H}$ NMR Spectroscopy.

NMR was employed here as a structural characterization technique for the free ligand, rhenium (I) and ruthenium (II) mono- and di-nuclear complexes. It is used extensively in this thesis in the structural elucidation and identification of compounds, reaction monitoring and determination of purity. Proton assignments were made with the use of a 2D-COSY spectrum where possible and all spectra are calibrated to the relevant solvent peak.

Interpretations of the dinuclear complexes described here became difficult at times due to the high number of protons present. Deuteration of the bipyridyl ligand was carried out on some mononuclear and dinuclear complexes in order to simplify structural assignment where ever possible. This lead to the removal of the bipyridyl protons which left the proton signals of the remaining ligands available for assignment. Figure 3.12 below shows the structures of the free ligands and the NMR assignment, while Table 3.1 indicates the chemical shifts in ppm, while Figure 3.13 shows the NMR spectra obtained.

### 3.3.4.1 $^1\text{H}$ NMR of Free Ligands.

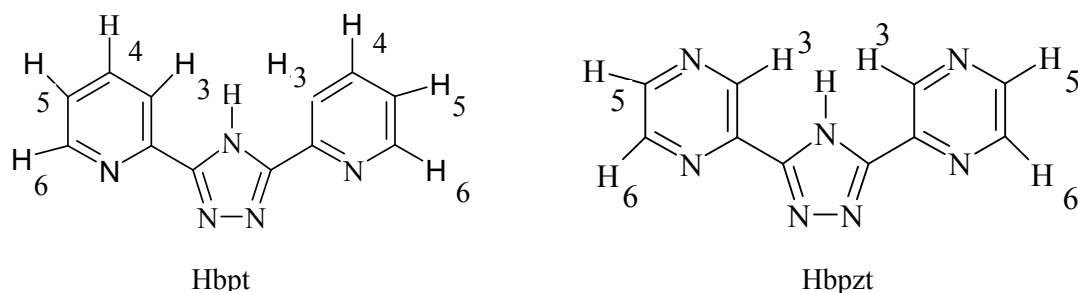


**Figure 3.12:** Labeling of the triazole ligands for  $^1\text{H}$  NMR assignment.

Ligand	H <sub>3</sub>	H <sub>4</sub>	H <sub>5</sub>	H <sub>6</sub>
Hbpt	8.15	7.98	7.50	8.75
Hbpzt	9.36	-	8.68	8.75

**Table 3.1:** Chemical shifts in ppm of the ligand protons measured in DMSO.

The NMR results obtained for the free ligands are uncomplicated and splitting patterns observed are as expected. Due to the symmetry of the free ligands only half the number of signals are observed as the protons are equivalent. For theazole ligands shown above the position of the H<sub>6</sub> proton, located next to the nitrogen, is found farthest downfield due to the shielding effect of the nitrogen. H<sub>4</sub> and H<sub>5</sub> of Hbpt and dptd are seen as multiplets and are located further upfield than the H<sub>6</sub> protons. In the Hbpzt ligand the H<sub>5</sub> and H<sub>6</sub> protons were found to overlap between 8.6 and 8.8 ppm, this is similar to the results reported by Hage *et al.*<sup>7</sup> while the proton signal for H<sub>3</sub> on the pyrazine ligand is located furthest downfield at 9.36 ppm. This NMR data will be used to aid in the assignment of the mononuclear and dinuclear complexes that follow.



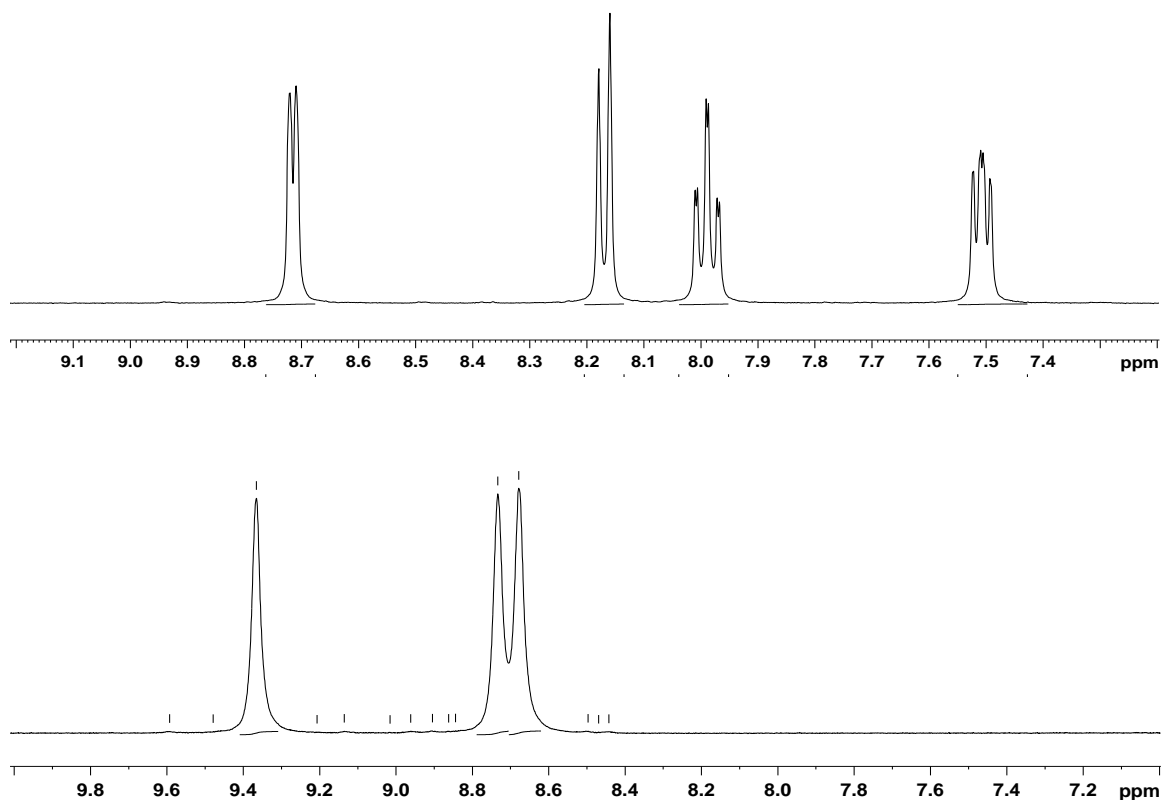


**Figure 3.13:**  $^1\text{H}$  NMR spectra for the Hbpt (top) and Hbpzt (bottom) carried out in DMSO at 298K.

The NMR results obtained for the free ligands are uncomplicated and splitting patterns observed are as expected. Due to the symmetry of the free ligands only half the number of signals are observed as the protons are equivalent. For theazole ligands shown above the position of the  $\text{H}_6$  proton, located next to the nitrogen, is found farthest downfield due to the shielding effect of the nitrogen.  $\text{H}_4$  and  $\text{H}_5$  of Hbpt and dptd are seen as multiplets and are located further upfield than the  $\text{H}_6$  protons. In the Hbpzt ligand the  $\text{H}_5$  and  $\text{H}_6$  protons were found to overlap between 8.6 and 8.8 ppm, this is similar to the results reported by Hage *et al.*<sup>8,9</sup> while the proton signal for  $\text{H}_3$  on the pyrazine ligand is located furthest downfield at 9.36 ppm. This NMR data will be used to aid in the assignment of the mononuclear and dinuclear complexes that follow.

### 3.3.4.2 $^1\text{H}$ NMR of Complexes.

#### 3.3.4.2.1 Complexes Containing Hbpt

The  $^1\text{H}$  NMR spectra of the complexes under discussion in this section are compared to that of the free ligands and relevant publications of known complexes. Complexes containing Hbpt will be discussed first followed by Hbpzt. The NMR spectrum of  $[\text{Ru}(\text{bpy})_2\text{bpt}]^+$  has been well documented<sup>2,3,7,8,9,14</sup> and is extremely complex. Hbpt is an asymmetric ligand forming N2 and N4 isomers upon coordination with ruthenium(II) as shown in Figure 3.14 below. The  $^1\text{H}$  NMR spectra obtained for these complexes gives rise to a more complicated spectrum in the aromatic region than that previously observed for the free ligands. However due to the nature of coordination there is a clear difference between the bound and unbound pyridine of the bpt ligand.

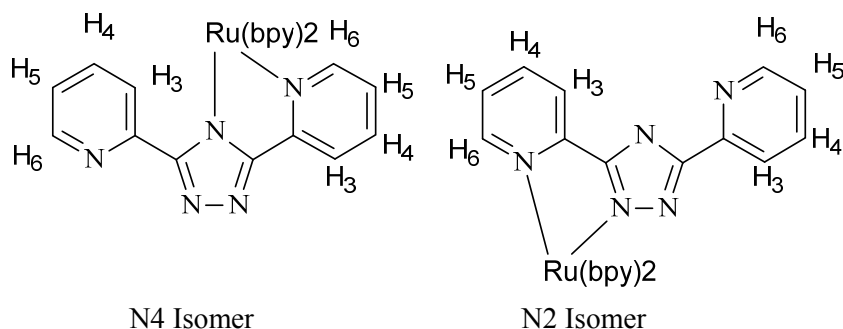


**Figure 3.14:** Structure of the N2/N4 isomers of  $[\text{Ru}(\text{bpy})_2\text{bpt}]^+$

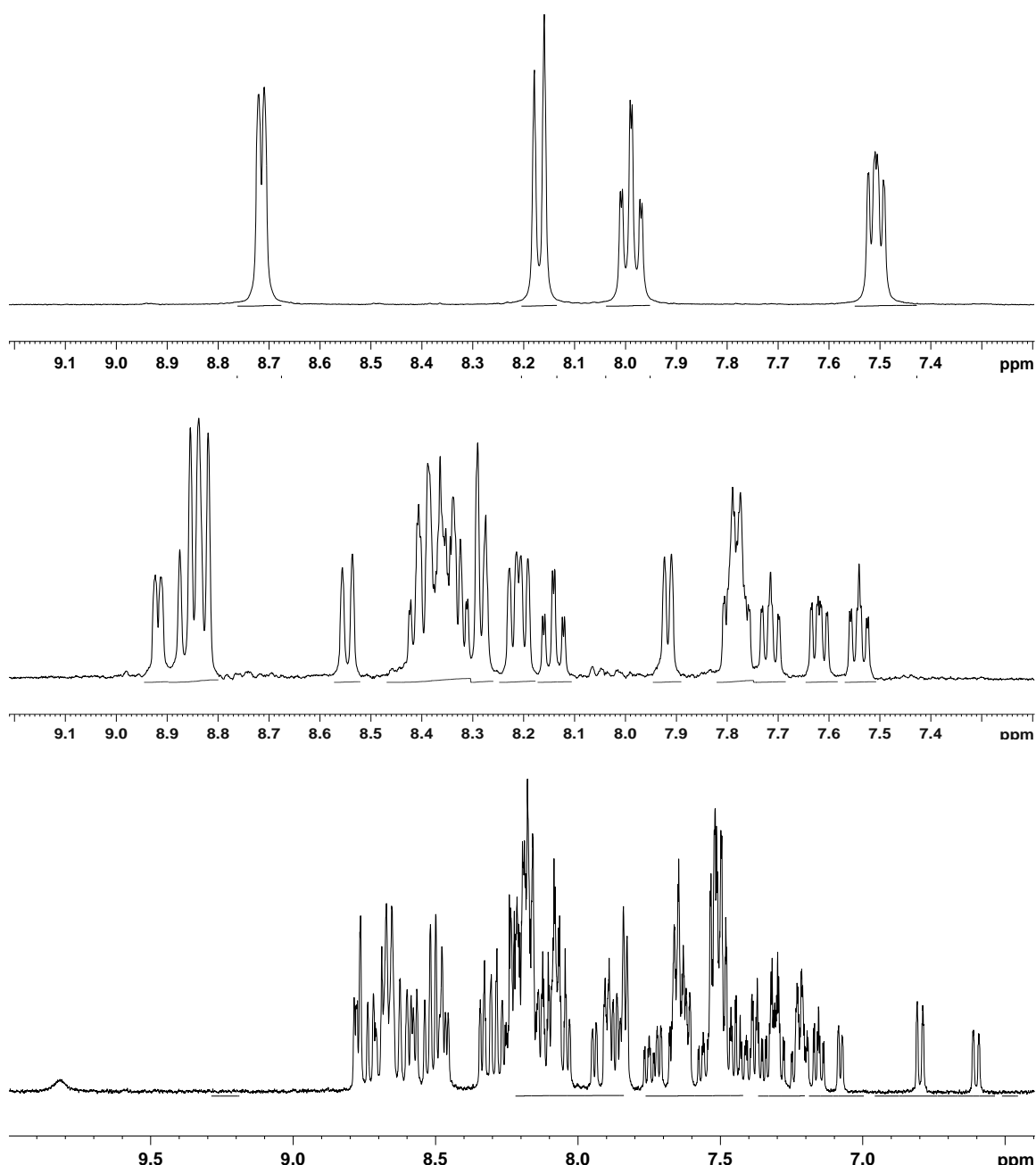


**Figure 3.15:**  $^1\text{H}$  NMR spectrum for Hbpt ligand (top),  $[\text{Ru}(\text{bpy})_2\text{bpt}]^+$  (middle) and  $[\{\text{Ru}(\text{bpy})_2\}_2\text{bpt}]^{3+}$  (bottom) carried out in DMSO at 298K.

Figure 3.15 above shows the numbering of the bpt<sup>−</sup> protons of the mononuclear ruthenium (II) complex, while Table 3.2 below details the chemical shift values. The bpy protons occur in the range expected and will not be further discussed here. Firstly the mononuclear complexes of bpt<sup>−</sup> containing Ru (II) and Re(I) will be discussed followed by the subsequent dinuclear complexes. Due to the nature of coordination of metal center to free ligand, the symmetry of the Hbpt previously observed, becomes lowered splitting the degeneracy and increasing the number of

protons signals in the aromatic region, this can be seen in Figures 3.14 and in 3.15 above in the mononuclear spectrum. The NMR data for these protons are reported as coordinated ring and free ring in Table 3.2 below.

	ppm			
	H3	H4	H5	H6
<b>Hbpt</b>	8.15	7.98	7.5	8.75
<b>[Ru(bpy)<sub>2</sub>bpt]<sup>+</sup></b>				
Ring A (co-ord)	8.54	8.29	7.62	7.91
Ring B (free)	8.43	8.11	7.54	8.92
bpy	8.81 - 8.89	8.18 - 8.21	7.69 - 7.71	8.37 - 8.31
<b>[Re(CO)<sub>3</sub>Cl(Hbpt)]</b>				
Ring A (co-ord)	8.42	8.26	7.52	8.78
Ring B (free)	8.40	8.22	7.52	9.05
<b>[(Ru(bpy)<sub>2</sub>)<sub>2</sub>bpt]<sup>3+</sup></b>	7.85	8.36	7.13	8.58
<b>[(Re(CO)<sub>3</sub>Cl)<sub>2</sub>(Hbpt)]</b>	8.25	8.25	7.68	9.02
<b>[Ru(bpy)<sub>2</sub>(bpt)Re(CO)<sub>3</sub>Cl]</b>				
<b>]</b>	8.09	7.43	6.74	8.38

**Table 3.2:** Chemical shifts in ppm obtained for Hbpt, [Ru(bpy)<sub>2</sub>(bpt)]<sup>+</sup>, [(Ru(bpy)<sub>2</sub>)<sub>2</sub>(bpt)]<sup>3+</sup>, [Re(CO)<sub>3</sub>Cl(Hbpt)], [(Re(CO)<sub>3</sub>Cl)<sub>2</sub>(Hbpt)] and [Ru(bpy)<sub>2</sub>(bpt)Re(CO)<sub>3</sub>Cl]<sup>+</sup> measured in DMSO at 298 K.

A clear observation of the effect of complexation is shown by the H6 bpt<sup>-</sup> proton for [Ru(bpy)<sub>2</sub>bpt]<sup>+</sup>. The metal bound H6 proton experiences changes in electron density due to the presence of the metal centre and adjacent bpy protons. This ring current of the adjacent bpy has a deshielding effect on the H6 proton resulting in a strong upfield shift from 8.92 ppm (free ring) to 7.91 ppm (co-ord). This is due to the presence of the bpy proton which decreases the applied magnetic field experienced at the nucleus of the H6 bpt<sup>-</sup> proton resulting in a lower frequency observed. The presence of the large metal centre also has a shielding effect on neighbouring protons which would result in an upfield shift of the protons in closest proximity.

The results obtained above in general, are in agreement to those previously reported by Hage and co-workers.<sup>8,9,17</sup> A shift of 1+ ppm can be observed due to the effect of the differing deuteriated solvents used for NMR analysis. Those reported by Hage are recorded in deuteriated acetone where as DMSO was the solvent of choice here.

The remaining proton assignment for the H3, H4 and H5 protons of the bpt<sup>-</sup> ligand were assigned with the use of a 2D- COSY and previously reported spectra.<sup>2,3,7,8</sup> Comparison of the deuteriated and non deuteriated spectra also greatly assisted in the assignment of the proton signals. A general shift can be observed from the free Hbpt protons to those located within the Ru (II) mononuclear complex which is reported to be due to the through space interactions between the bpy protons and those of the bpt<sup>-</sup> ligand.

The rhenium mononuclear complex of Hbpt has a much less complicated spectrum than that of the Ru monomer, due to the lack of the bpy protons. Assignment of the proton signals in the rhenium (I) complex was carried out by comparison with the spectra obtained for the free ligand. Again here the symmetry of the complex is reduced upon complexation of Re(CO)<sub>3</sub>Cl moiety resulting in the individual signals observed for free ring and coordinated ring of the triazole ligand. The H6 proton is again observed furthest downfield at 9.05 ppm (free) / 8.78 ppm (coord) due to the presence of the N atom and the Re (I) centre which is in agreement with previous publications of rhenium (I) bipyridine complexes.<sup>2,30</sup> The doublet furthest downfield at 8.78 ppm as the H<sub>6</sub> proton of the coordinated Hbpt the signals for the H<sub>3</sub>, H<sub>4</sub> and H<sub>5</sub> protons were then assigned accordingly. Unlike the ruthenium monomer [Re(CO)<sub>3</sub>Cl(Hbpt)] gave rise to no isomers in either the NMR or IR spectra.

Upon coordination of the second Re(CO)<sub>3</sub>Cl fragment to [Re(CO)<sub>3</sub>Cl(Hbpt)] the symmetry of the complex is reinstated and the number of proton signals observed are reduced as seen in Figure 3.16 below. Here proton H<sub>3</sub> and H<sub>4</sub> are seen to overlap as a multiplet at 8.25 ppm. H<sub>6</sub> is again seen as farthest downfield at 9.02 ppm with H<sub>5</sub> furthest upfield at 7.68 ppm. In progressing to the dinuclear [(Ru(bpy)<sub>2</sub>)<sub>2</sub>bpt]<sup>3+</sup> the spectra becomes more complicated due to the presence of the bipyridine protons, and the presence of geometrical isomers shown in Figure 3.14. The proton signals of [(Ru(bpy)<sub>2</sub>)<sub>2</sub>bpt]<sup>2+</sup> have obtained much attention<sup>3,7,8,9</sup> resulting in reported detailed characterization which greatly assisted in the assignment of this complicated spectra. The isomers observed are due to the orientations of the bipyridine rings but the formation of diastereoisomers of [(Ru(bpy)<sub>2</sub>)<sub>2</sub>(bpt)]<sup>3+</sup>. These separated isomers can be observed in Figure 3.16 below.

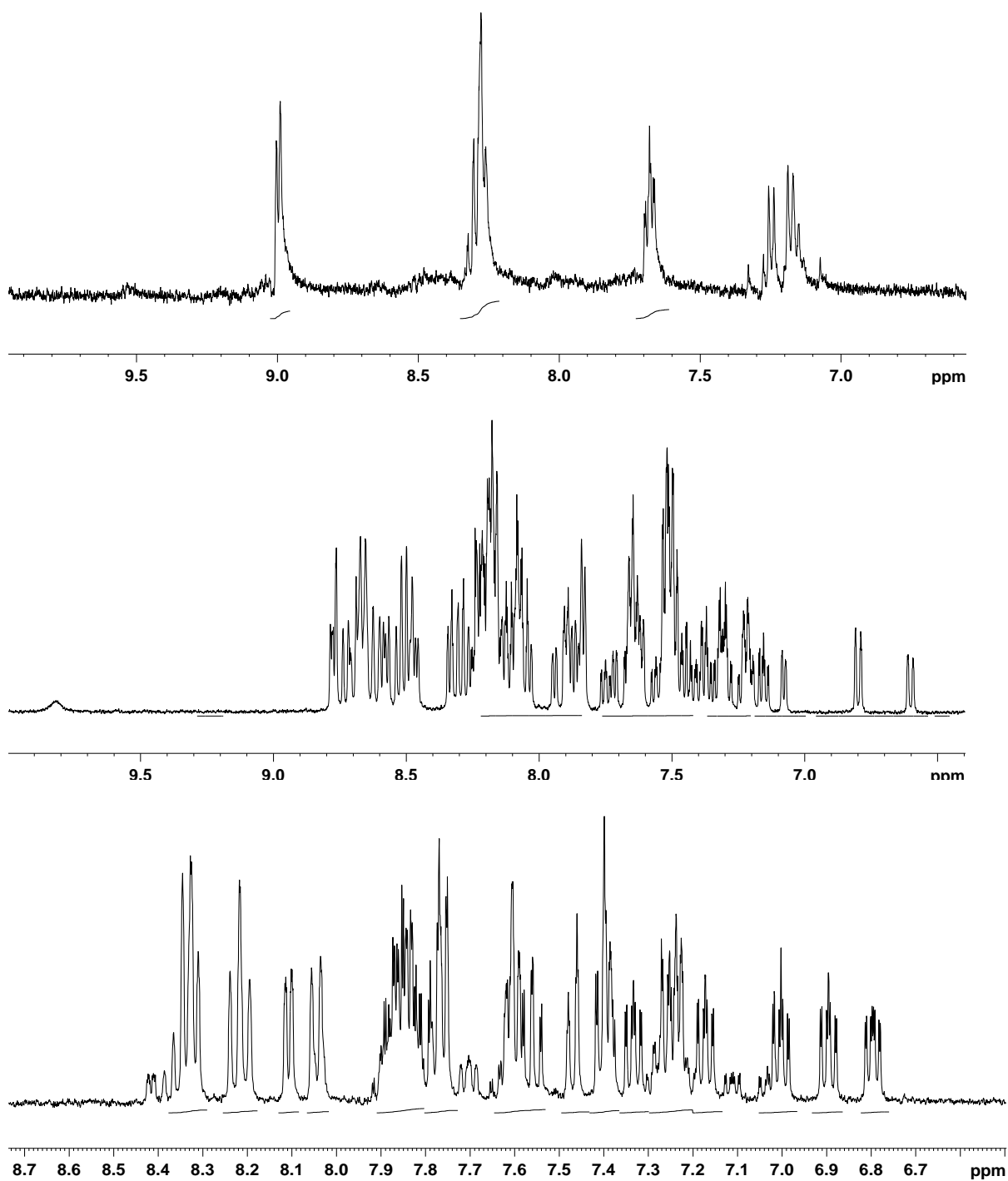


**Figure 3.16:**  $^1\text{H}$  NMR spectra for  $[(\text{Re}(\text{CO})_3\text{Cl})_2(\text{Hbpt})]$  (top) ,  $[(\text{Ru}(\text{bpy})_2)_2\text{bpt}]^{2+}$  (middle) and  $[\text{Ru}(\text{bpy})_2(\text{bpt})\text{Re}(\text{CO})_3\text{Cl}]^+$  (bottom) carried out in DMSO at 298K.

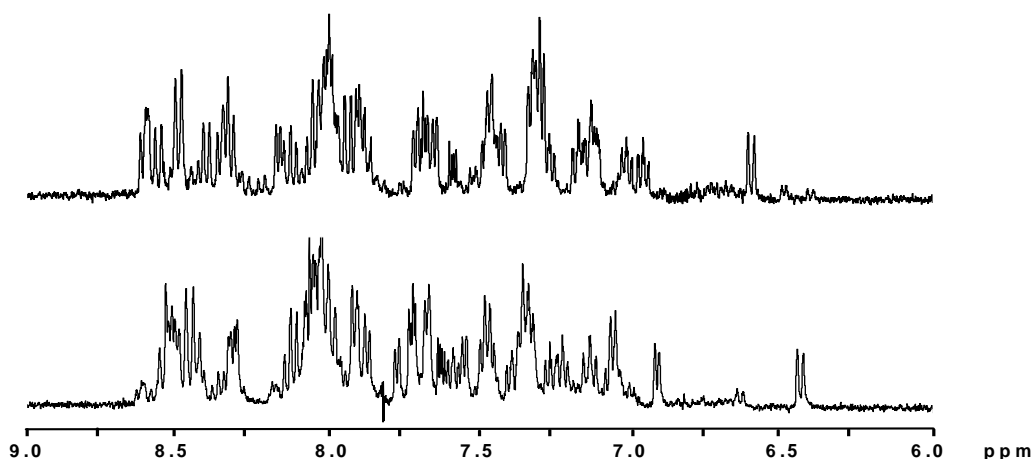


**Figure 3.17:**  $^1\text{H}$ NMR spectra obtained for fraction A (top) and B (bottom) of  $[(\text{Ru}(\text{bpy})_2)_2\text{bpt}]^{3+}$  in  $d_3$ -acetonitrile at 298K.

The heteronuclear complex  $[\text{Ru}(\text{bpy})_2(\text{bpt})\text{Re}(\text{CO})_3\text{Cl}]^+$  also gives rise to isomers as can be seen in Figure 3.14 above indicated by the protons at 6.78 ppm and 6.91 ppm, as observed previously in the homonuclear Ru (II) complex. Upon coordination of the  $\text{Re}(\text{CO})_3\text{Cl}$  moiety to the  $[\text{Ru}(\text{bpy})_2\text{bpt}]^+$  there is a characteristic shift upfield for all of the protons observed. Here the resonances of the triazole protons bound to the Re metal center are found at a higher chemical shift value than those of the ruthenium bound ring this has also been previously observed by C. Brennan.<sup>2</sup> The spectrum of  $[\text{Ru}(\text{bpy})_2(\text{bpt})\text{Re}(\text{CO})_3\text{Cl}]^+$  is complex and the values assigned to the proton signals have been carried out with the aid of the deuteriated complex  $[\text{Ru}(d\text{-bpy})_2(\text{bpt})\text{Re}(\text{CO})_3\text{Cl}]^+$  signals reported by C. Brennan<sup>2</sup> and are reported previously in Table 3.5.

#### 3.3.4.2.2 Complexes Containing Hbpzt.

Hbpzt coordinates to the ruthenium centre in the same way as the Hbpt complexes giving rise to the N2 and N4 isomers (Figure 3.14). Table 3.3 that follows contains the NMR data obtained for these systems, the bipyridine protons occur as expected and so will not be discussed in detail here.

	ppm		
	H <sub>3</sub>	H <sub>5</sub>	H <sub>6</sub>
<b>Hbpzt</b>	9.36	8.68	8.75
<b>[Ru(bpy)<sub>2</sub>bpzt]<sup>+</sup></b>			
Ring A (free)	9.34	7.58	8.55
Ring B (co-ord)	8.86	7.21	8.22
 bpy	8.48 - 8.60	7.43 - 7.62	8.13 - 8.78
<b>[(Ru(bpy)<sub>2</sub>)<sub>2</sub>bpzt]<sup>3+</sup></b>			
ligand (Hbpzt)	7.82	7.92	9.16
<b>[(Re(CO)<sub>3</sub>Cl)<sub>2</sub>(Hbpzt)]</b>	9.38	8.82	8.79

**Table 3.3:** Chemical shifts in ppm obtained for Hbpzt, [Ru(bpy)<sub>2</sub>(bpzt)]<sup>+</sup>, [(Ru(bpy)<sub>2</sub>)<sub>2</sub>(bpzt)]<sup>3+</sup> and [(Re(CO)<sub>3</sub>Cl)<sub>2</sub>(Hbpzt)] measured in DMSO at 298 K.

Figure 3.18 below shows the spectra for [Ru(bpy)<sub>2</sub>(bpzt)]<sup>+</sup>, [(Ru(bpy)<sub>2</sub>)<sub>2</sub>(bpzt)]<sup>3+</sup> and [(Re(CO)<sub>3</sub>Cl)<sub>2</sub>(Hbpzt)] measured in DMSO at 298 K. Here the free ligand proton furthest downfield is the H3 proton at 9.36 ppm due to the presence of the two neighboring N substituents of the pyrazine ring. Upon complexation with the ruthenium centre this shifts to 8.86 ppm for the co-ordinated pyrazine ring of the triazole, which is a similar effect to that reported by Hage<sup>7</sup> and Browne.<sup>23</sup> The H6 proton again here demonstrates the greatest effect of complexation with an upfield shift of approximately 0.5 ppm. Again the loss of symmetry is displayed upon formation of the Ru(II) mononuclear complex, with an increase in the number of proton signals for the free and coordinated triazole rings.



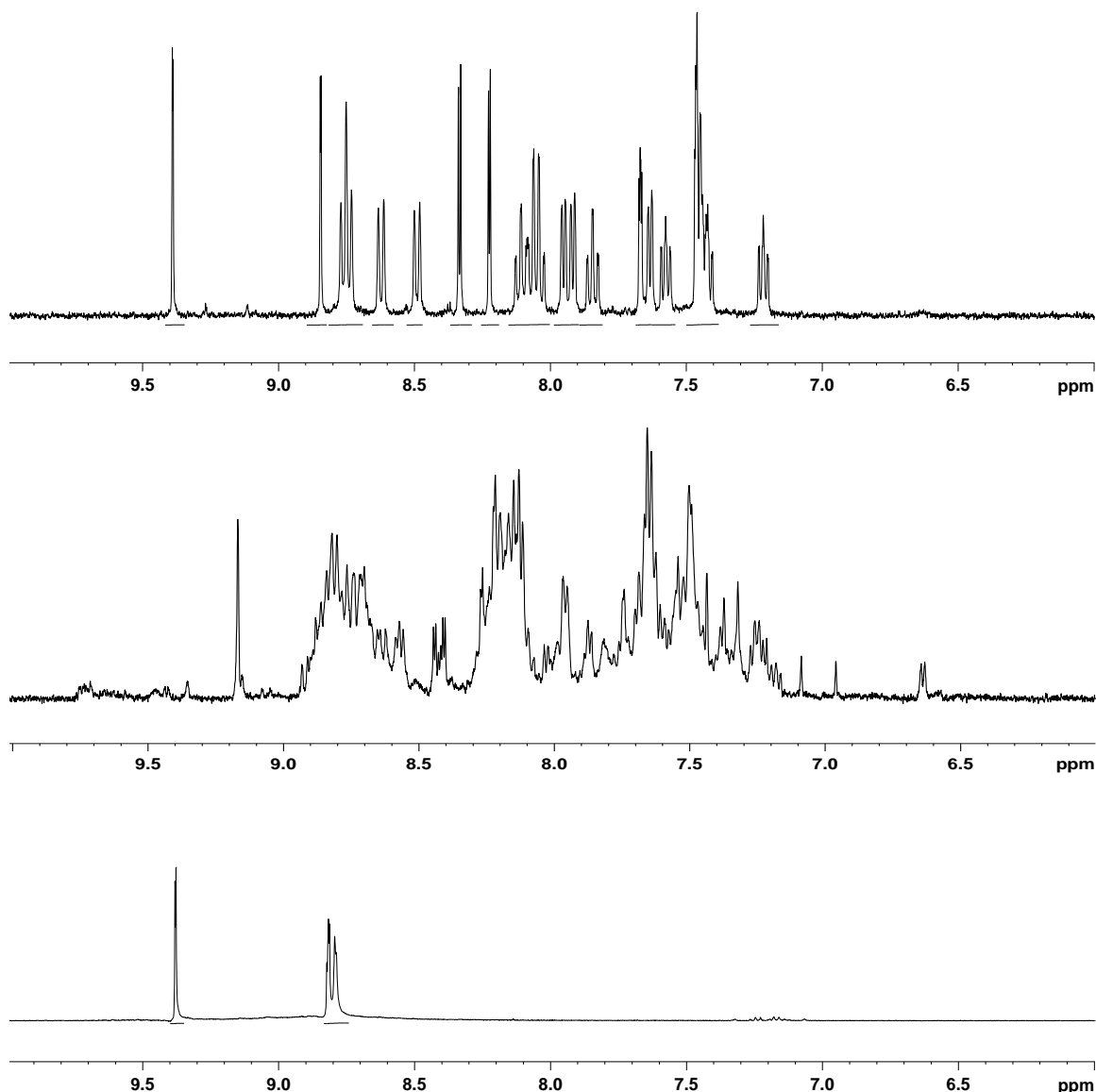


**Figure 3.18:**  $^1\text{H}$  NMR spectrum for  $[(\text{Ru}(\text{bpy})_2\text{bpzt})]^+$  (top),  $[(\text{Ru}(\text{bpy})_2)_2\text{bpzt}]^{3+}$  (middle) and  $[(\text{Re}(\text{CO})_3\text{Cl})_2(\text{bpzt})]$  (bottom) in DMSO at 298K.

The complexity of the homonuclear ruthenium dimer spectra in Figure 3.18 indicates the progression from the mononuclear to the dinuclear complex. Here the presence of isomers is also clearly seen due to the signals at 6.62 ppm and 6.97 ppm, though separation of these isomers has not yet been completed by HPLC the method of separation underway is that previously reported by Hughes *et al.*<sup>19,23</sup> Again the proton signals here for the bpzt<sup>-</sup> ligand were compared to those reported by Hage and Browne. As both the ligand rings are now coordinated the proton signals are expected to be similar. However, this is not the case with regard to the H6 proton. The H6 proton was previously observed at 8.22 ppm for the coordinated ring of  $[\text{Ru}(\text{bpy})_2\text{bpzt}]^+$  but is now seen at 9.16 ppm for  $[(\text{Ru}(\text{bpy})_2)_2\text{bpzt}]^{3+}$ , this is thought

to be due to the presence of the electronegative nitrogen atoms. The H3 protons of bpzt<sup>-</sup> shift upfield as expected due to the presence of the second metal centre in progressing from [Ru(bpy)<sub>2</sub>bpzt]<sup>+</sup> to [(Ru(bpy)<sub>2</sub>)<sub>2</sub>bpzt]<sup>3+</sup>. The H5 proton has a slight downfield shift which again may be due to the presence of the electronegative nitrogen atoms.

Attempts of Re (I) coordination to the free Hbpzt ligand has always resulted in the dinuclear [(Re(CO)<sub>3</sub>Cl)<sub>2</sub>bpzt] complex described in Figure 3.18 bottom spectra, the mononuclear complex has not been obtained. The proton signals for the H5 and H6 protons almost overlap, but the symmetry of the complex is maintained with only half the number of signals visible in the NMR spectra similar to the Hbpt rhenium dinuclear complex previously discussed. These can be further separated with the use of different deuteriated solvents. On complexation of the Re (I) centre with the bpzt<sup>-</sup> ligand, a shift downfield is observed for the H3, H5 and H6 protons, which is similar to that observed for [(Re(CO)<sub>3</sub>Cl)<sub>2</sub>bpt] which could be due to the presence and proximity of the two electronegative chlorine atoms.

### 3.4.2 Infra-red Spectroscopy.

IR spectra of the azole complexes were carried out in the CO vibrational region (2200 – 1700 cm<sup>-1</sup>) of the IR spectrum in dichloromethane. All of the complexes show CO bands, which are summarised in Table 3.4 below.

Complex		$\nu_{\text{CO}}$ (cm <sup>-1</sup> )	
[Re(CO) <sub>3</sub> (bpy)Cl]	2024	1990	1898
[Re(CO) <sub>3</sub> (Hbpt)Cl]	2020	1914	1894
[Re(CO) <sub>3</sub> Cl] <sub>2</sub> Hbpt]	2023	1916	1902
[{Re(CO) <sub>3</sub> Cl} <sub>2</sub> Hbpzt]	2025	1922	-
[Ru(bpy) <sub>2</sub> (bpt)Re(CO) <sub>3</sub> Cl] <sup>+</sup>	2022	1913	1896

**Table 3.4:** IR data for the carbonyl stretching obtained for the triazole complexes synthesised in this section carried out in DCM

$[\text{Re}(\text{CO})_3(\text{bpy})\text{Cl}]$  was prepared as a reference compound as the carbonyl bands in the IR spectrum are well understood<sup>24</sup> and is typical of complexes of the type  $[\text{Re}(\text{CO})_3(\text{L})\text{X}]$ . From Table 3.8 above it can be seen that the IR spectra for the above compounds shows that the facial isomer for the triazole complexes is dominant. This implies that the triazole ligands are bound in the equatorial region, trans to two carbonyls with a chlorine atom in the axial position and a CO in the final axial position. This is best described in Figure 3.16 below. These complexes are known to possess  $C_s$  symmetry<sup>25, 26</sup> where the IR bands from highest to lowest wavenumbers ( $\text{cm}^{-1}$ ), are assigned the symmetry labels  $A'$  (1),  $A''$  and  $A'$  (2) respectively.<sup>27</sup>

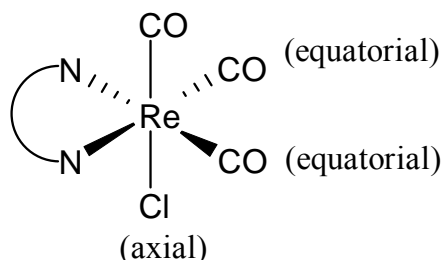


**Figure 3.19:** Example of the facial coordination of the rhenium tricarbonyl complexes discussed where N-N denotes the bidentate ligand.

The IR spectral results for the complexes  $[\text{Re}(\text{CO})_3(\text{Hbpt})\text{Cl}]$ ,  $[\text{Re}(\text{CO})_3\text{Cl}]_2\text{Hbpt}$  and  $[\text{Ru}(\text{bpy})_2(\text{bpt})\text{Re}(\text{CO})_3\text{Cl}]^+$  agree with those previously obtained.<sup>28</sup> Upon coordination of the second rhenium centre on the Hbpt ligand there appears to be very little spectral changes with the CO bands moving only slightly higher in frequency ( $3 \text{ cm}^{-1}$  for the  $A'$  (1) band). Upon coordination of the ruthenium metal center there is a slight shift from  $2020$  to  $2022 \text{ cm}^{-1}$  for the  $A'$  (1) band. Figure 3.20 below details a typical example for the IR spectra obtained for the Hbpt complexes.

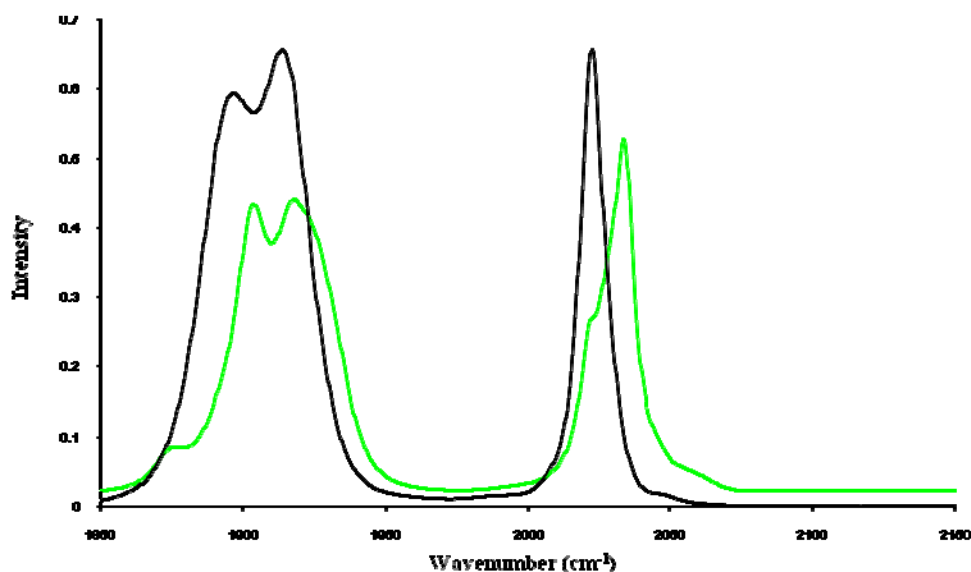


**Figure 3.20:** I.R. of  $[(\text{Re}(\text{CO})_3)_2\text{Hbpt}]$  (green) and  $[\text{Ru}(\text{bpy})_2(\text{bpt})\text{Re}(\text{CO})_3\text{Cl}]$  (black) in DCM at 298K.

IR spectra obtained for the complexes  $[(\text{Re}(\text{CO})_3\text{Cl})_2(\text{Hbpt})]$  and  $[\text{Ru}(\text{bpy})_2(\text{dptd})\text{Re}(\text{CO})_3\text{Cl}]$  show a combined  $A''$  and  $A'$  (2) bands, as a broad peak in the  $1900\text{ cm}^{-1}$  region, an example of which can be seen in Figure 3.21 below. Shoulders in both spectra can be seen at  $1907\text{ cm}^{-1}$  for  $[(\text{Re}(\text{CO})_3\text{Cl})_2(\text{Hbpt})]$  and  $1894\text{ cm}^{-1}$  for  $[\text{Ru}(\text{bpy})_2(\text{dptd})\text{Re}(\text{CO})_3\text{Cl}]$  indicating the formation of the fac isomer but due to solvent effects and solubility of these complexes, this band could not be resolved. Previous results for rhenium complexes containing bppz (2,3-bis(2-pyridyl)pyrazine) and ddpq (6,7-dimethyl-2,3-di(2-pyridyl)quinoxaline) ligands have also shown  $A''$  and  $A'$  (2) unresolved bands which may indicate the presence of isomers

29,30

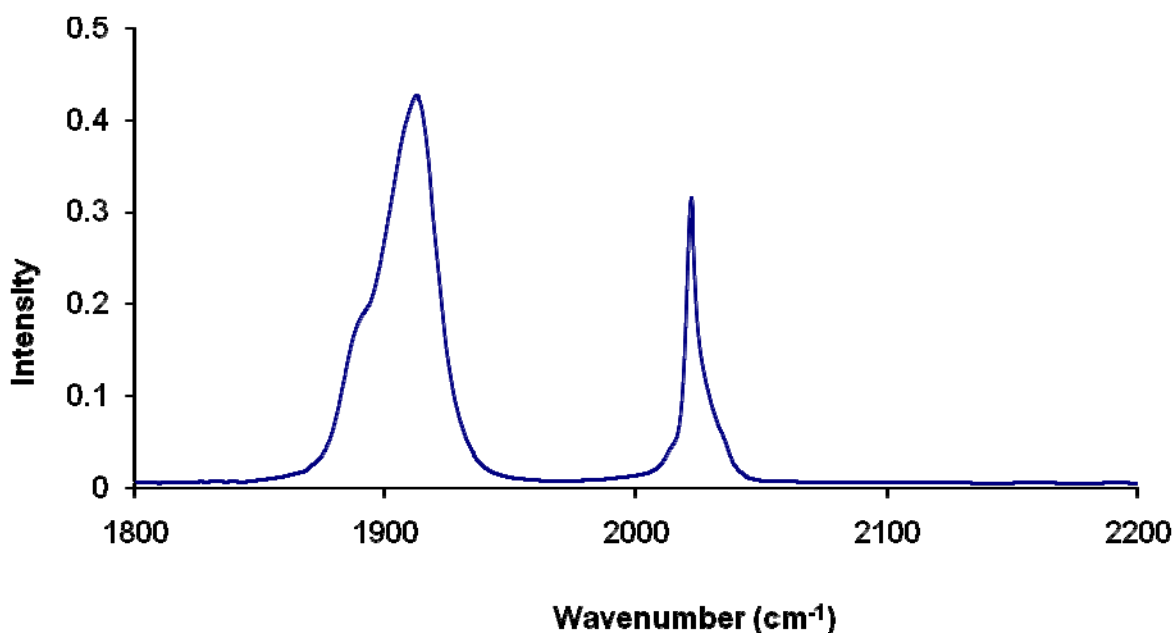


**Figure 3.21:** I.R. of  $[Ru(bpy)_2(dptd)Re(CO)_3Cl]$  in DCM at 298K.

Comparison of the results obtained for the  $[Re(CO)_3Cl]_2Hbpt$  and  $[Re(CO)_3Cl]_2Hbpzt$  show small shifts in the IR bands to higher frequencies. Pyrazine triazoles are known to exhibit stronger  $\pi$ -acceptor abilities than  $bpt^-$  and  $\pi^*$ -level of the pyrazine analogue reside at lower energies to that of the pyridine analogue. The CO band shift observed for the pyrazine complex could be attributed to the competition between the carbonyl and pyrazine ligands for  $\pi$ -electron density from the Rhenium metal centre.

### 3.4.3 Absorption Spectroscopy.

Examination of the electronic properties of the complexes prepared in this chapter, offers an insight to the effects of the bridging ligand on the ruthenium and rhenium metal centres. The introduction of electron withdrawing / donating ligands on the metal complexes can introduce a CM3CT band shift which can be monitored by absorption spectroscopy. The intensity of absorption at a particular wavelength can also indicate how effective the ruthenium moiety is as the light harvesting species of the photocatalyst.

Analysis of the complexes in this chapter were carried out in aerated acetonitrile at 298K, in the 200 nm – 800 nm region of the UV-vis spectrum. Absorption and

emission data for the complexes prepared in this section are shown in Table 3.5 below. Ruthenium complexes will be discussed first followed by rhenium, homonuclear and heteronuclear complexes.

Complex	$\lambda_{\text{abs}}$ (nm)	$\epsilon$ (LM <sup>-1</sup> cm <sup>-1</sup> )x 10 <sup>3</sup>	$\lambda_{\text{em}}$ (nm)
[Re(CO) <sub>3</sub> (bpy)Cl]	390	3.5	600
[Re(CO) <sub>3</sub> (Hbpt)Cl]	360	4.0	540
[Re(CO) <sub>3</sub> Cl] <sub>2</sub> Hbpt]	319	7.8	533
[{Re(CO) <sub>3</sub> Cl} <sub>2</sub> Hbpzt]	334	5.2	589
[Ru(bpy) <sub>3</sub> ] <sup>2+</sup>	452	12.9	612
[Ru(bpy) <sub>2</sub> bpt] <sup>+</sup>	480	10.8	677
[(Ru(bpy) <sub>2</sub> ) <sub>2</sub> bpt] <sup>2+</sup>	450	20.2	637
[Ru(bpy) <sub>2</sub> (bpt)Re(CO) <sub>3</sub> Cl] <sup>2+</sup>	440	15.8	640
[Ru(bpy) <sub>2</sub> bpzt] <sup>+</sup>	450	10.5	650
[(Ru(bpy) <sub>2</sub> ) <sub>2</sub> bpzt] <sup>2+</sup>	455	22.4	680

**Table 3.5:** Combined emission and absorption data carried out in aerated acetonitrile at 298K.

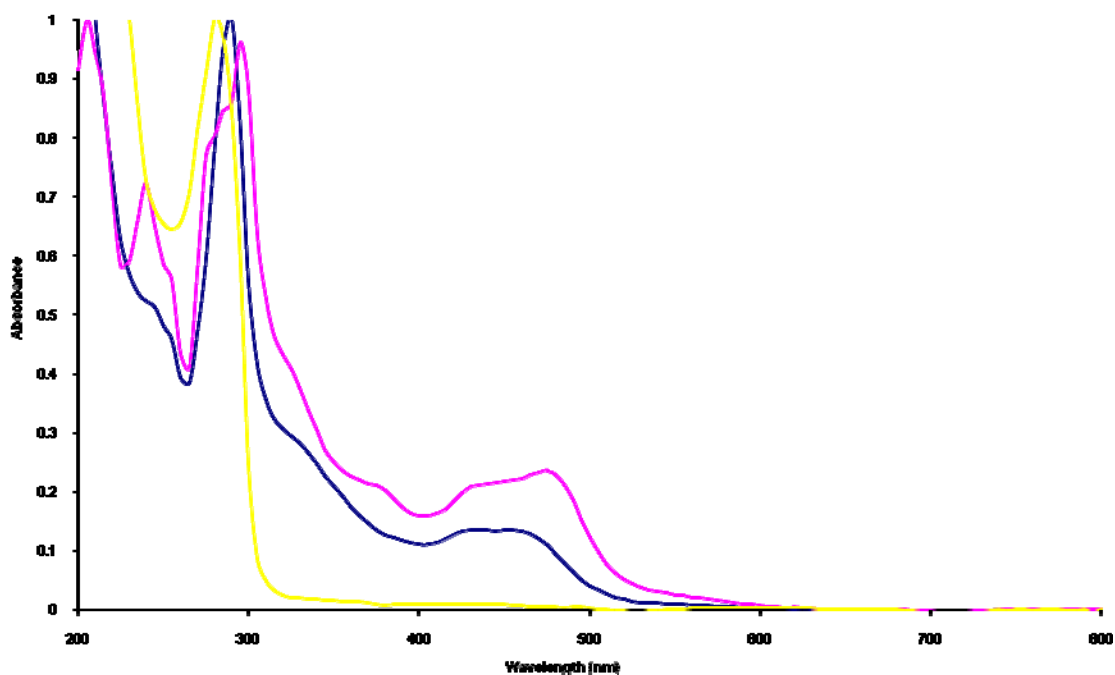


**Figure 3.22** Absorption spectra of Hbpt (yellow),  $[\text{Ru}(\text{bpy})_2\text{bpt}]^+$  (Pink) and  $[\text{Ru}(\text{bpy})_2(\text{bpt})\text{Re}(\text{CO})_3\text{Cl}]^+$  (blue) carried out at room temperature in acetonitrile.

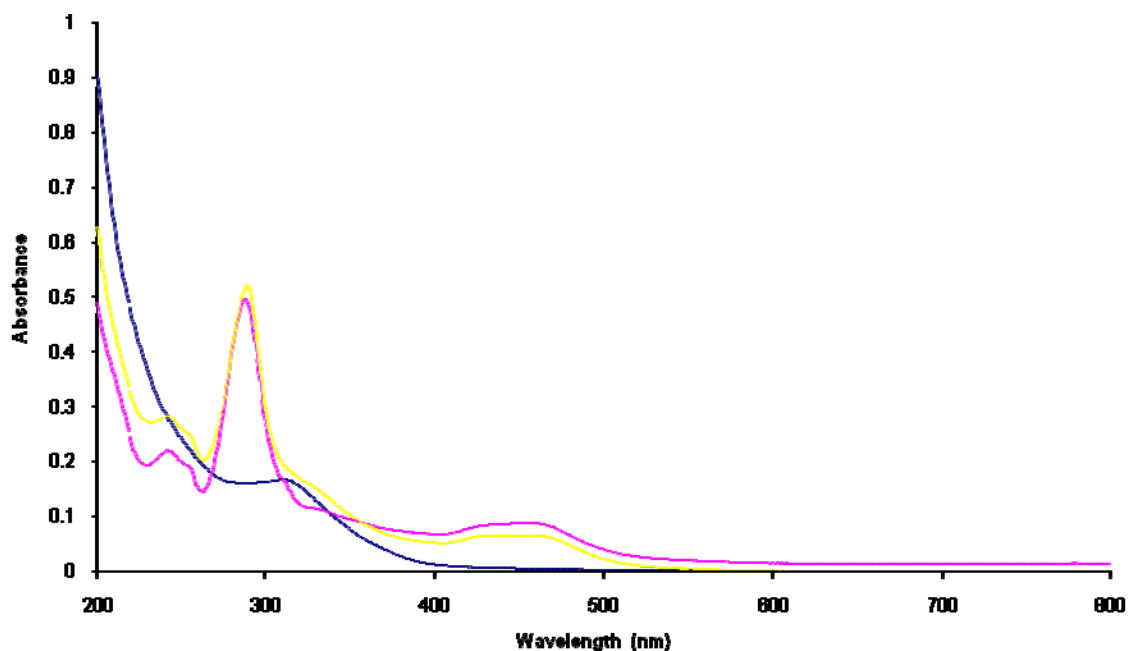


**Figure 3.23** Absorption spectra  $[\text{Ru}(\text{bpy})_2]_2\text{bpt}]^+$  (Pink) and  $[\text{Ru}(\text{bpy})_2(\text{bpt})\text{Re}(\text{CO})_3\text{Cl}]^+$  (yellow) and  $[\text{Re}(\text{CO})_3\text{Cl}]_2\text{Hbpt}]$  (blue) at room temperature in acetonitrile.

Figures 3.22 and 3.23 above display typical absorption spectra obtained from the complexes containing the Hbpt ligand. The extinction coefficients and CM3CT bands for the  $[\text{Ru}(\text{bpy})_2\text{bpt}]^+$  and  $[\text{Ru}(\text{bpy})_2)_2\text{bpt}]^{3+}$  agree with those previously reported by Hage and co-workers.<sup>8</sup> Comparison of the CM3CT bands of these complexes to the reference material  $[\text{Ru}(\text{bpy})_3]^{2+}$ , the CM3CT band is red shifted from 452 nm to 480 nm. This corresponds to the bpt<sup>-</sup> ligand donating electron density towards the metal center due to its strong  $\sigma$  – donor ability.<sup>31</sup> Upon complexation with another ruthenium center the electron density is spread between the two metal centers resulting in an CM3CT band that is blue shifted at 450 nm.

Similar CM3CT shifts are seen for the rhenium mononuclear and dinuclear complexes containing Hbpt. The CM3CT bands for  $[\text{Re}(\text{CO})_3(\text{Hbpt})\text{Cl}]$  and  $[\text{Re}(\text{CO})_3\text{Cl}]_2\text{Hbpt}]$  occur at 360 nm and 319 nm respectively, and concur with those previously reported. Comparing these to the reference  $[\text{Re}(\text{CO})_3(\text{bpy})\text{Cl}]$  with an CM3CT band at 390 nm, indicating an increased energy gap between the HOMO and LUMO of  $[\text{Re}(\text{CO})_3(\text{Hbpt})\text{Cl}]$  compared to the reference material. Coordination of the second  $\text{Re}(\text{CO})_3\text{Cl}$  fragment increases the energy gap between the HOMO and LUMO levels by stabilization of the HOMO level which results in the increased absorption of the CM3CT band. Carbonyl  $\pi^*$  transitions are masked here for the rhenium tricarbonyl species as the  $\text{Re} \rightarrow \pi^*(\text{CO})$  are known to be weak in intensity<sup>32</sup> and are overshadowed by the intense  $\pi \rightarrow \pi^*$  transitions of the triazole ligand. These bands can be seen in  $[\text{Re}(\text{CO})_5\text{Cl}]$  located at 280 nm in dichloromethane.

On comparison of the homonuclear complexes  $[(\text{Ru}(\text{bpy})_2)_2\text{bpt}]^{3+}$  and  $[(\text{Re}(\text{CO})_3\text{Cl})_2\text{Hbpt}]$  to that of the heteronuclear complex  $[\text{Ru}(\text{bpy})_2(\text{bpt})\text{Re}(\text{CO})_3\text{Cl}]^+$ , the CM3CT band at 440 nm is allocated to the  $\text{Ru} \rightarrow \pi^*(\text{bpt}^-)$ , as the  $\text{Re} \rightarrow \pi^*(\text{bpt}^-)$  in the mononuclear and dinuclear complexes occur at higher energies. The decrease in intensity of the band at 440 nm can also be attributed to the sharing of the negative charge of the triazolate anion upon coordination of the  $\text{Re}(\text{CO})_3\text{Cl}$  fragment to the ruthenium mononuclear complex. A rhenium CM3CT band in the heteronuclear complex is hard to distinguish as this band coincides with the intense LC transitions, which are commonly found in ruthenium bpt<sup>-</sup> complexes.<sup>3,7</sup>



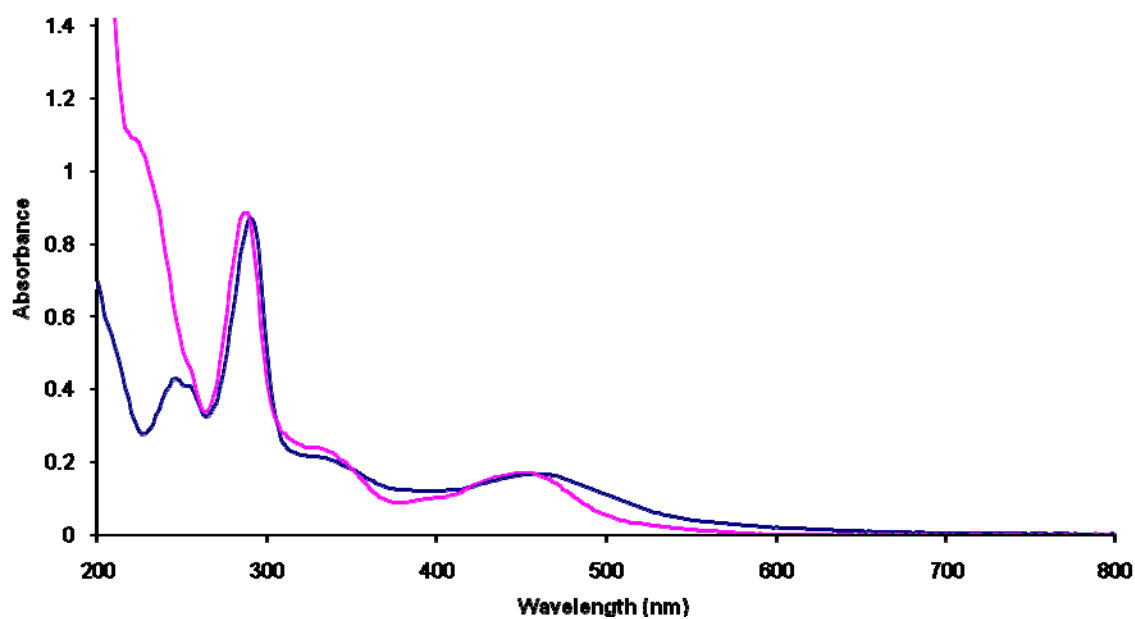


**Figure 3.24** Absorption spectra  $[(Ru(bpy)_2)_2bpzt]^{3+}$  (Pink) and  $[Ru(bpy)_2(bpzt)]^+$  (blue) and at room temperature in acetonitrile.

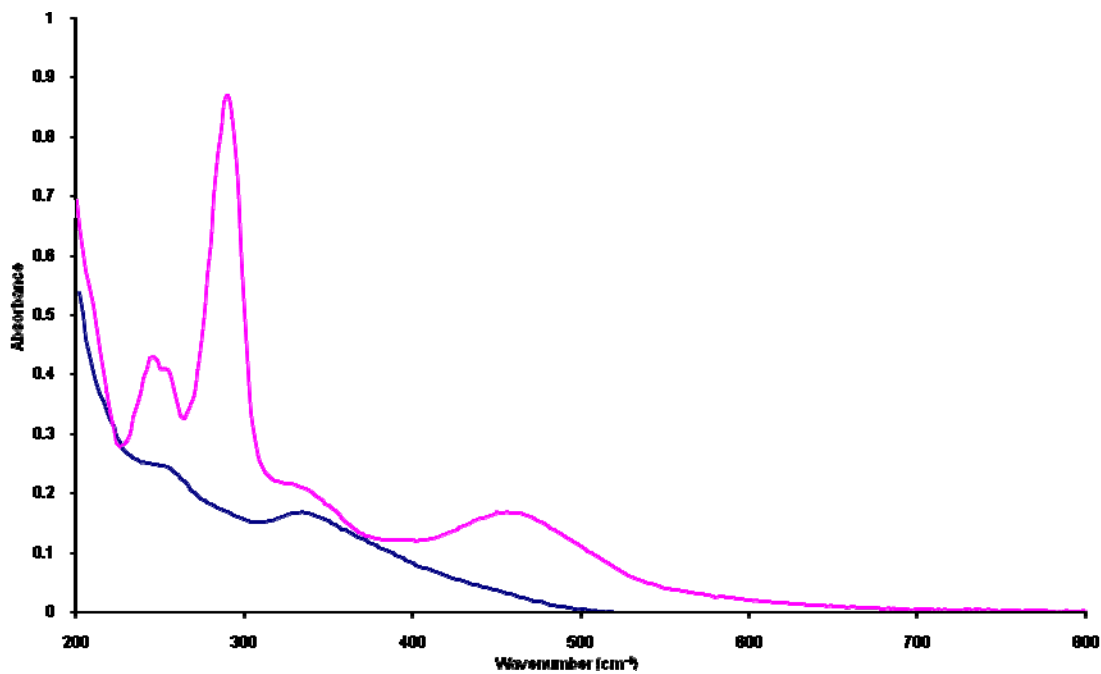


**Figure 3.25** Absorption spectra  $[(Ru(bpy)_2)_2bpzt]^{3+}$  (Pink) and  $[Re(CO)_3CL]_2Hbpzt$  (blue) and at room temperature in acetonitrile.

Figures 3.24 and 3.25 details the spectra obtained for the Ru(II) / Re(I) complexes containing the Hbpzt ligand. Pyrazine triazoles are known to exhibit stronger  $\pi$ -acceptor abilities than bpt<sup>-</sup> and  $\pi^*$ - level of the pyrazine analogue reside at lower energies to that of the pyridine analogue. Comparison of the spectra obtained for the complexes [Ru(bpy)<sub>2</sub>bpzt]<sup>+</sup> and [(Ru(bpy)<sub>2</sub>)<sub>2</sub>bpzt]<sup>3+</sup> to the reference [Ru(bpy)<sub>3</sub>]<sup>2+</sup>, show no significant shifts of the CM3CT bands at 450 nm and 455 nm respectively which would agree with the  $\pi$  – acceptor quality of the ligand. Though comparison of [Ru(bpy)<sub>2</sub>bpzt]<sup>+</sup> to [Ru(bpy)<sub>2</sub>bpt]<sup>+</sup>, the CM3CT transition is blue shifted from 480 nm to 450 nm indicating the weaker  $\sigma$  – donor ability of the pyrazine triazoles compared to the pyridine triazoles. This trend agrees with that previously reported by Hage *et al.*<sup>7,8,9</sup> Upon complexation of the second ruthenium there is a red shift from 450 nm to 455 nm, this is due to the lowering of the LUMO  $\pi^*$  level of the bpzt<sup>-</sup>. Comparison of the CM3CT bands of the dinuclear [(Re(CO)<sub>3</sub>Cl)<sub>2</sub>Hbpzt] complex to [(Re(CO)<sub>3</sub>Cl)<sub>2</sub>Hbpt] show a red shift of 15 nm which is expected due to the increased  $\pi$ - acceptor strength of the pyrazine triazole ligand. Similar trends are reported by Yoblinski and co-workers for pyrazine containing complexes.

### 3.4.4 Emission Spectroscopy

Emission analysis offers information about the <sup>3</sup>CM3CT and when combined with absorbance measurements can describe excited state geometries.<sup>33</sup> After the intake of energy an electron has moved from the HOMO to LUMO orbitals. Emission is then seen as the energy is rereleased from either the lowest singlet (fluorescence) or triplet state (phosphorescence). Table 3.5 above details the  $\lambda_{em}$  observed for the complexes under discussion in this chapter. All analysis was carried out at 298K in acetonitrile. All complexes exhibit strong emission bands between 580 and 720 nm. Complexes containing the Ru(bpy)<sub>2</sub> fragment will be compared to the reference [Ru(bpy)<sub>3</sub>]<sup>2+</sup> while those containing Re(CO)<sub>3</sub>Cl fragment will be compared to [Re(CO)<sub>3</sub>Cl(bpy)].

Figure 3.29 below shows typical emission spectra obtained for the complexes containing the Hbpt ligand. Comparing [Ru(bpy)<sub>2</sub>(bpt)]<sup>+</sup> to [Ru(bpy)<sub>3</sub>]<sup>2+</sup> there is a red shift of 25 nm from 612 to 637 nm. This trend agrees with those previously reported by Hage *et al.*<sup>7,8,9</sup> and further indicates the  $\sigma$ - donor ability of the Hbpt

ligand. In passing from the mononuclear  $[\text{Ru}(\text{bpy})_2(\text{bpt})]^+$  to the dinuclear  $[(\text{Ru}(\text{bpy})_2)_2(\text{bpt})]^{3+}$  there is a blue shift of 40 nm from 677 to 637 nm respectively. The addition of the second metal centre causes the negative charge on the triazole to be delocalized over both centers, therefore reducing the electron donating ability of the Hbpt ligand. This results in the red shift observed in both the absorption and emission spectra. Emission spectra for  $[\text{Ru}(\text{bpy})_2(\text{bpt})]^+$  and  $[(\text{Ru}(\text{bpy})_2)_2\text{bpt}]^{3+}$  are well understood and the bands observed at 677 and 637 nm are assigned as a decay from the  $^3\text{CM3CT}$  state and is known to be a bpy based emission.<sup>2,3</sup>

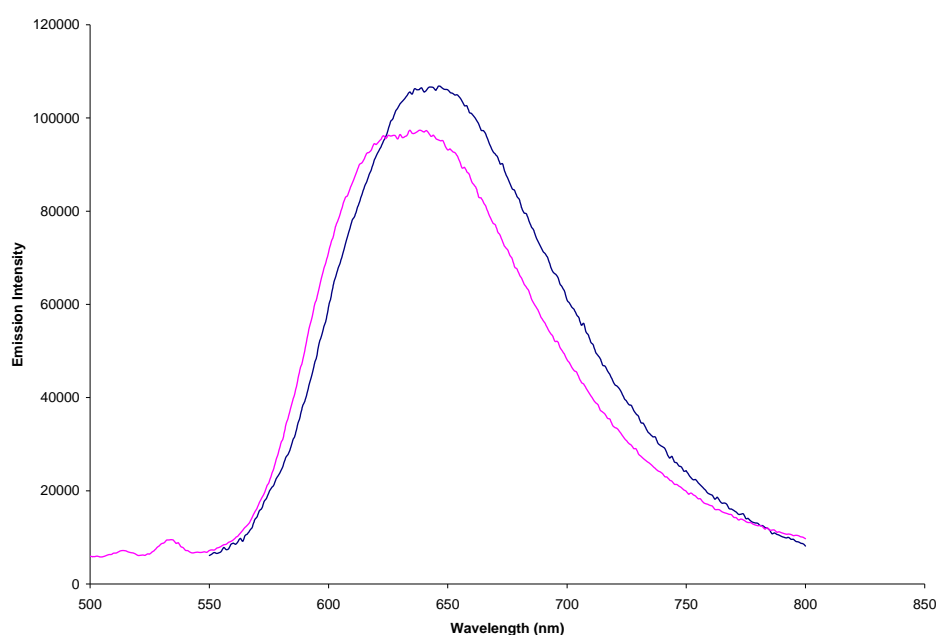


**Figure 3.26:** Emission spectrum of  $[\text{Ru}(\text{bpy})_2(\text{bpt})\text{Re}(\text{CO})_3\text{Cl}]^+$  (pink) and  $[(\text{Ru}(\text{bpy})_2)_2\text{bpt}]^{3+}$  (blue) in aerated acetonitrile solution.  $\lambda_{\text{exc}} = 460 \text{ nm}$ .

In progressing from  $[\text{Re}(\text{CO})_3\text{Cl}(\text{Hbpt})]$  to  $[(\text{Re}(\text{CO})_3\text{Cl})_2(\text{Hbpt})]$  a blue shift is also seen in progressing from the mononuclear to the dinuclear complex, 540 to 533 nm respectively, resulting in the stabilization of the  $t_{2g}$  energy level and an increase in the  $t_{2g} - ^3\text{CM3CT}$  energy gap. Both of these transitions are assigned as  $^3\text{CM3CT}$  bands and agree with results previously obtained.<sup>2</sup> Comparison of these emission bands to those obtained for  $[\text{Re}(\text{CO})_3\text{Cl}(\text{bpy})]$  at 600 nm show a blue shift in emission, this is in trend with previous publications where the addition of electron

donating groups near the metal centre cause a blue shift of the emission maxima.<sup>26,24,29</sup>

The heteronuclear complex  $[\text{Ru}(\text{bpy})_2(\text{bpt})\text{Re}(\text{CO})_3\text{Cl}]^+$  was found to have an emission maxima of 640 nm in acetonitrile at 298K. This emission appears to be based around the ruthenium fragment of the dinuclear complex as the previously described rhenium mononuclear and dinuclear complex have shown emission maxima around 540 nm. Upon coordination of the  $\text{Re}(\text{CO})_3\text{Cl}$  to the  $[\text{Ru}(\text{bpy})_2(\text{bpt})]^+$  there is a blue shift from 677 to 640 nm much like the homonuclear dimers of Hbpt. Indicating that again the electron density around the metal centres is shared resulting in the stabilisation of the  $t_{2g}$  level. These results are in keeping with the Ru(II)/Re(I) photocatalysts developed by *Ishitani and co-workers*<sup>34</sup> **Error! Bookmark not defined.** where the Ru/Re binuclear complex containing the bridging ligands 1,3-bis(4'-methyl-[2,2']bipyridinyl-4-yl)propan-2-ol (bpyC3-bpy) and 4-methyl-4'-[1,10]phenanthroline-[5,6-*d*]imidazol-4-methyl-4'-[1,10]phenanthroline-[5,6-*d*]imidazol-2-yl)bipyridine (mfibpy) showed emission maxima of 631nm and 646 nm respectively.

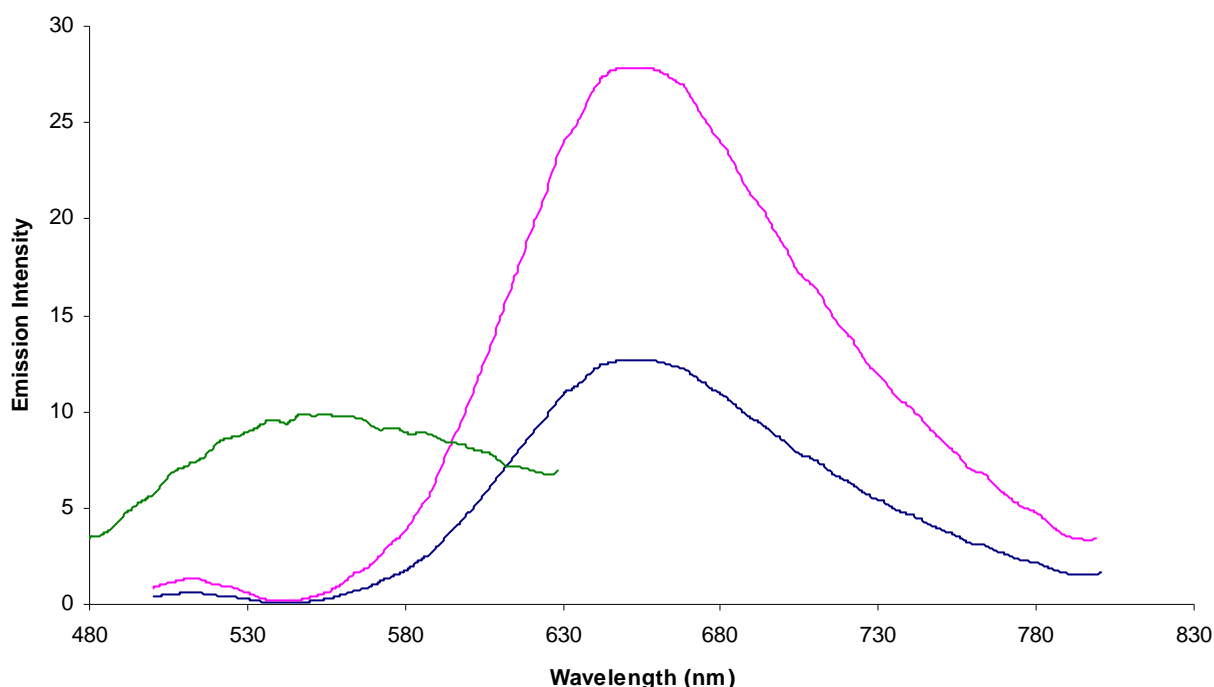


**Figure 3.27:** Emission spectrum of  $[\text{Ru}(\text{bpy})_2(\text{bpzt})]^+$  (blue),  $[\text{Ru}(\text{bpy})_2]_2\text{bpzt}^{3+}$  (pink) and  $[\text{Re}(\text{CO})_3\text{Cl}]_2\text{Hbpt}$  (green) in aerated acetonitrile solution.

Figure 3.27 details the emission spectra obtained for  $[\text{Ru}(\text{bpy})_2(\text{bpzt})]^+$ ,  $[(\text{Ru}(\text{bpy})_2)_2(\text{bpzt})]^{3+}$  and  $[\text{Re}(\text{CO})_3\text{Cl}(\text{Hbpzt})]$  and exhibit emission maxima of 650 nm, 680 nm and 589 nm respectively. For the ruthenium complexes these emissions are in agreement with those reported by Hage *et al.*<sup>7,8,9</sup>. As previously described Hbpzt is a weaker  $\sigma$ -donor than Hbpt but is a better  $\pi$ -acceptor.<sup>79</sup> This can be seen by the shift in emission maxima of the complexes containing Hbpzt when compared to Hbpt. There is a blue shift of 27 nm in passing from  $[\text{Ru}(\text{bpy})_2(\text{bpt})]^+$  (677 nm) to  $[\text{Ru}(\text{bpy})_2(\text{bpzt})]^+$  (650 nm). As Hbpzt is a weaker  $\sigma$  electron donor, the electron density around the Ru metal center in the pyrazine is reduced compared to that of the pyridine analogue due to the lower lying  $\pi^*$  orbital of the pyrazine ligand. Coordination of a second ruthenium metal to bpzt<sup>-</sup> leads to a red shift of 30 nm from 650 nm to 680 nm as can be seen in Table 3.5 previously. This is in contrast to that of the pyridine analogues where a blue shift is seen on coordination of a second ruthenium centre. Previously it was seen that the second metal center caused a stabilization of the  $t_{2g}$  energy level, thus increasing the  $t_{2g} - {}^3\text{CM}3\text{CT}$  energy gap resulting in a blue shift. Here a lowering of the  $\pi^*$  level of bpzt<sup>-</sup> is observed. These results agree with those previously reported for ruthenium complexes containing the Hbpzt ligand and other pyrazine based ligands<sup>35,19,36</sup>

The  $[(\text{Re}(\text{CO})_3\text{Cl})_2(\text{Hbpzt})]$  has a broad, featureless band whose position and shape are akin to previously reported rhenium carbonyl emitting complexes.<sup>37,38</sup> Comparison of  $[(\text{Re}(\text{CO})_3\text{Cl})_2(\text{Hbpzt})]$  (589 nm) to  $[(\text{Re}(\text{CO})_3\text{Cl})_2(\text{Hbpt})]$  (533 nm) shows a red shift of 56 nm. This again shows the  $\pi$ -acceptor qualities of the Hbpzt ligand over Hbpt. This also suggests a lower lying  $\pi^*$  orbital. Comparison of  $[(\text{Re}(\text{CO})_3\text{Cl})_2(\text{Hbpzt})]$  to the results reported for  $[\text{Re}(\text{CO})_3\text{Cl}(\text{dpp})]$  (where dpp = 2,2'-bipyrazine) by Cambron and co-workers<sup>39</sup> are interesting, the dimetallic  $[(\text{Re}(\text{CO})_3\text{Cl})_2(\text{dpp})]$  was found to be non emissive in fluid solution where the mononuclear pyrazine Re(I) complex was found to have an emission maxima at 670 nm in acetonitrile at room temperature. The red shift in the emission maxima of the dinuclear rhenium complex does follow a trend with the monodentate pyrazine triazoles previously reported by C. Brennan,<sup>2</sup> where the mononuclear

[Re(CO)<sub>3</sub>Cl(Hpztr)] was found to have an emission of 535 nm where the pyridine analogue has a maxima of 493 nm.

### **3.5 Conclusions**

This section describes the preparation and analysis of the complexes prepared for the purpose of reducing CO<sub>2</sub> catalytically. <sup>1</sup>HNMR spectroscopy detailed the formation of the complexes and the effects of the ligand protons upon complexation with a ruthenium or rhenium metal centre. IR analysis indicated that the rhenium (I) complexes prepared are all of the fac isomer due to the presence of the three carbonyl bands in the 1700cm<sup>-1</sup> - 2200 cm<sup>-1</sup> of the IR spectrum.

The effects of the bridging ligands Hbpt and Hbpzt were clearly seen in the IR, UV-vis and fluorescence measurements. Hbpzt was shown to be a better  $\pi$ -acceptor than Hbpt and dptd and results obtained are in agreement by those obtained by Hage *et al.*

Further synthetic studies are required to prepare the complexes [Re(CO)<sub>3</sub>Cl(Hbpzt)], [Re(CO)<sub>3</sub>Cl(dptd)] and [Ru(bpy)<sub>2</sub>(dptd)Re(CO)<sub>3</sub>Cl]<sup>2+</sup> to allow for comparison with the complexes already prepared. Lifetime measurements and excited state studies should be carried out to determine the location of the excited state in the dinuclear complexes obtained.

### **Biobibliography.**

- 
- <sup>1</sup> G. Denti, S. Campagna, S. Serroni, M. Ciano, V. Balzani, *J. Am. Chem. Soc.* **1992**, 114, 2944.
- <sup>2</sup> C. Brennan, Ph.D. Thesis, *Dublin City University*, Ireland, **2006**.
- <sup>3</sup> L. Cassidy, PhD Thesis, *Dublin City University*, **2008**.
- <sup>4</sup> Kalssen, D. M., Crosby, G. A., *J. Chem., Phys.*, 43, **1965**, 1498.
- <sup>5</sup> Crosby, G. A., Watts, R. J., *Science*, 170, **1970**, 1195.
- <sup>6</sup> Gafney, A. D., Adamson, A. W., *J. Am. Chem. Soc.*, 94, **1972**, 94, 8238.
- <sup>7</sup> R. Hage, Ph.D. Thesis, *Leiden University*, The Netherlands, **1991**.
- <sup>8</sup> R. Hage, A. H. J. Dijkhuis, J. G. Haasnoot, R. Prim, J. Reedijk, B. E. Buchanan, J. G. Vos, *Inorg. Chem.* 27, **1988**, 12, 2187.
- <sup>9</sup> R. Hage, J. G. Haasnoot, J. Reedijk, R. Wang, J. G. Vos, *Inorg. Chem.*, 30, **1991**, 3263.
- <sup>10</sup> J. Hawecker, J. M. Lehn, R. Ziessel, *J. Chem. Soc., Chem. Commun.* **1983**, 536.
- <sup>11</sup> O. Ishitani, M. W. George, T. Ibusuki, F. P. A. Johnson, K. Koike, K. Nozaki, C. Pac, J. J. Turner, J. R. Westwell, *Inorg. Chem.*, 33, **1994**, 4712.
- <sup>12</sup> B. P. Sullivan, T. J. Meyer, *Organometallics*, 5, **1986**, 1500.
- <sup>13</sup> J. Hawecker, J.-M. Lehn, R. Ziessel, *Helv. Chim. Acta*, 69, **1986**, 1990.
- <sup>14</sup> J. G. Vos, J. G. Haasnoot, G. Vos, *Inorg. Chim. Acta.*, 162, **1983**, 155.
- <sup>15</sup> W. R. Browne, C. M. O'Connor, C. Villani, J. G. Vos, *Inorg. Chem.*, 40, **2001**, 5461.
- <sup>16</sup> P. Passaniti, W. R. Browne, F. C. Lynch, D. Hughes, M. Nieuwenhuyzen, P. James, M. Maestri, J. G. Vos, *Dalton Trans.*, **2002**, 1740.
- <sup>17</sup> R. Hage, J. G. Haasnoot, H. A. Nieuwenhuis, J. Reedijk, D. J. A. de Ridder, J. G. Vos, *J. Am. Chem. Soc.*, 112, **1990**, 9245

- <sup>18</sup> B. P. Sullivan, D. J. Salmon, T. J. Meyer, *Inorg. Chem.*, **17**, **1978**, 3334.
- <sup>19</sup> C. G. Coates, T. E. Keyes, H. P. Hughes, P. M. Jayaweera, J. J. McGarvey, J. G. Vos, *J. Phys. Chem. A*, **102**, **1998**, 5013.
- <sup>20</sup> J. F. Geldard, F. Lions, *J. Org. Chem.*, **30**, **1965**, 318
- <sup>21</sup> G. Denti, S. Campagna, S. Serroni, M. Ciano, V. Balzani, *J. Am. Chem. Soc.* **114**, **1992**, 2944.
- <sup>22</sup> G. Denti, S. Serroni, S. Campagna, A. Juris, M. Ciano, V. Balzani, *In Perspectives in Coordination Chemistry*; A. F. Williams, C. Floriani, A. E. Merbach, Eds.; VCH: Basel, Switzerland, **1992**, p. 153.
- <sup>23</sup> W. R. Browne, C. M. O'Connor, H. P. Hughes, R. Hage, O. Walter, M. Doering, J. F. Gallagher, J. G. Vos *J. Chem. Soc. Dalton Trans.*, **2002**, 4048.
- <sup>24</sup> M. Wrighton, D. L. Morse, *J. Am. Chem. Soc.*, **96**, **1974**, 30, 4594.
- <sup>25</sup> L. W. Houk, G. R. Dobson, *Inorg. Chem.*, **5**, **1996**, 2119
- <sup>26</sup> S. L. Howell, K. C. Gordon, *J. Phys. Chem. A*, **110**, **2006**, 4880.
- <sup>27</sup> S. M. Fredricks, J. C. Luong, M. S. Wrighton, *J. Am. Chem. Soc.*, **101**, **1979**, 7415.
- <sup>28</sup> S. Rau, B. Schafer, D. Gleich, E. Anders, M. Rudlof, M. Friedrich, H. Górls, W. Henery, J. G. Vos, *Angew. Chem. Int. Ed.*, **45**, **2006**, 6125.
- <sup>29</sup> B. J. Yoblinski, M. Stathis, T. F. Guarr, *Inorg. Chem.*, **31**, **1992**, 5.
- <sup>30</sup> S. Van Wallendael, R. J. Shaver, D. P. Rillema, B. J. Yoblinski, M. Stathis, T. F. Guarr, *Inorg. Chem.*, **29**, **1990**, 1761.
- <sup>31</sup> S. Fanni, T. E. Keys, C. M. O'Connor, H. Hughes, R. Wang, J. G. Vos, *Coord. Chem. Rev.*, **2000**, 208.



- <sup>32</sup> G. L. Geoffry, M. S. Wrighton, *Academic Press: New York*, **1979**.
- <sup>33</sup> M. Klessinger, J. Michl, *Excited states and photochemistry of organic molecules*, **1995**.
- <sup>34</sup> B. Gholamkhash, H. Mametsuka, K. Koike, T. Tanabe, M. Furue, O. Ishitani, *Inorg. Chem*, 44, 2005, 2326.
- <sup>35</sup> H. Hughes, J. G. Vos, *Inorg. Chem.*, 34, **1995**, 4001.
- <sup>36</sup> W. R. Browne, N. M. O'Boyle, W. Henry, A. L. Guckian, S. Horn, T. Fett, C. M. O'Connor, M. Duati, L. De Cola, C. G. Coates, K. L. Ronayne, J. J. McGarvey, J. G. Vos, *J. Am. Chem. Soc.*, 127, **2005**, 1229.
- <sup>37</sup> A. Buris, S. Campagna, I. Bidd, J. M. Lehn, R. Ziessel, *Inorg. Chem.* 27, **1988**, 4007.
- <sup>38</sup> C. Creutz, H. Taube, *J. Am. Chem. Soc.*, 91, **1969**, 3988.
- <sup>39</sup> R. Ruminski, R. T. Cambron, *Inorg. Chem.*, 29, **1990**, 8.

## **Chapter 4: Synthetic Routes to $[\text{Ru}(\text{bpy})_2(\text{tpphz})\text{Re}(\text{CO})_3\text{Cl}](\text{PF}_6)_2$ .**

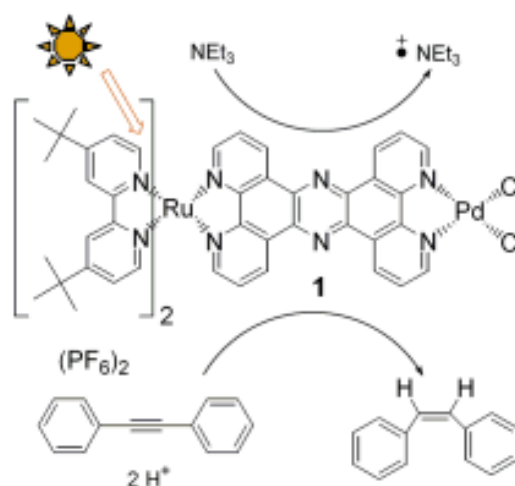
*The subject of the work presented in this chapter is the development of a synthetic pathway to prepare the dinuclear complex  $[\text{Ru}(\text{bpy})_2(\text{tpphz})\text{Re}(\text{CO})_3\text{Cl}](\text{PF}_6)_2$ . Synthesis and characterisation of the ruthenium (II) and rhenium (I) mononuclear complex intermediates are described. Preparation of the symmetric tetrapyrrodo[3,2-a:2',3':3'',2''-h:2''',3'''-j]phenazine (tpphz) ligand is discussed both as a free ligand and contained within mononuclear and dinuclear complexes.*

## 4.0 Introduction

The development of supramolecular assemblies for use as photocatalysts has received much attention throughout the years, as these assemblies allow for photoinduced electron and energy transfer processes under well defined geometries.<sup>1,2,3,4,5,6,7</sup> Of those complexes one particular bridging ligand, the symmetric tetrapyrido[3,2-a:2',3':3'',2''-h:2''',3'''-j]phenazine (tpphz) has received extensive attention and has been applied to areas such as molecular electronics<sup>8</sup>, DNA intercalators<sup>9</sup> and in the construction of rigid polymers<sup>10</sup> and dendrimers.<sup>11,12</sup>

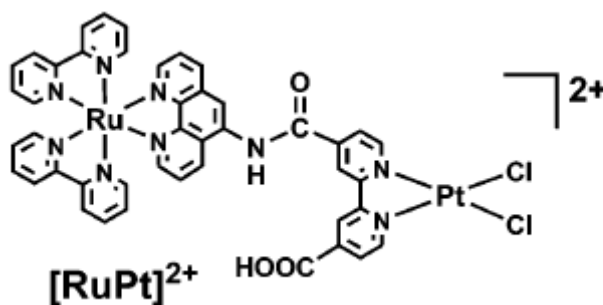
The reason for such an in depth study, is due to the rigidity of the complex when tpphz is used. Due to the high number of conjugated bonds within its structure, this ligand offers a rod like composition that is both longitudinally and torsionally rigid allowing a defined internuclear distance between the attached metal centres.<sup>13</sup> Such a defined orientation is desirable to increase the probability of communication between the metal centres. A reported consequence of this high degree of conjugation is the ability of the tpphz ligand, to act as an electron reservoir by storing an electron in the pyrazine midsection of its structure.<sup>14</sup>

One of the most successful photocatalysts in terms of its Hydrogen formation ability is a ruthenium/ palladium tpphz dimer ( $[\text{Ru}(\text{bpy})_2(\text{tpphz})\text{PdCl}_2]^{2+}$ ) by *Rau et al.* as shown in Figure 4.1 below.<sup>15</sup> For the formation of hydrogen, turnover numbers (TON) as high as 56 have been achieved using visible light ( $\lambda \geq 450$  nm) in acetonitrile using TEA (triethylamine) as a sacrificial donor to re-reduce the photocatalytically formed Ru(III) centre. These results also showed that the amount of hydrogen formed is highly dependant on the TEA concentration and the amount of time the photocatalyst is exposed to light the optimum of which was found to be 29 hours with 2 mol L<sup>-1</sup> of TEA.



**Figure 4.1:** Hydrogenation of Toluene to *cis*-stilbene using  $[\text{Ru}(\text{bpy})_2(\text{tpphz})\text{PdCl}_2]^{2+}$ .

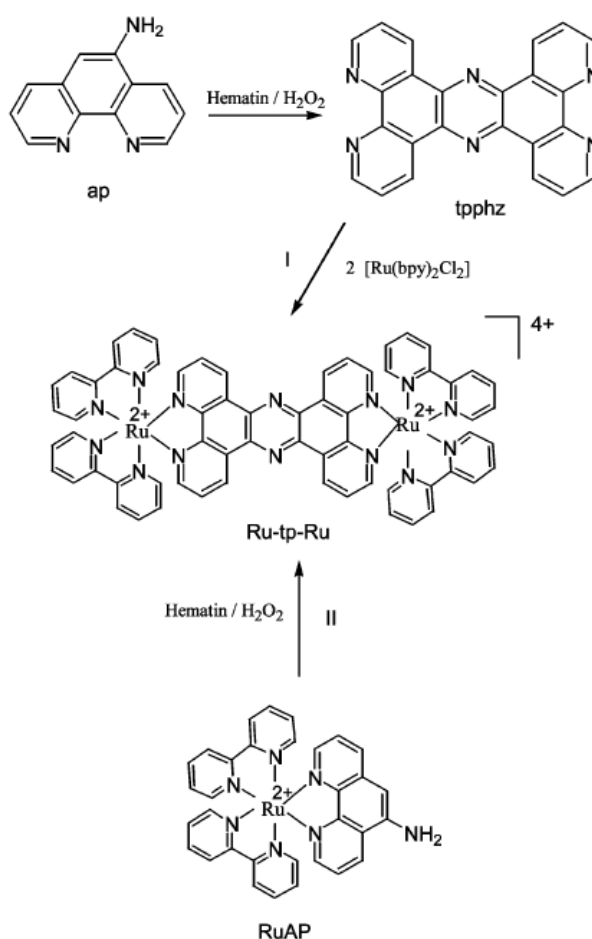
In addition to the formation of hydrogen,  $[\text{Ru}(\text{bpy})_2(\text{tpphz})\text{PdCl}_2]^{2+}$  was also shown to selectively reduce toluene (diphenylacetylene) to *cis*-stilbene with a TON of 63 .<sup>14,15</sup> The activity of the catalytic center ( $\text{PdCl}_2$ ) was illustrated by the generation of the *cis*- stilbene isomer only and the inactivity of the palladium free derivative. These results are much improved from those previously reported in 2006 by Sakai et al<sup>16</sup> who reported TON of 2 and 4 mol of  $\text{H}_2$  per mol of catalyst. The photocatalyst used by Sakai shown in Figure 4.2 was a ruthenium/platinum dinuclear complex but using a bridge that has lesser conjugation within its structure, indicating the importance of a reducible  $\pi$ -electron system as a bridging ligand.



**Figure 4.2:** Structure of the photocatalyst reported by Saki et al.<sup>16</sup>

Consideration of the success of the photocatalyst by *Rau et al.*,<sup>14, 15</sup> leads to an interesting postulation, on replacement of the catalytic centre with a rhenium moiety, a photocatalyst with the ability to reduce  $\text{CO}_2$  may be prepared. As previously discussed in Chapter 1, rhenium has been shown to be a metal of choice for the reduction of  $\text{CO}_2$ ,<sup>17,18,19,20,21</sup> so a dinuclear complex containing a ruthenium centre (as a light absorbing species), rhenium as a catalytic centre and tpphz ligand as a communication pathway has a high probability of working as a photocatalyst that reduces  $\text{CO}_2$ . The importance of using tpphz as a bridging ligand for intramolecular photoinduced electron transfer was also shown by *Chiorboli et al.*<sup>22</sup> in 2002 who found that in acetonitrile, electron transfer rates of a few picoseconds were observed. In the same study it was also determined that the presence of the tpphz ligand is that of a molecular component which actively participates in the energy and electron transfer process between the two metal centres.

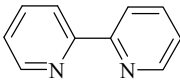
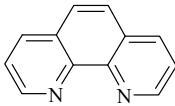
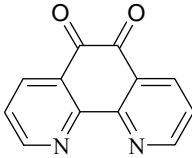
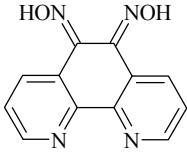
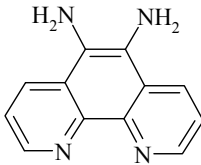
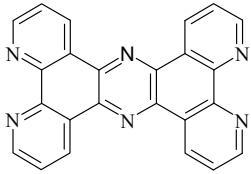
With this in mind a study into the synthetic preparation of the dinuclear complex  $[\text{Ru}(\text{bpy})_2(\text{tpphz})\text{Re}(\text{CO})_3\text{Cl}](\text{PF}_6)_2$  was conducted. Previous publications indicate the preparation of ruthenium tpphz dinuclear complexes are prepared from a condensation reaction between 1,10-phenanthroline and 1.10-phenanthroline-5,6-diamine.<sup>22,23,24</sup> Though in 2003 *Mosurkal et al.* reported a biocatalytic synthesis of  $[(\text{Ru}(\text{bpy})_2)_2(\text{tpphz})]^{4+}$  using Hematin as a catalyst in the presence of  $\text{H}_2\text{O}_2$ .<sup>25</sup> Hematin (hydroxyl ferriprotoporphyrin) the catalytic centre in certain enzymes, undergoes redox changes in the presence of  $\text{H}_2\text{O}_2$  in organic solvents such as DMF<sup>26</sup>. This unique approach taken by *Mosurkal et al.* shows the synthesis of the tpphz ligand, this is the first reported use of hematin for a small molecular system and the approach taken is shown below in Figure 4.3.<sup>25</sup> Carrying out the synthesis biocatalytically negated the use of long multistep synthesis and high reaction temperatures ( $180^\circ\text{C}$ ) that have been carried out previously. The reaction also appears to be specific as no formation of side products as reported. Currently the reported yields using hematin are low though it is suggested this could be improved during the work up procedure. Formation of the complex by Mosurkai was confirmed by UV-vis and emission spectra. MLCT based absorption bands were observed at 445 nm and an emission  $\lambda_{\text{max}}$  was found at 670 nm.



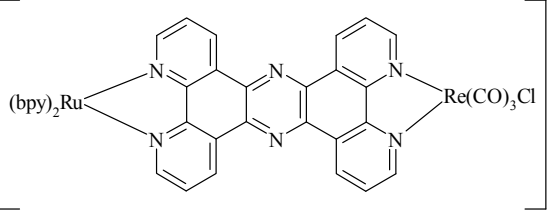
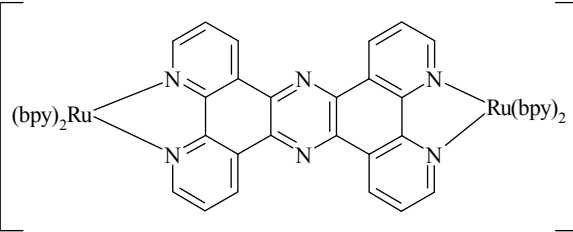
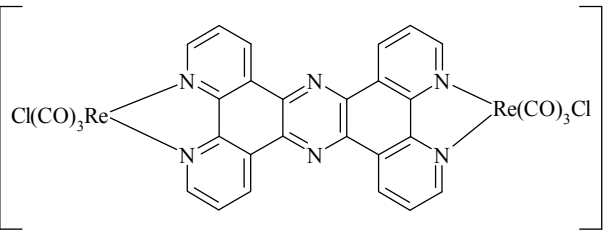
**Figure 4.3:** Biocatalytic synthesis reported by Mosurkal *et al.*

#### 4.1 Aim.

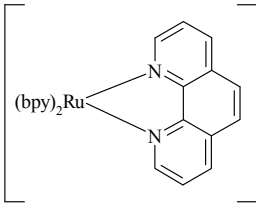
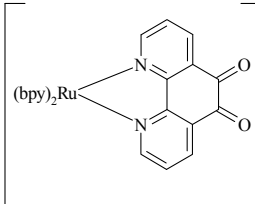
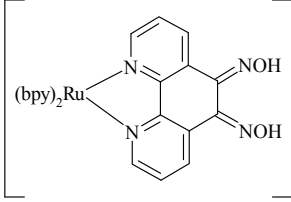
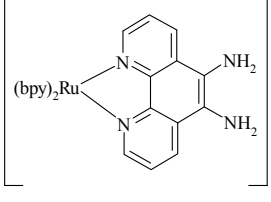
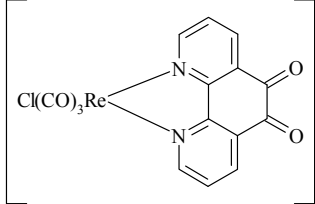
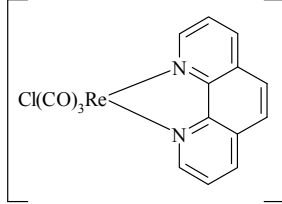
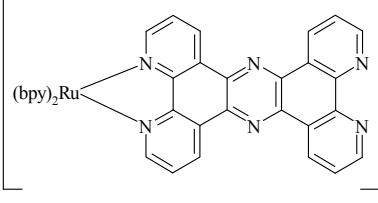
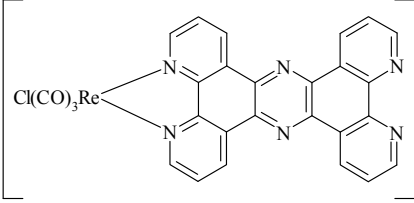
The work under discussion in this chapter describes the synthetic approaches undertaken to synthesise  $[\text{Ru}(\text{bpy})_2(\text{tpphz})\text{Re}(\text{CO})_3\text{Cl}](\text{PF}_6)_2$ . Tables 4.1, 4.2 and 4.3 that follow describe the ligands and complexes under discussion in this chapter. Initially the reactions reported by Bolger and Rau<sup>15</sup> amongst others, were used to create the tpphz ligand by means of a phenanthroline and phendiamine condensation reaction, from here novel synthetic routes were carried out to prepare  $[\text{Ru}(\text{bpy})_2(\text{tpphz})\text{Re}(\text{CO})_3\text{Cl}](\text{PF}_6)_2$ .

	
bpy, (2,2-bipyridine)	Phen, (1,10-phenanthroline)
	
Phendione, (1,10-phenanthroline-5,6-dione)	Phendioxime, (1,10-phenanthroline-5,6-dioxime)
	
Phendiamine, (1,10-phenanthroline-5,6-diamine)	Tp-phz, (tetrapyrido[3,2-a:2',3':3'',2''-h:2''',3'''-j]phenazine)

**Table 4.1:** Depicts the abbreviations and structures of the ligands discussed in this section.

$[\text{Ru}(\text{bpy})_2(\text{tpphz})\text{Re}(\text{CO})_3\text{Cl}](\text{PF}_6)_2$	
$[\{\text{Ru}(\text{bpy})_2\}_2\text{tpphz}](\text{PF}_6)_2$	
$[\{\text{Re}(\text{CO})_3\text{Cl}\}_2\text{tpphz}]$	

**Table 4.2:** Depicts the structures of the dinuclear complexes discussed in this section. bpy = 2,2-bipyridine.

 <p><math>[\text{Ru}(\text{bpy})_2(\text{phen})]^{2+}</math></p>	 <p><math>[\text{Ru}(\text{bpy})_2(\text{Phendione})]^{2+}</math></p>
 <p><math>[\text{Ru}(\text{bpy})_2(\text{Phendioxime})]^{2+}</math></p>	 <p><math>[\text{Ru}(\text{bpy})_2(\text{Phendiamine})]^{2+}</math></p>
 <p><math>[\text{Re}(\text{CO})_3\text{Cl}(\text{phendione})]</math></p>	 <p><math>[\text{Re}(\text{CO})_3\text{Cl}(\text{phen})]</math></p>
 <p><math>[\text{Ru}(\text{bpy})_2(\text{tpphz})]^{2+}</math></p>	 <p><math>[\text{Re}(\text{CO})_3\text{Cl}(\text{tpphz})]</math></p>

**Table 4.3:** Depicts the abbreviations and structures of the mononuclear complexes discussed in this section. *bpy* = 2,2-bipyridine.



## 4.2 Synthetic Procedures

### 4.2.1 Preparation of Ligands.

#### 1,10-phenanthroline-5,6-dione (dione)<sup>27</sup>

1,10-phenanthroline monohydrate (10.00 g, 50.46 mmol) was added in small portions to a stirring solution of 60 cm<sup>3</sup> concentrated sulphuric acid in a 500 cm<sup>3</sup> round bottom flask equipped with a reflux condenser. When the solid was completely dissolved, sodium bromide (5.19g 50.44 mmol) was added in small portions followed by 30 cm<sup>3</sup> of 70% HNO<sub>3</sub>. This was then brought to reflux (110 °C) for six hours and then the temperature was reduced to 95 °C, the reflux condenser removed to allow the bromine vapours to escape and left for sixteen hours.

The reaction was then brought to room temperature and poured over 800 g of ice and was carefully neutralised to pH 7 with approximately 300 cm<sup>3</sup> of 10 M NaOH. At this point the solution turned a green colour with a yellow precipitate. This precipitate was then collected, and this step repeated. The combined precipitate was then placed in a round bottom flask and refluxed in 200 cm<sup>3</sup> of water for 1 hour and the insoluble material was collected by vacuum filtration. This was repeated twice more and then the water was extracted with DCM until the organic layer remained clear. The DCM was then removed by rotary evaporation and an NMR obtained of the crude material. This was then recrystallised from toluene.

Yield: 8.16 g, 38.83 mmol, 77%.

Calc on C<sub>12</sub>H<sub>6</sub>N<sub>2</sub>O<sub>6</sub>, Mw: 210.12 g/mol

<sup>1</sup>H NMR: (*d*<sub>6</sub>- acetone, 298K) δ: 8.99 (2H, dd), 8.39 (2H, m), 7.67 (2H, d).

### **Tetrapyrido[3,2-a:2',3':3'',2''-h:2''',3'''-j]phenazine (Tpphz)**

1,10-phenanthroline-5,6-dione (0.3045 g, 1.449 mmol), sodium hydrosulphite (0.0318 g, 0.1826 mmol) and ammonium acetate (1.594 g, 20.67 mmol) were placed into a 50 cm<sup>3</sup> round bottom flask which was previously purged with nitrogen. This was slowly heated to 190°C with constant stirring for two hours. After the reagents have melted the reaction turns a yellow/brown colour. The reaction was then cooled to room temperature and 3cm<sup>3</sup> of water was added. The yellow precipitate was then collected under a vacuum, washed with water, methanol and acetone. The product was then triturated in refluxing ethanol, hot filtered, washed with ethanol and dried under vacuum.

Yield: 0.1526 g, 0.397 mmol, 52.8%.

Calc on C<sub>24</sub>H<sub>12</sub>N<sub>6</sub>, Mw: 384.39 g/mol

<sup>1</sup>H NMR:

(CDCl<sub>3</sub> TFA, 298K) δ: 10.06(dd, 4H), 9.47 (dd, 4H), 8.47 (dd, 4H).

(d<sub>3</sub>-ACN, TFA, 298K) δ: 10.03 (dd, 4H), 9.17 (dd, 4H), 8.25 (dd, 4H).

### **4.2.2 Preparation of Mononuclear Complexes.**

#### ***[Ru(bpy)<sub>2</sub>(1,10phenanthroline)](PF<sub>6</sub>)<sub>2</sub>*<sup>28</sup>**

[Ru(bpy)<sub>2</sub>Cl<sub>2</sub>].2H<sub>2</sub>O (0.200 g, 0.3845mmol) and (0.099 g, 0.549 mmol) of 1,10-phenanthroline monohydrate were refluxed at 120°C for 3 hours in 2:1 (v/v) ethanol : water. The reaction was cooled to room temperature and the ethanol removed. 5 cm<sup>3</sup> of water was added and the product was obtained by the addition of KPF<sub>6</sub>. The product was stored at +4 °C overnight and recrystallised from 2:1 (v/v) acetone: water.

Yield: 0.223 g, 0.253 mmol, 66%.

Calc on C<sub>32</sub>H<sub>22</sub>N<sub>6</sub> Ru<sub>1</sub>(PF<sub>6</sub>)<sub>2</sub>, Mw: 883.27 g/mol.

<sup>1</sup>H NMR (acetone, 298K) δ: 8.91 (m, bpy, 4H), 8.88 (m, phen, 2H), 8.40 (s, phen, 2H), 8.23 (dd, phen, 2H), 8.14 (dd, bpy, 4H), 7.89 (m, bpy, 4H), 7.58 (m, bpy, 4H), 7.38 (dd, phen, 2H).

**$[\text{Ru}(\text{bpy})_2(\text{phendione})](\text{PF}_6)_2$  (method 1)**

$[\text{Ru}(\text{bpy})_2(\text{phenanthroline})] \cdot 2(\text{PF}_6)$  (0.500g, 0.566 mmol) was dissolved in 10cm<sup>3</sup> of conc.  $\text{H}_2\text{SO}_4$  with stirring at room temperature. (0.858g, 8.34 mmol) of NaBr was added until completely dissolved. 7 cm<sup>3</sup> of 70%  $\text{HNO}_3$  was added and reaction was brought to 120 °C for 20 min. The reaction was cooled to room temperature and poured over 70 cm<sup>3</sup> of cold saturated  $\text{KPF}_6$  solution. This was stored at +4 °C overnight. The brown precipitate was collected by vacuum filtration and allowed to dry. The complex was recrystallised from 2:1 (v/v) acetone : water.

Yield: 0.465 g, 0.509 mmol, 90%.

Calc on  $\text{C}_{32}\text{H}_{22}\text{N}_6\text{O}_2 \text{Ru}_1 (\text{PF}_6)_2$ , Mw: 913.25 g/mol.

$^1\text{H}$  NMR (*acetone*, 298K)  $\delta$ : 8.52 (m, dione, 2H), 8.10 (dd, bpy, 2H) 7.98 (d, dione, 2H), 7.79 (d, bpy, 2H), 7.61 (d, dione 2H), 7.43 (dd, bpy, 2H)

**$[\text{Ru}(\text{bpy})_2(\text{phendione})](\text{PF}_6)_2^{28}$  (method 2)**

$[\text{Ru}(\text{bpy})_2\text{Cl}_2] \cdot 2(\text{H}_2\text{O})$  (0.074 g, 0.142 mmol) was dissolved in 5 cm<sup>3</sup> of ethanol. 1,10-phenanthroline-5,6-dione (0.029 g, 0.138 mmol) was added slowly with constant stirring. This was refluxed for 4 hours at 70 °C. The reaction was then cooled and filtered and saturated ethanolic  $\text{KPF}_6$  was added. The reaction was then placed at -20 °C overnight and a black solid was obtained. This was recrystallised from 1:1 (v/v) acetone: water.

Yield: 0.046 g, 0.048 mmol, 34 %.

Calc on  $\text{C}_{32}\text{H}_{22}\text{N}_6\text{O}_2 \text{Ru}_1 (\text{PF}_6)_2$ , Mw: 913.25 g/mol.

$^1\text{H}$  NMR (*acetone*, 298K)  $\delta$  8.52 (m, dione, 2H), 8.10 (dd, bpy, 2H) 7.98 (d, dione, 2H), 7.79 (d, bpy, 2H), 7.61 (d, dione 2H), 7.43 (dd, bpy, 2H).

**$[\text{Re}(\text{CO})_3\text{Cl}(\text{phen})]^{29}$**

20 cm<sup>3</sup> of anhydrous toluene was purged for 10 min.  $[\text{Re}(\text{CO})_5\text{Cl}]$  (0.100 g, 0.277 mmol) was weighed out carefully under nitrogen and added to 10 cm<sup>3</sup> of toluene. 1,10-phenanthroline monohydrate (0.0403 g, 0.203 mmol) was dissolved in 10 cm<sup>3</sup> of solvent along with a few drops of trifluoroacetic acid and brought to 25 °C. The  $[\text{Re}(\text{CO})_5\text{Cl}]$  was added slowly over a 15 minute period and then this solution was heated to reflux and left for 3 hours. The reaction had turned a bright yellow colour and was allowed to cool to room temperature and as this occurred, a bright yellow precipitate formed. The yellow product was collected by vacuum filtration and recrystallised from acetone: water 1:1 (v/v).

Yield: 0.093g, 0.191 mmol, 84%.

Calc on  $\text{C}_{15}\text{H}_8\text{N}_2\text{O}_3 \text{Cl}_1 \text{Re}_1$ , Mw: 485.80 g/mol.

<sup>1</sup>H NMR (*acetone*, 298K)  $\delta$ : 9.41 (dd, phen 2H), 8.85 (m, phen, 2H), 8.22 (s, phen, 2H), 7.38 (m, phen, 2H)

IR (CO)  $\nu\text{cm}^{-1}$ : 2020, 1918, 1894.

**$[\text{Re}(\text{CO})_3\text{Cl}(\text{phendione})]$**

As above except 1,10-phenanthroline-5,6-dione (0.0403 g, 0.192 mmol) and  $[\text{Re}(\text{CO})_5\text{Cl}]$  (0.100g, 0.276 mmoles) were used.

Yield: 0.085 g, 0.165 mmol, 86%.

Calc on  $\text{C}_{15}\text{H}_6\text{N}_2\text{O}_5 \text{Cl}_1 \text{Re}_1$ , Mw: 515.78 g/mol.

<sup>1</sup>H NMR (*acetone*, 298K)  $\delta$ : 9.22 (dd, phen, 2H), 8.77 (dd, phen, 2H), 7.98 (m, phen, 2H)

IR (CO)  $\nu\text{cm}^{-1}$ : 2023, 1923, 1989.

**[Re(CO)<sub>3</sub>Cl (tpphz)]**

Tpphz (0.192 g, 0.499 mmol) was dissolved in two drops of concentrated TFA and then placed in 10 cm<sup>3</sup> of anhydrous toluene and brought to 25 °C. To this a solution of [Re(CO)<sub>5</sub>Cl] (0.200 g, 0.553 mmol) in 10 cm<sup>3</sup> of anhydrous toluene was added over a 15 minute period. This was refluxed for three hours, toluene removed. The residue dissolved in acetone and filtered. The acetone was evaporated slowly to yield the yellow product.

Yield: 0.095g, 0.0954 mmol, 19. %.

Calc on C<sub>27</sub>H<sub>12</sub>N<sub>6</sub>O<sub>3</sub> Cl<sub>1</sub> Re<sub>1</sub>, Mw: 995.71 g/mol.

<sup>1</sup>HNMR (acetone, 298K) δ: 7.07(m, tpphz, 2H), 8.46(dd, tpphz, 1H), 9.66(m, tpphz, 2H) 10.46 (dd, tpphz, 1H).

IR (CO) νcm<sup>-1</sup>: 2026, 1927, 1908.

**4.2.3 Preparation of Dinuclear Complexes**

**[Ru(bpy)<sub>2</sub>(Tpphz)Re(CO)<sub>3</sub>Cl]·(PF<sub>6</sub>)<sub>2</sub>**

[Re(CO)<sub>3</sub>Cl(tpphz)] (0.050g, 0.07 mmol) was dissolved in ethanol. [Ru(bpy)<sub>2</sub>Cl<sub>2</sub>].2H<sub>2</sub>O (0.042g, 0.08mmol) was added slowly over a twenty minute period. This was left to reflux for six hours and the ethanol removed. 5 cm<sup>3</sup> of H<sub>2</sub>O was added and the solution filtered. The product was obtained by the addition of KPF<sub>6</sub>.

Yield 0.0137 g, 12%, 0.0097mmol.

Calc on C<sub>47</sub>H<sub>28</sub>N<sub>10</sub>O<sub>3</sub>Cl<sub>1</sub>Re<sub>1</sub>Ru<sub>1</sub>(PF<sub>6</sub>)<sub>2</sub>, Mw:1411.18 g/mol.

<sup>1</sup>HNMR (ACN, 298K) δ: 5.98 (dd, 2H), 6.05 (dd, 2H), 6.52 (m, 2H), 6.63 (m, 2H), 6.74 (m, 2H), 6.97 (m, 2H), 7.27 (m, 2H) 7.48 (dd, 2H), 7.51 (m, 2H), 7.63 (m, 2H) 8.46 (dd, 2H), 8.49 (dd, 2H), 8.97 (dd, 2H) 9.02 (dd, 2H) .

**$[(\text{Ru}(\text{bpy})_2)_2(\text{Tpphz})] \cdot (\text{PF}_6)_4$**

$[\text{Ru}(\text{bpy})_2\text{Cl}_2] \cdot 2\text{H}_2\text{O}$  (0.200g, 0.385 mmol) and tpphz (63mg, 0.165 mmol) were refluxed in 20cm<sup>3</sup> of 2:1 (v/v) ethanol: water for 24 hours. The reaction was cooled to room temperature and the ethanol removed. The reaction was allowed to stand at +4°C overnight and the reaction was filtered to remove any unreacted ligand. 10cm<sup>3</sup> of water was added and the product was obtained by the addition of  $\text{KPF}_6$  and was recrystallised from 2:1 (v/v) acetone : water.

Yield: 0.465 g, 0.260 mmol, 67%.

Calc on  $\text{C}_{64}\text{H}_{44}\text{N}_{14}\text{Ru}_1(\text{PF}_6)_4$ , Mw:1790.41 g/mol.

<sup>1</sup>HNMR (ACN, 298K)  $\delta$ : 7.00 (dd, bpy 2H), 7.25 (dd, bpy, 2H), 7.63 (m, bpy, 2H), 7.74 (m, bpy, 2H), 7.75 (dd, tpphz, 2H), 7.77 (m, bpy, 2H), 7.81 (m, bpy 2H) 7.96 (m, tpphz, 2H), 8.28 (m, bpy, 2H), 8.31 (m, bpy, 2H) 9.70 (dd, tpphz, 2H).

**$[(\text{Ru}(\text{d-bpy})_2)_2(\text{Tpphz})] \cdot (\text{PF}_6)_4$**

As above except  $[\text{Ru}(\text{d-bpy})_2\text{Cl}_2] \cdot 2\text{H}_2\text{O}$  (0.100g, 0.198 mmol) and tpphz (0.035g, 0.09 mmol) were used.

Yield: 0.198g, 0.113mmol, 57%.

Calc on  $\text{C}_{64}\text{N}_{14}\text{Ru}_1(\text{PF}_6)_4$ , Mw:1746.41 g/mol.

<sup>1</sup>HNMR (ACN, 298K)  $\delta$ : 7.75 (dd 2H), 7.96 (m, 2H), 9.70 (dd, 2H).

#### 4.2.4 Attempted Synthesis

##### 1,10-phenanthroline-5,6-dioxime (Phenoxime)

1,10-phenanthroline-5,6-dione (0.420g, 2.00 mmol),  $\text{NH}_2\text{OH}\cdot\text{HCl}$  (0.486g, 7.00 mmol) and  $\text{BaCO}_3$  (0.529g, 3.00 mmol) was refluxed in  $50\text{cm}^3$  of ethanol for 12 hours. The ethanol was then removed and the residue was stirred with  $40\text{cm}^3$  of 0.2M  $\text{HCl}$  for 1 hour and then filtered. The light yellow solid obtained was washed with water ( $20\text{cm}^3$ ), ethanol ( $20\text{cm}^3$ ) and finally dried under a vacuum at  $80^\circ\text{C}$ .

##### $[\text{Ru}(\text{bpy})_2(\text{Tpphz})\text{Re}(\text{CO})_3\text{Cl}]\cdot(\text{PF}_6)_2$

$[\text{Re}(\text{CO})_3\text{Cl}(\text{dione})]$  (50mg, 0.097mmol),  $[\text{Ru}(\text{bpy})_2(\text{dione})]2\text{PF}_6$  (91mg, 0.10 mmol) and ammonium acetate and  $\text{NaHS}$  were placed together in a round bottom flask and heated to  $40^\circ\text{C}$  until all of the ammonium acetate melted and a slurry was formed. The temperature was then brought to  $100^\circ\text{C}$  and left to stir for 5 hours. This was then cooled to room temperature and 5 ml of  $\text{H}_2\text{O}$  was added. A yellow precipitate was formed and removed by filtration.  $\text{KPF}_6$  was then added dropwise and a red precipitate was obtained.

##### $[(\text{Re}(\text{CO})_3\text{Cl})_2(\text{tpphz})]$

As for  $[\text{Re}(\text{CO})_3\text{Cl}(\text{tpphz})]$  except  $[\text{Re}(\text{CO})_5\text{Cl}]$  (0.10g, 0.2 mmol) and  $\text{tpphz}$  (0.053g, 0.1mmol) were used and the reaction was refluxed for 6 hours.  
IR (CO)  $\nu\text{cm}^{-1}$ : 2026, 1927, 1908.

### 4.3 Results and Discussion.

#### 4.3.1 Synthesis

##### *Ligand Preparation*

The tpphz ligand was prepared as described by Bolger *et al* with a solventless reflux using the solid with the lowest melting point (ammonium acetate) to form a slurry and then further reaction with the 1,10- phenanthroline-5,6-dione in the presence of a hydrogen donor (NaHS). The product was easily purified by trituration in ethanol. The reaction proceeded via a Schiff-base reaction between the amine and the aldehyde an example of such a reaction reaction is shown in Figure 4.4 below.

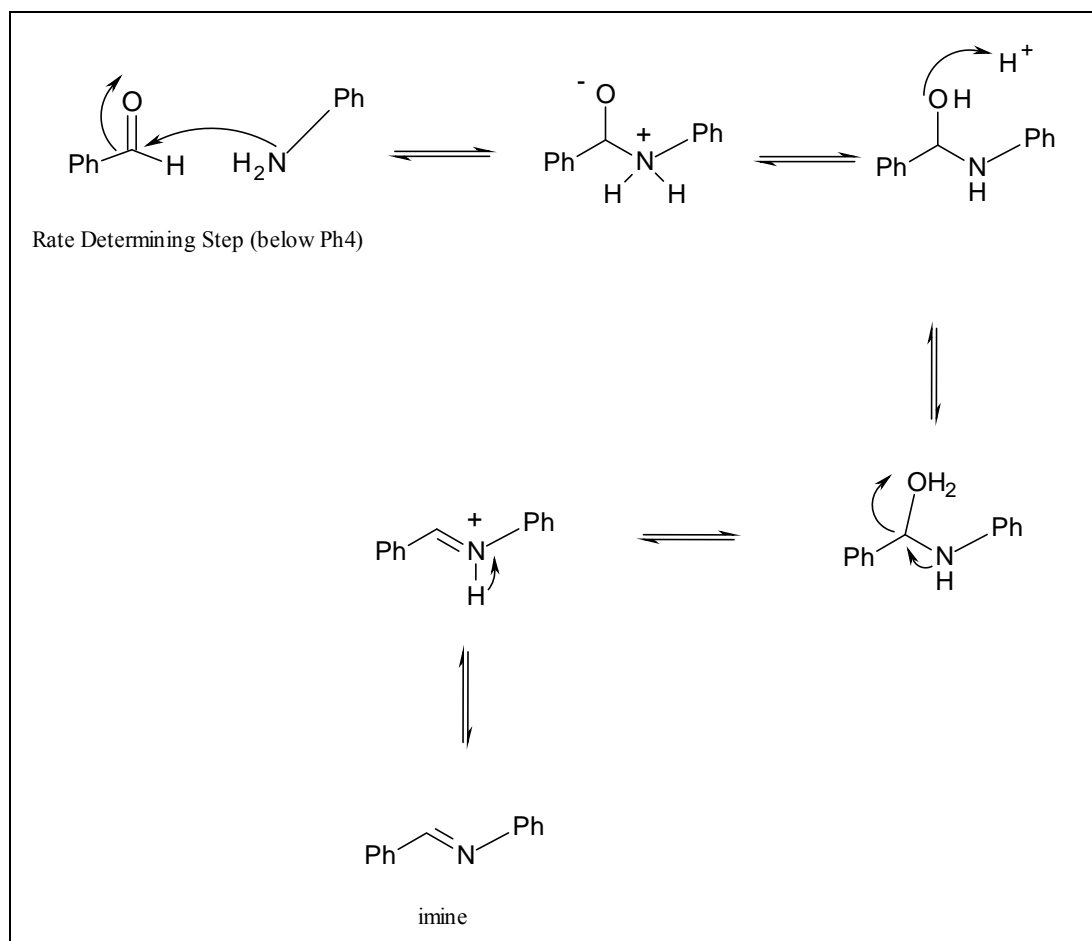


**Figure 4.4:** Example of a Schiff-base reaction.<sup>10</sup>



Problems were encountered as the ligand was found to be highly insoluble due to the high conjugation in its structure. Though the ligand itself is easily obtained, complexation to a metal (e.g. Ru or Re), or to gather experimental data, became a challenge.  $^1\text{HNMR}$  was carried out by the addition of TFA (trifluoroacetic acid) to the ligand and the deuteriated solvent was then added, though the ligand was found to be sparingly soluble in dichloromethane.

To overcome this problem it was thought that building the ligand on to the ruthenium and rhenium centres offered an increase in solubility. This required the preparation of an amine ligand bound to either the ruthenium or rhenium metal centers and an aldehyde on the remaining metal, followed by a coupling reaction. The approaches undertaken are described in the following section.

### ***Complex Preparation***

Previous publications<sup>24,22,27,30</sup> describe the formation of the mononuclear  $[\text{Ru}(\text{bpy})_2\text{tpphz}](\text{PF}_6)_2$ , via a Schiff base coupling reaction between 5,6-diamino-1,10-phenanthroline and  $[\text{Ru}(\text{bpy})_2\text{phendione}]^{2+}$  as shown in Figure 4.5 below. However the synthetic preparation of the 5,6-diamino-1,10-phenanthroline proved to be difficult. The publications mentioned above, report the formation of the diamine from a phendioxime intermediate. Phendioxime was formed from phendione in the presence hydroxylamine hydrochloride and barium carbonate as described in Figure 4.5. This reaction was problematic and  $^1\text{HNMR}$  data indicated that conversion of the  $\text{C}=\text{O}$  to the  $-\text{NOH}$  group only occurred on one side of the phendione ligand. Many attempts of synthesizing the phendioxime were made on the free phendione ligand itself and on  $[\text{Ru}(\text{bpy})_2(\text{phendione})](\text{PF}_6)_2$ , in preparation of the phendiamine but there were all unsuccessful, the reaction conditions used are described in Table 4.4 below.

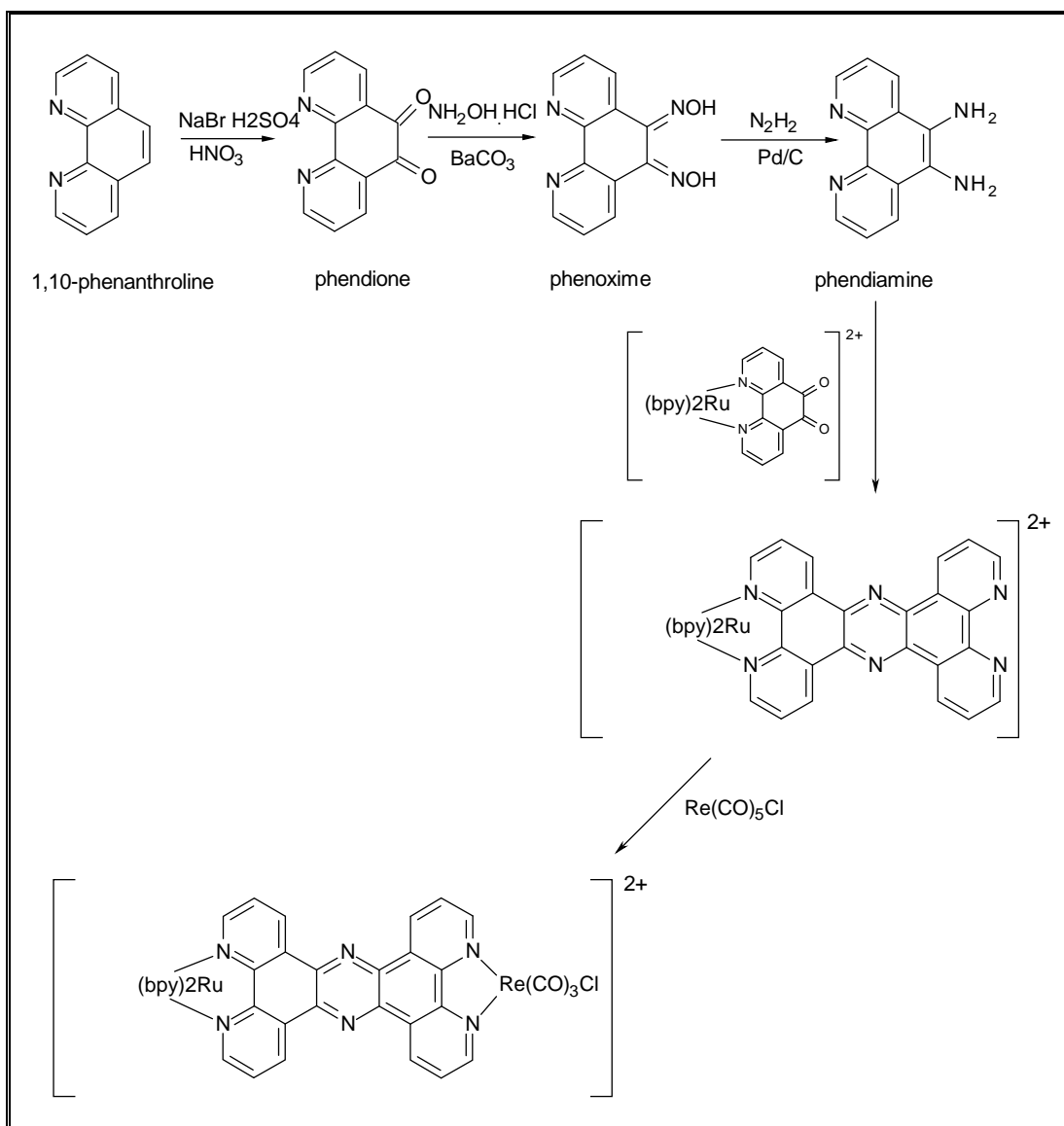


**Figure 4.5:** Synthetic Route 1 to the formation of the desired Ru (II) mononuclear complex and subsequent heterodimer.

Reaction #	Phendione mmol	$\text{NH}_2\text{OH.HCl}$ mmol	$\text{BaCO}_3$ mmol	Reaction Time (Hr)	Reaction Temp ( $^\circ\text{C}$ )
1	2	7	3	6	107
2	2	7	3	12	107
3	2	7	3	24	120
4	2	8	4	48	120
5	2	9	4	12	120
6	2	9	4	24	120

**Table 4.4:** Reaction conditions used in the preparation of the phendioxime ligand.

As the afore mentioned route was time consuming and problematic, a novel synthetic route was considered to prepare the Ru (II) mononuclear tpphz complex. The free tpphz ligand as shown above, was formed from the condensation of phendione with ammonium acetate. A new synthetic approach was subsequently taken to determine if the ruthenium when bound to the phendione ligand would couple with ammonium acetate to give the desired product shown in Figure 4.6 below.

The preparation of the ruthenium dione complex was interesting, as it was found that oxidation of the phenanthroline ligand while bound to the ruthenium gave a higher yield (89%) than the complexation of  $[\text{Ru}(\text{bpy})_2\text{Cl}_2]$  to a free ligand (tpphz) (34%). However upon coupling the  $[\text{Ru}(\text{bpy})_2\text{phendione}]^{2+}$  with free dione ligand no reaction was observed. Reactions of this type are very sensitive to the hydrogen donor.<sup>10</sup> Imine formation is fastest between pH 4 – 8 and though the catalyst is only required for the elimination of water, if too much amine is protonated the rate of reaction is slow to nonexistent. The amount of acid was varied along with the reaction solvent when no reaction was seen the hydrogen donor was also varied. Each reaction was monitored closely to determine if any signs of reaction were occurring e.g. colour change. These reactions are displayed below in Table 4.5.

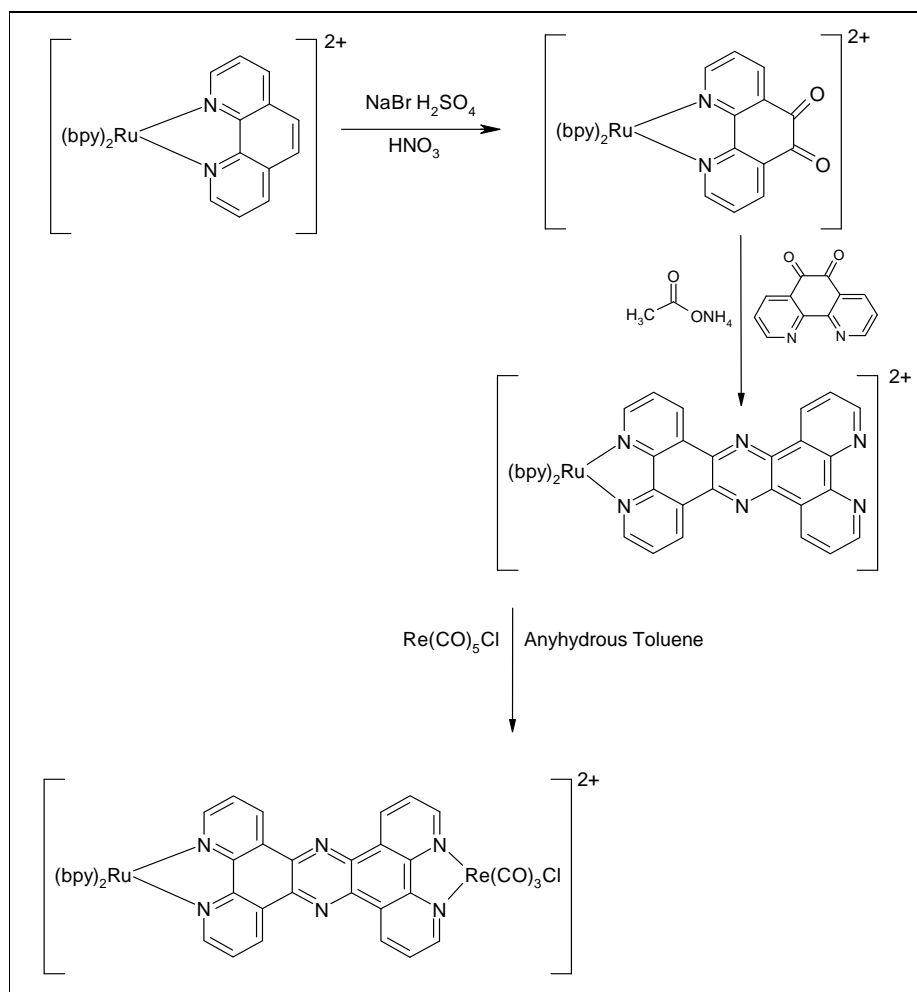


**Figure 4.6:** Synthetic Route 2 to the formation of the desired Ru (II) mononuclear complex and subsequent heterodimer.

Reaction #	$[\text{Ru}(\text{bpy})_2(\text{dione})]^{2+}$	Free Dione	Ammonium Acetate	H <sup>+</sup> Donor	Solvent	Temp. (°C)	Time (Hr)
1	1	1	6	NaHS	none	150	3
2	1	1	6	NaHS	none	150	6
3	1	1	6	NaHS	none	100	12
4	1	1.5	6	H <sub>2</sub> SO <sub>4</sub>	Ethanol	80	6
5	1	1.5	8	H <sub>2</sub> SO <sub>4</sub>	Ethanol: Water	120	6
6	1	1.5	8	H <sub>2</sub> SO <sub>4</sub>	Ethanol: Water	120	12
7	1	1.5	8	HNO <sub>3</sub>	Ethanol: Water	120	6

**Table 4.5:** Test reactions for the preparation of  $[\text{Ru}(\text{bpy})_2\text{tpphz}]^{2+}$ .

Even though the preparation of the ruthenium (II) mononuclear complex  $[\text{Ru}(\text{bpy})_2(\text{tpphz})]^{2+}$  was desired to complete the study, it is not necessary for the formation of the required Ru /Re dinuclear species. Following on from the previous reactions, a coupling reaction was conducted using ruthenium and rhenium phendione mononuclear complexes, in the presence of ammonium acetate and a hydrogen donor. This condensation reaction described in Figure 4.7, was carried out initially in 2:1 ethanol/ water (v/v) but no reaction was observed. The reaction was repeated using no solvent and the desired  $[\text{Ru}(\text{bpy})_2(\text{tpphz})\text{Re}(\text{CO})_3\text{Cl}]^{2+}$  was obtained in a small yield. This reaction is problematic as it may also give rise to  $[(\text{Ru}(\text{bpy})_2)_2(\text{tpphz})]^{4+}$  and  $[(\text{Re}(\text{CO})_3\text{Cl})_2(\text{tpphz})]$ .

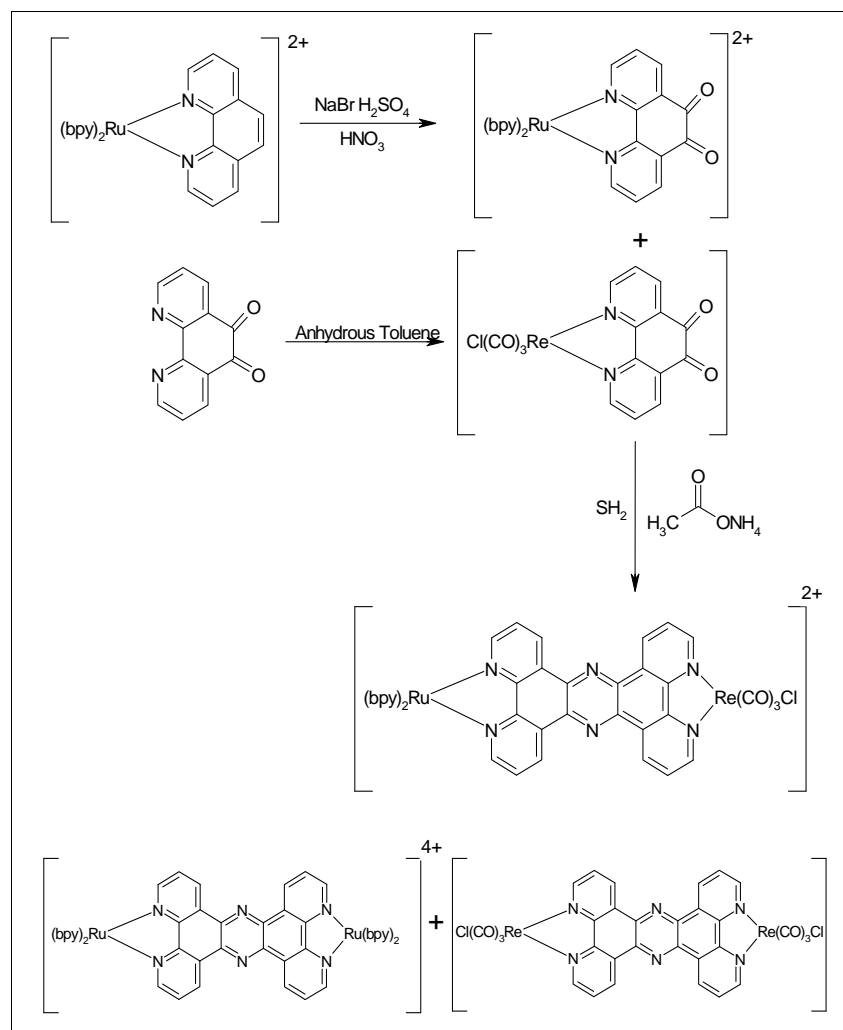


**Figure 4.7:** Synthetic Route 3 to the formation of the desired heterodimer.

A final route, (Figure 4.8) was devised in which the tpphz ligand was dissolved in a small amount of TFA and reacted with  $[\text{Re}(\text{CO})_5\text{Cl}]$  using toluene as a solvent to form the mononuclear complex. This reaction allowed the insoluble tpphz to be protonated turning a dark brown colour and dissolve into solution. Upon addition of the pentacarbonyl, a bright yellow solution was formed upon reaching the reflux temperature. As this formed a single mononuclear species  $[\text{Re}(\text{CO})_3\text{Cl}(\text{tpphz})]$  within 3 hours, the ruthenium bipyridyl moiety  $[\text{Ru}(\text{bpy})_2]$  was less complicated to attach. This attachment was carried out using methanol as a solvent with a 6 hour reaction time, though this dinuclear species so far has only been obtained in small yield.

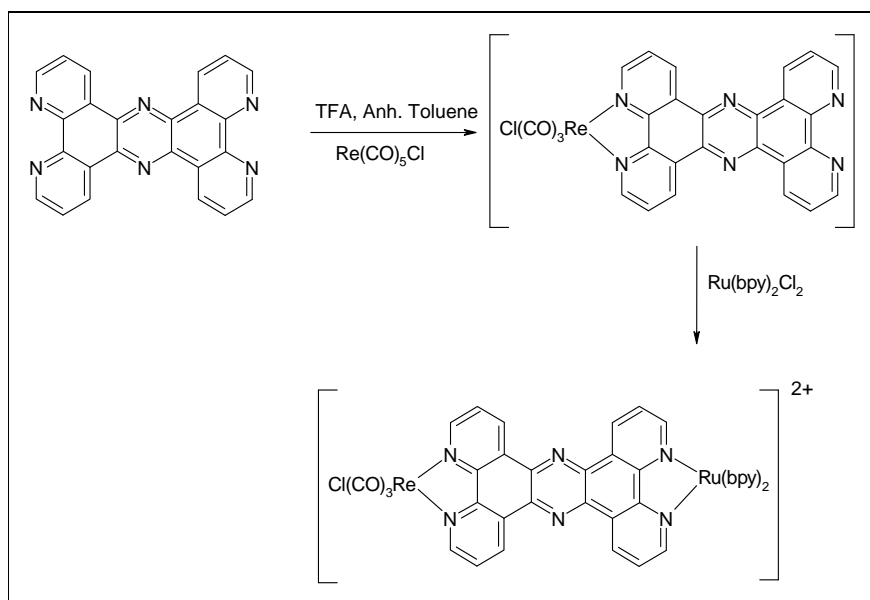


**Figure 4.8:** Synthetic Route 4 to the formation of the desired heterodimer.

### 4.3.2 <sup>1</sup>H NMR.

<sup>1</sup>H NMR was used in the elucidation of the structures of both the ligand and metal complexes with ruthenium (II) and rhenium (I). These metal centers form diamagnetic low-spin d<sup>6</sup> complexes that can be characterised with NMR spectroscopy. Firstly the NMR spectra obtained for the ligands will be discussed followed by the analysis of the NMR spectra of mononuclear and dinuclear species. Proton signals were assigned with the use of a 2D-COSY and all NMR spectra were calibrated to the correct solvent peak.

#### 4.3.2.1 <sup>1</sup>HNMR – Ligands.

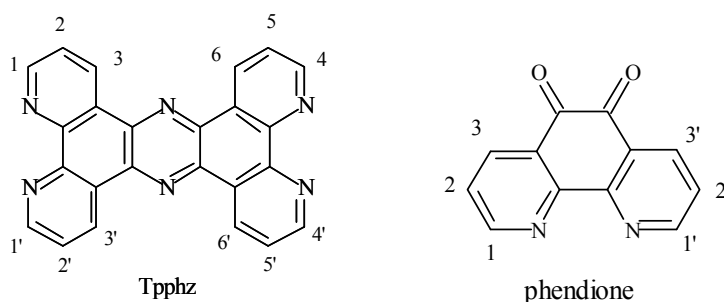


**Figure 4.9:** Labeling of the phenanthroline based ligands for <sup>1</sup>HNMR assignment.

<i>Ligand</i>	<i>Solvent</i>	<i>H1</i>	<i>H2</i>	<i>H3</i>	<i>H4</i>
<i>phen</i>	CD <sub>3</sub> CN	9.11	7.71	8.37	7.98
<i>phendione</i>	CD <sub>3</sub> CN	9.07	7.67	8.39	-
<i>phendione</i>	CDCl <sub>3</sub>	8.99	7.67	8.39	-
<i>phendione</i>	C <sub>3</sub> D <sub>6</sub> O	8.98	7.60	8.40	
<i>tpphz</i>	CD <sub>3</sub> CN	10.08	8.25	9.18	-
<i>tpphz</i>	CDCl <sub>3</sub>	10.06	8.47	9.47	-
<i>tpphz</i>	C <sub>3</sub> D <sub>6</sub> O	10.09	8.63	9.49	

**Table 4.6:** <sup>1</sup>H NMR data in ppm for phen, phendione and tpphz ligands.

The signals in the  $^1\text{H}$ -NMR spectra of free ligands 1,10-phenanthroline (phen), 1,10-phenanthroline-5,6-dione (phendione) and Tetrapyrrodo [3,2-a:2',3':3'',2''-h:2''',3'''-j]phenazine (tpphz) have been correctly assigned with the aid of 2D-COSY spectra, an example of which is shown below in Figure 4.10. The data obtained have been compared to the literature values reported.<sup>11,7</sup> Chemical shift values are presented in Table 4.6 above and relevant spectra can be observed in Figures 4.10 and 4.11 that follow.

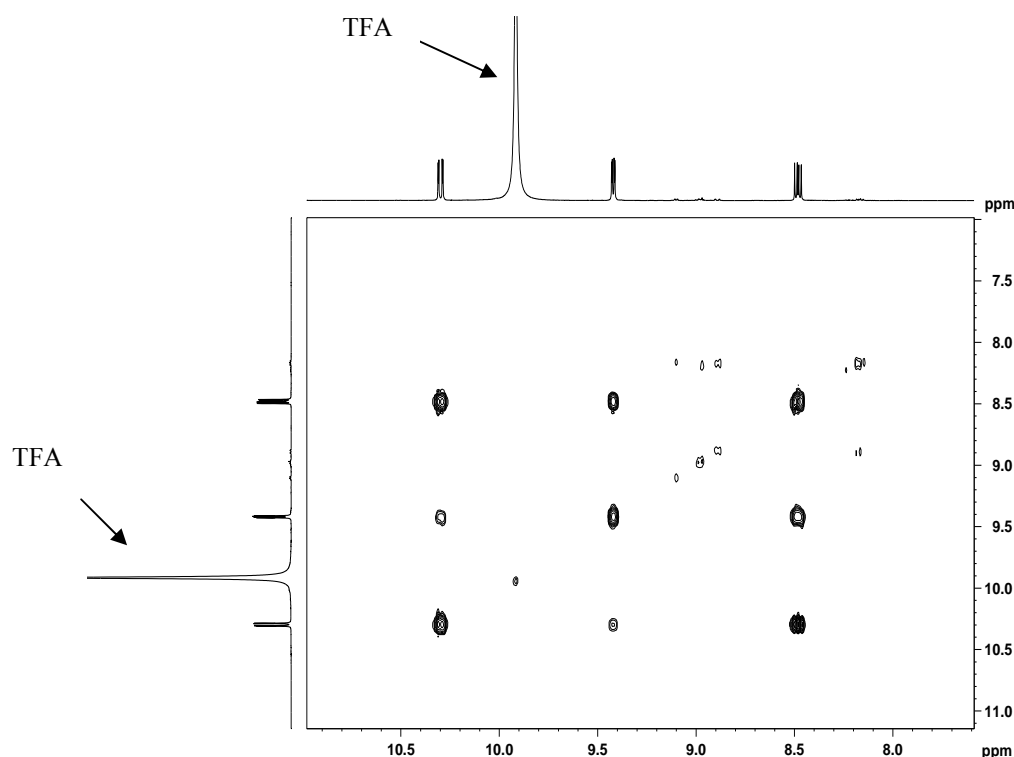


**Figure 4.10**  $^1\text{H}$ NMR COSY of tpphz ligand in  $d_3$ -acetonitrile at 298K.



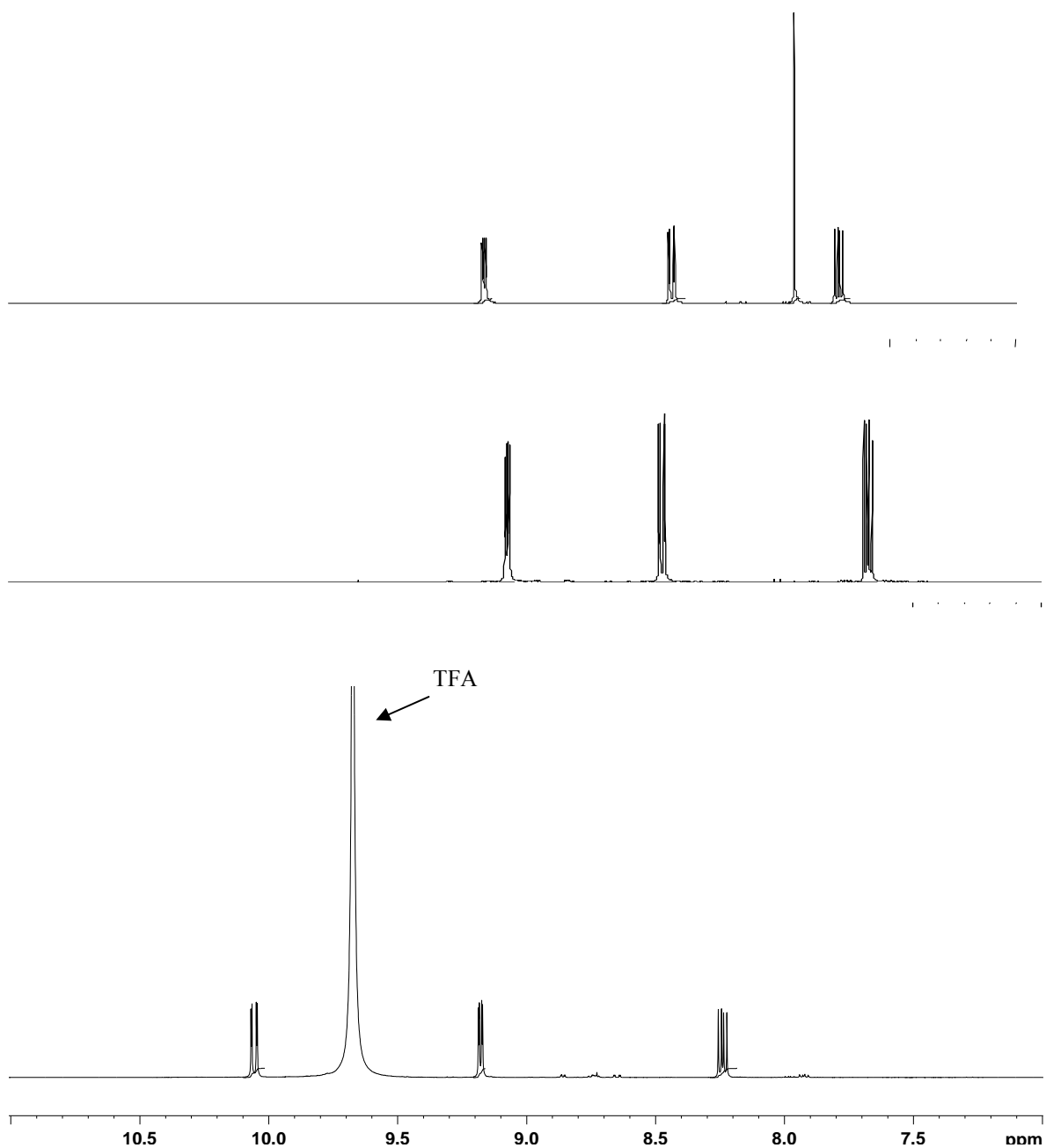


**Figure 4.11:**  $^1\text{H}$ NMR of phenanthroline (top), phendione (middle) and tpphz (bottom) ligands in  $d_3$ -acetonitrile at 298K. TFA peak can be seen at 9.66 ppm in the tpphz spectra.

The splitting obtained in the above spectra are explained with the use of a 2D-COSY analysis in each case. Observation of the data obtained indicated that the H2 proton lies the most upfield, as its position is far from the oxygen or nitrogen present to have an effect. The splitting of the H2 proton is also explained, as it is split by both the H1 and H3 protons. H1 is located as expected, the most downfield in each case due to the proximity of the nitrogen atom. The H3 proton in each case lies between the H1 and H2 protons, as the nearby oxygen deshielding the protons.

Comparison of the  $^1\text{H}$ -NMR data for a given proton, shows that in passing from the phenanthroline to phendione, a shift upfield is obtained. This is expected due to the presence of the oxygen on the phendione ligand that has a shielding effect on the protons. The  $\text{C}_2$  symmetry of phenanthroline and phendione ligands is revealed by the presence of 4 proton signals, each equivalent to 2 protons. In passing from phendione to the tpphz ligand, a down field shift is seen for a given proton, due to the absence of the oxygen and formation of the pyrazine center.

Obtaining an NMR spectrum of the tpphz ligand was much more complicated than the previous ligands due to the insolubility of the tpphz ligand in common organic solvents. TFA (tetrafluoroacetic acid) was required to dissolve the ligand (this peak can clearly be seen in Figures 4.10 and 4.11 at 9.66 ppm), followed by dissolution of the protonated ligand in a deuteriated solvent. Tpphz proton shifts are in agreement with those published by *Bolger et al.*<sup>2</sup> Due to high symmetry in the tpphz ligand, only three signals are observed for the 12 protons on the ligand itself, each signal referring to 4 protons.

**4.3.2.2  $^1\text{H}$  NMR - Mononuclear Complexes.**

The NMR spectra of the mononuclear complexes discussed in this section have been assigned with the use of a COSY spectrum in the aromatic region. Table 4.7 below contains the values obtained for the ligand protons (1,10-phenanthroline, 1,10-phenanthroline-5,6-dione and tpphz) of the mononuclear complexes prepared in  $d_6$ -acetone. As the bipyridine ligand proton signals appear as expected (see section 4.2), they are not further discussed here.

<i>Complex</i>	<i>H1</i>	<i>H2</i>	<i>H3</i>	<i>H4</i>
$[\text{Ru}(\text{bpy})_2(\text{phen})]^{2+}$	8.84	7.38	8.22	8.41
$[\text{Ru}(\text{bpy})_2(\text{phendione})]^{2+}$	8.58	7.61	7.98	-
$[\text{Re}(\text{CO})_3\text{Cl}(\text{phen})]$	9.41	8.85	8.03	8.22
$[\text{Re}(\text{CO})_3\text{Cl}(\text{phendione})]$	9.22	8.77	7.98	-
$[\text{Re}(\text{CO})_3\text{Cl}(\text{tpphz})]$	10.46	9.66	8.46	7.07

**Table 4.7:**  $^1\text{H}$  NMR data for the ligand protons of the Re (I) and Ru (II) mononuclear complexes carried out in  $d_6$ -acetone at 298K.

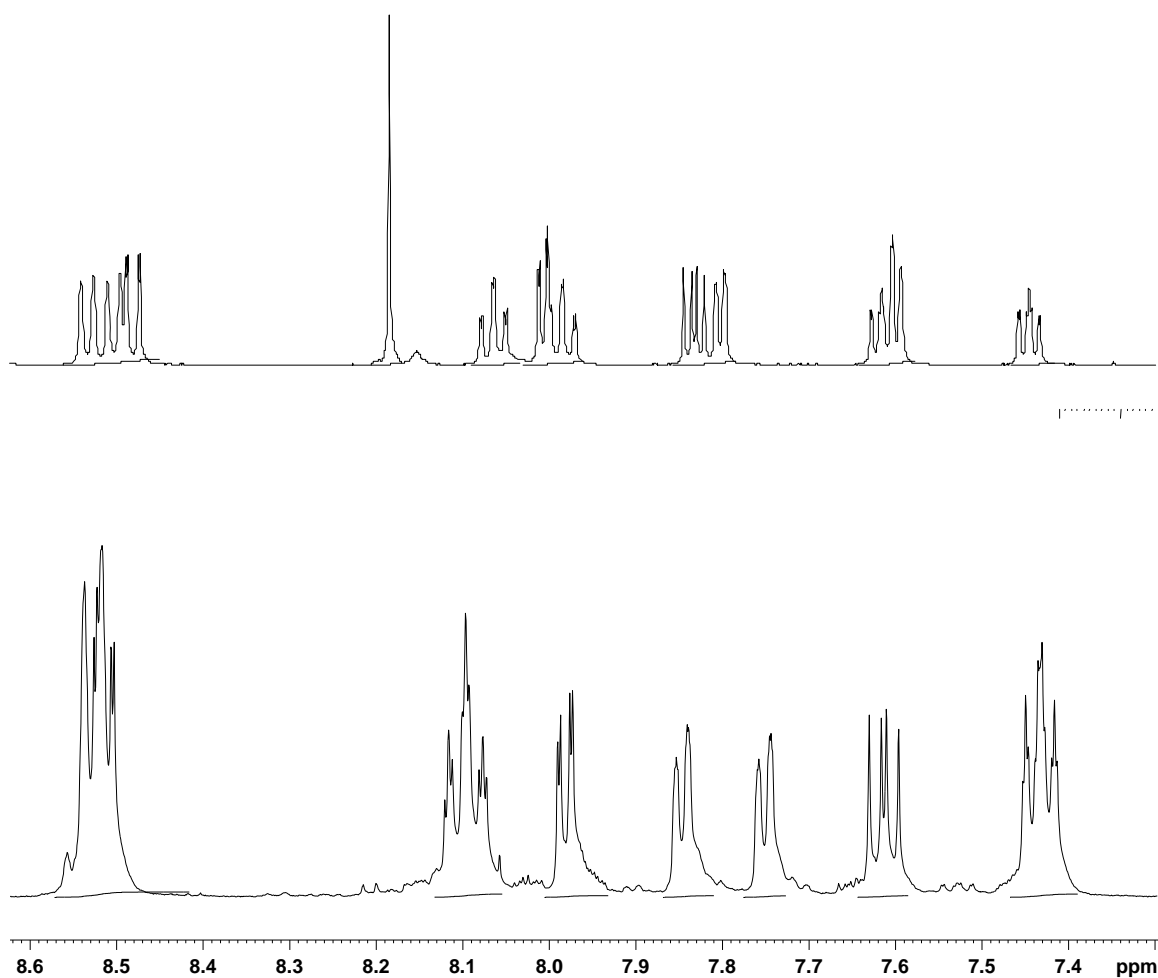


**Figure 4.12**  $^1\text{H}$ NMR spectrum for  $[\text{Ru}(\text{bpy})_2(\text{phen})]^{2+}$  (top) and  $[\text{Ru}(\text{bpy})_2(\text{phendione})]^{2+}$  (bottom) in  $d_3$ -acetone at 298K.

Figure 4.12 above details the spectra obtained for  $[\text{Ru}(\text{bpy})_2(\text{phen})]^{2+}$  and  $[\text{Ru}(\text{bpy})_2(\text{phendione})]^{2+}$  in  $d_6$ -acetone. There is a clear transformation in moving from the phenanthroline to the dione complex. There is a loss of 2 protons due to the formation of two oxygen double bonds, in the phenanthroline complex these two protons appear as a clear singlet at 8.23 ppm. This peak is absent from the dione complex which is a good indication of the formation of the  $[\text{Ru}(\text{bpy})_2(\text{phendione})]^{2+}$  complex. This was further confirmed by the IR data obtained for  $[\text{Ru}(\text{bpy})_2(\text{phendione})]^{2+}$ .

There is a small shift in the protons of the phenanthroline and the phendione when complexed to the Ru metal centre as the effect of binding is similar in both complexes. Comparing the free dione ligand and the complex  $[\text{Ru}(\text{bpy})_2(\text{dione})]^{2+}$  a shift of 0.41 ppm is observed for the H1 proton closest to the nitrogen, from 8.99 ppm to 8.58 ppm. This shift is due to the electron density of the metal centre which has a shielding effect on the hydrogens of the ligand resulting in an upfield shift of 0.33 ppm in this case.

Figure 4.13 below shows the proton NMR obtained for the free dione ligand,  $[\text{Re}(\text{CO})_3(\text{phen})\text{Cl}]$  and  $[\text{Re}(\text{CO})_3(\text{phendione})\text{Cl}]$ . The effect of complexation here is more prominent due to the lack of other protons in the complex. A clear shift of 0.2 – 0.4 ppm upfield for the ligand protons, is seen upon complexation of the dione ligand with the rhenium carbonyl species. Again only a small shift up field is noticed in progressing from  $[\text{Re}(\text{CO})_3(\text{phen})\text{Cl}]$  to  $[\text{Re}(\text{CO})_3(\text{phendione})\text{Cl}]$ . The singlet that appears at 8.22 ppm is missing from the dione complex indicating the formation of the two carbon – oxygen double bonds. This was further confirmed by IR analysis which showed peaks present at  $2023\text{ cm}^{-1}$ ,  $1923\text{ cm}^{-1}$  and  $1898\text{ cm}^{-1}$ . This is discussed in further detail in section 4.3.3.

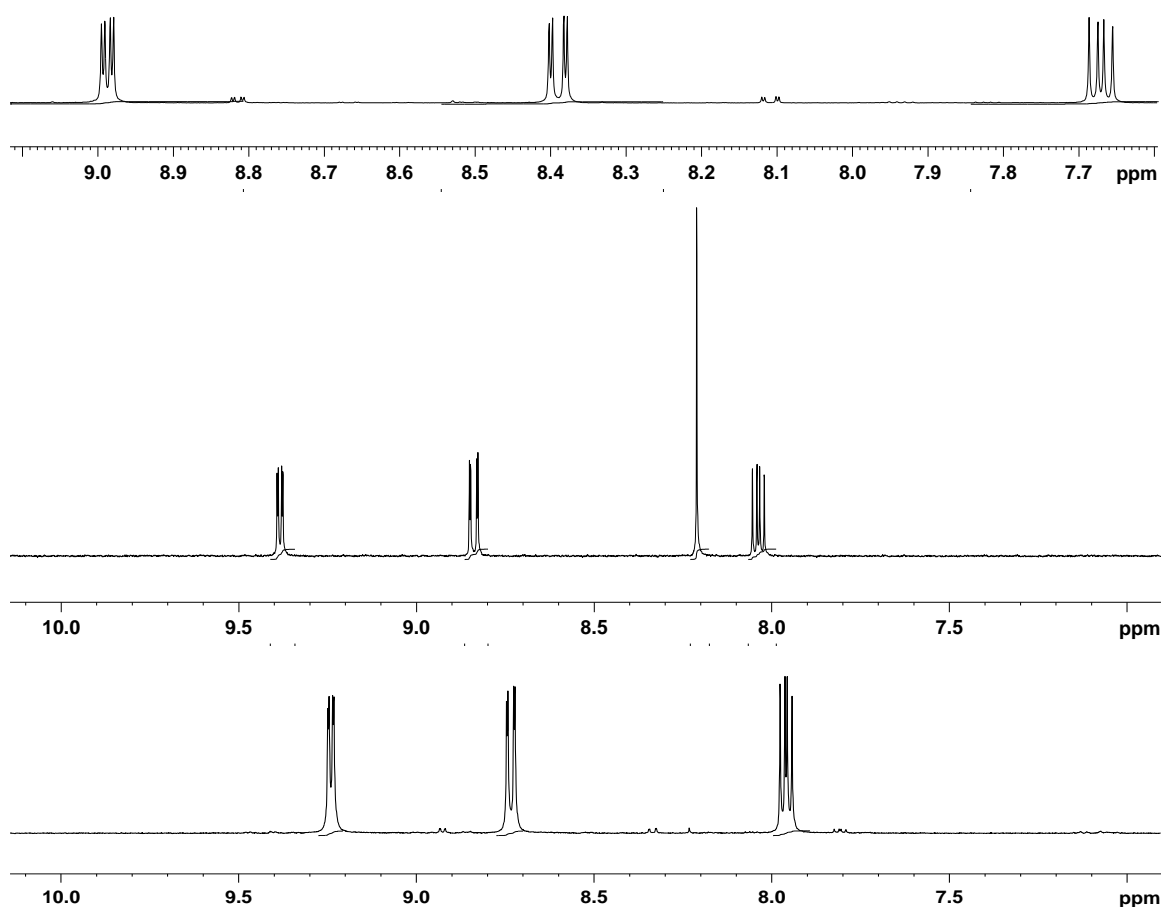


**Figure 4.13:**  $^1\text{H}$  NMR spectrum for phendione (top),  $[\text{Re}(\text{CO})_3(\text{phen})\text{Cl}]$  (middle) and  $[\text{Re}(\text{CO})_3(\text{phendione})\text{Cl}]$  (bottom) in  $d_6$ -acetone at 298K.

Analysis of the mononuclear complex  $[\text{Re}(\text{CO})_3\text{Cl}(\text{tpphz})]$  was difficult to obtain due to solubility issues and resulting NMR spectra depicted broad peaks with no identifiable proton signals. However IR data of this complex indicated that some formation had occurred due to a shift of carbonyl bands from  $2046\text{ cm}^{-1}$  and  $1922\text{ cm}^{-1}$  of the rhenium pentacarbonyl to  $2022\text{ cm}^{-1}$ ,  $1923\text{ cm}^{-1}$  and  $1902\text{ cm}^{-1}$  for  $[\text{Re}(\text{CO})_3\text{Cl}(\text{tpphz})]$  This is further discussed in section 4.3.3 that follows. It is of note that *Bolger et al.* have reported that the NMR spectra obtained for mononuclear complexes containing the tpphz ligand are concentration dependant due to the  $\pi$ - $\pi$  stacking that can occur on the free end of the ligand. The planarity and rigidity of the ligand allows for orientations where the stacking can occur though this has been shown to be solvent and concentration dependant. In the case of the rhenium

mononuclear complex  $[\text{Re}(\text{CO})_3\text{Cl}(\text{tpphz})]$  further nmr studies should be carried out to determine if this is what is occurring in this case.

#### 4.3.2.3 $^1\text{H}$ NMR - Dinuclear Complexes

To date the complexes  $[(\text{Ru}(\text{bpy})_2)_2(\text{tpphz})](\text{PF}_6)_4$ ,  $[(\text{Ru}(\text{d-bpy})_2)_2(\text{tpphz})](\text{PF}_6)_4$  and  $[\text{Ru}(\text{bpy})_2(\text{tpphz})\text{Re}(\text{CO})_3\text{Cl}](\text{PF}_6)_2$  have been synthesized. All NMR spectra carried out were calibrated to the relevant solvent peak and protons have been correctly assigned using a COSY spectra, an example of which can be seen in Figure 4.14.

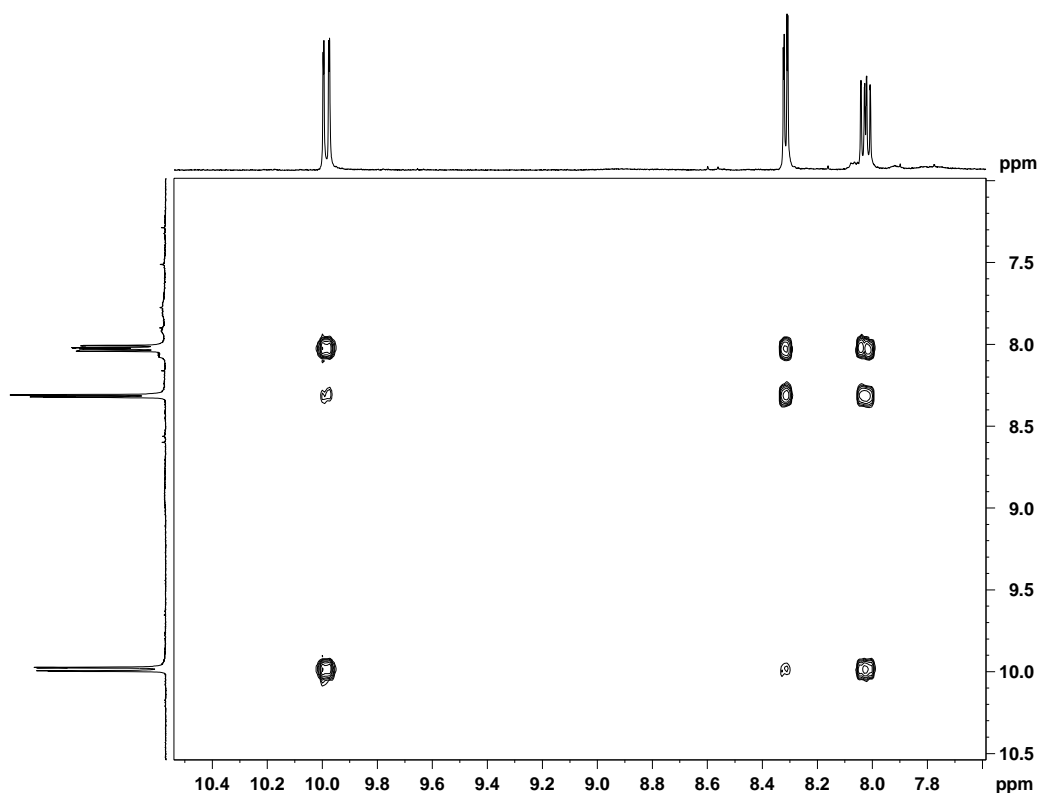


**Figure 4.14:** 2D-COSY spectrum for the complex,  $[(\text{Ru}(\text{d-bpy})_2)_2(\text{tpphz})]^{2+}$  in  $d_3$ -acetonitrile at 298K.

Figure 4.15 displays the NMR spectra obtained for  $[(\text{Ru}(\text{bpy})_2)_2(\text{tpphz})]^{2+}$ ,  $[(\text{Ru}(\text{d-bpy})_2)_2(\text{tpphz})]^{2+}$  and free tpphz ligand. Here the deuteriated complex was used to determine the position of the tpphz protons. The effect of complexation here can clearly be seen by a shift upfield for all ligand protons of approx 0.5 ppm for each proton. The NMR spectrum for  $[(\text{Ru}(\text{bpy})_2)_2(\text{tpphz})]^{2+}$ , still contains some

mononuclear  $[\text{Ru}(\text{bpy})_2(\text{tpphz})]^{2+}$  which is indicated by the presence of the two proton peaks at 9.48 ppm and 9.97 ppm which are in agreement with those reported by *Bolger et al.*<sup>24</sup> These peaks present are known to be the H1 and H4 protons located nearest to the N atom of the ligand. (see Figure 4.9 above and Figure 4.15 below.)

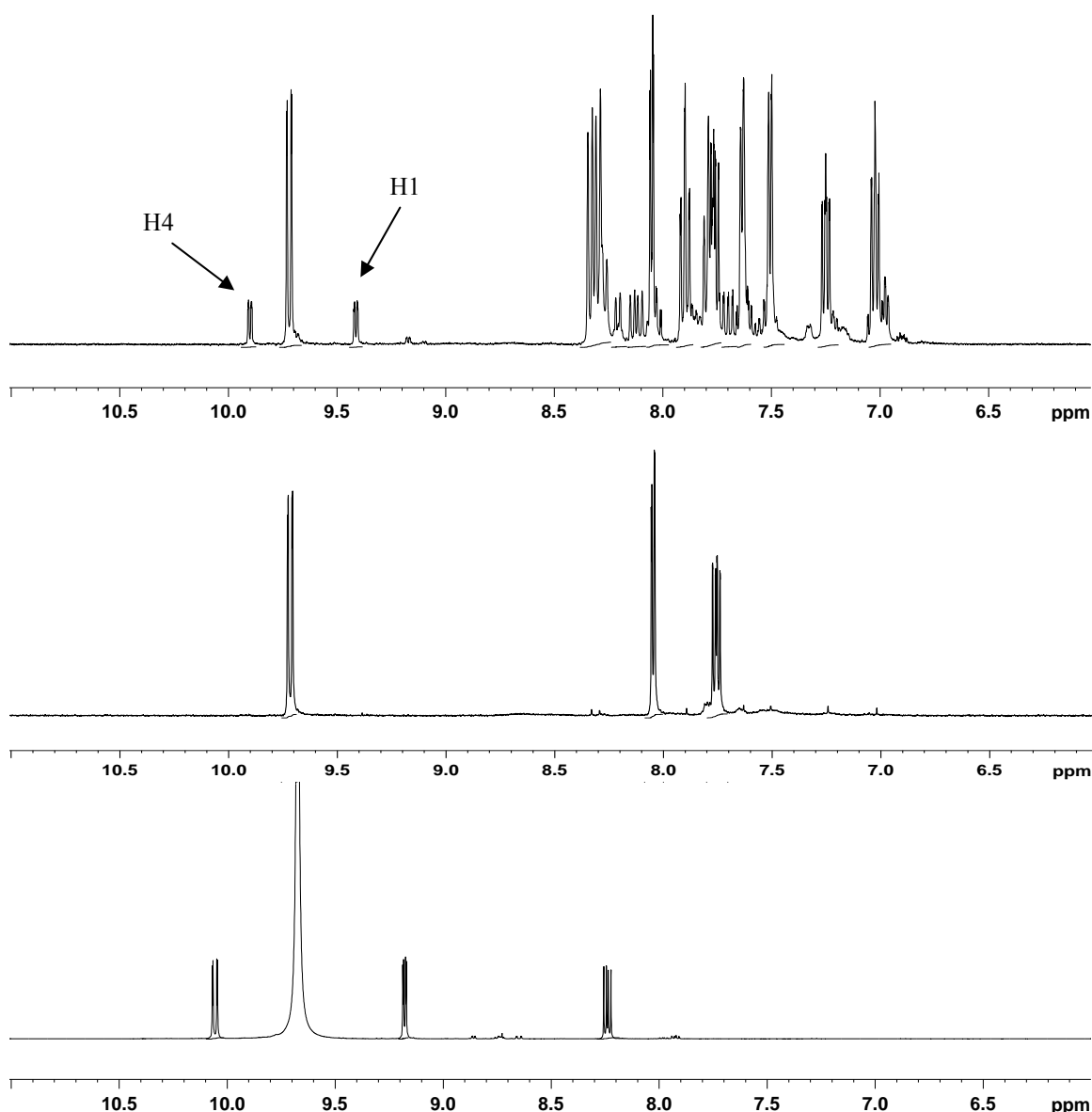


**Figure 4.15:**  $^1\text{H}$  NMR spectra for the complexes  $[\text{Ru}(\text{bpy})_2]_2(\text{tpphz})_2^{2+}$  (top),  $[\text{Ru}(\text{d-bpy})_2]_2(\text{tpphz})_2^{2+}$  (middle) and free  $\text{tpphz}$  ligand (bottom) in  $d_3$ -acetonitrile at 298 K.  $\text{Tp-phz}$  ligand was recorded in the presence of TFA (trifluoroacetic acid).



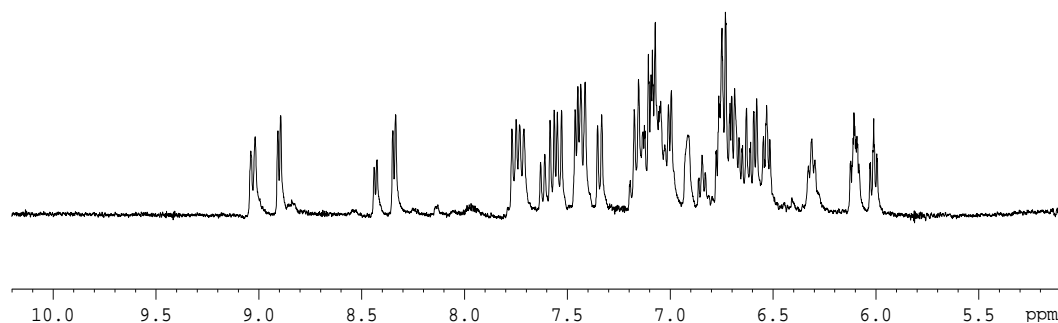


**Figure 4.16:**  $^1\text{H}$ NMR spectrum for  $[\text{Ru}(\text{bpy})_2(\text{tpphz})\text{Re}(\text{CO})_3\text{Cl}]^{2+}$  in  $d_3$ -Acetonitrile at 298K.

The NMR spectrum for the heteronuclear complex  $[\text{Ru}(\text{bpy})_2(\text{tpphz})\text{Re}(\text{CO})_3\text{Cl}]^{2+}$  is presented in Figure 4.16 above. This spectrum is difficult to interpret due to the presence of isomers which can be observed by the complexity of the spectrum obtained, and the presence of the peaks at 9.02 ppm, 9.04 ppm, 8.38 ppm and 8.41 ppm. To date the separation of these isomers has not been obtained. The separation of similar isomers has been reported by Bergman and Koi<sup>23</sup> using HPLC. To determine the positioning of the ligand protons a deuteriated complex  $[\text{Ru}(\text{d-bpy})_2(\text{tpphz})\text{Re}(\text{CO})_3\text{Cl}]^{2+}$  is required, but on comparing the NMR obtained by those presented by Bergman and Koi and Bolger, it can be theorized that the peaks at 9.04 ppm and 8.41 ppm are the H1 proton of the tpphz ligand of two differing isomers. It is also possible to say that the formation of the dinuclear complex has occurred due to the complexity of the spectrum and the positioning of the bpy protons, if a mononuclear species had formed the spectrum would be less complex and integrate for fewer protons.

### 4.3.3 Infra-red Analysis

IR spectra for the tpphz and related reactions were recorded in the carbonyl stretching region ( $2200 - 1700 \text{ cm}^{-1}$ ) in THF as a solvent. Table 4.6 below contains a summary of the results obtained while Figures 4.17 and 4.18 that follow, show IR spectra obtained for complexes of this type.

<i>Complex</i>	$\nu_{(\text{CO})} \text{ cm}^{-1}$	$\nu_{(\text{CO})} \text{ cm}^{-1}$	$\nu_{(\text{CO})} \text{ cm}^{-1}$
$[\text{Re}(\text{CO})_5\text{Cl}]$	2046	1922	-
$[\text{Re}(\text{CO})_3\text{Cl}(\text{phen})]$	2020	1918	1894
$[\text{Re}(\text{CO})_3\text{Cl}(\text{phendione})]$	2023	1923	1898
$[\text{Re}(\text{CO})_3\text{Cl}(\text{tpphz})]$	2022	1923	1902
$[\text{Ru}(\text{bpy})_2\text{tpphzRe}(\text{CO})_3\text{Cl}]^{2+}$	2024	1923	1900

**Table 4.8:** IR data for the carbonyl stretching region of the metal complexes in THF.

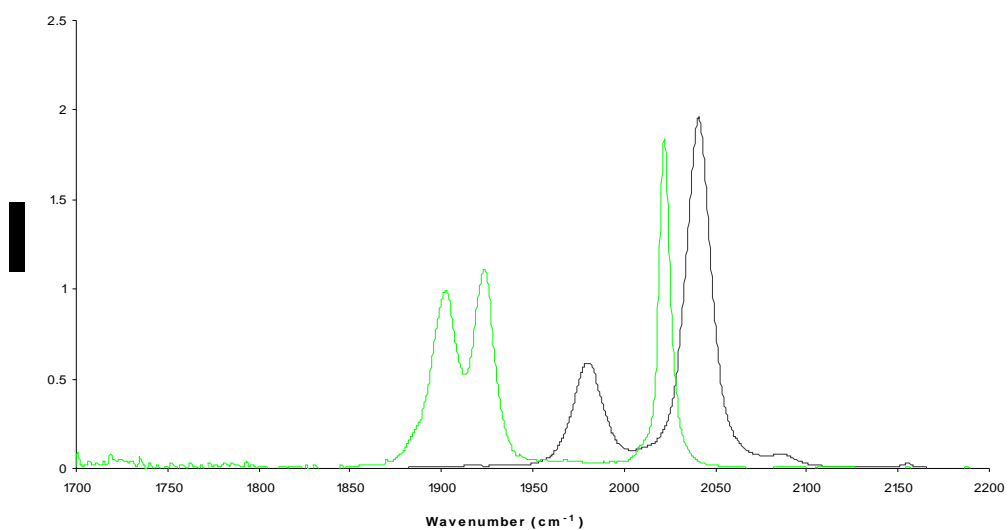


**Figure 4.17:** I.R. of  $[\text{Re}(\text{CO})_5\text{Cl}]$  (black) and  $[\text{Re}(\text{CO})_3\text{Cl}(\text{tpphz})]$  (green) in THF at 298K.

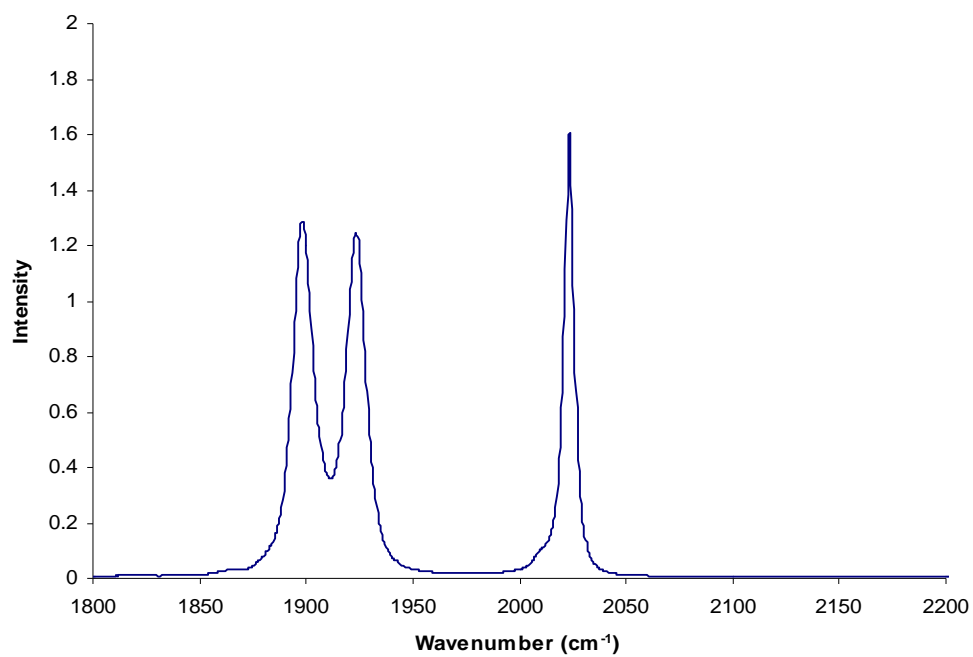


**Figure 4.18:** I.R. of  $[\text{Re}(\text{CO})_3\text{Cl}(\text{dione})]$  in THF at 298K.

All of the spectra obtained for the complexes  $[\text{Re}(\text{CO})_3\text{Cl}(\text{phen})]$ ,  $[\text{Re}(\text{CO})_3\text{Cl}(\text{phendione})]$ ,  $[\text{Re}(\text{CO})_3\text{Cl}(\text{tpphz})]$  and  $[\text{Ru}(\text{bpy})_2\text{-tpphz-Re}(\text{CO})_3\text{Cl}]^{2+}$  contain three carbonyl bands, which possess  $C_s$  symmetry<sup>12, 13</sup> where the IR bands from highest to lowest wavenumbers ( $\text{cm}^{-1}$ ), are assigned the symmetry labels  $A'$  (1),  $A''$  and  $A'$  (2) respectively.<sup>14</sup> Comparing these bands to those reported for  $[\text{Re}(\text{CO})_3\text{Cl}(\text{phen})]$ <sup>14,15</sup> indicate that the CO ligands are arranged around the Re metal center in a facial orientation. This means that the ligands are bound in the equatorial region, trans to two carbonyls with a chlorine atom in the axial position and a CO in the final axial position. This is best described in Figure 4.19 below.

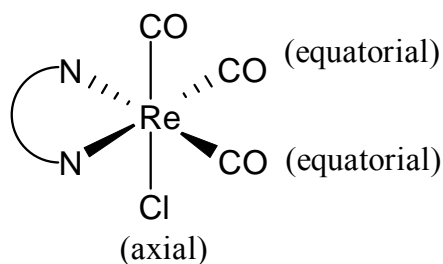


**Figure 4.19:** Example of the facial coordination of the rhenium tricarbonyl complexes discussed where N-N denotes a phenanthroline based ligand.

Upon chelation of the phenanthroline type ligands, these CO bands were found to move to a lower frequency compared to that of the pentacarbonyl complex as shown in Table 4.8 above. This is typical in the formation of a rhenium tricarbonyl species of the type  $[\text{Re}(\text{CO})_3(\text{L})\text{X}]$  where L is a bidentate N-coordinated ligand.<sup>14, 15</sup> This is due to the presence of back bonding on the Re centre. As the ligand becomes bound to the rhenium metal centre electron density of the rhenium  $d_\pi$  orbitals becomes increased and back bonding occurs between these and the CO  $\pi^*$  orbitals.

Coordination of the ruthenium moiety to the  $[\text{Re}(\text{CO})_3\text{tpphz}]$  monomer results in minor IR spectral changes ( $2 \text{ cm}^{-1}$  for the  $A'$  (1) band). This indicates that the ruthenium centre has no significant effect on the electron density around the tpphz ligand bound to the Re center and in turn the carbonyl ligands. This could be due to

the length of the planar tpphz ligand allowing both metal centers to coordinate to the ligand itself without changing electron density around the Re centre. If the  $\text{Ru}(\text{bpy})_2$  segment was to pull density away from the Re centre it would appear in the IR spectra as a shift in the CO bands to higher energies.<sup>16,17</sup>

#### **4.4 Conclusions.**

Preparation of the free ligands, mononuclear and dinuclear complexes discussed in this section have been confirmed by NMR spectroscopy with assignment of the peaks with the use of a 2D-COSY technique. Synthetic studies have shown that the preparation of the desired  $[\text{Ru}(\text{bpy})_2(\text{tpphz})\text{Re}(\text{CO})_3\text{Cl}]^{2+}$  is achievable from either a condensation reaction with the ruthenium and rhenium dione mononuclear complexes in the presence of ammonium acetate and a hydrogen donor or by coordination of the  $[\text{Ru}(\text{bpy})_2]$  moiety to the  $[\text{Re}(\text{CO})_3\text{Cl}(\text{tpphz})]$  mononuclear complex. The latter giving the highest yield with fewest impurities.

The rhenium mononuclear complexes obtained during this study have been analysed by IR spectroscopy and have shown that all of the complexes have formed in the fac isomer due to the three carbonyl bands present in the  $1700\text{ cm}^{-1} - 2200\text{ cm}^{-1}$  region of the IR spectrum.

For the complex  $[\text{Ru}(\text{bpy})_2(\text{tpphz})\text{Re}(\text{CO})_3\text{Cl}]^{2+}$  and precursors further analysis is required such as UV-vis analysis, fluorescence, mass spec and elemental analysis. At present the heteronuclear complexes that have been prepared and purified are currently under analysis for  $\text{CO}_2$  reduction, to determine the efficiency of the dyes prepared. Gas chromatography, ion chromatography IR and UV-vis measurements will be employed to determine the side products formed and the quantity in which they are formed. Results from these studies will determine those complexes which will require attachment groups for surface analysis. Due to the wide range of bridging ligands prepared an analysis of the effects of the ligand on  $\text{CO}_2$  reduction will also be studied

## 4.5 Bibliography

---

- <sup>1</sup> Wasielewski, M. R., *Chem Rev.*, **1992**, 92, 435.
- <sup>2</sup> Forster, R.J., Keys, T.E., Vos, J. G., *Interfacial Supramolecular Assemblies*, John Wiley, Chichester, UK., **2003**.
- <sup>3</sup> Kalyanasundaram, K., Gratzel, M., Nazeerudin, M. K., *J. Phys. Chem.*, **1992**, 96, 5865.
- <sup>4</sup> Bignozzi, C. A., Bortolini, O., Chiorboli, C., Indelli, M. T., Rampi, M. A., Scandola, F., *Inorg. Chem.*, **1992**, 31, 172.
- <sup>5</sup> Leob, B. L., Neyhart, G. A., Worl, L. A., Danielson, E., Sullivan, B. P., Mayer T. J., *J. Phy. Chem.*, **1989**, 93, 717.
- <sup>6</sup> Meyer, G. J., *J. Photochem. Photobio. A.*, **2003**, 158, 119.
- <sup>7</sup> Campagna S., Puntorireo F., Nastasi F., Bergamini G., Balzani V., *Top. Curr. Chem.*, **2007**, 280, 117.
- <sup>8</sup> Bolger, J., gourdon, A., Ishow, E., Launay, J. P., *J. Chem. Soc., Chem. Commun.*, **1995**, 1799.
- <sup>9</sup> Song Y. F., Yang, P., *Polyhedron*, **2001**, 20, 6, 501.
- <sup>10</sup> Kelch, S, Rehahn, M., *Macromolecules*, **1997**, 30, 6185.
- <sup>11</sup> Bodgie, S., Torres, A. S., Maloney D.J., Tate, D., Kinsel, G.R., Walker, A. K., MacDonnell, F. M., *J. Am. Chem. Soc.*, **1997**, 119, 10364.
- <sup>12</sup> Ishow, E., Gourdon, A., Launay, J.P., Lecante, P., Vereist, M, Chiorboli, C., Scandola, F., Bignozzi, C. A., *Inorg. Chem.*, **1998**, 37, 3603.

- <sup>13</sup> Chiorboli, C., Bignozzi, C. A., Scandola, F., *Inorg. Chem.*, **1999**, 38, 2402.
- <sup>14</sup> Rau S., Walther D., Vos J. G., *Dalton Trans.*, **2007**, 915.
- <sup>15</sup> Rau S., Schafer B., Gleich D., Anders E., Rudlof M., Friedrich M., Gorls H., Henery W., Vos J.G., *Angew. Chem. Int. Ed.*, **2006**, 45, 6125.
- <sup>16</sup> Ozawa H., Haga M. A., Sakai K., *J. Am. Chem. Soc.*, **2006**, **128**, 4926.
- <sup>17</sup> Hori H., Johnson F. P. A., Koike K., Takeuchi K., Ibusuki T., Ishitani O., *J. Chem. Soc., Dalton Trans.*, **1997**, 1019.
- <sup>18</sup> Hori H., Ishitani O., Koike K., Takeuchi K., Ibusuki T., *Analy. Sci.*, **1996**, 12, 4.
- <sup>19</sup> Hori H., Ishitani O., Koike K., Johnson F. P. A., Ibusuki T., *En. Conversion Manag.* **1995**, 36, 6-9, 621.
- <sup>20</sup> Hori H., Johnson F. P. A., Koike K., Ishitani O., Ibusuki T., *J. of Photochem. Photobio. A Chem.* (**1996**), 96, 1-3, 171.
- <sup>21</sup> Gholamkhash B., Mametsuka H., Koike K., Tanabe T., Furue M., Ishitani O., *Inorg. Chem.*, **2005**, 44, 7, 2326.
- <sup>22</sup> Chiorboli C., Rodgers M. A. J., Scandola F., *J. Am. Chem. Soc.*, **2003**, 125, 483.
- <sup>23</sup> Bergman S. D., Koi M., *Inorg. Chem.*, **2005**, 44, 1647.
- <sup>24</sup> Bolger J., Gourdon A., Ishow E., Launay J. P., *Inorg. Chem.*, 35, 10, **1996**, 2937.
- <sup>25</sup> Mousurkai R., Samuelson L. A., Kumar J., *Inorg. Chem.*, **2002**, 42, 5450.
- <sup>26</sup> Akkara J. A., Wang J., Yang D., Gonsalves K. F., *Macromolecules*, **2000**, 33, 2377.
- <sup>27</sup> Bodige S., McDonnell F., *Tetrahedron Letters*, 38, 47, **1997**, 8159.
- <sup>28</sup> Haung W., Ogawa T., *Polyhedron*, **2006**, 25, 1379.

<sup>29</sup> Wrighton M., Morse D. L., *JACS*, 96, 4, **1974**, 998.

<sup>30</sup> Chiorboli C., Bignozzi C. A., Scandola F., Ishow E., Gourdon A., Launay J. P., *Inorg. Chem.*, **1999**, 38, 2402.



***Chapter 5: Photochemical CO<sub>2</sub> Reduction Experiments.***

*Chapter 5 describes the analysis of the products of photochemical CO<sub>2</sub> reduction, formate and oxalate, using ion chromatography. The efficiency of the previously prepared photocatalysts in chapters 3 and 4 is discussed along with method development and the dionex 1500 ion chromatography system set up.*

## 5.0 Introduction.

The work described in chapter 5 was carried out to determine the efficiency of the previously prepared photocatalysts (Chapter 3 and 4) to reduced CO<sub>2</sub> by photochemical means. As shown in Figure 5.1 below, formate is a product, during the multi-step reduction of CO<sub>2</sub>, in the presence of a photocatalyst akin to those described in this body of work. An accurate determination of the quantity of formate and oxalate produced can lead to the determination of efficiency of a photocatalyst along with an insight to the mechanism and kinetics of CO<sub>2</sub> reduction occurring.

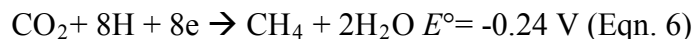
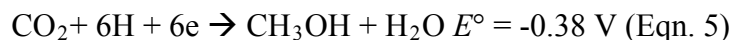
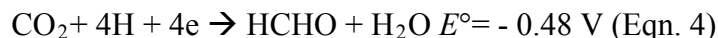
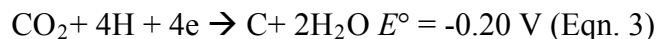
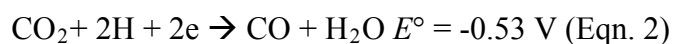


**Figure 5.1:** Redox potentials vs. NHE for the multi electron reduction of CO<sub>2</sub> at pH7 / 25°C<sup>1</sup>

This chapter is broken down into four main sections; section 5.1 relays the theory behind ion chromatography, specifically related to the work carried out within this chapter. Section 5.2 describes the system installation and initial calibration while section 5.3 details the method development for the anions oxalate and formate Section 5.4 concludes with sample analysis for formate and oxalate and an overview of suitability of the method chosen.

### 5.0.1. Ion Chromatography.

#### 5.0.1.1 Dionex ICS 1500 - Mode of Operation

To best describe the mode of operation of the ICS 1500, the flow of the mobile phase through the instrument will be described prior to sample injection, sample injection and system re-equilibration with the aid of Figure 5.2 below.

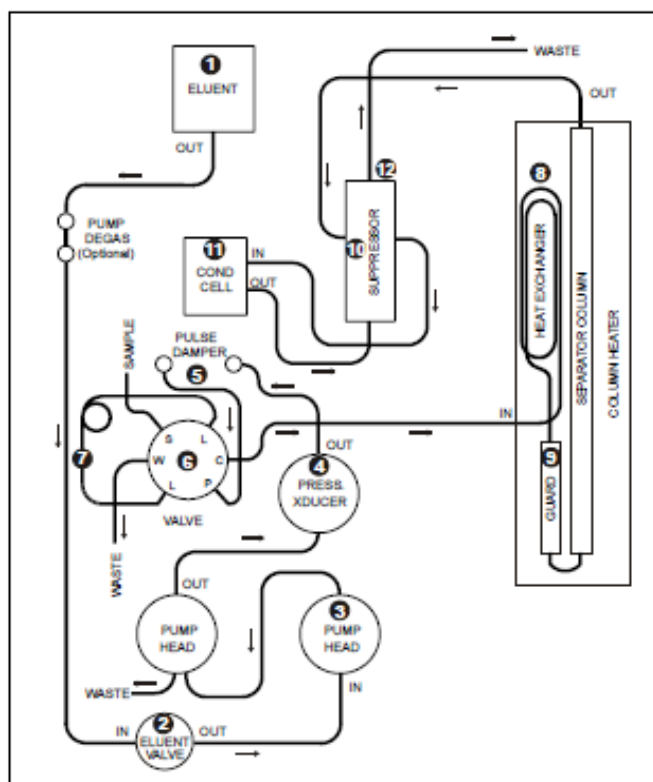


**Figure 5.2:** Diagram of Direction of Analysis Flow for the ICS 1500.<sup>2</sup>

As shown above, the mobile phase ( $\text{NaHCO}_3$  /  $\text{Na}_2\text{CO}_3$ ) passes from the reservoir through to the eluent valve, where it is pushed through to the pressure transducer which monitors the systems pressure. From here the mobile phase is pushed towards a pulse dampener, which minimises pressure variations from the pump, reducing background noise. From here the eluent passes on to the injection valve.

After a sample is loaded into the sample loop and injected, the mobile phase enters the loop, picks up the sample and moves on towards the heat exchanger, which warms the eluent to column temperature. This mixture (mobile phase\ sample) then passes through the guard column, separator column and towards the suppressor. From here the eluent / sample mixture passes through to the conductivity cell for detection. After detection the eluent is then passed back into the suppressor to act as a water source for the regenerant chamber. The flow is then directed towards waste and the cycle begins again.

### **5.0.2. Separation – Ion Exchange Chromatography.**

In order to discuss the mode of separation used within this chapter it is first important to understand the principles of ‘ion – exchange’ chromatography. Separation within an ion chromatography (IC) system is carried out within the analytical column containing anions, cations and water, where either the cations or anions are bound to an insoluble matrix (polymer resin), which are known as the *fixed ions*.<sup>3</sup> These fixed ions are the active sites of the exchange resin which determines the mode of exchange i.e. an anion exchange resin carries a *fixed ion* of positive charge. The *ion – exchange capacity* is then determined by the number of these active sites (functional groups) per weight of resin. Separation occurs stoichiometrically; as the electroneutrality of the solution is maintained during the exchange process e.g. a single monovalent anion displaces a single monovalent counter anion<sup>3</sup>

The mode of separation used here is anion exchange and the discussion of the mode of separation will be limited to the exchange interactions occurring within our system. The specifications of the columns fitted are located in Table 5.1 that follows along with limits of the parameters of operation.

<b>Packing Specifications</b>			
	<b>IonPac As22 (4 x 250 mm), Analytical</b>		<b>IonPac Ag22, (4 x 50 mm), Guard</b>
<b>Particle Diameter</b>	6.5		11
<b>% Substrate X - linking</b>	55		55
<b>Column Capacity (<math>\mu\text{eq}</math> / column)</b>	210		6
<b>Functional Group</b>	Alkyl / Alkanol Ammonium	Quaternary	Alkyl / Alkanol Ammonium Quaternary
<b>Hydrophobicity</b>	Low		Low
<b>Resin</b>	Supermacroporous ammonium polymer, (X - link = DVB)	PVB	Microporous PVB ammonium polymer, (X - link = DVB)
<b>Operating Parameters</b>			
<b>Typ. Back Pressure psi, (MPa)</b>	$\leq 1600$ (11.03)		$\leq 300$ (2.07) <sup>a</sup>
	$\leq 1900$ (11.03) <sup>a</sup>		$\leq 1900$ (11.03) <sup>a</sup>
<b>Standard Flow Rate (mL / min)</b>	1.2 (1.2) <sup>a</sup>		2.5 (1.2) <sup>a</sup>
<b>Maximum Flow Rate (mL / min)</b>	1.2 (1.2) <sup>a</sup>		2.5 (2.5) <sup>a</sup>
<i>a</i> = values for analytical and guard columns run in series, PVB = polyvinylbenzyl, DVB = divinylbenzene.			

**Table 5.1:** Column specifications and Operation Parameters for Dionex ICS 1500.

As can be seen in table 4.1 above the analytical column (ionpac AS22) contains a macroporous resin constructed from polyvinylbenzyl (PVB) ammonium polymer backbone with a 55% crosslinking with divinylbenzene to allow for mechanical strength.<sup>2,3</sup> This macroporous resin has a large surface area for surface derivitisation to give a high number of active sites for ion – exchange. The guard column is constructed from a microporous polymer of the same PVB polymer and degree of cross linking but with an increased pore size (and reduce surface area) as the function of the guard column is to protect the analytical column.

The Ionpac AS22 is an agglomerated ion exchange resin where the resin acts an internal core particle to which the functional groups (active sites) are attached. These functional groups are amminated latex particles and can be attached in three ways: electrostatic binding where the central core is functionalised with ionic groups of opposite charge to the functionalised latex, hydrophobic binding using an electrical double layer between the core and the latex or mechanical binding where a binding material is used to fix the latex to the neutral core.<sup>3,7</sup>

The addition of these functional groups will determine the ion exchange capacity of the resin which is varied by altering the type of latex particle. Extensive studies by Barron and Fritz were carried out to determine the effect of the alkyl linkage groups on the quaternary ammonium ion concluding that relative retention times are decreased with longer spacers only for large polarizable ions.<sup>4,5,6</sup>

The AS22 analytical column offers high chromatographic efficiency as the diffusion path is short leading to high mass transfer rates during exchange. The agglomerated exchanger is stable over a wide pH range with high selectivity which is required for most IC separations. The low degree of hydrophobicity within both the guard and analytical columns used here reduces the risk of column fouling by lipophilic sample components which may arise from sample analysis containing trace amounts of photocatalyst.<sup>7</sup>

### **5.0.3 Eluent**

Changing the eluting power of a solvent will alter the retention times of sample analytes, as the concentration of the eluent ions is increased more eluent ions are present to compete with the sample ions, therefore reducing the retention times of the sample ions. Ultimately the detector/ suppressor type used within a system will determine the types of eluent that can be used.

1. Type of eluent used.

Retention time of the analyte ion increases when the eluent ion is replaced by one with greater potential for dipole – dipole induction (increased polarizability).

Anion exchange: sulphate > nitrate > phosphate > chloride > hydroxide.

2. Ionic strength of eluent.

Retention time increases as concentration of eluent ions is decreased.

3. pH of eluent.

The exchange capacity of the exchange resin depends on the pH level at which it is used, which in turn affects the retention time of the analyte ions. The pH also affects the form in which the analyte ions are in and the eluent ions exist with the dissociation of the molecules depending on the pH

#### 5.0.4. Suppression.

The suppressor type used within the described system is the ASRS 300 4 mm self-regenerating suppressor 4mm. The role of a suppressor is to “suppress” the background conductance of the eluent (carbonate/bicarbonate mobile phase) thereby increasing the sensitivity of the detector. This is carried out by exchanging hydrogen ions from the membrane in the suppressor for cations in the eluent, prior to measurement of conductance by the detector. Figure 5.3 below describes the suppression mechanism with a carbonate/bicarbonate mobile phase.

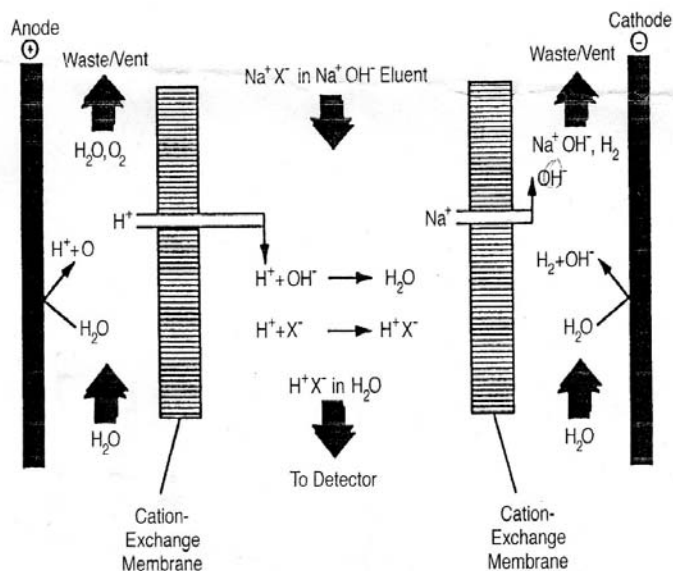
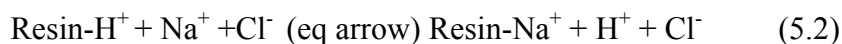


**Figure 5.3:** Mechanism of suppression for the Anion Self- Regenerating Suppressor.<sup>3,7,8</sup>

This ASRS suppressor is an electrolytic suppressor which electrolyses water to produce H<sup>+</sup> ions at the anode where they make their way across the first cation – exchange membrane where they come into contact with the mobile phase. The H<sup>+</sup> ions neutralise the basic eluent allowing the counter Na ions to make their way towards the negatively charged cathode to combine with hydroxide ions. An example



of this exchange is described below in equations 5.1 (eluent reaction in suppressor) and 5.2 (solute reaction), where Cl<sup>-</sup> ions denotes the solute and the eluent is sodium hydrogen carbonate.



The advantages of suppression are best described by Haddad and Jackson<sup>3</sup> are as follows:

- Decreased baseline noise resulting from pump pulsations.
- Decreased baseline conductance
- Virtual elimination of the water and carbonate dips from final chromatogram.
- Enhanced detectability of eluted anions since there is no loss of conductance signal due to reaction of H<sup>+</sup> ions in the analyte band with H<sub>2</sub>CO<sub>3</sub> in the suppressed eluent.

#### **5.0.5. Conductivity Detection.**

Conductivity is the ability of a solution containing a salt to conduct electricity across two electrodes in the presence of an electrical field. The intensity of conductance is directly proportional to the salt content i.e. as ionic strength increases, conductivity increases.<sup>2,3,7</sup> For this reason conductivity detection is commonly used in conjunction with suppressors as described above in section 5.1.4. Conductivity detection can either be direct (where the solute has a higher conductance than the eluent) or indirect (where the solute has a lower conductance than the eluent).

Here the DS6 conductivity cell is a flow through cell, using a direct detection method as is the most common mode of detection for the analysis of anions.<sup>3</sup> This cell is of simple design and is composed of two passivated stainless steel electrodes permanently sealed into the cell body with a volume of 1  $\mu$ L.<sup>2</sup> This is based on an alternating current bridge which supplies the electric potential between the two electrodes. Under the influence of this field the anions move towards the anode and the cations towards the cathode. The resulting current is dependent on the applied potential and the nature and concentration of the anions in the mobile phase.

As reported by Braunstein and Robbins<sup>9</sup> a cell design of this type can give rise to some problems as described below:

- Electrolytic processes (Faradaic) can occur at the electrodes, if removal of the ions at the electrodes occurs at a faster rate than supplied by the bulk solution.
- A double layer of ions can occur at the electrode surface which can act as a capacitor which is capable of storing a charge.
- The mobile phase in the cell itself can impose a resistance to the motion of ions in solution as they must overcome friction forces.

The effects mentioned above can be reduced by the introduction of a variable capacitance into the circuit, which can minimise the phase shift between the current and voltage. This is carried out by the introduction of parallel resistance-capacitance balancing arms as they can achieve smaller capacitances with higher accuracy.<sup>10</sup>

### ***5.1 Aim***

The Aim of this chapter is to describe the installation and calibration of the Dionex ICS 1500 system. Further described are the method developed for the analysis of the CO<sub>2</sub> reduction products formate and oxalate and the analysis of the previously synthesised dye [Ru(bpy)<sub>2</sub>(bpt)Re(CO)<sub>3</sub>Cl]<sup>2+</sup> described in chapter 3.

## 5.2 System Installation and Calibration.

### 5.2.1. System Installation.

As the *Dionex* ICS-1500 system was unused, an initial system calibration was carried out to determine the reliability of the system and the results generated. System calibration was carried out by three repeated injections of a 20 ppm mixed anion standard containing fluoride, chloride, nitrite, bromide and nitrate. This was then injected using the parameters described below in Table 5.2 and compared to the reported values by *Dionex* for the same separation of mixed anions.

<i>Separation Parameters for 20 ppm Mixed Anion Standard.</i>	
Eluent:	4.5 mM Na <sub>2</sub> CO <sub>3</sub> / 1.4 mM NaHCO <sub>3</sub> (pH = 9.1)
Flow Rate:	1.2 mL/min
Column Temperature:	30 °C
Detection:	Suppressed Conductivity Detector (CD25) @ 35 °C
Suppressor:	ASRS Ultra II, 4 mm
Applied Current:	31 mA
Injection Volume:	25 µL

**Table 5.2:** Operation parameters for the separation of a 20 ppm mixed anion standard.

### 5.2.2 Chemicals and Reagents.

Sodium formate,  $\geq 99.0\%$  ACS reagent Sigma, potassium oxalate monohydrate  $\geq 99.0\%$  ACS reagent Sigma, sodium carbonate  $\geq 99.0\%$  ACS reagent Sigma, sodium hydrogen carbonate and sodium chloride  $\geq 99.5\%$  ACS reagent Sigma. All the above solid reagents were used as received.

Deionised water was obtained prior to use from a Millipore milliQ plus system only used when above 18M $\Omega$ .

### 5.2.3. Separation and Resolution.

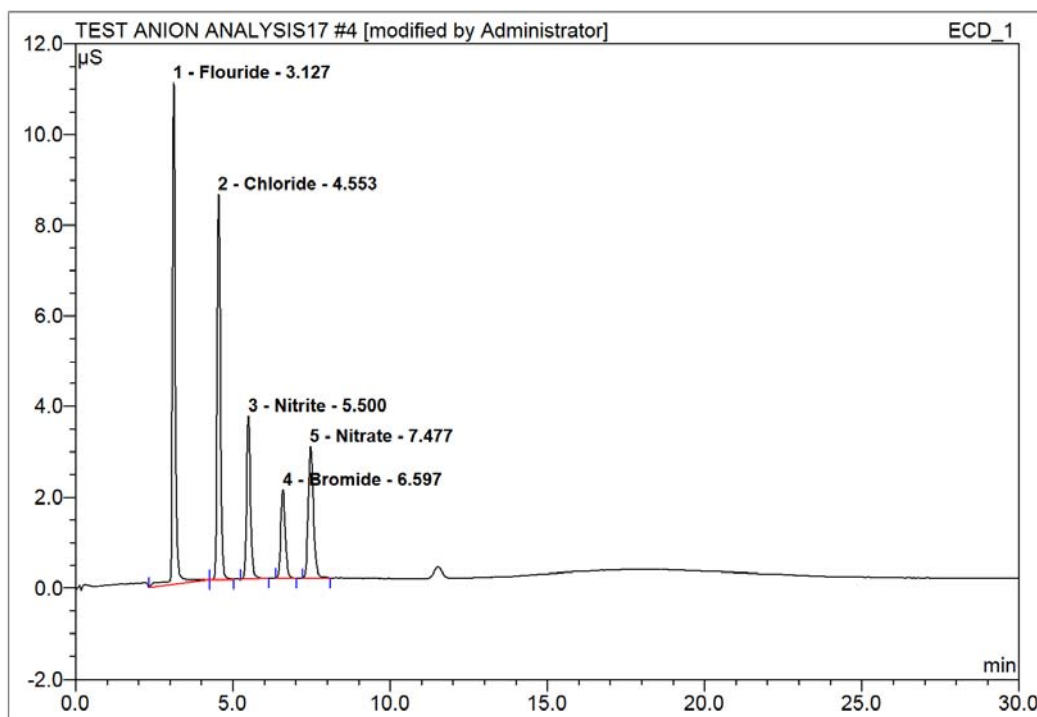


**Figure 5.4:** Separation chromatogram of a 20 ppm mixed anion standard.

<i>Analyte</i>	<i>Ret (t<sub>r</sub>)</i>	<i>Void (t<sub>0</sub>)</i>	<i>Adjusted ret (t<sub>r</sub>)</i>	<i>K'</i>	<i>α</i>	<i>N</i>	<i>Rs</i>
Fluoride	3.12	2.12	1.00	0.47	-	6812	-
Chloride	4.53	2.12	1.14	0.54	1.14	9817	1.06
Nitrite	5.5	2.12	1.59	0.75	1.40	9741	3.02
Bromide	6.58	2.12	2.10	0.99	1.32	10209	3.31
Nitrate	7.47	2.12	2.52	1.19	1.20	9829	2.23

Where :

$(\alpha) = \text{Selectivity Factor (relative retention)} = (t_{r2} - t_{r1}) / 0.5(w_2 + w_1)$ ,

$K' = \text{Capacity Factor} = ((t_r - t_0) / t_0)$

$Rs = \text{Resolution} = 1/4 (K'/K' + 1)(N)^{1/2}(\alpha - 1/\alpha)$

**Table 5.3:** Separation and Resolution results obtained for the 20 ppm mixed anion standard.

Figure 5.4 above depicts the separation achieved for a 20 ppm mixed anion standard for an initial system check. Table 5.3 above details the separation achieved for each individual anion. The above anions were deemed adequately resolved as there were no overlap of peak areas observed. For reasonable accuracy peak maxima must be at least  $4\sigma$  apart which is equivalent to an  $Rs = 1.0$ .<sup>10</sup> Capacity factors and selectivity factors for each of the anions are reasonable.

The relative retention times were compared to those obtained by Dionex as shown in Table 5.4 below. One difference of note between the system tested by Dionex and the system used here was injection volume, the Dionex system ran with an injection volume of 10  $\mu\text{L}$  where here an injection volume of 25  $\mu\text{L}$  was used. As the system peaks were eluting in the same order with similar retention times the system was deemed ready to use and a series of experiments were carried out to determine reproducibility and efficiency.

<i>Analyte</i>	<i>Ret (t<sub>r</sub>)</i>	<i>Ret (t<sub>r</sub>) (Dionex)</i>
Fluoride	3.12	2.88
Chloride	4.53	4.33
Nitrite	5.5	5.30
Bromide	6.58	6.41
Nitrate	7.47	7.32

**Table 5.4:** Comparison of retention times obtained by in house ICS- system and those reported by Dionex.

#### 5.2.4. Reproducibility and Efficiency

<i>Analyte</i>	<i>Avg. Rt</i>	<i>%RSD Rt</i>	<i>%RSD Pk Area</i>	<i>HETP (L/N)</i>	<i>N</i>	<i>K' (tr-t0)/t0</i>
Flouride	3.12	0.834	0.55	0.036	6812	0.47
Chloride	4.53	0.47	0.54	0.025	9817	1.14
Nitrite	5.35	0.43	0.49	0.026	9741	1.52
Bromide	6.58	0.32	0.49	0.244	10209	2.10
Nitrate	7.47	0.39	0.56	0.254	9829	2.52

Where: L= column length (250mm), T0 (void volume) = 2.12 min,

**Table 5.5:** Results obtained for the 20 ppm mixed anion standard, containing average retention time and relative standard deviation (%RSD) for peak area and retention time and column efficiency (HETP, N and capacity factor).

Reproducibility and efficiency were carried out using triplicate injections of the same standard. The relative percentage standard deviations of retention time and peak area were then calculated as shown above in Table 5.5. As can be seen above all %RSD for retention time and peak area are below 1%, the system has proved to be reliable when tested to the specification laid out by Dionex.

#### ***5.2.5. Conclusion.***

As seen above all % RSD for retention time and peak areas are below 1%, the system has proved to be reliable and reproducible when tested to the specification laid out by Dionex. The separation achieved for each of the anions is above those required for a reliable quantification method. These experiments have shown that the system can give reproducible and efficient results, knowing this the development of a method for oxalate and formate can be preformed.

### ***5.3 Method Development for the Analysis of Oxalate and Formate.***

The following section describes the steps taken to determine the retention times and reproducibility of the anions oxalate and formate, upon obtaining these values limits of detection and linearity were determined using sodium formate and potassium oxalate as standards. System suitability was then determined before the development of a sample pre-treatment with a view to analysis of irradiated samples of previously prepared photocatalyst. Each of these steps will be described in detail below with a final section on CO<sub>2</sub> irradiation experiments carried out.

### 5.3.1 Determination of Retention Times and Reproducibility.

Determination of retention times for oxalate and formate were carried out by preparing a series of solutions containing 20 ppm NaCl, 20 ppm Sodium Formate and 20 ppm potassium oxalate. The NaCl was used as an internal standard to determine the retention times of the other anions, as the retention time of the chloride peak was determined during the 20 ppm mixed anion standard injections described previously in section 5.2. Initial system conditions are described in Table 5.6 below.

<i>Separation Parameters for Chloride, Oxalate and Formate Standards</i>	
Eluent:	4.5 mM Na <sub>2</sub> CO <sub>3</sub> / 1.4 mM NaHCO <sub>3</sub> (pH = 9.1)
Flow Rate:	1.2 mL/min
Column Temperature:	30 °C
Detection:	Suppressed Conductivity Detector (CD25) @ 35 °C
Suppressor:	ASRS Ultra II, 4 mm
Applied Current:	31 mA
Injection Volume:	25 µL
Run Time:	15.00 mins
<i>Table 5.6: Operation parameters for chloride, oxalate and formate standards.</i>	



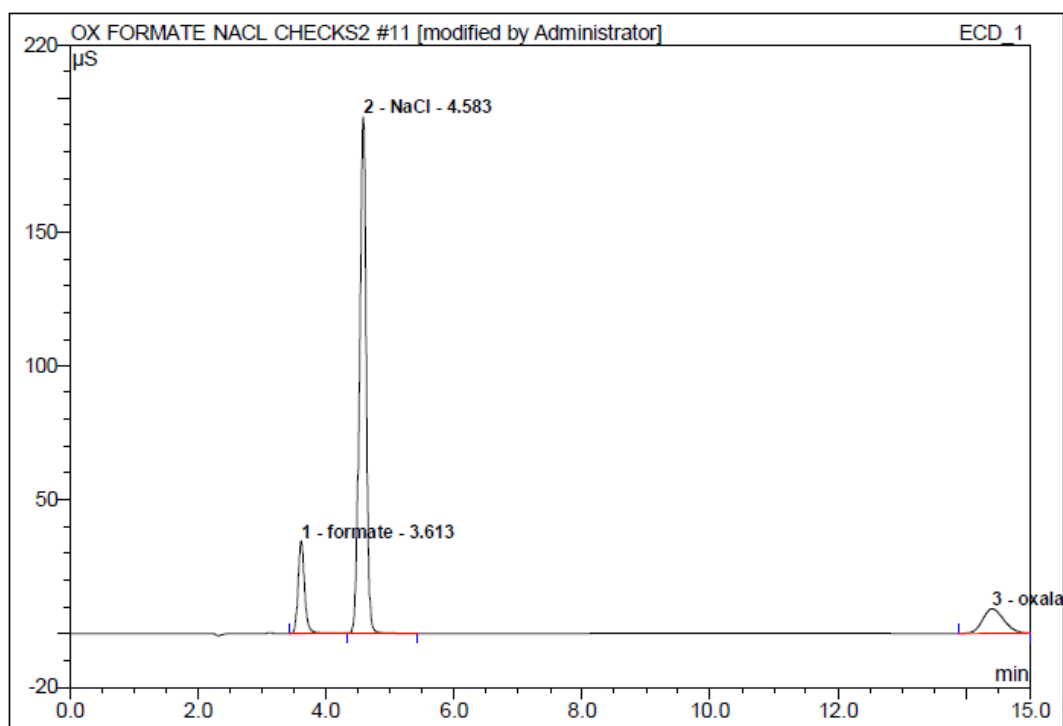


**Figure 5.5:** Chromatogram obtained for chloride, oxalate and formate standards.

Initially a series of triplicate injections of a 20 ppm solution containing the internal standard NaCl and oxalate and formate were injected on to the system. The results obtained are shown above in Figure 5.5. As can be seen from the chromatogram the run time of the experiment at 15 mins was too short, it did allow time for the oxalate peak to resolve but subsequent experiments were extended to 20 mins. The retention times for the formate and oxalate peaks were determined as 3.8 mins and 14.4 mins respectively. Knowing this the internal standard could be removed allowing the system to be calibrated with oxalate and formate standards. The results of this calibration are shown in Table 5.7 that follows.

### 5.3.2. Calibration and Quantification.

Calibration of the internal standards oxalate and formate was carried out by a 3 injection repeat from a  $10^{-3}$ M standard where retention time and peak area were monitored. Quantification was carried out by preparing 3 different solutions of  $10^{-3}$ M with two injections per sample. % RSD Rt and % RSD Pk area were monitored to determine that the system was reliable.

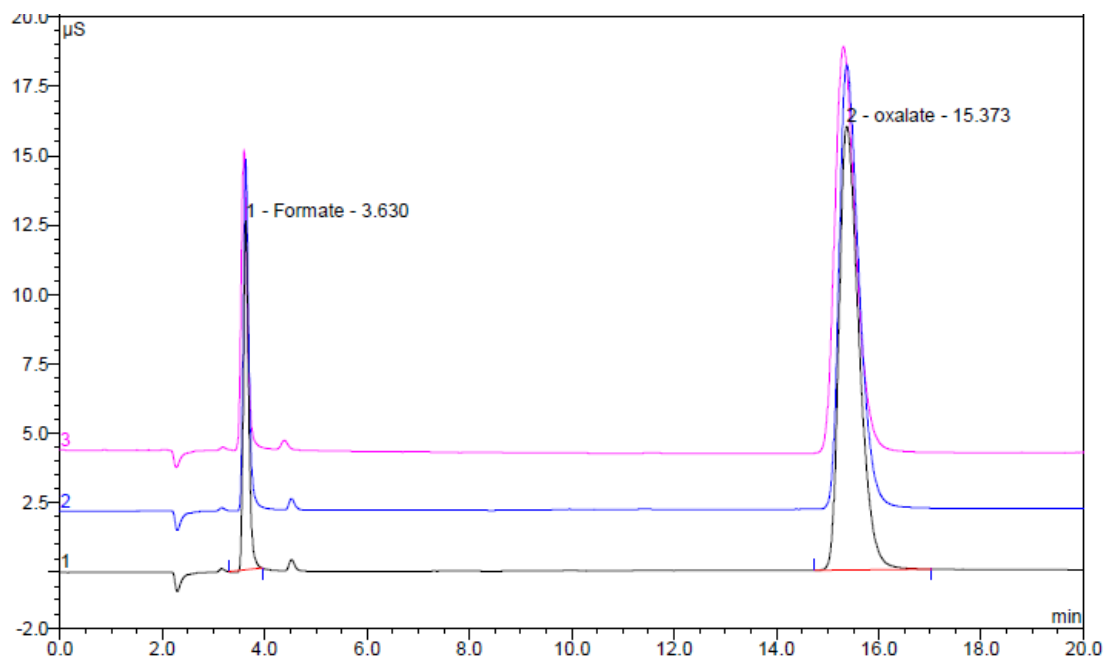


**Figure 5.6:** Chromatogram of  $10^{-3}$ M oxalate/ formate standard repeat injections using the system parameters described in Table 5.6.

<i>Analyte</i>	<i>Avg. Rt</i>	<i>%RSD Rt</i>	<i>%RSD Area</i>	<i>Pk</i>	<i>HETP (L/N)</i>	<i>N</i>
Formate	3.8	0.46	0.57	0.031	9835	
Oxalate	14.4	0.38	0.64	0.22	9972	

**Table 5.7:** Results obtained for formate and oxalate internal standards, containing average retention time and relative standard deviation (%RSD) for peak area and retention time and column efficiency (HETP and N).

### 5.3.3 Detection Limits.

Dilute standards were made up and diluted until no longer discernable from the baseline. Detection limits were then calculated as the concentration of each anion that was equivalent to three times the signal to noise ratio. Initial blank injections were carried out to determine any interference from water / eluent and to determine if any carry over was occurring between injections. The detection range was found to be  $\geq 10^{-5}$ M.

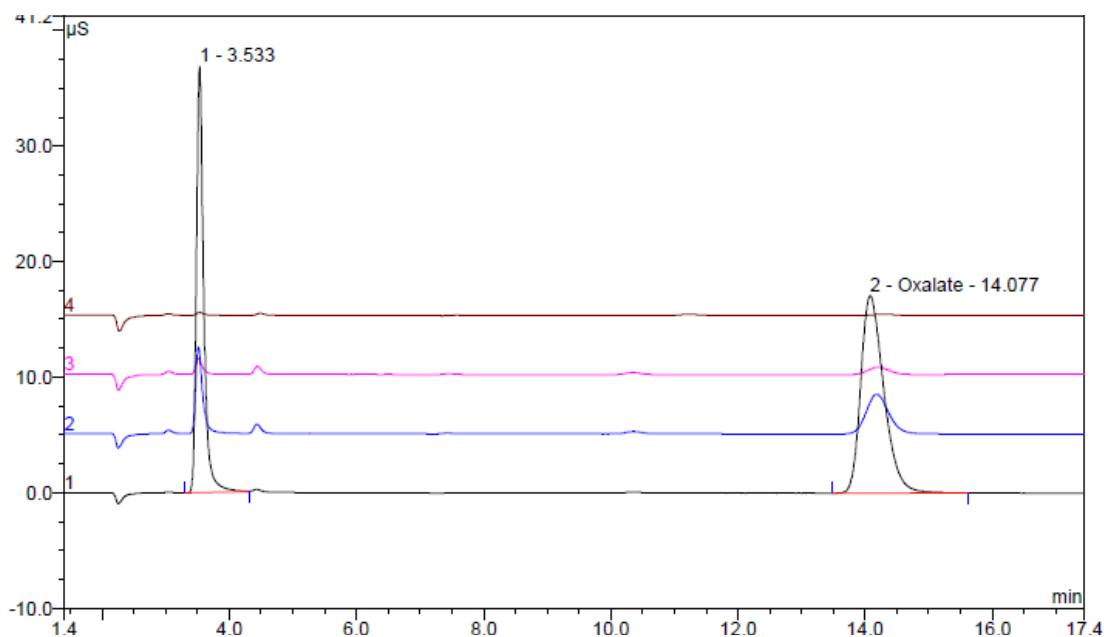


**Figure 5.7:** Chromatogram of oxalate and formate standards during limit of detection studies.

Linearity was then carried out between  $10^{-2}$ M and  $10^{-5}$ M with duplicate injections of each standard. With such a wide range linearity is difficult to obtain, but with each sample injection the system showed a significant response in peak area.

#### 5.4. Photochemical CO<sub>2</sub> Reduction Experiment.

A series of standards ( $10^{-2}\text{M}$ ,  $10^{-3}\text{M}$ ,  $10^{-4}\text{M}$ ,  $10^{-5}\text{M}$ ) were prepared using oxalate and formate. Each of these solutions were injected in duplicate, using the system set up parameters described previously in Table 5.6. 4 samples of  $10^{-3}\text{M}$   $[\text{Ru}(\text{bpy})_2(\text{bpt})\text{Re}(\text{CO})_3\text{Cl}]^{2+}$  were prepared in acetonitrile with TEA as a sacrificial donor. These solutions were then degassed with argon followed by purging with CO<sub>2</sub>. These were then irradiated at 0, 6, 12 and 24 hours under blue light. Table 5.8 describes the results obtained for this experiment while Figure 5.10 shows the chromatogram from the 24 hour sample.

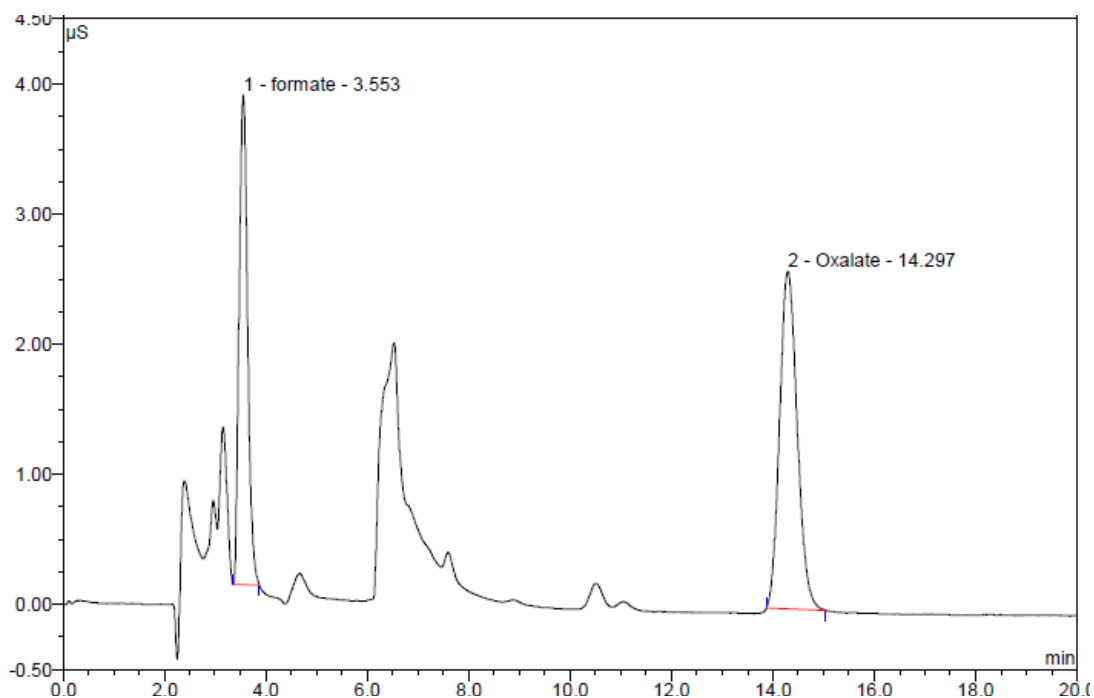


**Figure 5.8:** Chromatogram of  $[\text{Ru}(\text{bpy})_2(\text{bpt})\text{Re}(\text{CO})_3\text{Cl}]^{2+}$  after 24 hours irradiation under blue light.

<i>Hours Irrad.</i>	<i>Analyte</i>	<i>Ret.Time min</i>	<i>Area μS*min</i>	<i>Amount</i>	<i>Height μS</i>	<i>Rel.Area %</i>	<i>Area μS*min</i>
6	formate	3.52	0.5992	0.3078	3.707	58.28	0.599
6	oxalate	0	0	0	0	0	0
12	formate	3.467	0.0858	0.0441	0.426	13.42	0.086
12	oxalate	14.247	0.0319	0.0199	0.078	4.99	0.032
24	formate	3.553	0.7573	0.3891	3.793	41.42	0.757
24	oxalate	14.297	1.071	0.6698	2.625	58.58	1.071

**Table 5.8:** Results obtained from the 24 hour irradiation study of  $[Ru(bpy)_2(bpt)Re(CO)_3Cl]^{2+}$ .

From the above results, it is clear that some CO<sub>2</sub> reduction is occurring during irradiation due to the presence of formate and oxalate in the above samples. For this method to be quantitative another method of degassing the samples needs to be found so that the amount of CO<sub>2</sub> in each sample vial can be monitored and assessed. From the above results the formation of formate and oxalate appears to form in higher yields at longer irradiation times. A further time dependant study should be performed to determine if/ when the dye decomposes and the reduction process appears to cease. From the above results it is also of interest that the amount of formate in the 12 hour sample compared to the 6 hour sample is much less. This could be due to a badly sealed vial or student error. These measurements should be repeated in full to check the amounts of formate and oxalate formed. The chromatograms also show the elution of other products between the formate and oxalate peaks which could be decomposition products of the dye itself. Further investigations are required to determine a proper quantitative analysis where a rate of reduction and turn over numbers can be calculated.

### 5.5 Conclusions and Future Work.

Installation and calibration of the Dionex ICS 1500 was carried out successfully. The retention times of the oxalate and formate standards were determined independently and relative to the internal standard NaCl. This method was then used to determine if any CO<sub>2</sub> reduction products were observed when [Ru(bpy)<sub>2</sub>(bpt)Re(CO)<sub>3</sub>Cl]<sup>2+</sup> was irradiated under blue light for a period of 24 hours. These results showed that the dye did produce the CO<sub>2</sub> reductions products oxalate and formate with the oxalate forming between the 6 hour and 12 hour period.

Subsequent investigations are required to determine the CO<sub>2</sub> turnover numbers for the dye along with investigations into the degassing procedure of the dye samples. These results are encouraging and prompt further investigation into the use of the inorganic dye [Ru(bpy)<sub>2</sub>(bpt)Re(CO)<sub>3</sub>Cl]<sup>2+</sup> to reduce carbon dioxide.

---

### 5.6 Bibliography.

- <sup>1</sup> Lhen, J.M., Zeissel, R., *Proc. Natl. Acad. Sci. USA.*, 79, **1982**, 701.
- <sup>2</sup> Dionex Manual of Operation, 2005, Dionex Cooperation.
- <sup>3</sup> Haddad P.R., Jackson P.E., *Ion Chromatography: Principles and Applications*, Journal of Chromatography Library vol. 46, Elssvier **1990**
- <sup>4</sup> Barron R.E., Fritz J.S., *J. chromatography.*, 316 **1984** 201.
- <sup>5</sup> Barron R.E., Fritz J.S., *J. chromatography.*, 284 **1984** 13.
- <sup>6</sup> Warth L.M., Fritz J.S., Naples J.O., *J. chromatography.*, 462 **1989** 165.
- <sup>7</sup> Fritz J.S., Gjerde D.T., *Ion Chromatography* wiley VCH **1995**
- <sup>8</sup> Rabian S., Stillian J., Barreto V., Friedman K., Toofan M., *J. Chromatogr.*, 640, **1993**, 97.
- <sup>9</sup> Braunstein J., Robbins G.D., *J. Chem. Educ.*, 48, **1983**, 1129.

<sup>10</sup> Willard H.H., Merritt L.L. Jr., Dean J.A., Settle F.A. Jr., *Instrumental methods of Analysis*, 7<sup>th</sup> ed., wadsworth publishing company **1988**.

***Chapter 6: Conclusions and Future Work.***

*Chapter 6 concludes this thesis by providing an overall conclusion from the investigations carried out in the previous chapters. Future work into the area of CO<sub>2</sub> reduction is also proposed.*



## 6.0 Conclusions and Future Work.

The main focus of this thesis has been synthetic investigations into the development of inorganic dyes to be used within the area of CO<sub>2</sub> reduction. Due to the increasing size of the bridging ligands and of the ruthenium and rhenium moieties themselves novel synthetic pathways were developed, before and initial investigation into the ability of the dye to reduce CO<sub>2</sub>.

It was described in chapter 3 that the traditional approach “*complexes as metals / complexes as ligands*” was successful in the development of the inorganic complex [Ru(bpy)<sub>2</sub>(bpt)Re(CO<sub>3</sub>)Cl]<sup>2+</sup>. Investigations into the development of the pyrazine analogue where unsuccessful and further synthetic investigations into the attachment of the rhenium moiety to the [Ru(bpy)<sub>2</sub>(bpzt)]<sup>+</sup> mononuclear complex still need to be carried out possibly in the direction of a new synthetic pathway.

However this traditional approach to the preparation of inorganic supramolecular complexes was unsuccessful in the development of [Ru(bpy)<sub>2</sub>(tpphz)Re(CO)<sub>3</sub>Cl]<sup>2+</sup> discussed in chapter 4. This spurred the development of novel synthetic pathways, the most successful of which required the “building” of the complex stepwise from the rhenium moiety. Further analysis and investigations of this complex are required including life time of the excited state along with photochemical CO<sub>2</sub> reduction studies. The novel complexes [Ru(*d*-bpy)<sub>2</sub>(tpphz)]<sup>2+</sup> and [(Ru(*d*-bpy)<sub>2</sub>)<sub>2</sub>(tpphz)]<sup>4+</sup> were also prepared with high purity, these also required further investigation and analysis including adsorption and emission studies.

Chapter 5 describes the initial installation and calibration carried out on the Dionex ICS 1500 system. The retention times and calibration of the internal standards oxalate and formate was also carried out before the initial investigation of the photochemical reduction of CO<sub>2</sub> using [Ru(bpy)<sub>2</sub>(bpt)Re(CO)<sub>3</sub>Cl]<sup>2+</sup>. Initial results showed that oxalate and formate are produced during this reduction process but further investigation into the degassing of the samples prior to irradiation under blue light is required to determine an accurate and quantifiable method.

## Appendix A - List of Figures

### Chapter 1

**Figure 1.1:** General scheme of photosynthesis occurring within a chloroplast ( pg 3).

**Figure 1.2:** Activation mechanism of rubisco in the presence of CO<sub>2</sub> ( pg 4)

**Figure 1.3:** Structure of the metal containing segment of rubisco. ( pg 5).

**Figure 1.4:** Redox potentials vs. NHE for the multi electron reduction of CO<sub>2</sub> at pH7 / 25°C ( pg 7)

**Figure 1.5:** Shows the two electron reduction potentials as a function of pH for carbon dioxide to carbon monoxide, carbon dioxide to formic acid and hydrogen ion /water to dihydrogen. ( pg 7)

**Figure 1.6:** Shows the oxidative and reductive quenching equations as described by E. Fujita. ( pg 9)

**Figure 1.7:** Possible CO<sub>2</sub> reduction pathways as described by Fujita et al. ( pg 10)

**Figure 1.8:** Equations for the bimolecular process for CO<sub>2</sub> reduction. ( pg 11)

**Figure 1.9:** Structures of [Ni(14-aneN4)]<sup>2+</sup> and [Ni(12-aneN4)]<sup>2+</sup> investigated by Craig et al. ( pg 14)

**Figure 1.10:** Preparation of the supramolecular complex [ Ru<sup>(II)</sup> (bpy)<sub>2</sub>(bpy-cyclam)Ni<sup>(II)</sup>] ( ClO<sub>4</sub>)<sub>4</sub>.2H<sub>2</sub>O(3) via[ Ni<sup>(II)</sup> cyclam] (1) and [ Ru(bpy)<sub>2</sub>(bpy-H<sub>2</sub>cyclam<sup>2+</sup>)](ClO<sub>4</sub>)<sub>4</sub>.3H<sub>2</sub>O. ( pg 15)

**Figure 1.11:** Preparation of the supramolecular complex [Ru(phen)<sub>2</sub>(phen-cyclam-Ni)(ClO<sub>4</sub>)<sub>4</sub>].2H<sub>2</sub>O from the Ni(II) cyclam ligand (1) and Ru(phen)<sub>2</sub>(phen-cyclam-H<sub>2</sub>)(ClO<sub>4</sub>)<sub>4</sub>.3H<sub>2</sub>O (2).( pg 16)

**Figure 1.12:** Structure of [Ru(bpy)<sub>2</sub>(4-((4-methylpyridinium-1-yl)methyl)-4'-methyl-2,2'-bipyridine)](ClO<sub>4</sub>)<sub>3</sub> ( pg 17)

**Figure 1.13:** Proposed mechanisms for CO<sub>2</sub> reduction for metal metaltetraaza-macrocycles.( pg 18)

**Figure 1.14:** Supramolecular complexes studied by Ishitani et al.( pg 20)

**Figure 1.15:** Diagram of the trinuclear supramolecular structures investigated by Ishitani et al.( pg 21)

**Figure 1.16:** Structures of Re(II)-Re(I) complexes using MebpyC<sub>2</sub>H<sub>4</sub>Mebpy, MebpyC<sub>4</sub>H<sub>8</sub>Mebpy, MebpyC<sub>6</sub>H<sub>12</sub>Mebpy and corresponding alcohol (1,3-bis(4-methyl-2,2'-bipyridinyl-4-yl)-propan-2-ol) as bridging ligands (pg 22)

**Figure 1.17:** Equations describing type II catalysis. (pg 23)

**Figure 1.18:** Metallomacrocycles investigated for CO<sub>2</sub> reduction where MP = metalloporphyrin, MN = metallocorrin, MPc = metallophthalocyanine, MC = metallocorrole. (pg 25)

**Figure 1.19:** Results of Photochemical production of CO in CO<sub>2</sub>-saturated acetonitrile solutions containing 5% TEA and Co porphyrin conducted by Fujita et al. (pg 27)

**Figure 1.20:** Structures of the zinc porphyrin diad prepared by Ishitani et al. (pg 28)

**Figure 1.21:** Photochemical production of CO preformed by Grodkowski and Neta. (pg 30)

**Figure 1.22:** Preparation of the Zn-Phthalocyanine catalyst reported by Zhao et al. (pg 31)

**Figure 1.23:** Time dependence of formic acid yields of the various catalysts prepared by Zhao et al (pg 32)

**Figure 1.24:** Improved sol-gel technique by Zhao et al. (pg 33)

**Figure 1.25:** Illustration of photo-catalytic reduction of CO<sub>2</sub> at ZnPc absorbed TiO<sub>2</sub>. (pg 34)

**Figure 1.26:** Proposed Mechanistic Steps in the Reduction of CO<sub>2</sub> by Metal Porphyrin Derivatives (M) Fe or Co) via a Type II catalysts by Morris et al. (pg 35)

**Figure 1.27:** Kinetic results reported for CO<sub>2</sub> insertion for fac-[Re(bpy)(CO)<sub>3</sub>H] by Sullivan et al (pg 36)

**Figure 1.28:** First reported photochemical synthesis of mer-[Re(CO)<sub>3</sub>(bpy)Cl]. (pg 37)

**Figure 1.29:** Proposed mechanism for CO<sub>2</sub> reduction using a rhenium mononuclear complex by Ishitani et al. (pg 39)

**Figure 1.30:** Dinuclear complexes prepared as potential photocatalysts for CO<sub>2</sub> reduction. (bpy = 2,2'-bipyridine). (pg 41)

## Chapter 2

**Figure 2.1:** Diagram of Reflux Setup. (pg 54)

**Figure 2.2:** Illustration of solvent removal from sample. (pg 55)

## Chapter 3

**Figure 3.1:** An example of the triazole ligand Hbpt with the coordination sites N2 and N4 available. (pg 58)

**Figure 3.2:** General synthesis of a mononuclear complex. (pg 59)

**Figure 3.3:** Example of a homonuclear complex synthesis. (pg 59)

**Figure 3.4:** Example of a heteronuclear complex synthesis. (pg 60)

**Figure 3.5:** Depicts the structures of the ligands discussed in this section. (pg 61)

**Figure 3.6:** Depicts the structures of the mononuclear complexes discussed in this section. (pg 62)

**Figure 3.7:** Depicts the structures of the dinuclear complexes discussed in this section. (bpy = 2,2-bipyridine). (pg 63)

**Figure 3.8:** Synthetic route used to synthesise Hbpt. (pg 71)

**Figure 3.9:** Route used to synthesise Hbpzt. (pg 72)

**Figure 3.10:** Schematic representation of the pathways employed in the synthesis of the dinuclear metal complexes. (L = Hbpt, Hbpzt, dptd ). (pg 74)

**Figure 3.11:**  $^1\text{H}$ NMR spectra for  $[\text{Ru}(\text{bpy})_2\text{Cl}_2]$  and  $[\text{Ru}(\text{bpy})_2\text{bpt}]^+$  carried out in DMSO at 298K. (pg 75)

**Figure 3.12:** Labeling of the triazole ligands for  $^1\text{H}$  NMR assignment. (pg 76)

**Figure 3.13:**  $^1\text{H}$  NMR spectra for the Hbpt (top) and Hbpzt (bottom) carried out in DMSO at 298K. (pg 77)

**Figure 3.14:** Structure of the N2/N4 isomers of  $[\text{Ru}(\text{bpy})_2\text{bpt}]^+$  (pg78)

**Figure 3.15:**  $^1\text{H}$  NMR spectrum for Hbpt ligand (top),  $[\text{Ru}(\text{bpy})_2\text{bpt}]$  (middle) $^+$  and  $[\{\text{Ru}(\text{bpy})_2\}_2\text{bpt}]^{3+}$  (bottom) carried out in DMSO at 298K. (pg 79)

**Figure 3.16:**  $^1\text{H}$  NMR spectra for  $[(\text{Re}(\text{CO})_3\text{Cl})_2(\text{Hbpt})]$  (top),  $[\text{Ru}(\text{bpy})_2\text{bpt}]^{2+}$  (middle) and  $[\text{Ru}(\text{bpy})_2(\text{bpt})\text{Re}(\text{CO})_3\text{Cl}]^+$  (bottom) carried out in DMSO at 298K. (pg 82)

**Figure 3.17:**  $^1\text{H}$ NMR spectra obtained for fraction A (top) and B (bottom) of  $[\text{Ru}(\text{bpy})_2\text{bpt}]^{3+}$  in  $\text{d}_3$ -acetonitrile at 298K. (pg 83)

**Figure 3.18:**  $^1\text{H}$  NMR spectrum for  $[(\text{Ru}(\text{bpy})_2\text{bpzt})^+]$  (top),  $[(\text{Ru}(\text{bpy})_2)_2\text{bpzt}]^{3+}$  (middle) and  $[(\text{Re}(\text{CO})_3\text{Cl})_2(\text{bpzt})]$  (bottom) in DMSO at 298K. (pg 85)

**Figure 3.19:** Example of the facial coordination of the rhenium tricarbonyl complexes discussed where N-N denotes the bidentate ligand. (pg 87)

**Figure 3.20:** I.R. of  $[(\text{Re}(\text{CO})_3)_2\text{Hbpt}]$  (green) and  $[\text{Ru}(\text{bpy})_2(\text{bpt})\text{Re}(\text{CO})_3\text{Cl}]$  (black) in DCM at 298K. (pg 88)

**Figure 3.21:** I.R. of  $[\text{Ru}(\text{bpy})_2(\text{dptd})\text{Re}(\text{CO})_3\text{Cl}]$  in DCM at 298K. (pg 89)

**Figure 3.22** Absorption spectra of Hbpt (yellow),  $[\text{Ru}(\text{bpy})_2\text{bpt}]^+$  (Pink) and  $[\text{Ru}(\text{bpy})_2(\text{bpt})\text{Re}(\text{CO})_3\text{Cl}]^+$  (blue) carried out at room temperature in acetonitrile. (pg 91)

**Figure 3.23** Absorption spectra  $[(\text{Ru}(\text{bpy})_2)_2\text{bpzt}]^+$  (Pink) and  $[\text{Ru}(\text{bpy})_2(\text{bpt})\text{Re}(\text{CO})_3\text{Cl}]^+$  (yellow) and  $[(\text{Re}(\text{CO})_3\text{Cl})_2\text{Hbpt}]$  (blue) at room temperature in acetonitrile. (pg 91)

**Figure 3.24** Absorption spectra  $[(\text{Ru}(\text{bpy})_2)_2\text{bpzt}]^{3+}$  (Pink) and  $[\text{Ru}(\text{bpy})_2(\text{bpzt})]^+$  (blue) and at room temperature in acetonitrile. (pg 93)

**Figure 3.25** Absorption spectra  $[(\text{Ru}(\text{bpy})_2)_2\text{bpzt}]^{3+}$  (Pink) and  $[(\text{Re}(\text{CO})_3\text{Cl})_2\text{Hbpzt}]$  (blue) and at room temperature in acetonitrile. (pg 93)

**Figure 3.26:** Emission spectrum of  $[\text{Ru}(\text{bpy})_2(\text{bpt})\text{Re}(\text{CO})_3\text{Cl}]^+$  (pink) and  $[(\text{Ru}(\text{bpy})_2)_2\text{bpzt}]^{3+}$  (blue) in aerated acetonitrile solution.  $\lambda_{\text{exc}} = 460 \text{ nm}$ . (pg 95)

**Figure 3.27:** Emission spectrum of  $[\text{Ru}(\text{bpy})_2(\text{bpzt})]^+$  (blue),  $[(\text{Ru}(\text{bpy})_2)_2\text{bpzt}]^{3+}$  (pink) and  $[(\text{Re}(\text{CO})_3\text{Cl})_2\text{Hbpzt}]$  (green) in aerated acetonitrile solution. (pg 96)

## **Chapter 4**

**Figure 4.1:** Hydrogenation of Tolane to cis-stilbene using  $[\text{Ru}(\text{bpy})_2(\text{tpphz})\text{PdCl}_2]^{2+}$ . (pg 104)

**Figure 4.2:** Structure of the photocatalyst reported by Saki et al. (pg 104)

**Figure 4.3:** Biocatalytic synthesis reported by Mosurkal et al. (pg 107)

**Figure 4.4:** Example of a Schiff-base reaction. (pg 116)

**Figure 4.5:** Synthetic Route 1 to the formation of the desired Ru (II) mononuclear complex and subsequent heterodimer. (pg 118)

**Figure 4.6:** Synthetic Route 2 to the formation of the desired Ru (II) mononuclear complex and subsequent heterodimer. (pg 120)

**Figure 4.7:** Synthetic Route 3 to the formation of the desired heterodimer (pg 121)

**Figure 4.8:** Synthetic Route 4 to the formation of the desired heterodimer (pg 122)

**Figure 4.9:** Labelling of the phenanthroline based ligands for  $^1\text{H}$ NMR assignment. (pg 123)

**Figure 4.10:**  $^1\text{H}$ NMR of phenanthroline (top), phendione (middle) and tpphz (bottom) ligands in  $\text{d}_3$ -acetonitrile at 298K. TFA peak can be seen at 9.66 ppm in the tpphz spectra. (pg 125)

**Figure 4.11**  $^1\text{H}$ NMR COSY of tpphz ligand in  $\text{d}_3$ -acetonitrile at 298K. (pg 126)

**Figure 4.12**  $^1\text{H}$ NMR spectrum for  $[\text{Ru}(\text{bpy})_2(\text{phen})]^{2+}$  (top) and  $[\text{Ru}(\text{bpy})_2(\text{phendione})]^{2+}$  (bottom) in  $\text{d}_3$ -Acetone at 298K. (pg 128)

**Figure 4.13:**  $^1\text{H}$  NMR spectrum for phendione (top) ,  $[\text{Re}(\text{CO})_3(\text{phen})\text{Cl}]$ (middle) and  $[\text{Re}(\text{CO})_3(\text{phendione})\text{Cl}]$ (bottom) in  $\text{d}_6$ -Acetone at 298K. (pg 129)

**Figure 4.14:** 2D-COSY spectrum for the complex  $^+[(\text{Ru}(\text{d-bpy})_2)_2(\text{tpphz})]^{2+}$  in  $\text{d}_3$ -acetonitrile at 298K. (pg 131)

**Figure 4.15:**  $^1\text{H}$ NMR spectra for the complexes  $[(\text{Ru}(\text{bpy})_2)_2(\text{tpphz})]^{2+}$ ,  $[(\text{Ru}(\text{d-bpy})_2)_2(\text{tpphz})]^{2+}$  and free tpphz ligand in  $\text{d}_3$ -acetonitrile at 298K. (pg 132)

**Figure 4.16:**  $^1\text{H}$ NMR spectrum for  $[\text{Ru}(\text{bpy})_2(\text{tpphz})\text{Re}(\text{CO})_3\text{Cl}]^{2+}$  in  $\text{d}_3$ -Acetonitrile at 298K. (pg 133)

**Figure 4.17:** I.R. of  $[\text{Re}(\text{CO})_5\text{Cl}]$ (black) and  $[\text{Re}(\text{CO})_3\text{Cl}(\text{tpphz})]$  (green) in THF at 298K. (pg 135)

**Figure 4.18:** I.R. of  $[\text{Re}(\text{CO})_3\text{Cl}(\text{dione})]$  in THF at 298K. (pg 135)

**Figure 4.19:** Example of the facial coordination of the rhenium tricarbonyl complexes discussed where N-N denotes a phenanthroline based ligand. (pg 136)

### **Chapter 5.**

**Figure 5.1:** Redox potentials vs. NHE for the multi electron reduction of  $\text{CO}_2$  at pH7 / 25°C. (pg 149)

**Figure 5.2:** Diagram of Direction of Analysis Flow for the ICS 1500. (pg 150)

**Figure 5.3:** Mechanism of suppression for the Anion Self- Regenerating Suppressor.(pg 155)

**Figure 5.4:** Separation chromatogram of a 20 ppm mixed anion standard. (pg 159)

**Figure 5.5:** Chromatogram obtained for chloride, oxalate and formate standards. (pg 164)

**Figure 5.6:** Chromatogram of  $10^{-3}\text{M}$  oxalate/ formate standard repeat injections using the system parameters described in Table 5.6. (pg 165)

**Figure 5.7:** Chromatogram of oxalate and formate standards during limit of detection studies. (pg 166)

**Figure 5.8:** Chromatogram of  $[\text{Ru}(\text{bpy})_2(\text{bpt})\text{Re}(\text{CO})_3\text{Cl}]^{2+}$  after 24 hours irradiation under blue light. (pg 167)





## **Appendix B - List of Tables**

### **Chapter 1**

**Table 1.1:** Summary of Type I catalyst experiments for CO<sub>2</sub> reduction via bimolecular process. (pg 12)

**Table 1.2:** Summary of Type I catalyst experiments for CO<sub>2</sub> reduction via bimolecular process. (pg 13)

**Table 1.3:** Summary of Type II catalyst experiments for CO<sub>2</sub> reduction. (pg 24)

### **Chapter 3**

**Table 3.1:** Chemical shifts in ppm of the ligand protons measured in DMSO. (pg 78)

**Table 3.2:** Chemical shifts in ppm obtained for Hbpt,

$[\text{Ru}(\text{bpy})_2(\text{bpt})]^+$ ,  $[\text{Ru}(\text{bpy})_2)_2(\text{bpt})]^{3+}$ ,  $[\text{Re}(\text{CO})_3\text{Cl}(\text{Hbpt})]$ ,  $[(\text{Re}(\text{CO})_3\text{Cl})_2(\text{Hbpt})]$  and  $[\text{Ru}(\text{bpy})_2(\text{bpt})\text{Re}(\text{CO})_3\text{Cl}]^+$  measured in DMSO at 298 K. (pg 81)

**Table 3.3:** Chemical shifts in ppm obtained for Hbpzt,  $[\text{Ru}(\text{bpy})_2(\text{bpzt})]^+$ ,  $[\text{Ru}(\text{bpy})_2)_2(\text{bpzt})]^{3+}$  and  $[(\text{Re}(\text{CO})_3\text{Cl})_2(\text{Hbpzt})]$  measured in DMSO at 298 K. (pg 85)

**Table 3.4:** Chemical shifts in ppm of the dptd protons of dptd and  $[\text{Ru}(\text{bpy})_2(\text{dptd})]^+$  as measured in DMSO at 298K. (pg 87)

**Table 3.5:** IR data for the carbonyl stretching obtained for the azole complexes synthesised in this section carried out in DCM. (pg 90)

**Table 3.6:** Combined emission and absorption data carried out in aerated acetonitrile at 298K. (pg 93)

### **Chapter 4**

**Table 4.1:** Depicts the abbreviations and structures of the ligands discussed in this section. (pg 113)

**Table 4.2:** Depicts the abbreviations and structures of the dinuclear complexes discussed in this section. Where bpy = 2,2-bipyridine. (pg 113)

**Table 4.3:** Depicts the abbreviations and structures of the mononuclear complexes discussed in this section. Where bpy = 2,2-bipyridine. (pg 114)

**Table 4.4:** Reaction conditions carried out in the preparation of the phendioxime ligand. (pg 115)

**Table 4.5:** Test reactions for the preparation of  $[\text{Ru}(\text{bpy})_2\text{tpphz}]^{2+}$ . (pg 126)

**Table 4.6:**  $^1\text{H}$  NMR data in ppm for phen, phendione and tpphz ligands. (pg 130)

**Table 4.7:**  $^1\text{H}$  NMR data for the ligand protons of the Re(I) and Ru (II) mononuclear complexes carried out in  $\text{d}_6$ -acetone at 298K. (pg 133)

**Table 4.8:** IR data for the carbonyl stretching region of the metal complexes in THF. (pg 141)

## **Chapter 5.**

**Table 5.1:** Column specifications and Operation Parameters for Dionex ICS 1500. (pg 152)

**Table 5.2:** Operation parameters for the separation of a 20 ppm mixed anion standard. (pg 158)

**Table 5.3:** Separation and Resolution results obtained for the 20 ppm mixed anion standard. (pg 160)

**Table 5.4:** Comparison of retention times obtained by in house ICS- system and those reported by Dionex. (pg 161)

**Table 5.5:** Results obtained for the 20 ppm mixed anion standard, containing average retention time and relative standard deviation (%RSD) for peak area and retention time and column efficiency (HETP, N and capacity factor). (pg 161)

**Table 5.6:** Operation parameters for chloride, oxalate and formate standards. (pg 163)

**Table 5.7:** Results obtained for formate and oxalate internal standards, containing average retention time and relative standard deviation (%RSD) for peak area and retention time and column efficiency (HETP and N). (pg 165)

**Table 5.8:** Results obtained from the 24 hour irradiation study of  $[\text{Ru}(\text{bpy})_2(\text{bpt})\text{Re}(\text{CO})_3\text{Cl}]^{2+}$ . (pg 169)